

AD/A-007 135

**CLOSED-LOOP OPTIMIZATION PROGRAM
FOR THE M60A1 TANK GUN STABILIZATION
SYSTEM**

W. Binroth, et al

Bendix Research Laboratories

Prepared for:

Rock Island Arsenal

February 1975

DISTRIBUTED BY:

NTIS

**National Technical Information Service
U. S. DEPARTMENT OF COMMERCE**

Best Available Copy

The findings of this report are not to be construed as an Official Department of the Army position, unless so designated by other authorized documents.

DISPOSITION INSTRUCTIONS:

Destroy this report when it is no longer needed. Do not return it to the originator.

ACCESSION NO.		
DTIC		
DATE		
CLASSIFICATION		
BY		
EXTENSION-NO.		
GR.	ATAC	
A		

Best Available Copy

UNCLASSIFIED

SECURITY CLASSIFICATION OF THIS PAGE (When Data Entered)

REPORT DOCUMENTATION PAGE		READ INSTRUCTIONS BEFORE COMPLETING FORM
1. REPORT NUMBER R-CR-75-011	2. GOVT ACCESSION NO.	3. RECIPIENT'S CATALOG NUMBER AD/A-007135
4. TITLE (and Subtitle) CLOSED-LOOP OPTIMIZATION PROGRAM FOR THE M60A1 TANK GUN STABILIZATION SYSTEM		5. TYPE OF REPORT & PERIOD COVERED FINAL JUN 74 - FEB 75
		6. PERFORMING ORG. REPORT NUMBER BRL/TR-75-7484
7. AUTHOR(s) W. BINROTH G.A. CORNELL R.W. PRESLEY		8. CONTRACT OR GRANT NUMBER(s) DAAA-09-74-C-2068
		10. PROGRAM ELEMENT, PROJECT, TASK AREA & WORK UNIT NUMBERS 1T162114AH73
9. PERFORMING ORGANIZATION NAME AND ADDRESS BENDIX RESEARCH LABORATORIES SOUTHFIELD, MICHIGAN 48076		12. REPORT DATE FEB 75
11. CONTROLLING OFFICE NAME AND ADDRESS		13. NUMBER OF PAGES 240
		15. SECURITY CLASS. (of this report) U
14. MONITORING AGENCY NAME & ADDRESS (if different from Controlling Office) ARTILLERY & ARMORED WEAPONS SYSTEMS DIRECTORATE ROCK ISLAND, ILLINOIS 61201		15a. DECLASSIFICATION/DOWNGRADING SCHEDULE N/A
16. DISTRIBUTION STATEMENT (of this Report) APPROVED FOR PUBLIC RELEASE DISTRIBUTION UNLIMITED		
17. DISTRIBUTION STATEMENT (of the abstract entered in Block 20, if different from Report) Reproduced by NATIONAL TECHNICAL INFORMATION SERVICE U S Department of Commerce Springfield VA 22151		
18. SUPPLEMENTARY NOTES PRICES SUBJECT TO CHANGE		
19. KEY WORDS (Continue on reverse side if necessary and identify by block number) STABILIZATION CONTROL SYSTEM ACCELEROMETER FLUIDICS RATE CONTROL HYDRAULIC COMPENSATION POSITION CONTROL PNEUMATIC NON-LINEAR FLOW RATE SENSOR		
20. ABSTRACT (Continue on reverse side if necessary and identify by block number) THE OBJECTIVE OF THIS STUDY WAS TO PROVIDE A GUN STABILIZATION SYSTEM FOR THE M60A1 TANK GUN IN WHICH PERFORMANCE WAS OPTIMIZED. A MATHEMATICAL MODEL OF THE VEHICLE AND THE APPROPRIATE CONTROL SYSTEM WAS DERIVED AND PROGRAMMED ON A HYBRID COMPUTER. PERFORMANCE REQUIREMENTS WERE ESTABLISHED WITH RESPECT TO GUN POINTING ACCURACY AND CONTROL SYSTEM STABILITY. HARDWARE CHARACTERISTICS REQUIRED TO MEET ACQUISITION RATE REQUIREMENTS WERE ALSO DEFINED. A COMPLETE ANALYTICAL SYSTEMS STUDY WAS PERFORMED TO YIELD A BASIS FOR THE HYBRID COMPUTER ANALYSIS. IN THE COMPUTER ANALYSIS, SYSTEM PERFORMANCE		

DD FORM 1473 1 JAN 73 EDITION OF 1 NOV 65 IS OBSOLETE

UNCLASSIFIED

SECURITY CLASSIFICATION OF THIS PAGE (When Data Entered)

Best Available Copy

UNCLASSIFIED

SECURITY CLASSIFICATION OF THIS PAGE(When Data Entered)

— WAS INVESTIGATED IN DETAIL AND FIVE PROSPECTIVE SENSORS WERE STUDIED WITH
RESPECT TO SYSTEM PERFORMANCE CRITERIA. ↗

UNCLASSIFIED

11 SECURITY CLASSIFICATION OF THIS PAGE(When Data Entered)

FOREWORD

This final report describes the study conducted under Army Contract DAAA09-74-C-2068, "Closed-Loop Optimization Program for the M60A1 Tank Gun Stabilization System." The work was administered under the direction of the Thomas J. Rodman Laboratories. Mr. Jack Connors and Mr. Verlin Baumgarth were the Contracting Officer's Representative and Alternate, respectively. The work was conducted during the period 1 July 1974 to 31 December 1974.

This report was prepared by the Information Processing Department, Bendix Research Laboratories, Southfield, Michigan. Mr. W. Binroth was project supervisor for this program, and responsible for the analytical effort, along with Mr. G. A. Cornell and Mr. R. W. Presley. The computer simulation studies were supported by Mr. T. A. Somer and Ms. J. A. Lindsay.

The report number assigned to this report by the Bendix Research Laboratories is BRL/TR-75-7484.

TABLE OF CONTENTS

	<u>Page</u>
SECTION 1 - INTRODUCTION AND SUMMARY	1-1
1.1 Introduction	1-1
1.2 Scope	1-1
1.3 Summary	1-2
SECTION 2 - MATHEMATICAL MODELS DESCRIPTION	2-1
2.1 General	2-1
2.2 Vehicle Models	2-1
2.2.1 Elevation Axis Vehicle Model	2-1
2.2.2 Azimuth Axis Vehicle Model	2-4
2.2.3 Friction	2-5
2.3 Servovalve and Motor Models	2-6
2.4 Sensor Model Descriptions	2-11
2.4.1 General	2-11
2.4.2 Electric Rate Gyro Model	2-11
2.4.3 Hydraulic Rate Sensor Model	2-12
2.4.4 Integrating Accelerometer Model	2-12
2.4.5 Laminar Vortex Rate Sensor Model	2-13
2.4.6 Pneumatic Accelerometer Model	2-14
2.5 Controller Models	2-14
SECTION 3 - CONTROL SYSTEMS APPROACH	3-1
3.1 General	3-1
3.2 Performance Criteria	3-1
3.3 Control Law Derivation	3-2
3.3.1 Rate Control System	3-2
3.3.2 Position Control System	3-4
SECTION 4 - HARDWARE SELECTION PROCEDURE	4-1
4.1 General	4-1
4.2 Hardware Considerations and Assumptions	4-1
4.3 Mathematical Model of the Actuator System	4-3
4.4 Elevation Axis Hardware Selection	4-6
4.5 Azimuth Axis Hardware Selection	4-9
SECTION 5 - Analytical System Analysis	5-1
5.1 General	5-1
5.2 Linear System Derivation	5-1
5.2.1 Rate Control System	5-1
5.2.2 Position Control System	5-5

Preceding page blank

	<u>Page</u>
5.2.3 Linear Model Parameters	5-8
5.2.4 Linear System Response	5-11
5.3 Tracking Error Reduction	5-11
5.4 Sensor Error Analysis	5-14
5.4.1 General	5-14
5.4.2 Two Rate Sensors	5-14
5.4.3 Single Acceleration Sensor	5-15
5.5 Method of Eliminating the Effects of Integrator Drifts and Sensor Offsets	5-17
5.6 Effects of Gyros on Response	5-18
5.7 Forward Versus Feedback Compensation	5-19
5.8 System Stiffness	5-21
5.9 Coupling	5-22
5.10 Summary of Analytical Systems Study	5-26
 SECTION 6 - SIMULATION ANALYSIS RESULTS	 6-1
6.1 General	6-1
6.2 Simulation Approach	6-2
6.3 Comparison Study of Rate and Position Control for Stabilization	6-3
6.4 Preliminary Simulation Studies	6-5
6.4.1 Effect of Nonlinear Valve Flow	6-5
6.4.2 Effect of Hull Dynamics	6-5
6.4.3 Effects of Changes in Fluid Compressibility and Bulk Modulus	6-5
6.5 Evaluation of Sensors in Elevation Axis	6-5
6.5.1 Evaluation of Electric Rate Gyros	6-6
6.5.2 Evaluation of Hydraulic Rate Sensors	6-14
6.5.3 Evaluation of Integrating Accelerometer	6-14
6.5.4 Evaluation of Laminar Vortex Sensor	6-22
6.6 Evaluation of Sensors in Azimuth Axis	6-27
6.6.1 Evaluation of Electric Rate Gyros	6-27
6.6.2 Evaluation of Pneumatic Accelerometer	6-30
6.7 Summary of Simulation Results	6-37
 SECTION 7 - CONCLUSIONS	 7-1
 SECTION 8 - RECOMMENDATIONS	 8-1
 SECTION 9 - BIBLIOGRAPHY	 9-1
 APPENDIX A - DIGITAL COMPUTER PROGRAMS	 A-1
 APPENDIX B - ANALOG AND HYBRID WIRING DIAGRAMS	 B-1
 DISTRIBUTION	 C-1

LIST OF ILLUSTRATIONS

<u>Figure No.</u>	<u>Title</u>	<u>Page</u>
2-1	Simplified Block Diagram of the Rate Command Stabilization System	2-2
2-2	Elevation Axis Vehicle Model	2-2
2-3	Azimuth Axis Vehicle Model	2-4
2-4	Block Diagram for Simulating Friction	2-7
2-5	Idealized Block Diagram for Simulating Friction	2-7
2-6	Servo valve and Motor Simulation Block Diagram	2-8
2-7	Block Diagram of the Pneumatic Accelerometer	2-14
2-8	Controller for Rate Command with Two Rate Sensors	2-16
2-9	Controller for Rate Command with Single Acceleration Sensor	2-16
2-10	Controller for Position Command with Two Rate Sensors	2-17
2-11	Controller for Position Command with Single Acceleration Sensor	2-17
3-1	Simplified Block Diagram of a Rate Command Stabilization System	3-3
3-2	Simplified Block Diagram of a Position Command Stabilization System	3-5
4-1	Model for Actuator Systems	4-2
4-2	Pump Control System Schematic	4-2
4-3	Hardware Selection Results for Elevation Axis	4-7
4-4	Servo valve Conversion Diagram	4-7
4-5	Time History Plot for Elevation Angle, Rate, and Gas Volume	4-8
4-6	Hardware Selection Results for Azimuth Axis	4-8
4-7	Accumulator Sizing Effects Diagram	4-10
4-8	Azimuth Rotation Requirements Plot	4-10
4-9	Time History Plot for Azimuth Angle, Rate, and Gas Volume	4-11
4-10	Curves of Constant Products of Transmission Ratio and Motor Displacement for Azimuth and Elevation Axes	4-11
5-1	Block Diagram of Linearized Rate Control System	5-2
5-2	Block Diagram of Linearized Position Control System	5-6
5-3	Linear System Step Response	5-12
5-4	Linear System Frequency Response	5-12
5-5	Simplified Block Diagram of the Rate Command System	5-13
5-6	Simplified Block Diagram of the Rate Control System with Two Rate Sensors	5-15
5-7	Simplified Block Diagram of the Rate Control System with a Single Acceleration Sensor	5-16

<u>Figure No.</u>	<u>Title</u>	<u>Page</u>
5-8	Method of Eliminating the Effects of Integrator Drift and Sensor Offsets	5-18
5-9	Block Diagram for Effect of Rate Sensor Dynamics on Response	5-20
5-10	Simplified Block Diagram of System with Feedback Compensation	5-20
5-11	Simplified Block Diagram of System with Compensation in Forward Path	5-20
5-12	Dynamic Stiffness Curve	5-23
5-13	Schematic for Coupling of Hull Pitch Rate to Gun	5-25
6-1	Frequency Response - Position Control	6-4
6-2	Frequency Response - Position Control and Rate Control	6-4
6-3	Response to a Command Step Input - Elevation Rate Control with Electric Gyros	6-7
6-4	Response to Sinusoidal Pitch Rate - Elevation Rate Control with Electric Gyros	6-9
6-5	Closed Loop Frequency Response Curves - Elevation Rate Control with Electric Gyros	6-9
6-6	Response to HITPRO Simulated Bump Course - Elevation Rate Control with Electric Gyros	6-11
6-7	Response to HITPRO Bump Course with Hull Sensor Gain Error - Elevation Rate Control with Electric Gyros	6-11
6-8	Response to HITPRO Bump Course with Coulomb and Stiction Friction - Elevation Rate Control with Electric Gyros	6-12
6-9	Graph of Tracking Error Versus Hull Sensor Gain Error - Elevation Rate Control with Electric Gyros	6-12
6-10	Graph of Tracking Error Versus Friction - Elevation Rate Control with Electric Gyros	6-13
6-11	Dynamic Stiffness - Elevation Rate Control with Electric Gyros	6-13
6-12	Response to a Step Rate Command - Hydraulic Rate Sensor	6-15
6-13	Response to Sinusoidal Hull Motion - Hydraulic Rate Sensor	6-15
6-14	Frequency Response - Hydraulic Rate Sensors	6-16
6-15	Response to HITPRO Simulated Bump Course - Hydraulic Rate Sensor	6-16
6-16	Response to HITPRO Bump Course with Coulomb and Stiction Friction - Hydraulic Rate Sensor	6-17
6-17	Response to HITPRO Bump Course with Coulomb and Stiction Friction - Hydraulic Rate Sensor	6-17
6-18	Graph of Tracking Error Versus Hull Sensor Gain Error - Hydraulic Rate Sensor	6-18

<u>Figure No.</u>	<u>Title</u>	<u>Page</u>
6-19	Tracking Error Versus Sensor Deadband - Hydraulic Rate Sensor	6-18
6-20	Effects of Combined Hull Sensor Deadband and Friction - Hydraulic Rate Sensor	6-19
6-21	Response to a Step Rate Command - Integrating Accelerometer	6-20
6-22	Response to Sinusoidal Hull Motion - Integrating Accelerometer	6-20
6-23	Response to HITPRO Bump Course - Integrating Accelerometer	6-21
6-24	Response to HITPRO Bump Course with Coulomb and Stiction Friction - Elevation Rate Control with Integrating Accelerometer	6-21
6-25	Maximum Tracking Error Versus Friction - Integrating Accelerometer	6-23
6-26	Frequency Response - Integrating Accelerometer	6-23
6-27	Response to a Step Rate Command - Laminar Vortex Sensor	6-24
6-28	Response to HITPRO Bump Course - Laminar Vortex Sensor	6-25
6-29	Response to HITPRO Bump Course with Hull Sensor Gain Error - Laminar Vortex Sensor	6-25
6-30	Tracking Error Versus Hull Sensor Gain - Laminar Vortex Sensor	6-26
6-31	Frequency Response - Laminar Vortex Sensor	6-26
6-32	Step Response - Azimuth Rate Control with Electric Gyros	6-28
6-33	Response to Sinusoidal Hull Motion - Azimuth Rate Control with Electric Gyros	6-28
6-34	Response to HITPRO Bump Course - Azimuth Rate Control with Electric Gyros	6-29
6-35	Response to HITPRO Bump Course with Hull Sensor Gain Error - Azimuth Rate Control with Electric Gyros	6-29
6-36	Tracking Error Versus Hull Sensor Gain Error - Azimuth Rate Control with Electric Gyros	6-30
6-37	Response to HITPRO Bump Course with 2 ms Sensor Deadband - Azimuth Rate Control with Electric Gyros	6-31
6-38	Response to HITPRO Bump Course with 6 ms Sensor Deadband	6-31
6-39	Effects of Deadband and Friction on Tracking Error - Azimuth Rate Control with Electric Gyros	6-32
6-40	Frequency Response - Azimuth Rate Control with Electric Gyros	6-32

<u>Figure No.</u>	<u>Title</u>	<u>Page</u>
6-41	Response to Pivot Steer Maneuver - Azimuth Rate Control with Electric Gyros	6-33
6-42	Step Response - Pneumatic Accelerometer	6-34
6-43	Response to Sinusoidal Hull Motion - Pneumatic Accelerometer	6-34
6-44	Response to HITPRO Bump Course - Pneumatic Accelerometer	6-35
6-45	Response to HITPRO Bump Course with Coulomb and Stiction Friction - Pneumatic Accelerometer	6-35
6-46	Maximum Tracking Error Versus Friction - Pneumatic Accelerometer	
6-47	Frequency Response - Pneumatic Accelerometer	

LIST OF TABLES

<u>Table No.</u>	<u>Title</u>	<u>Page</u>
2-1	Elevation Vehicle Parameters	2-3
2-2	Azimuth Vehicle Parameters	2-4
2-3	Hardware Parameters	2-10
4-1	Parameters for Hardware Selection Study	4-6
6-1	Results of the Sensor Evaluation Study	6-38

LIST OF SYMBOLS AND ABBREVIATIONS

<u>Symbol</u>	<u>Definition</u>	<u>Units</u>
A_p	Piston area	cm^2
A_v	Servo valve flow area	cm^2
A_{v0}	Effective servo valve flow area	cm^2
$A_{v \max}$	Maximum servo valve flow area	cm^2
a_1, a_2, a_3, a_4	Dummy constants in stiffness transfer function	--
B	Bulk modulus	kg/cm^2
C	Flow coefficient	$\text{cm} / (\text{s} - \sqrt{\text{kg}/\text{cm}^2})$
C_h	Hull suspension constant	$\text{kg-m}/\text{rad}$
D_a	Denominator of the actuator and gun transfer function	--
D_c	Coulomb friction coefficient	kg-m
D_g	Denominator of gyro transfer function	--
D_{gh}	Gun trunnion friction coefficient	kg-m
D_m	Motor displacement	cm^3/rad
D_s	Stiction friction coefficient	kg-m
D_{sa}	Hull suspension damping-azimuth	kg-m-s
D_{se}	Hull suspension damping-elevation	kg-m-s
D_{th}	Turret friction coefficient	kg-m-s
D_v	Viscous friction coefficient	kg-m-s
G_A	Servo valve transfer function	--

<u>Symbol</u>	<u>Definition</u>	<u>Units</u>
G_c	Cubic denominator of linearized system transfer function	-
G_p	Pressure feedback transfer function	-
G_1	Controller transfer function	-
G_2	Actuator transfer function	-
H_x	Angular momentum about x-axis	-
J_g	Gun inertia	kg-m-s^2
J_{gx}	Gun inertia about the roll axis	kg-m-s^2
J_{gy}	Gun inertia about the yaw axis	kg-m-s^2
J_{ha}	Hull inertia-azimuth	kg-m-s^2
J_{he}	Hull inertia-elevation	kg-m-s^2
J_m	Motor inertia	kg-m-s^2
J_t	Turret inertia	kg-m-s^2
J_{tx}	Turret inertia about the roll axis	kg-m-s^2
J_{tz}	Turret inertia about the pitch axis	kg-m-s^2
J_x	Inertia about x axis	kg-m-s^2
K	Gain of nulling network	-
k_a	Servo valve gain	$\text{cm}^2/(\text{rad/s})$
K_{bg}	Gun sensor gain	-
K_{bh}	Hull sensor gain	-
K_h	Control gain of hull rate cancellation term	-
K_i	Integral controller gain	1/s
K_o	Static stiffness	kg-m/rad
K_p	Pressure feedback gain	$\text{rad}(\text{s-kg/cm}^2)$

<u>Symbol</u>	<u>Definition</u>	<u>Units</u>
K_r	Proportional controller gain	-
K_s	Open loop system gain	-
K_{sa}	Hull suspension spring constant-azimuth	kg-m/rad
K_{se}	Hull suspension spring constant-elevation	kg-m/rad
k	Ratio of specific heats	-
L	Leakage coefficient	$\text{cm}^3/(\text{s}-\text{kg}/\text{cm}^2)$
$L_s M_s$	Gun mass unbalance	-
$L_t M_t$	Turret mass unbalance	-
l	Lever arm of piston actuator	cm
N_c	Numerator of feedback compensation transfer function	-
P_f	Output of pressure feedback network	rad/s
P_m	Motor differential pressure	kg/cm^2
P_o	Effective motor pressure	kg/cm^2
P_s	Supply pressure	kg/cm^2
P_{so}	Initial supply pressure	kg/cm^2
Q_l	Leakage flow	cm^3/s
Q_m	Motor flow	cm^3/s
Q_o	Dummy variable used in linear analysis	-
Q_p	Pump flow	cm^3/s
Q_v	Servo valve flow	cm^3/s
R	Transmission ratio	-

<u>Symbol</u>	<u>Definition</u>	<u>Units</u>
R_h, R_p	Distance between the hull centers of rotation and the trunnion	cm
s	Laplace operator	s
T_A	Actuator torque	kg-m
T_c	Coulomb friction	kg-m
T_d	Disturbance torque	kg-m
T_E	Tracking error	rad
T_f	Total friction	kg-m
T_{fg}	Trunnion friction torque	kg-m
T_{gc}	Gun gyroscopic torque	kg-m
T_{gf}	Gun firing torque	kg-m
T_{g1}	Coupling torque due to turret angle	kg-m
T_{g2}	Coupling torque due to hull acceleration	kg-m
T_s	Stiction friction	kg-m
T_t	Coupling torque due to mass unbalance	kg-m
T_{tc}	Turret gyroscopic torque	kg-m
T_v	Viscous friction	kg-m
T_z	Gyroscopic torque about z axis	kg-m
V	Actuator volume	cm ³
V_a	Accumulator gas volume	cm ³
V_o	Steady state gas volume in accumulator	cm ³
$Y(s)$	Sensor transfer function	-

<u>Symbol</u>	<u>Definition</u>	<u>Units</u>
α, β	Dummy variables used in linear analysis	-
e	Controller error	rad/s
e_d	Integrator drift	rad/s
e_h	Hull sensor offset error	rad/s
e_g	Gun sensor offset error	rad/s
e_s	Input to system open loop transfer function	rad/s
e_t	Sensed tracking error	mils
ζ	Sensor damping ratio	-
ΔA_v	Change in servovalve area	cm ² /s
ΔP_m	Change in motor pressure	(kg/cm ²)/s
ΔT	Breakaway torque in friction model	kg-m
$\dot{\theta}$	Threshold speed in friction model	rad/s
$\Delta \theta_g$	Change in gun angle	rad
$\Delta \theta_h$	Change in hull angle	rad
θ_g	Gun angle	rad
$\dot{\theta}_{gs}$	Gun sensor output	rad/s
θ_h	Hull pitch angle	rad
$\dot{\theta}_{hs}$	Hull sensor output	rad/s
$\dot{\theta}_{ht}$	Terrain pitch rate	rad/s
$\dot{\theta}_{hv}$	Relative hull pitch rate	rad/s
θ_s	Position command	rad
$\dot{\theta}_s$	Rate command	rad/s
τ_1, τ_2	Time constants in forward compensation network	s

<u>Symbol</u>	<u>Definition</u>	<u>Units</u>
τ_3, τ_4	Time constants in feedback compensation network	s
τ_a	Integrator gain in the integrating accelerometer rate computation network	s
τ_b	Time constant of the integrating accelerometer transfer function	s
τ_c	Compressibility time constant	s
τ_d	Time delay of laminar vortex sensor	s
τ_f	Stiction friction time constant	s
τ_i	Time constant of the pseudo-differentiator in the input compensation network	s
τ_n	Time constant of servovalve dynamics	s
τ_p	Pressure feedback time constant	s
τ_s	Time constant of laminar vortex sensor	s
ψ_h	Hull roll angle	rad
$\dot{\psi}_{ht}$	Terrain yaw rate	rad/s
$\dot{\psi}_{hv}$	Relative hull yaw rate	rad/s
ψ_t	Turret angle	rad
ω_b	Bandwidth of integrating accelerometer	rad/s
ω_n	Natural frequency of sensor	rad/s
ω_{NS}	Dummy variable used in linear analysis	—
ω_x, ω_y	Angular rates about x and y axes, respectively	rad/s

<u>Symbol</u>	<u>Definition</u>	<u>Units</u>
$\frac{\partial T}{\partial n}$	Slope of torque-speed curve	kg-m-s
$\frac{\partial T}{\partial e}$	Slope of torque-error signal curve	kg-m/rad

ABBREVIATIONS

cc	cubic centimeter
cm	centimeter
gpm	gallons per minute
Hz	Hertz
in	inch(es)
kg-m	kilogram-meter
kg/cm ²	kilogram/square centimeter
mil	milliradian
p-p	peak to peak
psi	pounds/square inch
rad	radian(s)
s	second(s)

SECTION 1
INTRODUCTION AND SUMMARY

1.1 INTRODUCTION

The "Closed-Loop Optimization Program for the M60A1 Tank Gun Stabilization System" study project was undertaken by the Bendix Research Laboratories under Contract DAAA09-74-C-2068 for the Rock Island Arsenal. The objective was to develop a gun stabilization system in which performance and reliability are optimized. It had been concluded prior to the initiation of this contract that fluidic approaches appeared attractive from the reliability and cost standpoint. The purpose of this contract is to provide the Contracting Officers with conclusive evidence and recommendations regarding the applicability of the fluidic approach to tank weapons systems, while supplying a mathematical model of the entire vehicle/control system. In order to provide this information, fluidic devices were to be considered without forcing incorporation of a particular existing fluidic device.

The results of Phase I, discussed in this report, consist of a requirement analysis, a model definition, and a system stability and performance analysis. A detailed performance study of the different applicable sensors consisting of electronic rate gyros, a hydraulic rate sensor, an integrating accelerometer, a laminar vortex sensor, and a pneumatic accelerometer were also included for future trade studies. A complete error analysis for two of the sensors is recommended in order to augment a decision on the applicability of fluidic approaches in this area.

Control system design was performed in accordance with specifications which call for a pointing accuracy of 1/2 mil rms diameter circle without a gunner operating the controls. A 3 dB bandwidth of at least 15 Hz is also desired. It is required that the system hardware be out of saturation 98 to 99 percent of the time. The duration of an engagement was specified to be 15 to 20 s.

1.2 SCOPE

For the purpose of deriving a realistic mathematical model of the stabilization system, a study was made of existing literature on the M60A1 tank, and of previous system studies on the vehicle. Upon simplifying models of the vehicle in the literature, where appropriate, and independently developing realistic models of the servovalve, actuators and sensors, a complete control system model was derived. Selection of the appropriate actuator system hardware to be used was carried out in close cooperation with the Contracting Officer's Representatives. Models were defined separately for the azimuth (turret) and elevation

(gun) axes. In addition to the vehicle and gun models, the mathematical model included the controller and compensation, the effects of nonlinear valve flow, and static, coulomb, and viscous friction effects. The effect of hull dynamics on the system was also evaluated. A mathematical model of coupling between axes due to roll motion was investigated analytically with respect to the approximate effects on system performance and pointing accuracy. Control laws were derived analytically in accordance with the performance specifications set forth prior to the start of the contract. A control law was specified for both rate and position command input concepts.

From the model definition, an analog computer program was defined and programmed for each control concept. Diagrams and descriptions of all programs used in this study are contained in Appendices A and B. The Rock Island Arsenal digital program "HITPRO" was adapted to the Bendix Research Laboratories computer, and the analog programs were, at that point, modified to hybrid programs in order to accept inputs from HITPRO. These inputs consisted of vehicle rates corresponding to those experienced by an M60 tank while traversing the Aberdeen Proving Ground terrain. Additional hybrid functions of these programs consisted of a time delay property of the laminar vortex sensor.

Prior to a complete hybrid computer analysis of the system, an analytical systems study was conducted in order to develop a fuller comprehension of the overall system behavior. The study also aided in the development of digital check solutions for all of the hybrid computer analyses. In addition, the analytical study includes a sensor error analysis and an evaluation of coupling of axes on pointing errors.

The hybrid computer simulation results consist of an evaluation of the effects of nonlinear valve flow and hull dynamics, a comparison of the rate and position control concepts, and a detailed evaluation of each of the five sensors studied. The electric rate gyros, as they are presently used in the field, were evaluated in both the elevation and azimuth axes. The hydraulic rate sensor, the integrating accelerometer, and the laminar vortex sensor were evaluated in the elevation axis, and the pneumatic accelerometer was evaluated in the azimuth axis.

The conclusions reached on the basis of the computer analysis are contained in Section 7. Recommendations as to future studies and stabilization approaches are contained in Section 8.

1.3 SUMMARY

A mathematical model of a suitable stabilization system for the M60A1 tank main gun was formulated and programmed. The model was formulated so as to include most of the significant nonlinearities such as nonlinear valve flow and hull dynamics due to gun motion. A hybrid computer analysis was performed to determine the operating characteristics of the stabilization system, to evaluate prospective sensors for sensing gun and/or hull rate, and to determine whether a rate or a

position command control concept is preferable with respect to specified performance criteria.

The analytical study revealed that both the rate and the position control concepts required a proportional plus integral control law in order to minimize the gun tracking error. It was also shown that the rate and the position concepts are equivalent in terms of nulling out the effects of hull motions, and thus in terms of stabilizing the gun after the target is in the sight. A computer analysis which followed verified this equivalence. In addition, it was possible to show that the effect of hull motions on the system can be minimized by either a high control loop gain along with a lead-lag compensation network or by using a hull sensor signal in the control law.

The extensive computer simulation analysis revealed several significant conclusions in the areas of stabilization control philosophy and sensor applicability. In the process of arriving at a full computer model of the system for sensor evaluation, it was found that the effect of hull dynamics on the gun was negligible. Nonlinear valve flow, however, was found to have a significant influence on system performance. A linearized flow model was not sufficiently accurate for use in this study.

It was found that all five of the sensors studied meet the performance criteria set forth by the Contracting Officer's Representative. In addition, this study indicates that these criteria can be met by using only a gun sensor. If verified by further studies, the need for a corresponding hull sensor may be eliminated.

The detailed sensor study revealed that automatic offset and integrator drift nulling circuits are required when using an acceleration sensor. A method which can be used for this purpose is described in Section 5.5. In addition, it was determined that increasing the gain of the acceleration sensor will decrease the sensor offset effects and, hence, the drift rate. More generally, in the sensor study it was found that sensor gain errors have a small effect on the tracking error. Also, a combination of sensor deadband and gun or turret friction will cause the system to limit cycle.

In order to compensate for sensor phase lag, feedback compensation was found to be required. Forward path compensation is desirable for obtaining stability with higher loop gains for this system.

SECTION 2
MATHEMATICAL MODEL DESCRIPTION

2.1 GENERAL

This section contains the mathematical model of the gun stabilization system as programmed on the hybrid computer. This model consists of the vehicle model, servovalve and motor, sensor models, and the controller. The azimuth and elevation systems are presented separately. The effects of coupling are not included. The individual system components are described in Sections 2.2 through 2.4. Also presented are the controller models for the following configurations:

- (1) Rate control with two rate sensors
- (2) Rate control with one acceleration sensor in gun axis
- (3) Position control with two rate sensors
- (4) Position control with one acceleration sensor in gun axis

A simplified block diagram of a rate control system with two rate sensors is shown in Figure 2-1.

2.2 VEHICLE MODELS

The vehicle models consist of an elevation (gun) axis model and an azimuth (turret) axis model. They include, respectively, the gun and turret inertias, effects of friction, and hull suspension effects.

2.2.1 Elevation Axis Vehicle Model

The elevation axis vehicle model shown in Figure 2-2 consists of the combined gun and hull dynamics. For the gun dynamics, the torque applied to the gun equals the actuator torque T_A , plus the disturbance torque T_d acting on the gun, minus the trunnion friction torque T_{fg} . It follows that the gun angular acceleration with respect to inertial space is given by:

$$\ddot{\theta}_g = \frac{1}{J_g} (T_A + T_d - T_{fg})$$

The friction model is discussed in Section 2.2.3. The disturbance torque T_d is generated, for example, by a gun firing. The hull dynamics generate a hull angular acceleration θ_{hv} with respect to the tracks. This

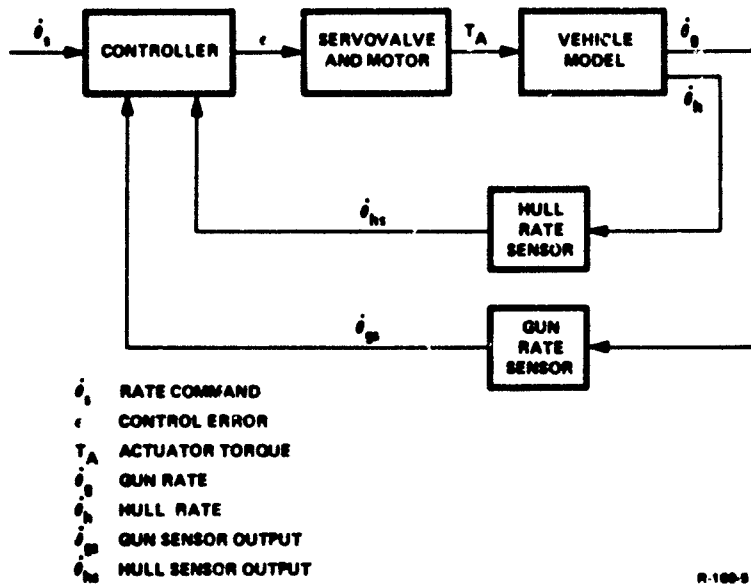


Figure 2-1. Simplified Block Diagram of the Rate Command Stabilization System

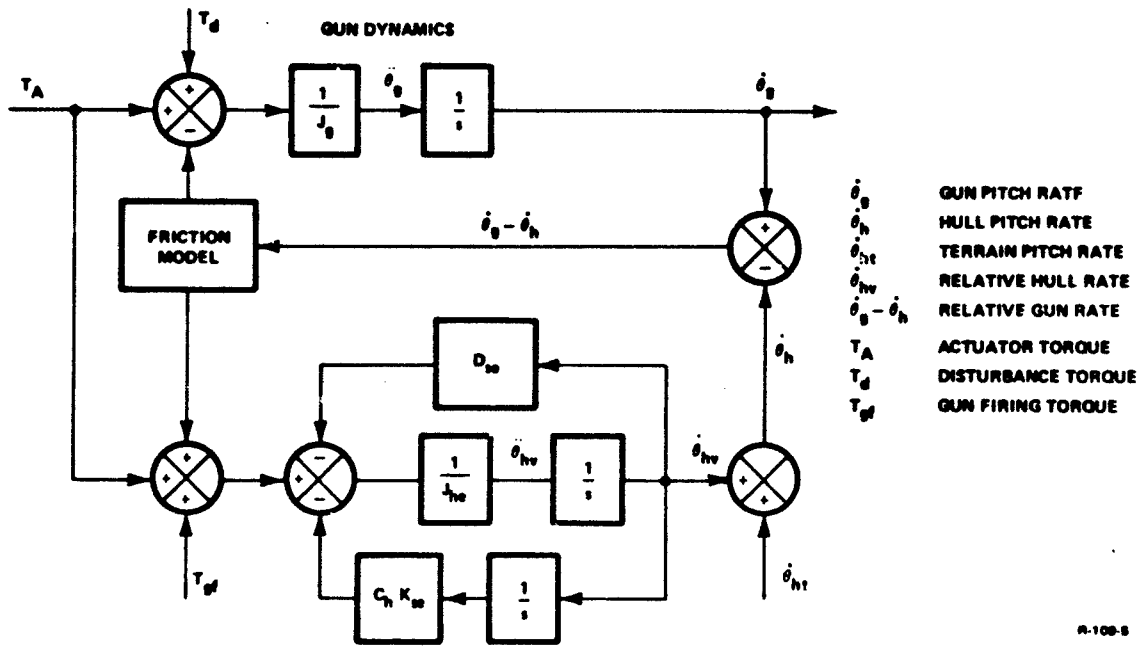


Figure 2-2. Elevation Axis Vehicle Model

acceleration results from the reaction of the actuator torque and the gun firing torque T_{gf} . The acceleration is given by:

$$\ddot{\theta}_{hv} = \frac{1}{J_{he}} [T_A + T_{gf} - D_{se} \dot{\theta}_{hv} - (K_{se} + C_h) \theta_{hv}]$$

where the last two terms represent the hull suspension.

The terrain pitch rate $\dot{\theta}_{ht}$ added to the relative hull rate $\dot{\theta}_{hv}$ gives the total hull pitch rate $\dot{\theta}_h$ as shown below.

$$\dot{\theta}_h = \dot{\theta}_{hv} + \dot{\theta}_{ht}$$

The angular rate of the gun with respect to the hull (relative gun rate) is given by:

$$(\dot{\theta}_g - \dot{\theta}_h).$$

A list of the vehicle elevation parameters is contained in Table 2-1.

Table 2-1. Elevation Vehicle Parameters

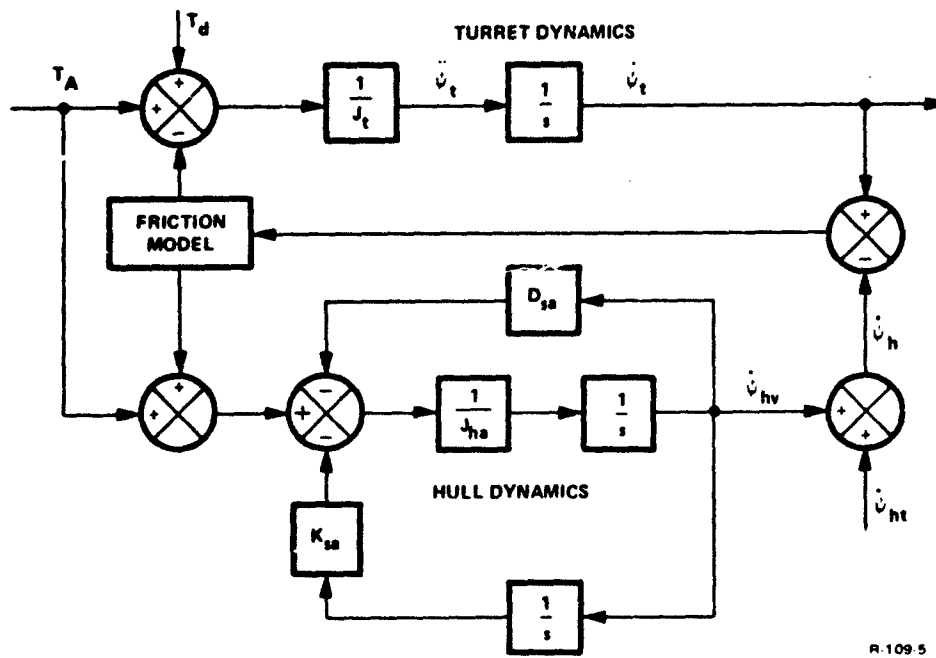
Parameter	Value	Units
D_{se}	7.8×10^4	kg-m-s
D_{gh}	166	kg-m-s
J_g	527	kg-m-s ²
J_{he}	1.73×10^4	kg-m-s ²
K_{se}	9.85×10^6	kg-m/rad
C_h	40,500	kg-m/rad
τ_f	0.01	s

2.2.2 Azimuth Axis Vehicle Model

The azimuth axis vehicle model, shown in Figure 2-3, is the same as the elevation model, except for the values of the moments of inertia and friction. Angular position is denoted by ψ rather than θ , as in the elevation model. A list of the vehicle azimuth parameters is contained in Table 2-2.

Table 2-2. Azimuth Vehicle Parameters

Parameter	Value	Units
D_{sa}	8.3×10^4	kg-m-s
D_{th}	7.75	kg-m-s
J_t	3140	kg-m-s ²
J_{ha}	1.84×10^4	kg-m-s ²
K_{sa}	9.4×10^6	kg-m/rad



R-109.5

Figure 2-3. Azimuth Axis Vehicle Model

2.2.3 Friction

Three types of friction, viscous, coulomb, and stiction, are considered here. Actuators generally have significant quantities of all three types. In addition, the turret and the gun trunnion may have one or more of the friction types. The three types of friction are described below.

Viscous Friction

Viscous friction is proportional to the speed of the gun relative to the hull.

$$T_v = D_v (\dot{\theta}_g - \dot{\theta}_h) \quad (2-1)$$

Coulomb Friction

Coulomb friction is constant in magnitude. The sign, or direction, changes when the direction of motor rotation changes.

$$T_c = D_c \text{sign} (\dot{\theta}_g - \dot{\theta}_h) \quad (2-2)$$

Stiction Friction

Stiction occurs each time the motor starts or reverses direction. It rapidly decays to zero. The sign changes when the direction of rotation reverses. Stiction friction is modeled by the following equation:

$$T_s = D_s \frac{\tau_f s}{1 + \tau_f s} \text{sign} (\dot{\theta}_g - \dot{\theta}_h) \quad (2-3)$$

Total friction is the sum of the three types of friction for both axes:

$$T_f = T_v + T_c + T_s \quad (2-4)$$

When compliance is added to the model, the actuator and trunnion frictions have different equations. When compliance is not used, the equations are the same, and the actuator and trunnion friction can be combined as is done here. The friction values given in equations (2-1) through (2-4) are the combined friction of the actuator and

trunnion, for elevation. For the azimuth axis, equation (2-4) represents the combined friction of the actuator and the turret.

The block diagram used for simulating friction is shown in Figure 2-4.

An ideal circuit for friction simulation is shown in Figure 2-5. In this diagram, the breakaway torque ΔT is the minimum actuator torque that will result in actuator movement. When the magnitude of T_A is less than ΔT and the gun is at rest, the friction torque exactly equals the actuator torque. At this point, no torque is applied to the gun. For this region of operation, the friction is called static friction.

$$T_f = T_A \quad (T_f = \text{static friction})$$

When the actuator torque exceeds the breakaway torque, the circuit switches to running friction, and T_f is given by equation (2-4). A torque is then applied to the gun, and gun motion starts. As long as the gun speed exceeds the threshold value $\Delta \theta$, the circuit stays in the running friction mode regardless of the value of T_A . The parameters in the friction model must be adjusted so that at the instant of switching from static to running friction, the two friction values are equal.

2.3 SERVOVALVE AND MOTOR MODELS

The servovalve and motor for both the elevation and azimuth systems are modeled as shown in Figure 2-6. This model includes a pressure feedback servovalve with nonlinear flow dynamics. The voltage applied to the servovalve is the sum of ϵ and P_f . The quantity ϵ is the output of the control law as described in Section 3. The quantity P_f is the output of the pressure feedback network. The servovalve dynamics G_a are represented by a first order lag, i.e.,

$$G_a = \frac{1}{\tau_n s + 1}$$

The servovalve gain is K_a . In the simulation, the deadband was assumed zero while the valve area A_v was limited to $A_v \text{ max}$. The servovalve flow rate Q_v is given by:

$$Q_v = C A_v \sqrt{\frac{P_s - P_m}{2}}, \quad \text{for } A_v > 0$$

$$Q_v = C A_v \sqrt{\frac{P_s + P_m}{2}}, \quad \text{for } A_v < 0$$

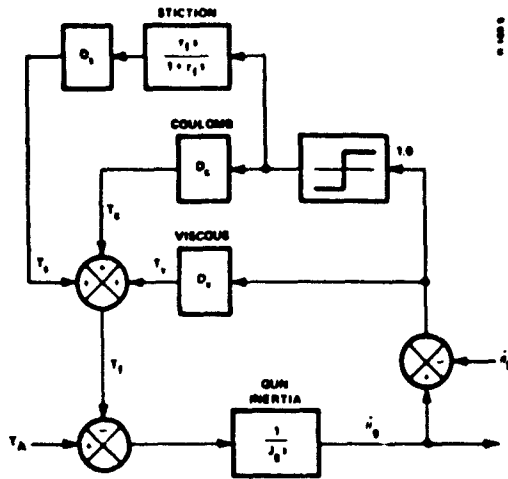


Figure 2-4. Block Diagram for Simulating Friction

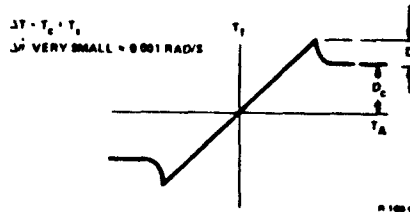
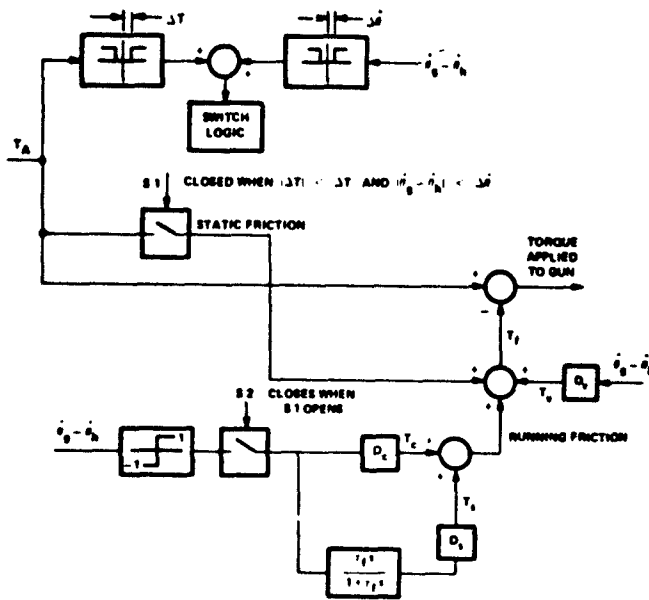


Figure 2-5. Idealized Block Diagram for Simulating Friction

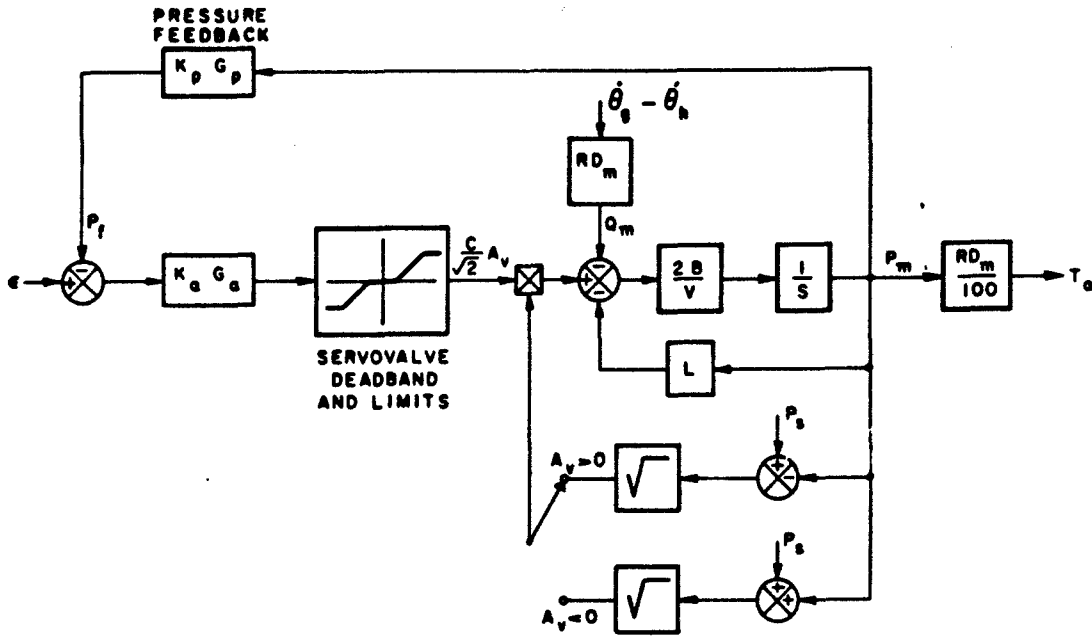


Figure 2-6. Servovalve and Motor Simulation Block Diagram

where

C = flow coefficient

P_s = supply pressure

P_m = motor pressure

The rate of change of motor pressure P_m is given by:

$$\dot{P}_m = \frac{2B}{V} (Q_v - Q_m - Q_l)$$

where

B = bulk modulus

V = volume

Q_m = displacement flow rate, i.e.

$$Q_m = RD_m (\dot{\theta}_g - \dot{\theta}_h)$$

and where RD_m is the motor displacement reflected to the gun. For a piston actuator, RD_m is replaced by lA_p . The model is otherwise unchanged. Leakage flow Q_l is assumed proportional to the motor pressure and is thus given by:

$$Q_l = L P_m$$

The resultant actuator torque T_A is then given by:

$$T_A = \frac{RD_m}{100} P_m$$

The dynamic pressure feedback network $K_p G_p$ is utilized for stabilizing and improving the servovalve/motor response. The compensator G_p is used to wash out the pressure feedback at low frequency or at steady state. Pressure feedback without the washout would reduce the static stiffness. The function G_p can either be provided by a servovalve designed to have dynamic pressure feedback, or by an electrical network. For each axis, the gain K_p is a system parameter that was varied to obtain the desired system response. The pressure feedback transfer function is given by:

$$K_p G_p = K_p \frac{\tau_p s}{1 + \tau_p s}$$

Table 2-3 contains the parameters of the servovalve and motor for both the elevation and azimuth systems.

Table 2-3. Hardware Parameters

Parameter	Value	Units
B	10,550	kg/cm ²
C	955	cm/s√kg/cm ²
D _c	Variable	kg-m
D _s	Variable	kg-m
D _v	Variable	kg-m-s
J _m	Negligible	kg-m-s ²
L	0.116	cm/s-kg/cm ²
P _s	210 (nominal)	kg/cm ²
τ _p	0.07	s
K _a	1	cm ² /(rad/s)
τ _n	0.008	s
<u>Elevation</u>		
A _{v max}	0.22	cm ²
RD _m	2970 (initial studies)	cm ³ /rad
	1311 (optimum value)	cm ³ /rad
V	855	cm ³
<u>Azimuth</u>		
A _{v max}	0.45	cm ²
RD _m	1639	cm ³ /rad
V	492	cm ³
<u>Linear Model</u>		
∂T/∂n	2.08 x 10 ⁴	kg-m-s
∂T/∂ε	6.25 x 10 ⁴	kg-m/rad
τ _c	0.016	s

2.4 SENSOR MODEL DESCRIPTIONS

2.4.1 General

A set of five different sensors was selected by the Contracting Officers for study. All five sensors were likely candidates for this application, and it was desired to establish the performance characteristics of each sensor on a relative and absolute basis, in an appropriate realistic environment. Properties of the electric rate gyros, the General Electric hydraulic rate sensors, and the Honeywell laminar vortex sensor were provided to Bendix by the Contracting Officers. The model of the Airsearch pneumatic accelerometer was provided directly to Bendix by Airsearch. The model of the Bendix integrating accelerometer was obtained from Bendix personnel. For each of the three rate sensors, a configuration was used in which a sensor was placed at the gun and in the hull. For the two accelerometers, a sensor was placed only at the gun.

The models for the sensors are presented in terms of transfer functions. All sensor models have provisions for adding threshold and varying the sensor gains. All nominal sensor gains were considered unity. The sensor gain has no effect on response to command inputs or terrain disturbances. Gain distribution does, however, affect the response to noise, and drift due to offsets. Noise and drift were not studied in detail in this phase. When these effects are studied, the actual sensor gains must be used.

2.4.2 Electric Rate Gyro Model

The electric rate gyros which measure the angular gun rate and hull rate can be represented by a second order transfer function as given by:

$$\dot{\theta}_{gs} = \frac{1}{1 + \frac{2\zeta}{\omega_n} s + \frac{1}{\omega_n^2} s^2} \dot{\theta}_g$$

$$\dot{\theta}_{hs} = \frac{1}{1 + \frac{2\zeta}{\omega_n} s + \frac{1}{\omega_n^2} s^2} \dot{\theta}_h$$

where

$$\omega_n = 157 \text{ rad/s}$$

$$\zeta = 0.7$$

2.4.3 Hydraulic Rate Sensor Model

The hydraulic rate sensor utilized in this study is manufactured by the General Electric Corporation. The dynamics of this sensor can be represented by a second order transfer function as follows:

$$\dot{\theta}_{gs} = \frac{1}{1 + \frac{2\zeta}{\omega_n} s + \frac{1}{\omega_n^2} s^2} \dot{\theta}_g$$

$$\dot{\theta}_{hs} = \frac{1}{1 + \frac{2\zeta}{\omega_n} s + \frac{1}{\omega_n^2} s^2} \dot{\theta}_h$$

where

$$\zeta = 0.707$$

and

$$\omega_n = 40 \times 2\pi \text{ rad/s}$$

The following are additional characteristics of this sensor:

Scale factor: 0.13 psi/deg/s

Mass unbalance drift: 2 deg/s/g at 1800 psi

Noise: 0.6 deg/s (peak to peak)

Supply pressure drift: 0.3 deg/s/percent change in supply pressure

Scale factor drift: 0.8 percent/percent change in supply pressure

2.4.4 Hydraulic Integrating Accelerometer Model

The hydraulic integrating accelerometer produced by Bendix measures the gun acceleration $\ddot{\theta}_g$. Its transfer function is given by:

$$\ddot{\theta}_{gs} = \frac{\tau_b}{1 + \tau_b s} \ddot{\theta}_g$$

where

$$\tau_b = \frac{1}{\omega_b}$$

and

$$\omega_b = 2\pi \times 0.1 \text{ rad/s}$$

The sensed acceleration is converted to a rate signal $\dot{\theta}'_g$ by the rate computation network shown below.

$$\dot{\theta}'_{gs} = \left(1 + \frac{1}{\tau_a s} \right) \ddot{\theta}_g$$

where τ_a is set equal to τ_b which is the time constant of the integrating accelerometer.

If the sensor break frequency varies due to temperature changes or other factors, the sensed rate signal becomes

$$\dot{\theta}'_{gs} = \frac{\tau_b s}{1 + \tau_b s} \left(1 + \frac{1}{\tau_a s} \right) \ddot{\theta}_g = \frac{\tau_b}{\tau_a} \left(\frac{1 + \tau_a s}{1 + \tau_b s} \right) \ddot{\theta}_g$$

Above the break frequency, the signal is not affected by the change in break frequency. At lower frequencies, there is a gain change proportional to the change in break frequency.

2.4.5 Laminar Vortex Rate Sensor Model

The transfer function for the laminar vortex sensor produced by Honeywell is a first order lag with transport delay, i.e.,

$$\dot{\theta}_{gs} = \frac{e^{-\tau_d s}}{1 + \tau_s s} \dot{\theta}_g$$

$$\dot{\theta}_{hs} = \frac{e^{-\tau_d s}}{1 + \tau_s s} \dot{\theta}_h$$

where

$$\tau_d = 0.01 \text{ s (transport delay)}$$

$$\tau_g = 0.002 \text{ s (time constant)}$$

2.4.6 Pneumatic Accelerometer Model

The basic pneumatic accelerometer produced by Garrett Airsearch has a second order transfer function, with lead-lag compensation, in a closed loop configuration. The block diagram of the sensor is shown in Figure 2-7 where

$$\omega_n = 14.8 \text{ rad/s}$$

$$\zeta = 0.6$$

The accelerometer saturates at 0.7 rad/s^2 .

The rate computation network which transforms the sensed acceleration into a rate is a simple integrator.

2.5 CONTROLLER MODELS

The four controller model variations developed for this study are described in this section, and are listed below.

- (1) Rate command with two rate sensors
- (2) Rate command with single acceleration sensor
- (3) Position command with two rate sensors
- (4) Position command with single acceleration sensor

Two of the variations considered are rate command systems where the gunner commands angular rates. One of the rate systems utilizes two rate sensors (gun and hull) while the other utilizes a single acceleration sensor (gun). Two of the models are position control where the gunner commands an angular position. Again, one of these systems utilizes two rate sensors

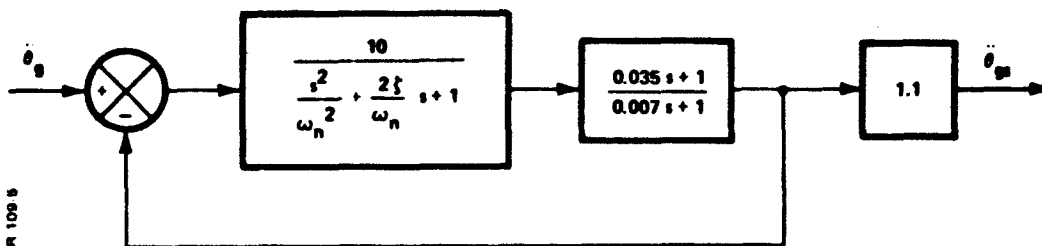
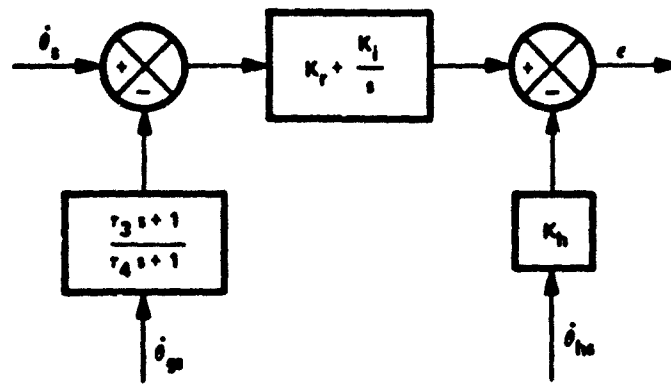


Figure 2-7. Block Diagram of the Pneumatic Accelerometer

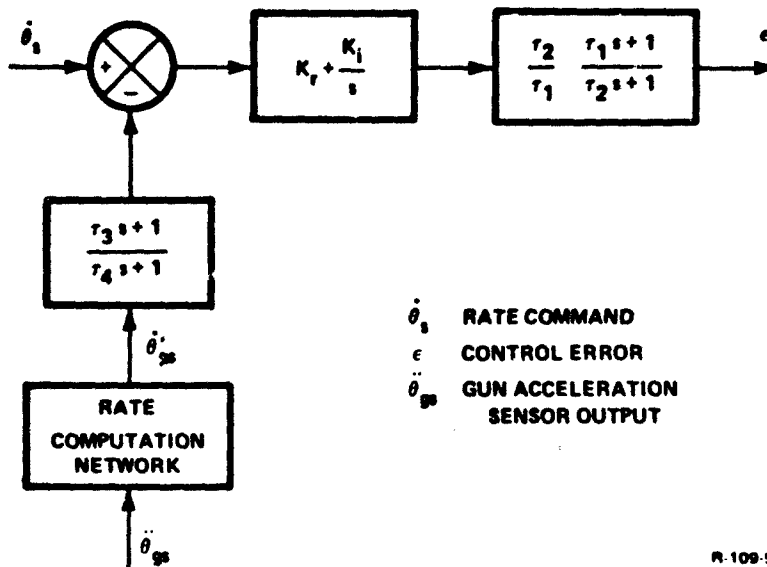
while the other utilizes a single acceleration sensor. Block diagrams of each of these controllers are shown in Figures 2-8 through 2-11. Proportional and integral control is utilized along with compensation networks in the forward and feedback paths and on the input in the position command system. The controller utilizing a single acceleration sensor requires a rate computation network to transform the sensed acceleration into a rate. These rate computation networks are defined with the acceleration sensor models in Section 2.4.4 and 2.4.6.



$\dot{\theta}_s$ RATE COMMAND
 e CONTROL ERROR
 $\dot{\theta}_{gs}$ GUN RATE SENSOR OUTPUT
 $\dot{\theta}_{hs}$ HULL RATE SENSOR OUTPUT

R-109-5

Figure 2-8. Controller for Rate Command with Two Rate Sensors



$\dot{\theta}_s$ RATE COMMAND
 e CONTROL ERROR
 $\ddot{\theta}_{gs}$ GUN ACCELERATION
 SENSOR OUTPUT

R-109-5

Figure 2-9. Controller for Rate Command with Single Acceleration Sensor

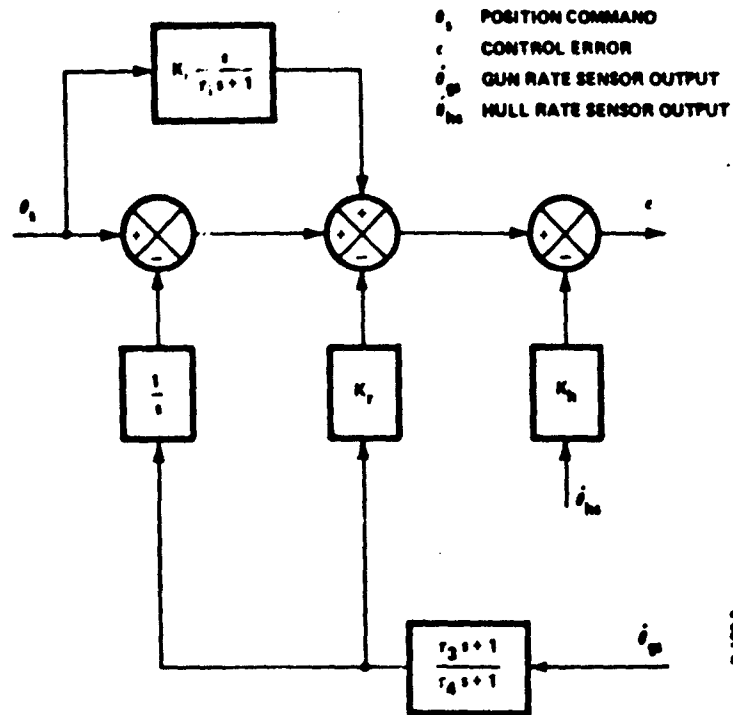


Figure 2-10. Controller for Position Command with Two Rate Sensors

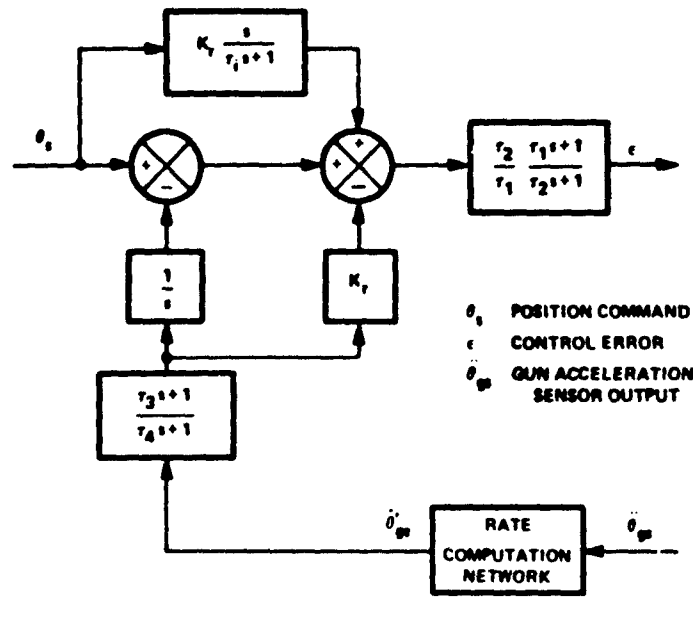


Figure 2-11. Controller for Position Command with Single Acceleration Sensor

SECTION 3
CONTROL SYSTEMS APPROACH

3.1 GENERAL

General requirements of the M60A1 tank gun stabilization system are as follows:

- (1) To rapidly attain a target by means of gunner commands after the target has been sighted by the gunner.
- (2) To keep the gun on target after the gun has been aimed by the gunner in spite of hull motions.

In order to satisfy criterion (1), it is necessary that the response of the system be sufficiently fast so that the time from sighting the target until firing of the first round be minimum. For satisfying criterion (2), it is necessary to minimize the effects of vehicle hull rates on the tracking error of the stabilization system.

Since the design of a control system for a given application is subject to all performance criteria, the criteria for the M60A1 gun stabilization system are described in Section 3.2. Note that these criteria are given in terms of pointing requirements as well as general performance. Hardware acceleration performance criteria are also given.

The control systems approach utilized in this study for achieving the specified performance criteria is described in detail in Sections 3.3.1 and 3.3.2, for the rate and the position command inputs, respectively. It was specified at the start of the program that contemporary conventional control system techniques would be used to achieve the desired performance. If conventional techniques could not achieve the performance goals, more complex optimal procedures would be utilized. At this point in the development of the complete stabilization system, conventional methods of synthesis appear satisfactory.

3.2 PERFORMANCE CRITERIA

The following performance criteria were utilized in the control system design and hardware selection procedure for the stabilization system.

(1) Tracking Error Requirements

The requirement for the tracking error is that it be within a circle of 0.5 mil diameter 67 percent of the time. Data to verify conformance with this requirement will not be obtained in Phase I. Therefore, a goal was set for the tracking error to be 0.5 mil peak to peak or less for the HITPRO bump course at 8 mph.

(2) Frequency Response and Stability Requirements

The frequency response goal was 15 Hz bandpass. Bandpass is defined as the frequency at which the amplitude ratio is -3 dB.

Gain margin and phase margin are two criteria which are frequently used to indicate the system stability. In this study, the following definitions are used to establish stability goals:

- (a) Gain Margin = 1.0 - (open loop amplitude ratio at 180 deg open loop phase lag)
- (b) Phase Margin = 180 deg - (open loop phase lag at gain crossover)
- (c) Gain Crossover = frequency at which the open loop amplitude ratio is 1.0 (or zero dB)

A gain or phase margin of zero indicates an unstable system. The greater the gain or phase margin, the less likely it is that instability will occur due to variation in control system components. The goals are a gain margin of 0.5 or greater and a phase margin of 35 deg or greater.

(3) Acceleration and Speed Capability of Actuators

The goal for the elevation actuator system is to accelerate to a speed of 60 deg/s in 10 deg of gun rotation, starting from rest. The goal for the azimuth actuator system is to accelerate to 90 deg/s in 45 deg of turret rotation, starting from rest.

(4) Gain Variation

The control system shall be designed to minimize the effects of rate sensor gain variation and friction.

3.3 CONTROL LAW DERIVATIONS

The control synthesis approach utilized for this study is outlined in the following two sections, for the rate command input (rate control system) and the position command input (position control system), respectively. For the rate control system, a hull rate cancellation technique and a lead-lag stabilization technique are presented. The position control system is mathematically compared to the rate control system.

3.3.1 Rate Control System

A simplified block diagram of a rate command stabilization system is shown in Figure 3-1. The inputs are the command rate $\dot{\theta}_s$ and the hull rate $\dot{\theta}_h$. The output gun rate $\dot{\theta}_g$, which is compared with $\dot{\theta}_s$ to generate an error, is processed by the controller G_1 . An additional output is the gun attitude angle θ_g .

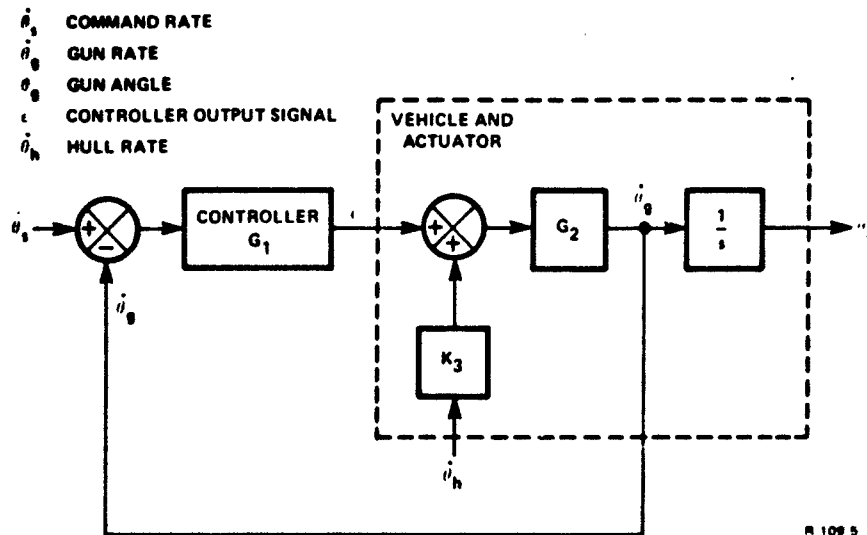


Figure 3-1. Simplified Block Diagram of a Rate Command Stabilization System

The objectives of the control system are to have the gun rate follow the command rate and to have the gun angle θ_g stabilized with respect to hull rate inputs.

Using proportional plus integral control, it follows that:

$$G_1 = K_r + \frac{K_i}{s}$$

where

K_r = proportional gain

K_i = integral gain

By use of integral control, the steady state tracking error $TE = \theta_s - \theta_g$ is a constant for command rate and hull rate inputs. Increasing the gain K_i will decrease the tracking error. Stability considerations, however, dictate a practical limit on K_i . In order to handle this problem in an alternate way, two methods were devised to reduce tracking errors due to vehicle motions. These two methods are described in detail in Section 5.3.

The first of these methods is a hull rate cancellation technique. The hull motion $\dot{\theta}_h$ is sensed and is then used in the control laws. The control signal output ϵ is therefore given by:

$$\epsilon = \left(K_r + \frac{K_i}{s} \right) (\dot{\theta}_s - \dot{\theta}_g) - K_h \dot{\theta}_h$$

where

$K_h = K_3$ = gain of the hull motion effect on the gun rate

The second method uses a single gun sensor and does not use a hull sensor. The tracking error is reduced by increasing the loop gain and introducing a lead-lag network to maintain stability. The control signal output in this case is given by:

$$\epsilon = \frac{\tau_2}{\tau_1} \left(\frac{\tau_1 s + 1}{\tau_2 s + 1} \right) \left(K_r + \frac{K_i}{s} \right) (\dot{\theta}_s - \dot{\theta}_g)$$

where

$$\tau_2/\tau_1 = 10$$

3.3.2 Position Control System

The block diagram for position control with proportional plus integral control is shown in Figure 3-2. The gunner generates an angular position command θ_g rather than a rate command $\dot{\theta}_g$. The position command signal is differentiated and compared with the gun rate signal to obtain the rate error signal. Since perfect differentiation cannot be achieved, a first order lag with time constant τ_1 is included in the input compensation.

In addition, the gun rate signal is integrated and compared with the input position command to obtain the position error signal. Potentiometer feedback was not used as this would have resulted in increased sensitivity to hull sensor gain errors, and increased drift rate.

The position command system can be shown to be mathematically identical to the rate system except for the first order lag τ_1 in the input compensation. (This is discussed in more detail in Sections 5.2.2 and 6.3.) On this basis, the tracking error for hull rate inputs is identical for the rate and the position control systems. In order to

perform a meaningful comparison of the two control system concepts, a rate command input was assumed for both. Under these conditions, for ramp position command inputs, the tracking error is also the same for both the rate and the position systems, as long as the input lag τ_1 is zero. If τ_1 is large enough to affect the system response, or if input compensation is not used, response of the position control system to rate inputs will be slower. However, one advantage with the position control system is that a position command signal can be used. This results in considerably faster response to the process of aiming the gun at a target for the position control system, even if input compensation is not used.

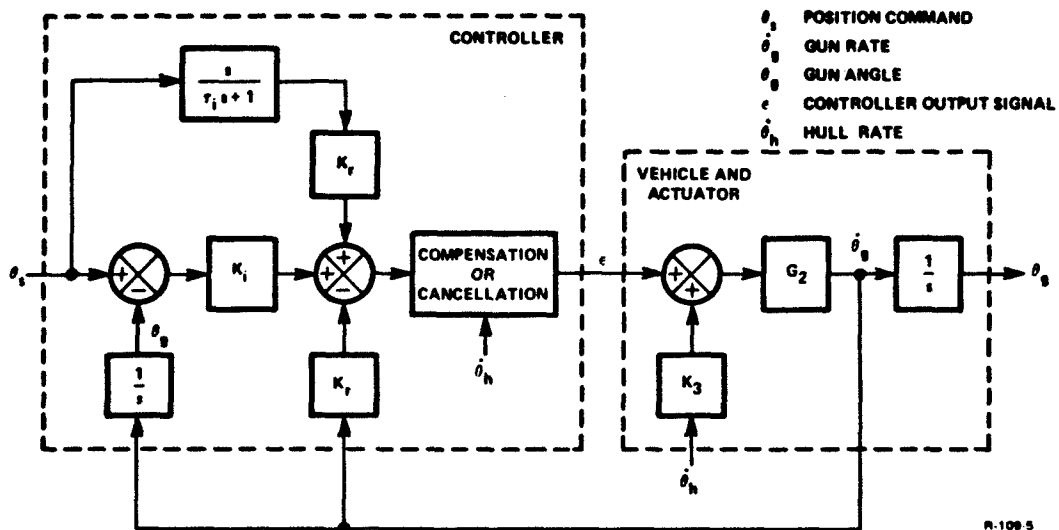


Figure 3-2. Simplified Block Diagram of a Position Command Stabilization System

SECTION 4
HARDWARE SELECTION PROCEDURE

4.1 GENERAL

For the purpose of this contract, a study was performed for selecting the appropriate actuator hardware in each of the two axes to meet the following set of specifications set forth by the Contracting Officer's Representatives:

Axis	Slew Rate Requirement
Azimuth	90 deg/s in 45 deg
Elevation	60 deg/s in 10 deg

These specifications were not previously required for the M60A1 actuators. A mathematical model of the hardware was thus derived (Section 4.3), and from this model the appropriate servovalve, accumulator volume, transmission gear ratio, and motor displacement were selected. The selection results for the elevation and azimuth axes are given in Sections 4.4 and 4.5, respectively. A total pump flow capacity of 30 gpm was assumed in this study.

Upon completion of the study, the hardware was jointly selected by Bendix and personnel from Rock Island Arsenal, for inclusion in the subsequent computer study.

4.2 HARDWARE CONSIDERATIONS AND ASSUMPTIONS

An actuator is considered optimal if it achieves a maximum turret or gun acceleration. If the actuator displacement is too small, the actuator torque will not be great enough to rapidly accelerate the load inertia. If the actuator displacement is too large, the pump will not provide sufficient flow to reach the desired speed. It follows that an optimum actuator displacement exists which is small enough to obtain the desired speed with the available pump flow, and large enough to obtain rapid acceleration. Likewise, the servovalve flow area should be large enough so that significant pressure drop does not occur across the servovalve during acceleration. A model for the actuator system is illustrated in Figure 4-1.

For the purpose of this analysis, it was assumed that a variable delivery constant pressure pump would be used. The schematic for this type of pump is shown in Figure 4-2. The pump servovalve passes fluid

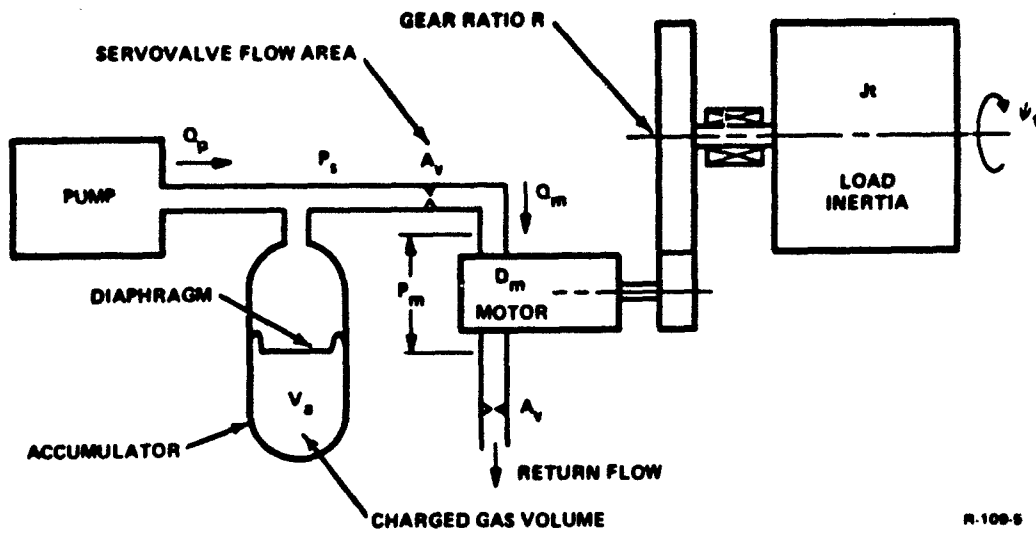


Figure 4-1. Model for Actuator Systems

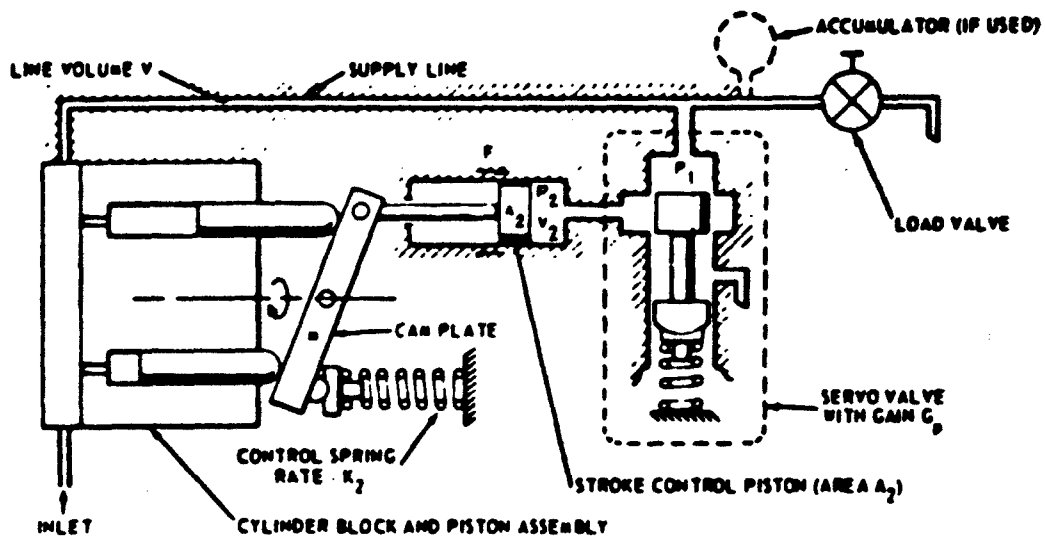


Figure 4-2. Pump Control System Schematic

either to or from the control piston, depending on the sign of the pressure error. If the pressure is higher than the set pressure, the valve passes fluid from the main circuit into the stroking piston cylinder, thus decreasing the delivery of the pump so that the pressure will be reduced. On the other hand, if the pressure is low, the valve passes fluid to the pump case and the control spring forces the pump displacement to increase.

Thus, as the flow demand changes, the pump displacement automatically changes to maintain the supply pressure constant, within the flow range of the pump.

The following hardware and fluid properties were neglected, since they would not affect the choice of the optimum actuator system.

- Pump dynamics
- Fluid leakage
- Fluid compressibility
- Friction

The pump dynamics and the compressibility lag are generally sufficiently fast to have negligible effect on acceleration. Use of an accumulator slows the pump response. This effect was neglected for this study. The addition of pump dynamics would add considerably to the complexity of the simulation.

The turret and gun acceleration achieved in practice will be a little less than the values obtained in the study due to the effects of friction and leakage.

The parameters which must be optimized to obtain the best performance are the product of transmission ratio and motor displacement RD_m , the maximum servovalve flow area ($A_{v \max}$), and accumulator volume V_a . The product RD_m is the motor displacement reflected to the turret or gun, respectively.

4.3 MATHEMATICAL MODEL OF THE ACTUATOR SYSTEM

The pump model assumed here provides that pump flow Q_p equal to that of the motor Q_m below the maximum pump flow in accordance with:

$$\begin{aligned} Q_p &= Q_m & , & \text{ for } Q_m < 20 \text{ gpm} \\ Q_p &= 20 \text{ gpm} & , & \text{ for } Q_m \geq 20 \text{ gpm} \end{aligned} \tag{4-1}$$

The maximum pump flow for a single axis was taken to be 20 gpm. However, a 30 gpm pump should be used to provide the required flow when both axes are activated simultaneously.

It follows for the azimuth axis that equating the motor flow to the servovalve flow yields:

$$RD_m \dot{\psi}_t = CA_v \sqrt{\frac{P_s - P_m}{2}} \quad (4-2)$$

Squaring equation (4-2) and solving for P_m :

$$P_m = P_s - \left(\frac{RD_m}{CA_v} \right)^2 \dot{\psi}_t^2 \quad (4-3)$$

The turret acceleration is:

$$\ddot{\psi}_t = \frac{RD_m}{100 J_t} P_m \quad (4-4)$$

The accumulator is shown in Figure 4-1. The volume of gas under the diaphragm is initially charged to the supply pressure. The volume above the diaphragm is filled with hydraulic fluid. When the hydraulic fluid is at the desired supply pressure, approximately one-half of the accumulator volume is filled with gas. As long as the servovalve flow does not exceed the pump flow capability, the pump will maintain the desired supply pressure, and the hydraulic fluid and gas volumes will not change. When the valve flow exceeds the pump flow, hydraulic fluid will flow from the accumulator, the gas volume will expand, and the supply pressure will drop. This process is adiabatic and it follows that:

$$P_s V_a^k = C \quad (4-5)$$

Differentiating with respect to time:

$$k P_s V_a^{k-1} \dot{V}_a + V_a^k \dot{P}_s = 0$$

Solving for \dot{P}_s :

$$\dot{P}_s = \frac{kP_s \dot{V}_a}{V_a} \quad (4-6)$$

The rate of change of gas volume equals the difference between the motor flow and pump flow.

$$\begin{aligned} \dot{V}_a &= Q_m - Q_p, \quad \text{when } Q_m > Q_p \\ \dot{V}_a &= 0, \quad \text{when } Q_m < Q_p \end{aligned} \quad (4-7)$$

For a hydraulic motor, the displacement flow is given by:

$$Q_m = RD_m \dot{\psi}_t \quad (4-8)$$

The gas volume in the accumulator and the supply pressure are:

$$V_a = V_o + \int \dot{V}_a dt \quad (4-9)$$

where

V_o = steady state gas volume in accumulator at 3000 psi

$$P_s = P_{so} + k \int P_s \frac{\dot{V}_a}{V_a} dt \quad (4-10)$$

Equations (4-1), (4-3), (4-4), and (4-7) through (4-10) were used for the computer study to determine the actuator system sizing. The same set of equations was used for the elevation axis, with only a change in parameters and a substitution of θ_g for ψ_t .

Table 4-1 lists the actuator system parameters.

Table 4-1. Parameters for Hardware Selection Study

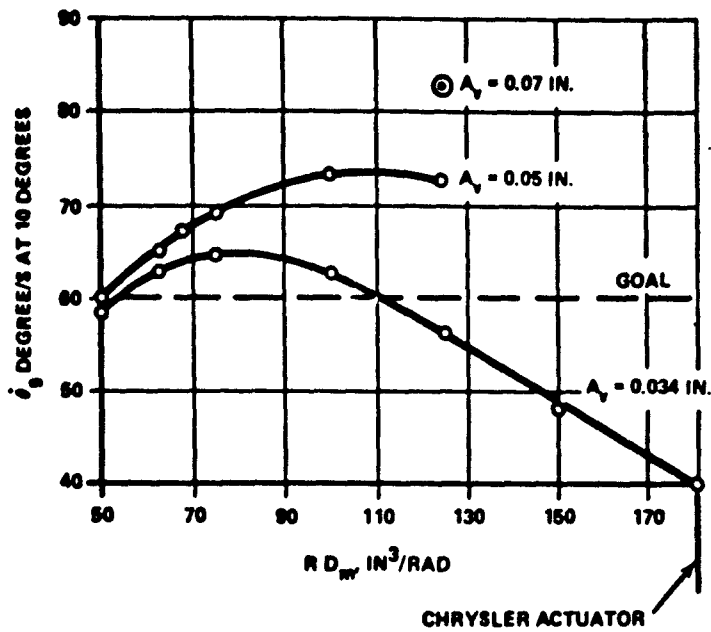
Parameter	Value	Units
C	100	in/s $\sqrt{\text{psi}}$
J _G	3800	slugs
J _c	22,700	slugs
k	1.4	-
P _{so}	3000	psi
V _o	one-half accumulator volume	in ³

4.4 ELEVATION AXIS HARDWARE SELECTION

Results of the hardware selection procedure for the elevation axis are summarized in Figure 4-3. Gun elevation rate achieved at an elevation angle displacement of 10 deg is plotted for three different servovalve areas and numerous values of the product of transmission ratio R and motor displacement D_m. It is evident from Figure 4-3 that with a servovalve area of 0.034 in², the gun elevation rate exceeds 60 deg/s in 10 deg of displacement for values of RD_m between 50 and 110. For maximum rate, a value of 80 for RD_m was selected for elevation.

Since servovalves are generally rated in terms of gpm flow at a pressure drop of 1000 psi instead of effective flow area, an appropriate conversion is achieved by use of Figure 4-4. This figure also indicates which commercially available valves can handle a given application. The flow area of 0.034 in² is thus equivalent to a 20 gpm servovalve, and the largest available MOOG series 30 valve can be utilized for this application. A 20 gpm servovalve was therefore selected. A MOOG Series 30 valve was also used in an actuator system utilized in the past by the Chrysler Corporation for the M60A1 main gun.

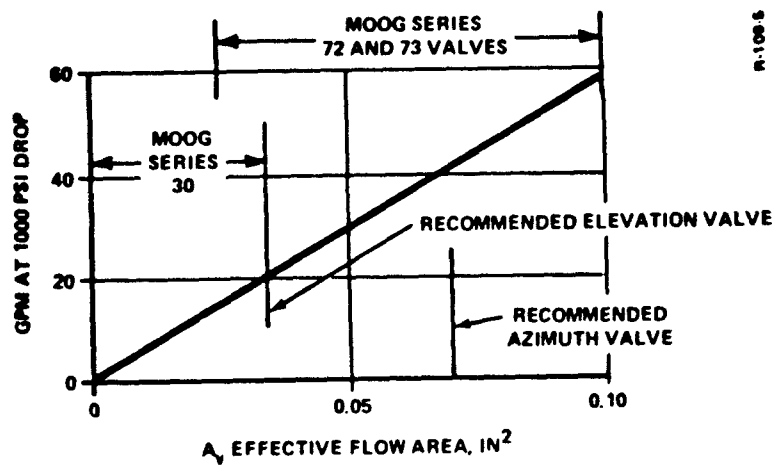
A time history plot for the gun elevation angle, the elevation rate, and the accumulator gas volume is contained in Figure 4-5. As indicated by this figure, the accumulator was not used in the first 10 deg of elevation displacement. Therefore, an accumulator is not required for elevation. An elevation accumulator may be of value, however, when both the gun and turret are rotated simultaneously.



3000 PSI, 20 GPM PUMP FLOW
 1 GAL. ACCUMULATOR USED. NO ACCUMULATOR FLOW OCCURRED DURING FIRST 10-DEGREE ROTATION. ACCUMULATOR MAY HELP WHEN AVAILABLE PUMP FLOW IS REDUCED DUE TO TURRET ROTATION.
 30 GPM PUMP REQUIRED
 FRICTION AND FLOW LOSSES NEGLECTED

R-1006

Figure 4-3. Hardware Selection Results for Elevation Axis



R-1006

Figure 4-4. Servovalve Conversion Diagram

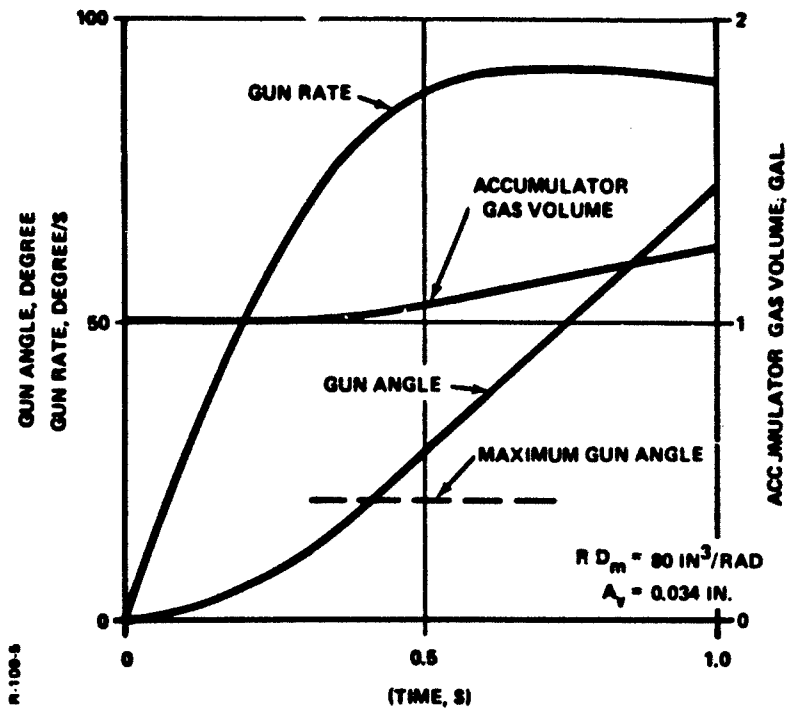


Figure 4-5. Time History Plot for Elevation Angle, Rate, and Gas Volume

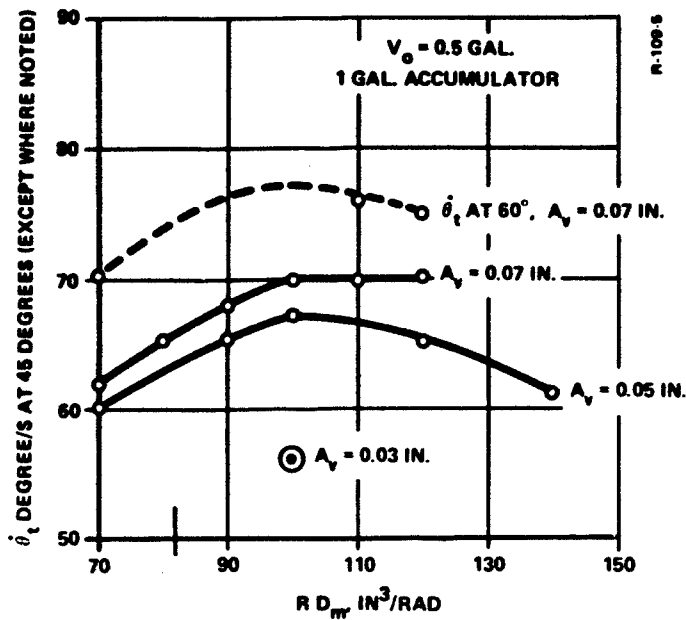


Figure 4-6. Hardware Selection Results for Azimuth Axis

4.5 AZIMUTH AXIS HARDWARE SELECTION

Results of the hardware selection for the azimuth axis are summarized in Figure 4-6. Turret azimuth rate achieved at an azimuth displacement angle of 40 deg is plotted for three different servovalve areas and numerous values of the product RD_m . It is evident from Figure 4-6 that a rate of 90 deg/s in 45 deg displacement is not possible. It was therefore decided to choose the valve and motor combination which maximizes rate at 45 deg displacement.

In accordance with Figure 4-6, a turret speed of 70 deg/s is obtained with A_v equal to 0.07 in² and RD_m values of 100 to 120 in³/rad using a 1 gallon accumulator. Therefore, these are the recommended values.

Figure 4-7 demonstrates the effect of reducing or increasing the accumulator volume from 1 gallon. Increasing the accumulator volume above 1 gallon has no effect, while reducing the volume has only a minimal effect.

Figure 4-8 shows the turret rotation required to accelerate to a speed of 90 deg/s. If this criterion had been used, an RD_m of 90 and a 2 gal accumulator would have been selected. However, an RD_m of 100 appears to be the best overall choice when allowance is made for torque loss due to friction.

As indicated by Figure 4-4, the selected 0.07 in² servovalve flow area is equivalent to 40 gpm flow at 1000 psi pressure drop. This is within the range of the MOOG 72 and 73 flow control servovalves.

A time history plot for the turret azimuth angle, the turret azimuth rate, and the accumulator gas volume is contained in Figure 4-9 for the selected values of RD_m and A_v .

A curve for each of the azimuth and elevation axes, which shows the range of values available for R and D_m , is contained in Figure 4-10. The product RD_m was determined to be 100 and 80 for the azimuth and elevation axes respectively.

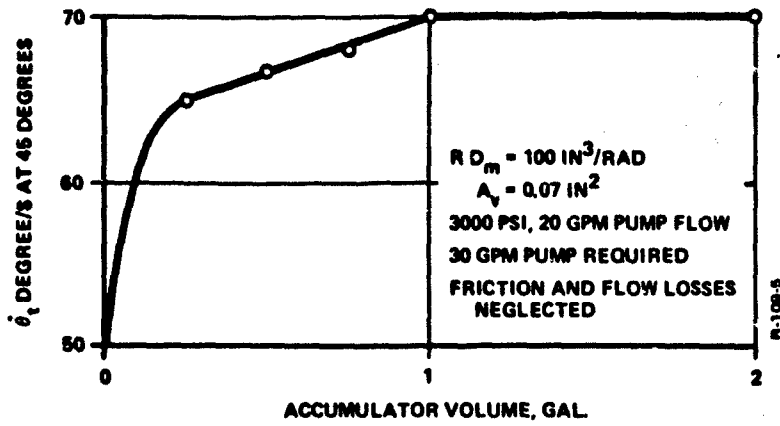


Figure 4-7. Accumulator Sizing Effects Diagram

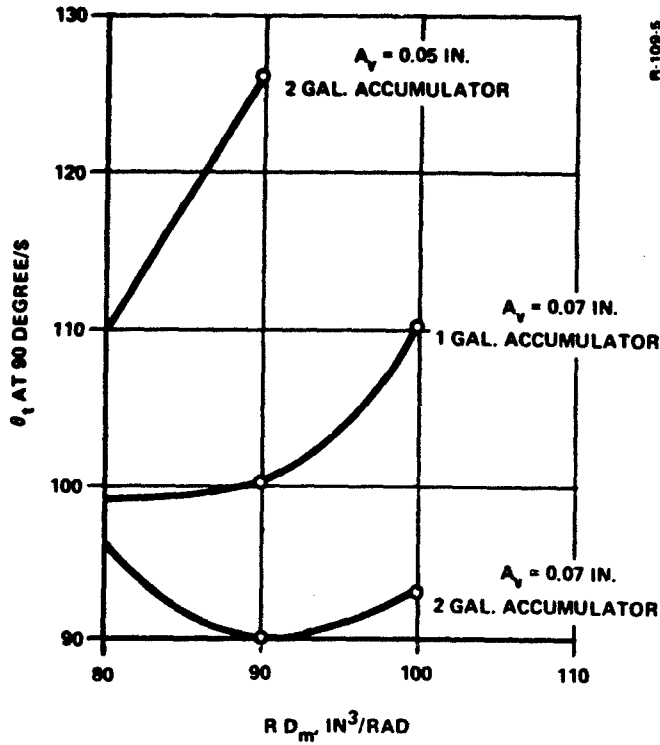


Figure 4-8. Azimuth Rotation Requirements Plot

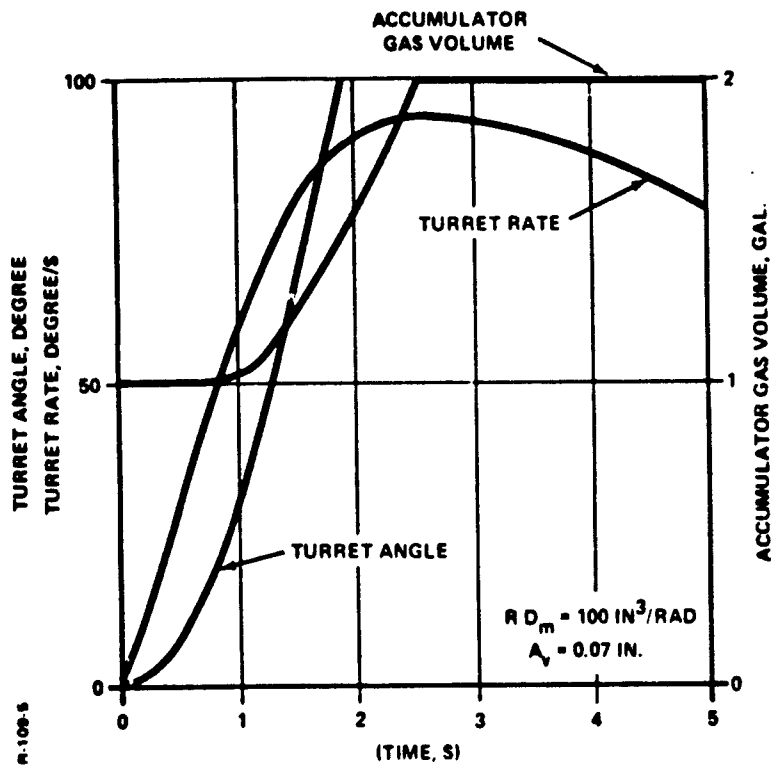


Figure 4-9. Time History Plot for Azimuth Angle, Rate, and Gas Volume

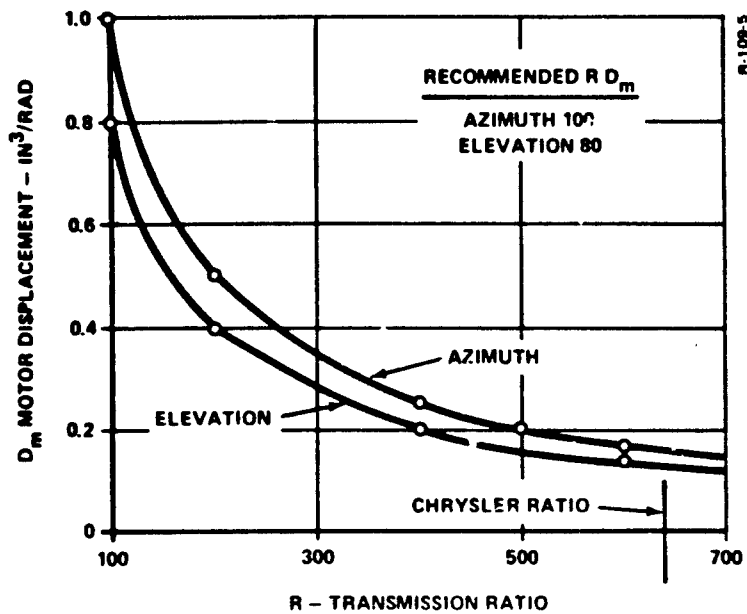


Figure 4-10. Curves of Constant Products of Transmission Ratio and Motor Displacement for Azimuth and Elevation Axes

SECTION 5
ANALYTICAL SYSTEM ANALYSIS

5.1 GENERAL

This section contains an extensive analytical analysis of the rate and position control systems which was performed prior to the simulation analysis. By means of this study, it was possible to gain valuable insight into the behavior of the system and to derive starting values for the rate, proportional, and integral gains of the control law. In addition, two methods were derived to reduce system tracking errors. An analytical sensor error study and an outline of a coupling model are also presented.

For the purpose of this analytical study, the control system was linearized and simplified, where possible, while retaining basic system functions. This simplification of the system is described in Sections 5.2.1 and 5.2.2 for the rate and the position control concepts, respectively. Transfer functions for the system described here showed how the systems should be designed to achieve the desired performance.

Initial gain values for the nonlinear computer models were also determined from the linear study. These gain values were varied, and compensation was used to achieve the desired performance with the nonlinear flow equations, sensor dynamics, and other nonlinear effects and lags.

5.2 LINEAR SYSTEM DERIVATION

5.2.1 Rate Control System

This section contains the derivation of the linearized rate control system shown in Figure 5-1. The following nonlinearities were omitted in order to simplify the transfer function:

- (1) Friction
- (2) Sensor dynamics
- (3) Compliance

Since pressure feedback dynamics have negligible phase shift at the natural frequency, this effect can be represented by a constant as shown in Figure 5-1.

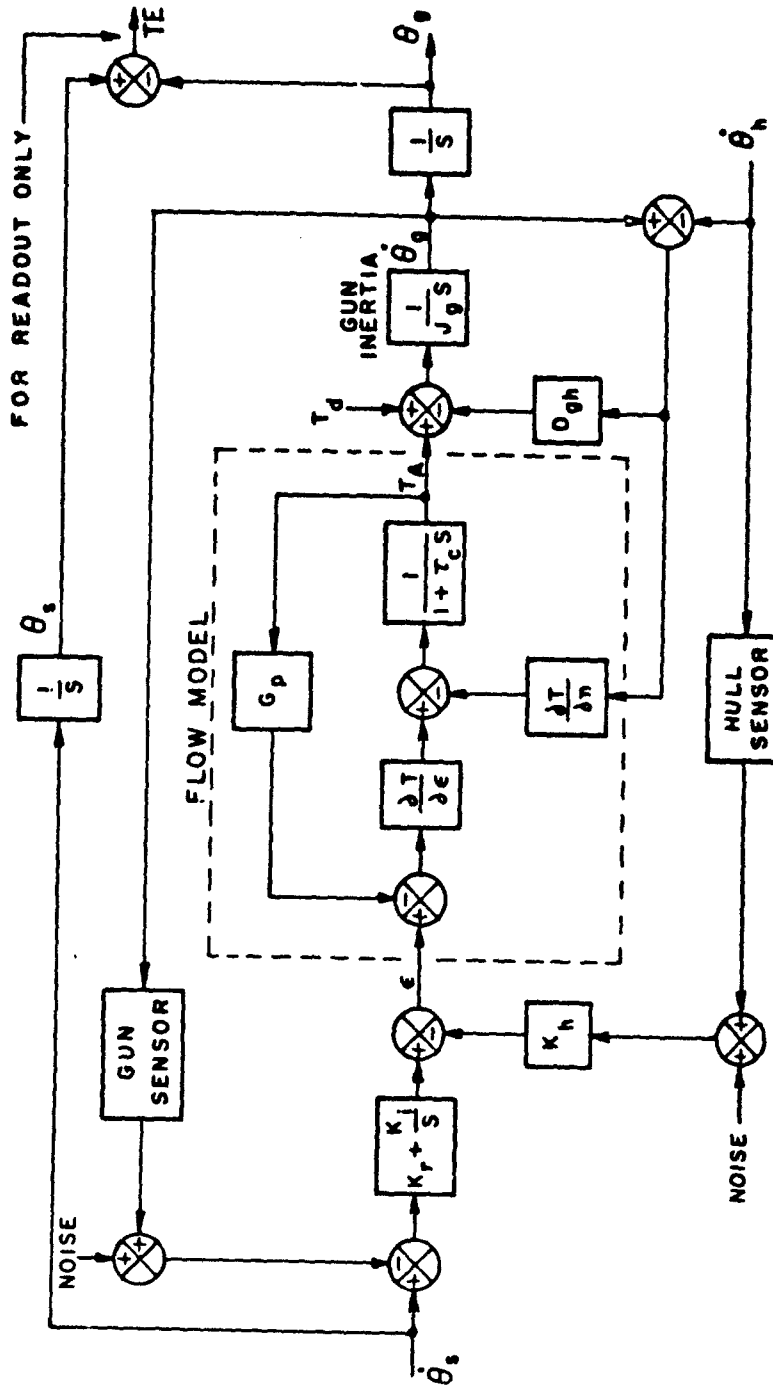


Figure 5-1. Block Diagram of Linearized Rate Control System

The nonlinear flow and torque equations from Figure 2-6 are given by:

$$C A_v \sqrt{\frac{P_s - P_m}{2}} = R D_m (\dot{\theta}_g - \dot{\theta}_h) + L P_m + \frac{V}{2B} s P_m \quad (5-1)$$

$$T_A = R D_m P_m \quad (5-2)$$

Linearizing by partial differentiation yields:

$$C \sqrt{\frac{P_s - P_o}{2}} \Delta A_v - \frac{C A_{vo}}{2 \sqrt{2 (P_s - P_o)}} \Delta P_m = R D_m s (\Delta \theta_g - \Delta \theta_h) + L \Delta P_m + \frac{V}{2B} s \Delta P_m \quad (5-3)$$

Substituting for P_m from equation (5-2) and rearranging terms gives:

$$C \sqrt{\frac{P_s - P_o}{2}} \Delta A_v = \frac{Q_o}{2 R D_m (P_s - P_o)} \Delta T_A + \frac{V}{2 B R D_m} s \Delta T_A + R D_m s (\Delta \theta_g - \Delta \theta_h) \quad (5-4)$$

where

$$Q_o = C A_{vo} \sqrt{\frac{P_s - P_o}{2}} + 2L (P_s - P_o)$$

Rearranging terms, and defining new parameters gives:

$$T_A = \frac{1}{1 + \tau_c s} \left[\frac{\partial T}{\partial \epsilon} \epsilon - \frac{\partial T}{\partial n} (\dot{\theta}_g - \dot{\theta}_h) \right] \quad (5-5)$$

where

$$\begin{aligned} \epsilon &= A_v \\ \tau_c &= \frac{v}{Q_o} \frac{(P_s - P_o)}{B} \\ \frac{\partial T}{\partial n} &= 2 (RD_m)^2 \frac{(P_s - P_o)}{Q_o} \\ \frac{\partial T}{\partial \epsilon} &= \frac{2CRD_m (P_s - P_o)}{CA_{vo} + 2L \sqrt{2 (P_s - P_o)}} \end{aligned}$$

Assuming $T_d = T_{fg} = 0$, gun acceleration is given by:

$$\ddot{\theta}_g = \frac{T_A}{J_g} \quad (5-6)$$

The control law developed in Section 3.2 is:

$$\epsilon = \left(K_r + \frac{K_i}{s} \right) (\dot{\theta}_s - \dot{\theta}_g) - K_h \dot{\theta}_h \quad (5-7)$$

Upon solving equations (5-4) through (5-7), the system transfer function is:

$$\frac{\dot{\theta}_g}{\dot{\theta}_s} = \frac{1 + \frac{K_r}{K_i} s}{1 + \frac{s}{\beta \omega_{NS}} + \frac{\alpha s^2}{\beta \omega_{NS}^2} + \frac{s^3}{\beta \omega_{NS}^3}} \quad (5-8)$$

where

$$\omega_{NS}^2 = \frac{1}{J_g \tau_c} \left(\frac{\partial T}{\partial n} + K_r \frac{\partial T}{\partial \epsilon} \right) \quad (5-9)$$

$$\beta \omega_{NS} = \frac{K_i \frac{\partial T}{\partial \epsilon}}{\frac{\partial T}{\partial n} + K_r \frac{\partial T}{\partial \epsilon}} \quad (5-10)$$

$$\alpha \omega_{NS} = \frac{1 + K_p \frac{\partial T}{\partial \epsilon}}{\tau_c} \quad (5-11)$$

The steady state $T_d/\dot{\theta}_g$ gain is:

$$\frac{T_d}{\dot{\theta}_g} = \frac{K_i \frac{\partial T}{\partial \epsilon}}{1 + K_p \frac{\partial T}{\partial \epsilon}} \quad (5-12)$$

The response to terrain input is:

$$\frac{\dot{\theta}_g}{\dot{\theta}_h} = \frac{\frac{\partial T}{\partial n} - K_h \frac{\partial T}{\partial \epsilon}}{K_i \frac{\partial T}{\partial \epsilon}} \cdot \frac{1}{G_c} \quad (5-13)$$

where

G_c = cubic denominator of the transfer function

It follows that the gun motion, or tracking error, for a terrain input is zero if

$$K_h = \frac{\partial T / \partial n}{\partial T / \partial \epsilon}$$

However, since the torque speed slope is nonlinear, perfect cancellation over the complete range of operation may not be possible.

5.2.2 Position Control System

This section contains a derivation of the linearized elevation position control system shown in Figure 5-2. As indicated in the figure, the inertial gun position feedback signal is obtained by integrating

the gun rate sensor signal. A potentiometer was not used for the position feedback because it would have been necessary to add the hull position to the potentiometer signal to obtain the inertial position signal. This would have made the system very sensitive to hull sensor gain variation.

The control law for this system is given by:

$$c = K_i (\theta_s - \theta_g) + K_r (\dot{\theta}_s - \dot{\theta}_g) - K_h \dot{\theta}_h$$

Since a position command input will generally be used for the position command system, the command rate signal $\dot{\theta}_s$ will not be readily available. This signal can be omitted, or it can be obtained by pseudo differentiation of the input command signal as shown below.

$$\dot{\theta}_s = \frac{s}{1 + \tau_i s} \theta_s$$

Including the $\dot{\theta}_s$ term results in faster response to command inputs.

Other equations for the position control concept take the same form as those for the rate control concept.

It follows therefore that the position control transfer function is given by:

$$\frac{\theta_g}{\theta_s} = \frac{1 + \frac{K_r}{K_i} \cdot \frac{1}{1 + \tau_i s} s}{1 + \frac{s}{\beta\omega_{NS}} + \frac{\alpha s^2}{\beta\omega_{NS}^2} + \frac{s^3}{\beta\omega_{NS}^3}}$$

The steady state response to a hull rate step input is:

$$\dot{\theta}_g = \frac{\frac{\partial T}{\partial n} - K_h \frac{\partial T}{\partial \epsilon}}{K_i \frac{\partial T}{\partial \epsilon}} \dot{\theta}_h$$

The transfer functions for hull rate and disturbance torque inputs are the same as for the rate control system. Therefore, the response to these inputs is identical for the two systems.

The response to identical rate command inputs will be the same for both systems if the pseudo differentiator lag τ_1 equals zero. This condition was used in the simulation for showing the equivalence of the two systems, as discussed in Section 6.3. Since position command inputs will generally be used with the position control system, the response time to rotate the gun to a commanded angle will be shorter whether or not the input rate signal θ_s is used.

5.2.3 Linear Model Parameters

For model development and preliminary studies, the actuator displacement and volume under compression were obtained from the bibliography. The parameters developed here corresponded to the elevation axis:

$$RD_m = LA_p = 38.4 \text{ in.} \times 4.72 \text{ in}^2 \times 16.37 \frac{\text{cm}^3}{\text{in}^3}$$

where

$$RD_m = 2970 \text{ cm}^3/\text{rad}$$

$$V = 895 \text{ cm}^3$$

The supply pressure and maximum servovalve area were taken to be

$$P_s = 210 \text{ kg/cm}^2$$

$$A_{v \text{ max}} = 0.2 \text{ cm}^2$$

The linearized actuator parameters are:

$$\frac{\partial T}{\partial n} = \frac{2}{100} (RD_m)^2 \frac{P_s - P_o}{Q_o}$$

$$\tau_c = \frac{V}{B} \frac{P_s - P_o}{Q_o}$$

$$\frac{\partial T}{\partial \epsilon} = \frac{2}{100} RD_m \frac{P_s - P_o}{A_{vo}}$$

The effective servovalve area A_{vo} and pressure P_o are typically taken to be equal to one-half the maximum servovalve area and one-half supply pressure for linear analysis. Thus, the linearized servovalve parameters are:

$$Q_o = CA_{vo} \sqrt{\frac{P_s - P_o}{2}} = 955 \times 0.1 \sqrt{\frac{210 - 105}{2}}$$

giving

$$Q_o = 695 \text{ cm}^3/\text{s}$$

Also

$$\frac{\partial T}{\partial n} = \frac{2}{100} (2970)^2 \frac{105}{695} = 2.66 \times 10^4 \text{ kg-m-s}$$

$$\tau_c = \frac{895}{10,550} \times \frac{105}{695} = 0.013 \text{ s}$$

$$\frac{\partial T}{\partial \epsilon} = 0.02 \times 2970 \times \frac{105}{0.1} = 6.25 \times 10^4 \text{ kg-m/rad}$$

Generally, the linearized parameters must be varied somewhat to obtain the best correlation with the nonlinear system. To achieve this correlation, the following values were used:

$$\frac{\partial T}{\partial n} = 2.08 \times 10^4 \text{ kg-m/s}$$

$$\tau_c = 0.016 \text{ s}$$

$$\frac{\partial T}{\partial \epsilon} = 6.25 \times 10^4 \text{ kg-m/rad}$$

The initial gain values for K_i , K_r and K_p were determined as follows. The bandpass goal was 15 Hz. Thus, a bandpass of 16 Hz was selected for the linear system, to allow some performance margin. From equation (5-9)

$$K_r = \frac{1}{\partial T / \partial \epsilon} \left(\tau_c J \omega_{NS}^2 - \frac{\partial T}{\partial n} \right)$$

and for

$$\omega_{NS} = 2\pi \times 16 = 100 \text{ rad/s}$$

it follows that:

$$K_r = \frac{1}{6.25 \times 10^4} (0.016 \times 527 \times 100^2 - 2.08 \times 10^4) = 1.0$$

From equation (5-10)

$$K_i = \beta \omega_{NS} \left(K_r + \frac{\partial T / \partial n}{\partial T / \partial \epsilon} \right)$$

In this expression, β should equal 0.35 for the best linear system response, and α should equal 0.7. Thus:

$$K_i = 0.35 \times 100 \left(1.0 + \frac{2.08}{6.25} \right) = 47$$

Equation (5-11) specifies that:

$$K_p = \frac{1}{\partial T / \partial \epsilon} (\alpha \tau_c \omega_{NS} - 1)$$

Upon substituting numerical values, it follows that:

$$K_p = \frac{1}{6.25 \times 10^4} (0.016 \times 0.7 \times 100 - 1) = 2 \times 10^{-6}$$

5.2.4 Linear System Response

Based on the transfer functions presented in Sections 5.2.1 and 5.2.2, a digital computer solution for time and frequency response was obtained. Using ideal sensors and the parameters for the elevation axis, the resulting time response is illustrated in Figure 5-3. Note that the time response exhibits a 7 percent overshoot. A solution for system frequency response is illustrated in Figure 5-4. This figure shows that a bandpass of 18 Hz was achieved.

5.3 TRACKING ERROR REDUCTION

This section deals with the method of reducing the gun tracking error due to motions of the hull. Referring to Figure 5-5, which is a simplified block diagram of the rate command stabilization system with proportional and integral control, assume a constant hull rate input $\dot{\theta}_h$ and no command input ($\dot{\theta}_g = 0$). In steady state, $\dot{\theta}_g = 0$ and $Q_v = Q_m$. Then:

$$\epsilon = - \frac{\partial T / \partial n}{\partial T / \partial \epsilon} \dot{\theta}_h$$

Since the tracking error TE is given by:

$$TE = \theta_s - \theta_g$$

$$\epsilon = K_p (\dot{\theta}_s - \dot{\theta}_g) + K_i (\theta_s - \theta_g)$$

then the steady state tracking error is:

$$TE = -\theta_g = \frac{\epsilon}{K_i} = - \frac{\partial T / \partial n}{K_i \partial T / \partial \epsilon} \dot{\theta}_h$$

It is desired to reduce this tracking error so that the gun is stabilized with respect to hull motions.

Two methods can be used to reduce the tracking error: The first method is a cancellation technique. Equation (5-13) shows that hull motion will cause no gun motion, and thus will result in no tracking error, if

$$K_h = \frac{\partial T / \partial n}{\partial T / \partial \epsilon}$$

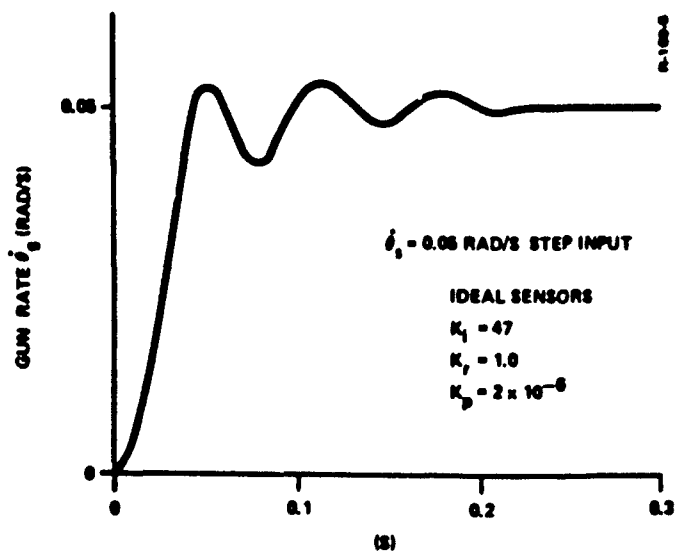


Figure 5-3. Linear System Step Response

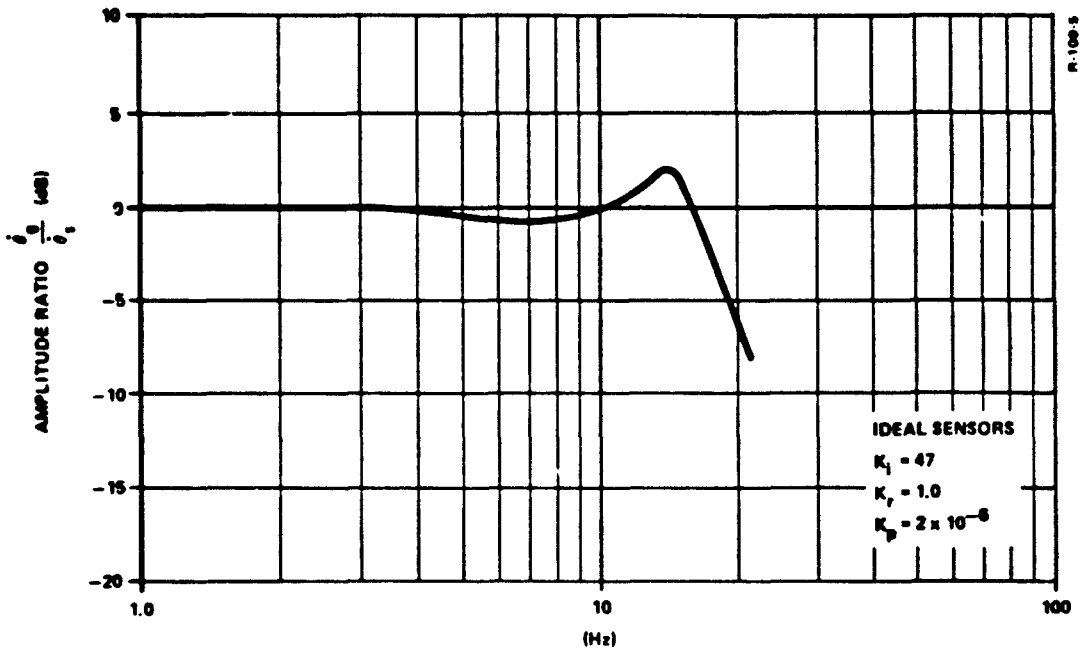


Figure 5-4. Linear System Frequency Response

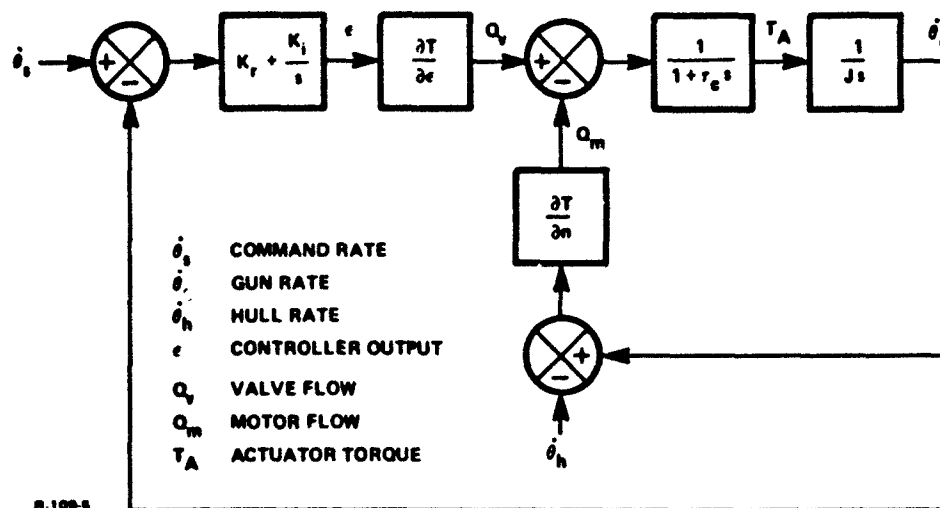


Figure 5-5. Simplified Block Diagram of the Rate Command System

Therefore, hull motion can be effectively cancelled by using the output signal of an inertial hull sensor with gain K_h in the control law. Complete cancellation of hull motion coupling for the actual system, however, cannot be obtained due to nonlinearities and compressibility. In addition, gain variations due to such factors as aging and temperature will cause some tracking error. The cancellation technique, however, is very effective in reducing gun motion.

The second method uses only a single gun sensor. No vehicle motion signal input is provided for this system. The tracking error for the system will be inversely proportional to the error signal amplification and, therefore, a very high gain must be used. A lag-lead network is required to lower the high frequency gain for stability. The design technique is to first adjust the gains for the stable operation with the desired response. The gain required to lower the tracking error to an acceptable level is then determined. The lag-lead network is designed to maintain the high frequency gains at the original values for stable operation, while a higher gain is obtained at low frequency for low tracking error.

The higher gain and lag-lead network can also be used with the cancellation technique to reduce the sensitivity to variation of some of the gains.

5.4 SENSOR ERROR ANALYSIS

5.4.1 General

The effect of sensor errors on the control and stabilization system is the subject of this section. Sensor errors considered here are gain errors and offset errors. Only the rate command system is analyzed in this section. It is assumed that in both the rate and position command systems, the gunner will zero the tracking error with or without sensor errors. On that basis, sensor errors have an effect only on stabilizing the gun in the presence of hull motions. As described in Section 5.2.2, the response to hull motions is identical for both the rate and the position command systems.

The analysis presented here will consider a system utilizing:

- (1) Two rate sensors (Section 5.4.2)
- (2) A single acceleration sensor in the gun axis (Section 5.4.3)

5.4.2 Two Rate Sensors

Figure 5-6 is a simplified block diagram of the rate control system with two rate sensors. The transfer function of the sensors is assumed to be $Y(s)$ with unity gain. For zero sensor gain error, $K_{bh} = K_{bg} = 1$. The sensor offset errors are ϵ_h and ϵ_g .

A hull sensor gain error has the same effect as a change in K_h . The effects of changes in K_h were investigated using the simulation and are described in Section 6.

A hull sensor offset error will give a constant steady state tracking error. This is determined as follows: Assuming that $\theta_s = \theta_h = 0$ and $\theta_g = 0$ (in steady state), then $\epsilon = 0$ and $-K_i \theta_g = K_h \epsilon_h$. Since the tracking error $TE = -\theta_g$,

$$TE = \frac{K_h}{K_i} \epsilon_h$$

Typical gain values are $K_h = 0.15$ and $K_i = 50$. Therefore, the tracking error in radians for an offset error in rad/s is $TE = 0.003 \epsilon_h$.

A gun sensor gain error will have little effect on the stabilization system since it only changes the loop gain and is like changing K_r and K_i . The effect of a gun sensor offset error ϵ_g is analyzed as follows: Assuming $\theta_s = 0$, and $\theta_h = \text{constant}$, then in steady state, $\theta_{gs} = 0$. Therefore, $\theta_g = -\epsilon_g$. Since the tracking error is given by $TE = \theta_s - \theta_g$, it follows that $TE = \int \epsilon_g dt$. The tracking error for a gun

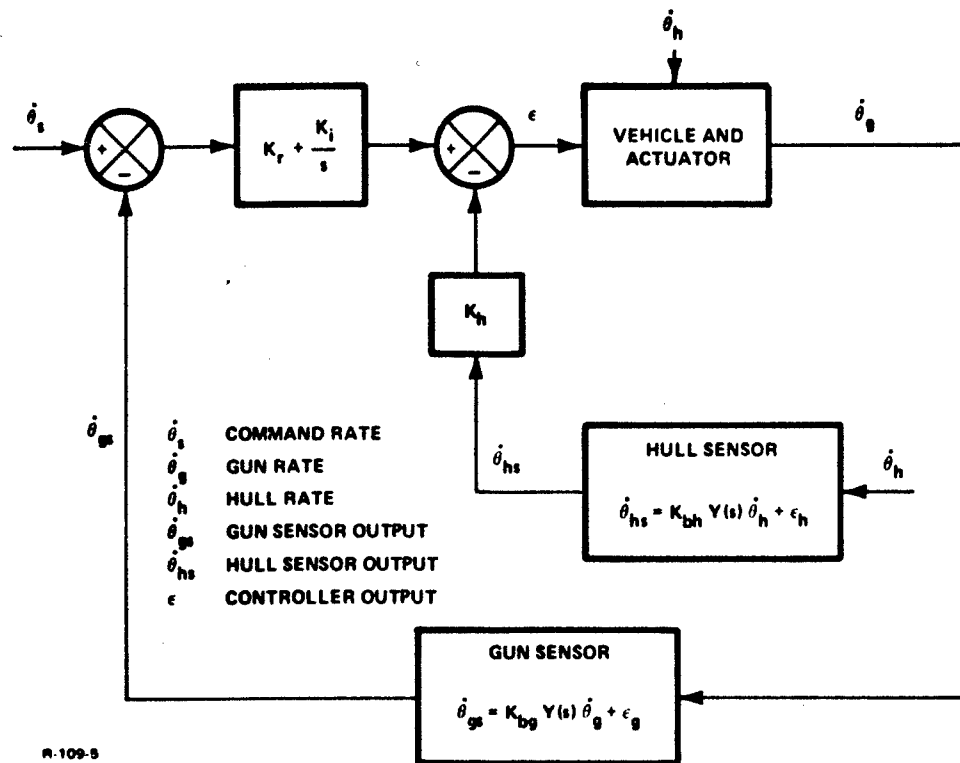


Figure 5-6. Simplified Block Diagram of the Rate Control System with Two Rate Sensors

sensor offset will therefore increase with time. As a result, it is mandatory to minimize the gun sensor offset error or devise a method of eliminating its effect. Section 5.5 discusses a method of eliminating sensor offset errors.

5.4.3 Single Acceleration Sensor

A simplified block diagram of a rate control system with a single acceleration sensor in the gun axis is presented in Figure 5-7. Both an integrating and a pneumatic accelerometer are shown, along with the corresponding rate computation networks.

For both of these acceleration sensors, a gain error (i.e., $K_{bg} \neq 1$) has the same effect as the rate sensors. The loop gain changes with the gain error, but the influence on the tracking error is small.

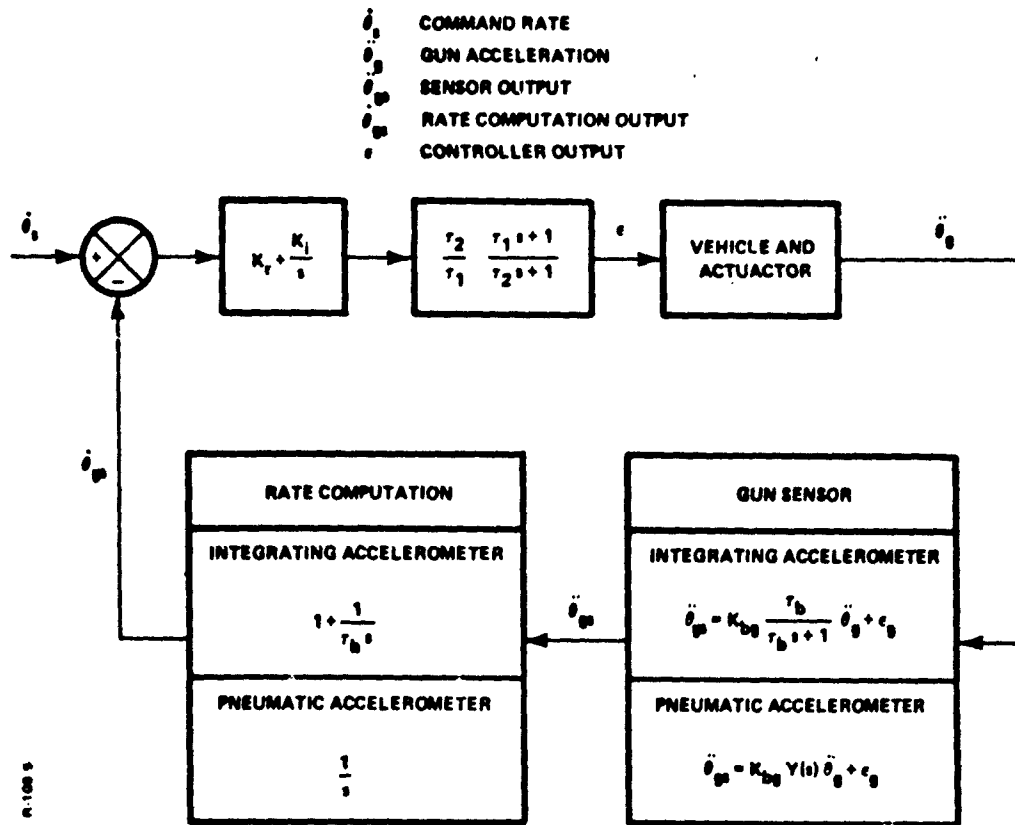


Figure 5-7. Simplified Block Diagram of the Rate Control System with a Single Acceleration Sensor

For the integrating accelerometer, the effect of an offset error is synthesized as follows: In steady state, $\dot{\theta}_{gs} = 0$. Therefore,

$$\dot{\theta}_{gs} = 0 = \left(1 + \frac{1}{\tau_b s} \right) \left(\frac{\tau_b}{\tau_b s + 1} \ddot{\theta}_g + c_g \right)$$

It follows that

$$\ddot{\theta}_g = -s \epsilon_g - \frac{1}{\tau_b s} \epsilon_g$$

Since the tracking error is $TE = -\theta_g$,

$$TE = \int \epsilon_g dt + \iint \frac{\epsilon_g}{\tau_b} dt dt$$

The tracking error will therefore increase with time for a constant offset error. Its effect, however, can be minimized by increasing the time constant τ_b . For the pneumatic accelerometer, the effect of an offset error is determined in a similar manner. In steady state, $\dot{\theta}_{gs} = 0$ so that

$$\dot{\theta}_{gs} = 0 = \frac{1}{s} (\ddot{\theta}_{gs} + \epsilon_g)$$

The tracking error is therefore

$$TE = \theta_g = \iint \epsilon_g dt dt$$

Again the tracking error will increase with time for a constant sensor offset error.

5.5 METHOD OF ELIMINATING THE EFFECTS OF INTEGRATOR DRIFT AND SENSOR OFFSETS

The sensor error analysis in Section 5.4 shows that gun sensor offsets cause the gun to drift, and hence the tracking error to increase with time. A method has been developed which automatically nulls out the effects of integrator drift and sensor offsets. This method is illustrated in Figure 5-8. The sensor and integrator shown are parts of the original system. The track/store amplifier operates such that the output tracks (equals) the input when in the track mode, and stores (holds) the output when in the store mode.

The amplifier is ordinarily in the store mode so that the output of the sensor θ_{gs} (gun rate in this case) is integrated to give the gun angle. At the time it is desired to null the sensor offset ϵ_g and the integrator drift ϵ_d , the track/store amplifier is put into the track mode. This must be accomplished during a period when the actual gun rate $\dot{\theta}_g$ is zero. Under these conditions, when the network reaches steady state, its output is zero, effectively nulling the offset and drift. Switching the amplifier to the store mode returns the system to normal operation except that now the drift and offset are nulled out.

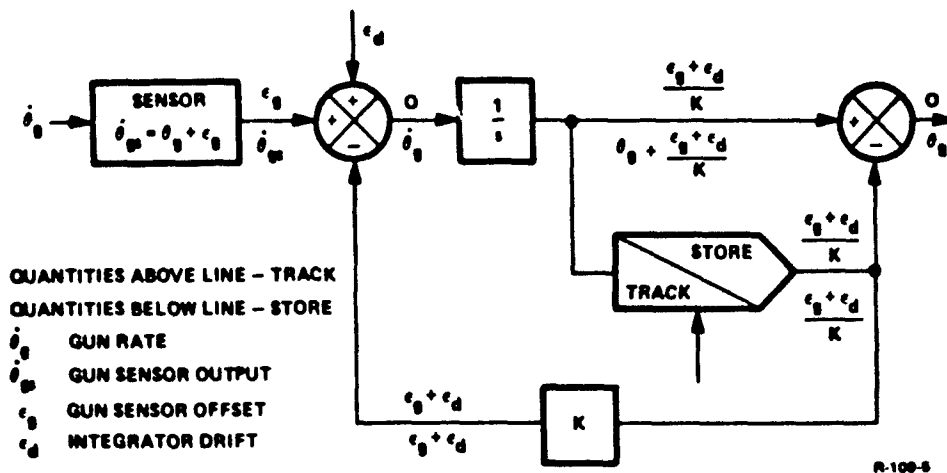


Figure 5-8. Method of Eliminating the Effects of Integrator Drift and Sensor Offsets

Two of these networks are required for an acceleration sensor system while only one is required for a rate sensor system. In addition, the network is required only for the gun sensor since an offset error in the hull sensor results in a small tracking error which does not increase with time.

In order to implement this type of drift and offset elimination, the gunner can be provided with a pushbutton switch which activates all the nulling networks. A timer could also be utilized to automatically return the system to normal operation after the nulling process is completed.

5.6 EFFECT OF GYROS ON RESPONSE

A block diagram for analysis of the effect of rate sensor dynamics on response is presented in Figure 5-9. The transfer function for a command input is

$$\frac{\dot{\theta}_g}{\dot{\theta}_s} = \frac{\left(1 + \frac{K_r}{K_i} s\right) D_g}{1 + \left(\frac{K_r}{K_i} + \frac{D_a D_g}{K_a K_i}\right) s}$$

where

D_g = denominator of gyro transfer function

K_a = gain of actuator and gun transfer function

D_a = denominator of the actuator and gun transfer function

The gyro dynamics, represented by D_g , add a lead term to the transfer function, which will increase the overshoot to a step input command. The gyro dynamics also add phase lag to the open loop system, and thus will reduce the damping. Therefore, compensation must be used to reduce the overshoot and phase lag resulting from the sensor dynamics.

5.7 FORWARD VERSUS FEEDBACK COMPENSATION

Lead-lag compensation must be used to reduce the overshoot and phase lag resulting from the sensor dynamics. In this section, a comparison is made between using this type of compensation in the forward or in the feedback path.

The block diagram in Figure 5-10 shows a system open loop transfer function with a gain term K_s in the numerator, dynamic terms D_s in the denominator, and with feedback compensation N_c/D_c .

The closed loop transfer function is

$$\frac{\dot{\theta}_g}{\dot{\theta}_s} = \frac{K_s D_c}{K_s N_c + D_c D_s}$$

The block diagram in Figure 5-11 shows the same system with forward compensation. The closed loop response is

$$\frac{\dot{\theta}_g}{\dot{\theta}_s} = \frac{K_s N_c}{K_s N_c + D_c D_s}$$

The response with feedback compensation has a lead term equal to the compensation denominator D_c . The response with forward compensation has a lead term equal to the compensation numerator N_c . Generally, the smaller the lead time constant, the less the overshoot will be. Therefore, when lead-lag compensation is used, it should be in the feedback path. When lag-lead compensation is used, it should be in the forward path.

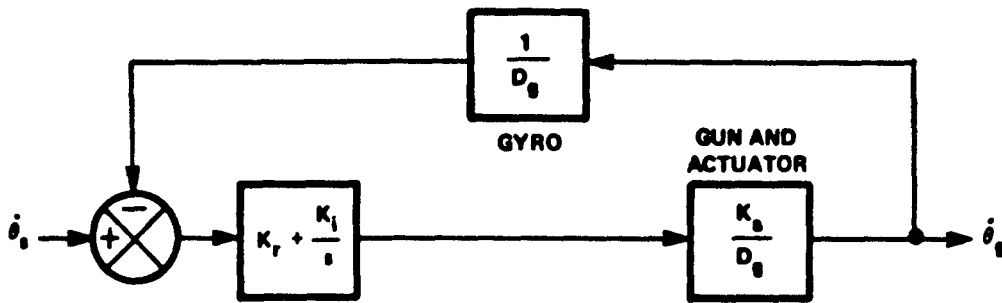


Figure 5-9. Block Diagram for Effect of Rate Sensor Dynamics on Response

R-109-8

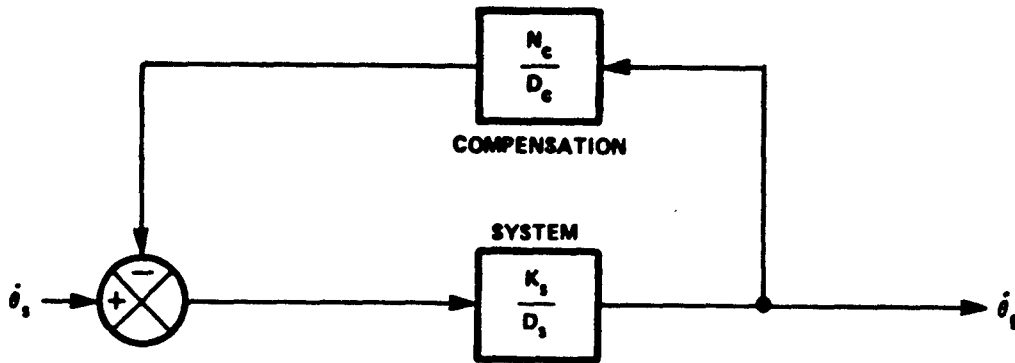


Figure 5-10. Simplified Block Diagram of System with Feedback Compensation

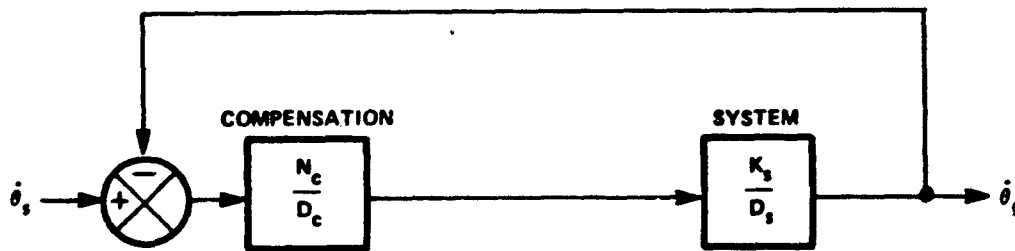


Figure 5-11. Simplified Block Diagram of System with Compensation in Forward Path

5.8 SYSTEM STIFFNESS

Stiffness is the reciprocal of the response to a disturbance torque. The static stiffness can be considered as the equivalent spring rate of the system. The tracking error resulting from a constant disturbance torque equals the disturbance torque divided by the static stiffness. The stiffness transfer function is

$$\frac{T_d}{\theta_g} = K_o \frac{1 + a_1 s + a_2 s^2 + a_3 s^3 + a_4 s^4}{(1 + \tau_p s) (1 + \tau_c s) + K_p \tau_p \frac{\partial T}{\partial \epsilon} s^2}$$

where

$$a_1 = \frac{1}{K_i \frac{\partial T}{\partial \epsilon}} \left[\frac{\partial T}{\partial n} + (K_r + K_i \tau_p) \frac{\partial T}{\partial \epsilon} \right]$$

$$a_2 = \frac{1}{K_i \frac{\partial T}{\partial \epsilon}} \left[J_g + \tau_p \frac{\partial T}{\partial n} + K_r \frac{\partial T}{\partial \epsilon} \right]$$

$$a_3 = \frac{1}{K_i \frac{\partial T}{\partial \epsilon}} \left[J_g (\tau_p + \tau_c) + K_p \tau_p \frac{\partial T}{\partial \epsilon} \right]$$

$$a_4 = \frac{1}{K_i \frac{\partial T}{\partial \epsilon}} J_g \tau_c \tau_p$$

The static stiffness is given by

$$K_o = K_i \frac{\partial T}{\partial \epsilon}$$

The stiffness should be high to minimize the effects of disturbance torques. Disturbance torques can result from gun bending mode vibrations, coupling, and bumps in the road. The static stiffness can be increased by increasing the system integral gain K_i . When K_i is increased, a low frequency dipole must be used in the forward path to lower the gain at high frequency as required for stability.

The analysis in Section 5.9 shows the effect of stiffness on tracking errors resulting from coupling.

5.9 COUPLING

The azimuth and elevation stabilization systems are coupled by both gyroscopic and hull roll rate effects. This section discusses this coupling and methods of minimizing their effect.

One cause of coupling between the azimuth and elevation axes is gyroscopic moments. According to the law for a gyroscope, if a mass is rotating about the x axis with angular momentum H_x , simultaneous rotation about the y axis will result in a torque about the z axis. Thus,

$$T_z = \omega_y \cdot H_x \quad (5-14)$$

where

$$H_x = J_x \omega_x \quad (5-15)$$

Applying this law to the elevation axis, with the gun pointing straight ahead, gives:

$$T_{gc} = \dot{\phi}_h \cdot J_{gy} \dot{\psi}_t + \dot{\psi}_t \cdot J_{gx} \dot{\phi}_h \quad (5-16)$$

where

J_{gx} = inertia of the gun about the roll axis

J_{gy} = inertia of the gun about the yaw axis

Thus, when turret rotation and roll occur simultaneously, the resulting torque T_{gc} is applied to the gun.

The gun moments of inertia about the yaw and roll axes are not known. A rough estimate of the inertia about the yaw axis was calculated by multiplying the gun mass by the square of the estimated distance from the gun's center of gravity to the center of turret rotation.

$$J_{gy} = 1.5^2 \times 100 = 225 \text{ kg-m-s}^2$$

The gun moment of inertia about the roll axis is assumed to be negligible.

The peak roll rate, from the HITPRO program, is 0.24 rad/s. The peak turret rate is assumed to be 1.571 rad/s.

The torque applied to the gun by the gyroscopic effect is thus

$$T_{gc} = \dot{\phi}_h \cdot J_{gy} \cdot \dot{\psi}_t = 0.24 \cdot 225 \times \frac{\pi}{2} = 85 \text{ kg-m}$$

The tracking error resulting from this torque is T_{gc} divided by the stiffness. The stiffness curve determined from the nonlinear computer simulation of the rate control system with electric gyro is shown in Figure 5-12. The stiffness at 0.6 Hz, the fundamental frequency of the bump course, is 5.6×10^5 kg-m/rad. Thus

$$TE = \frac{85}{5.6 \times 10^5} = 0.00015 \text{ rad (0.15 mil)}$$

When the gun is not pointing straight ahead, the coupling equation becomes

$$T_{gc} = (J_{gx} \cdot J_{gy}) (\dot{\phi}_h \cos \psi_t + \dot{\theta}_h \sin \psi_t) \dot{\psi}_t \quad (5-17)$$

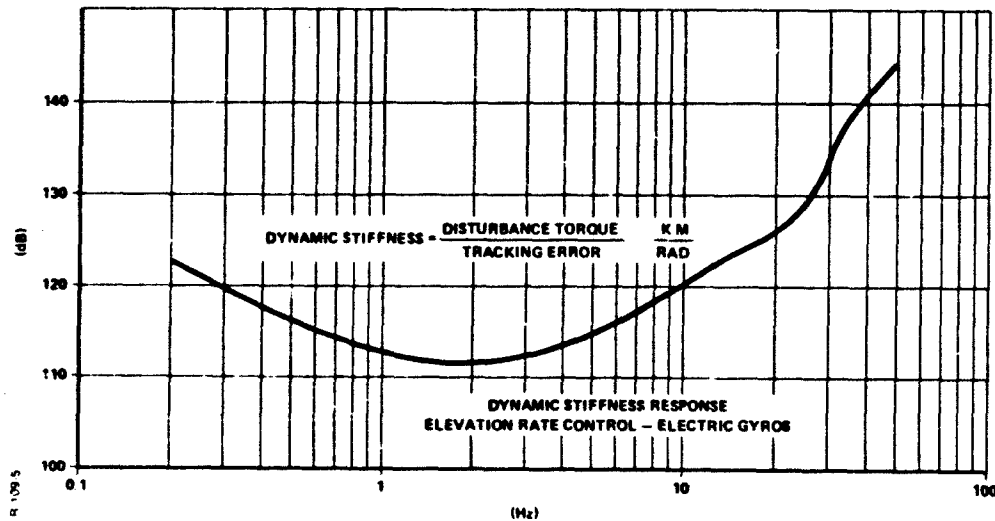


Figure 5-12. Dynamic Stiffness Curve

Similarly, for the azimuth axis, a torque T_{tc} is applied to the turret when the vehicle rolls while the gun is being rotated about the pitch axis, and when vehicle pitch and roll occur simultaneously.

$$T_{tc} = \dot{\phi}_h \cdot J_{tz} \dot{\theta}_h + \dot{\theta}_h \cdot J_{tx} \dot{\phi}_h + \dot{\phi}_h \cdot J_g \dot{\theta}_g$$

where

J_{tx} = inertia of turret about the roll axis

J_{tz} = inertia of turret about the pitch axis

The turret inertias are assumed to be equal about all three axes. The torque applied to the turret, using hull rates from HITPRO, is

$$\begin{aligned} T_{tc} &= 2 J_t \dot{\phi}_h \dot{\theta}_h + \dot{\phi}_h J_g \dot{\theta}_g = 2 \times 3140 \times 0.24 \times 0.18 + 0.24 \times 527 \times 1.05 \\ &= 408 \text{ kg-m} \end{aligned}$$

The dynamic stiffness curve was not run for azimuth. However, azimuth stiffness should be about six times higher than for elevation, due to the higher inertia of the turret. The higher stiffness in azimuth was indicated by the smaller tracking errors on the bump course with this axis. The estimated tracking error resulting from gyro effect is thus

$$TE = \frac{408}{6 \times 5.6 \times 10^5} = 0.00012 \text{ rad (0.12 mil)}$$

The estimated tracking errors are within the goal of 0.25 mil, but are large enough to be significant. The calculated values could be considerably in error if the estimated inertias are significantly in error.

Two methods can be used to reduce the tracking errors resulting from coupling. The first method is by increasing the stiffness. Stiffness is proportional to the integral gain K_I , as shown in Section 5.8. Therefore, increasing K_I will reduce the coupling error. It is also important to tune the system parameters and compensation so that the stiffness remains high over the frequency band of coupling.

The second method uses a hull roll rate sensor to cancel the coupling effect. The coupling error can probably be reduced to an acceptable level by increasing the stiffness. Therefore, the second method was not studied in detail.

A second coupling effect, for elevation, is the result of hull pitch angle, as seen by the gun, varying with turret angle. When the turret angle is zero, the torque acting on the gun is given by

$$T_{gl} = T_A - \left(D_{gh} + \frac{\partial T}{\partial n} \right) (\dot{\theta}_g - \dot{\theta}_h)$$

where D_{gh} is the trunnion friction and $\partial T/\partial n$ is the slope of the actuator torque-speed curve. The significance of the $\partial T/\partial n$ term will now be discussed. Figure 5-13 shows the gun with a piston actuator, and with the servovalve represented by orifice area A_v . If there were no oil in the cylinder, and no trunnion friction, hull pitch motion would not apply any torque to the gun. The gun inertia would then maintain the gun orientation fixed in space. However, when there is oil in the cylinder, any motion of the hull relative to the gun results in oil being pumped through orifice A_v . This flow causes a differential pressure to act on the piston, and thus applies a torque to the gun. The ratio of the torque to the relative velocity is the term $\partial T/\partial n$.

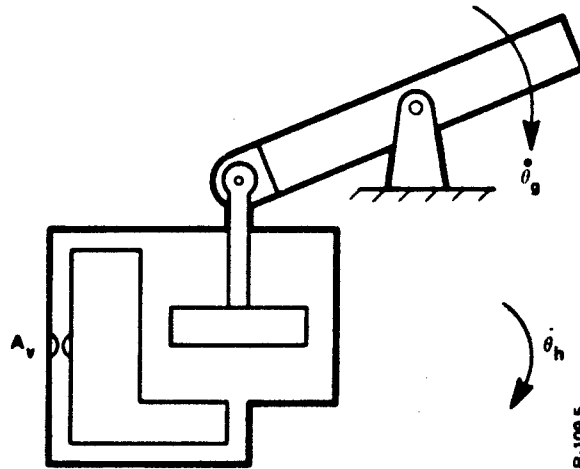


Figure 5-13. Schematic for Coupling of Hull Pitch Rate to Gun

The equation for friction coupling becomes considerably more complex when vehicle roll is considered.

A torque also results from hull acceleration. This torque is proportional to the gun mass unbalance $L_g M_g$ and the distance between the hull centers of rotation and the trunnion.

$$T_{g2} = L_g M_g (R_p \ddot{\theta}_h \cos \psi_t + R_h \ddot{\phi}_h \sin \psi_t)$$

The mass unbalance of the gun is small. Therefore, this term will probably be negligible.

A second coupling for azimuth results from the turret mass unbalance with respect to the turret center of rotation $L_t M_t$. When the turret angle is zero, hull roll motion applies a torque to the turret, but hull pitch has no effect. When the turret angle is 90 deg, hull pitch motion applies a torque to the turret, and hull roll has no effect. The equation for the torque applied to the turret by these effects is

$$T_t = L_t M_t (\sin \theta_h \sin \psi_t + \sin \phi_h \cos \psi_t)$$

5.10 SUMMARY OF ANALYTICAL SYSTEMS STUDY

Following is a summary of the results obtained and methods of synthesis accomplished by means of the analytical systems study. Some of these items proved to be irvaluable in the subsequent computer analysis of the system.

- (1) A linear model of the stabilization system was derived which aided in the design of the control system and allowed the establishment of an initial set of control gains.
- (2) For terrain inputs, the responses of the rate and position command systems are identical.
- (3) Two methods can be used to reduce the tracking error resulting from hull motion. These are:
 - (a) Cancellation of hull rate using hull rate sensor
 - (b) Lag-lead compensation with high loop gain
- (4) A sensor error analysis restricted to gain and offset errors showed that only gun sensor offset errors are significant and cause the tracking error to increase with time.
- (5) A method was developed for eliminating the effects of sensor offset errors and integrator drift.

- (6) Sensor dynamics increase overshoot and reduce stability.
- (7) Lead-lag compensation will be required if the gun rate sensor phase lag is significant.
- (8) When a lead-lag configuration is used, it should be in the feedback path.
- (9) The integral control gain K_I should be high to maximize system stiffness and minimize the effects of disturbance torques.
- (10) When vehicle roll rates occur, significant coupling between the azimuth and elevation axes takes place in the form of gyroscopic moments and other effects.

SECTION 6
SIMULATION ANALYSIS RESULTS

6.1 GENERAL

This section contains a detailed description of the analog and digital computer results obtained in this study for the gun stabilization system. The objectives of the computer study are outlined here. The organization of the relevant computer program as well as a summary of the types of inputs and outputs are discussed in Section 6.2. Section 6.3 compares the rate and position command systems. The results of a preliminary computer analysis evaluating the effects of nonlinear valve flow, vehicle hull dynamics, and hydraulic fluid compressibility are described in Section 6.4. The effects of these nonlinearities needed to be evaluated in order to judge whether or not they would be included in the detailed simulation models. A detailed evaluation of the complete stabilization system and the five candidate sensors are contained in Sections 6.5 and 6.6.

The following is a summary of the objectives considered in this systems study.

- (1) Evaluate the effects of the nonlinear valve flow equations versus linearized flow, and the effect of hull dynamics.
- (2) Derive stabilization system configurations for each of the sensors, and define gains and compensation networks required to meet the performance goals with each system.
- (3) Investigate the effects of sensor gain variation, sensor dead-band, and actuator friction on tracking error.
- (4) Perform detailed evaluation of the five prospective sensors for this application.
- (5) Determine the system time response for step and sinusoidal inputs.
- (6) Determine the tracking error for sinusoidal hull rates and for bump course using the HITPRO digital computer program.
- (7) Determine the gain and phase margins for each configuration.

The following sensors were analyzed in detail.

- (1) Elevation Axis
 - Two electric gyros.
 - Two hydraulic rate sensors (GE).
 - Two laminar vortex rate sensors (Honeywell).
 - One integrating accelerometer (Bendix).

(2) Azimuth Axis

Two electric gyros

One pneumatic accelerometer (AiResearch)

Rate sensors can be used in either one (gun) or two (gun and hull) sensor configurations. Only the rate sensor configuration utilizing two sensors was analyzed in this study.

Accelerometers can be used in only the one sensor configuration. Since the accelerometer signal is integrated to obtain the rate signal, an accelerometer for sensing hull rate would have an open loop integrator which would result in excessive drift rates. On the other hand, the gun sensor integrator is within a closed control loop. Under those conditions, integrator drift will have less effect.

6.2 SIMULATION APPROACH

The organization of the computer programming approach utilized for the analog, hybrid, and digital computer programs is described in this section. The types of inputs, organization of the analog computer boards, analog computer switch logic utilized, and the hybrid computer inputs are also described. Detailed listings of all digital computer programs are contained in Appendix A. Analog and hybrid program wiring diagrams are presented in Appendix B.

Digital computer solutions were obtained for each system configuration as checks on the analog computer simulations. The following inputs were generally used for the digital computer simulations.

- (1) Command rate step inputs
- (2) Hull rate step inputs
- (3) Hull rate sinusoidal inputs

The analog program of the control system was initiated by means of a simplified linear model. The nonlinear flow equations, sensor dynamics, nonlinear friction, and deadband were added one at a time, so that their effects could be assessed individually.

In order to facilitate the selection of the various components for a particular computer simulation run, automated computer switches were used for the following purposes.

- (1) Selecting one of the five sensors.
- (2) Selecting either a two sensor configuration using a hull sensor and a gun sensor or a one sensor configuration using only a gun sensor.
- (3) Selecting either forward or feedback path compensation.

The following inputs were used for the hybrid computer study for determining time and frequency responses.

- (1) Step command rate input.
- (2) Sinusoidal rate command input.
- (3) Step hull rate input.
- (4) Sinusoidal hull rate input.
- (5) Simulated bump course from program HITPRO.

The step and sinusoidal command inputs used were sufficiently small to avoid saturation of any component of the simulation. A hull rate input in the azimuth axis as used here is representative of a pivot steer maneuver. The digital program HITPRO was used to provide realistic hull motion for the simulated bump course. To implement these rates in the simulation, the hull pitch motion was stored in the digital part of the hybrid computer from a magnetic tape and was then used for providing the elevation hull rate inputs. The same rate input was used for the azimuth axis because no comparable azimuth rates were available from the HITPRO program. This is a valid procedure since the power spectral densities of the hull pitch and yaw motions are approximately the same.

The sinusoidal hull rate input used was of approximately the same amplitude as the maximum hull rate observed for the bump course, and of approximately the same frequency as the bump course fundamental frequency.

6.3 COMPARISON STUDY OF RATE AND POSITION CONTROL FOR STABILIZATION

As discussed in Section 5.2.2, the transfer functions for hull rate inputs are the same for both the rate and position command systems. Also, the transfer functions for command inputs are the same if, for the position control system, the input compensation term $s/(\tau_1 s + 1)$ is a perfect derivative.

In order to verify the above results, a computer study was made to compare responses using the rate and position command simulation models. Each of the rate and position command systems was modelled with equal gains and compensation networks and with two electric gyro sensors. A perfect derivative of the position command θ_g was used in the position system. The frequency response curves of the two systems are shown in Figures 6-1 and 6-2. Figure 6-1 verifies that the two systems are, in fact, equivalent.

In an actual system, a perfect derivative cannot be generated; instead, an approximation to it must be generated by the input compensation network of the type $s/(\tau_1 s + 1)$. Figure 6-2 shows the system frequency response using a perfect derivative and with $\tau_1 = 0.01$ s for the input compensation network.

As a result of this study, the performance evaluations of each of the five sensor configurations were conducted using the rate command system only.

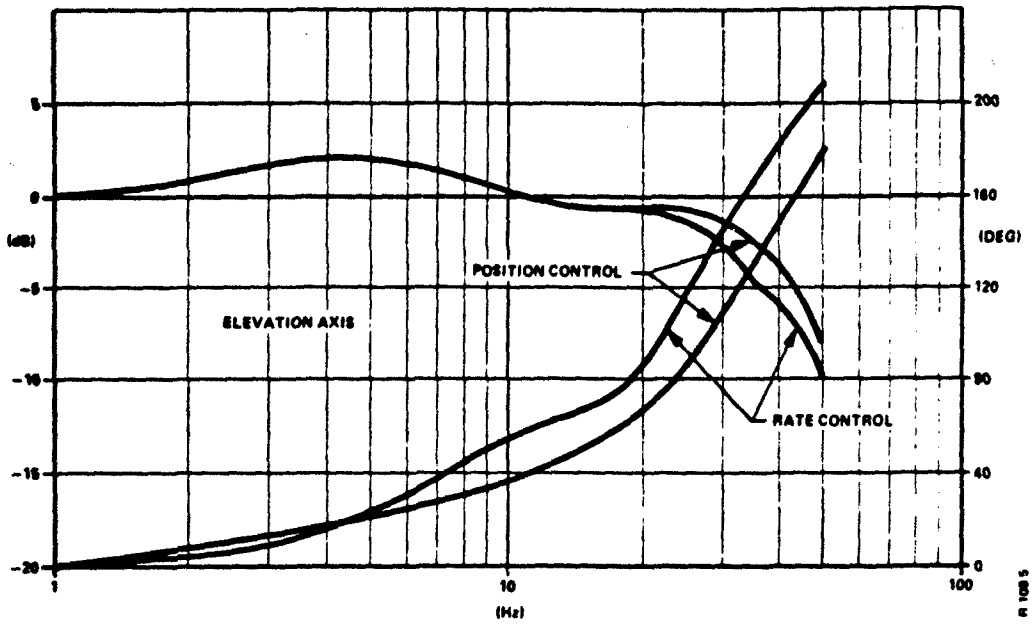


Figure 6-1. Frequency Response - Position Control

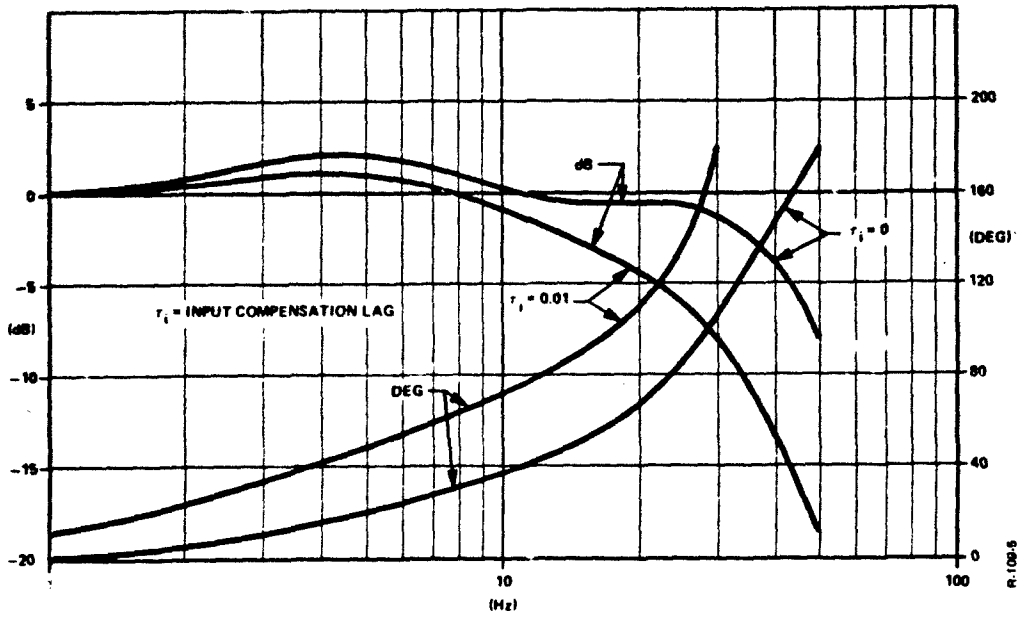


Figure 6-2. Frequency Response - Position Control and Rate Control

6.4 PRELIMINARY SIMULATION STUDIES

6.4.1 Effect of Nonlinear Valve Flow

It was found by means of the computer simulation that the rate command system (with ideal sensors) exhibited basically the same step response with the linear flow models as with the nonlinear. When the electric gyro dynamics were added, the nonlinear model became unstable, while the linear model remained stable. This indicates that the nonlinear flow model has less phase margin than the linear model. The nonlinear flow model was therefore used for all subsequent system studies.

6.4.2 Effect of Hull Dynamics

Hull dynamics modelled in this simulation represent the effect observed when the actuator applies torque to the gun. At that point an equal and opposite torque is applied to the hull and the resulting hull motion affects the gun. The simulation was used to determine system response to command and hull rate inputs, with and without hull dynamics. It was found that hull dynamics had a negligible effect on system response and on the tracking error. As a result, hull dynamics were not included in the model for subsequent studies.

6.4.3 Effects of Changes in Fluid Compressibility and Bulk Modulus

The volume under compression V modelled in this simulation consists of the high pressure fluid in the servovalve, actuator, and connecting lines. The numerical value for V used here was obtained from the bibliography. This value seems large and indicates that in the past, long connecting lines were used. To determine whether this significantly affected system performance, a step response simulation was performed with a 10 percent reduction in the value of V . A negligible change in the step response of the system was observed.

The effect of a drastic change in the bulk modulus was also determined. This effect represents the process of air entering the hydraulic fluid. It was found that reducing the fluid bulk modulus B by 50 percent, has a negligible effect on the system step response and stability. These results indicate that the amount of pressure feedback used here was great enough to compensate for the large volume under compression.

Compressibility may have different effects when compliance and gun bending modes are added to the model. These effects should therefore be evaluated again in future studies when bending modes and compliance have been modelled.

6.5 EVALUATION OF SENSORS IN ELEVATION AXIS

Sections 6.5 and 6.6 contain the evaluation of each of the five sensors studied. Time and frequency response plots are presented to

illustrate the results. The results for the sensors in Section 6.5.1 through 6.5.4 are based on elevation (gun) axis parameters while the results for the pneumatic accelerometer in Section 6.6 are based on azimuth axis parameters. All simulation results presented here are based on the rate command control concept as pointed out in Section 6.3.

6.5.1 Evaluation of Electric Rate Gyros

A block diagram of the rate command system with two electric rate gyros is presented in Figure 5-6. A hull rate sensor is used for cancellation of hull rate coupling, and a gun rate sensor is used for closing the control loop. Lead-lag compensation is used to compensate for sensor phase lag, and thus to improve stability. Compensation is in the feedback path. This is the best location for the compensation in order to reduce the overshoot to command step inputs. (See Section 5.7.)

Using the hybrid computer simulation, the gains were adjusted to obtain the desired frequency response, stability, and tracking error. The resulting gain values and compensation are:

$$K_i = 50 \text{ 1/s}$$

$$K_r = 7.5$$

$$K_p = 2.5 \times 10^{-4} \text{ rad/(s-kg-cm}^2\text{)}$$

$$K_h = 0.15$$

$$\text{Feedback compensation } \frac{1 + 0.008 \text{ s}}{1 + 0.0016 \text{ s}}$$

The response to a command step input $\dot{\theta}_g = \text{rad/s}$ was obtained, and is shown in Figure 6-3. The gun rate reaches the commanded speed, 0.05 rad/s, in about 0.04 s, overshoots about 15 percent, then settles to the commanded speed with no oscillations. The absence of oscillations indicates good damping. In the absence of a specific performance requirement for step response, the speed of response as well as damping appear satisfactory.

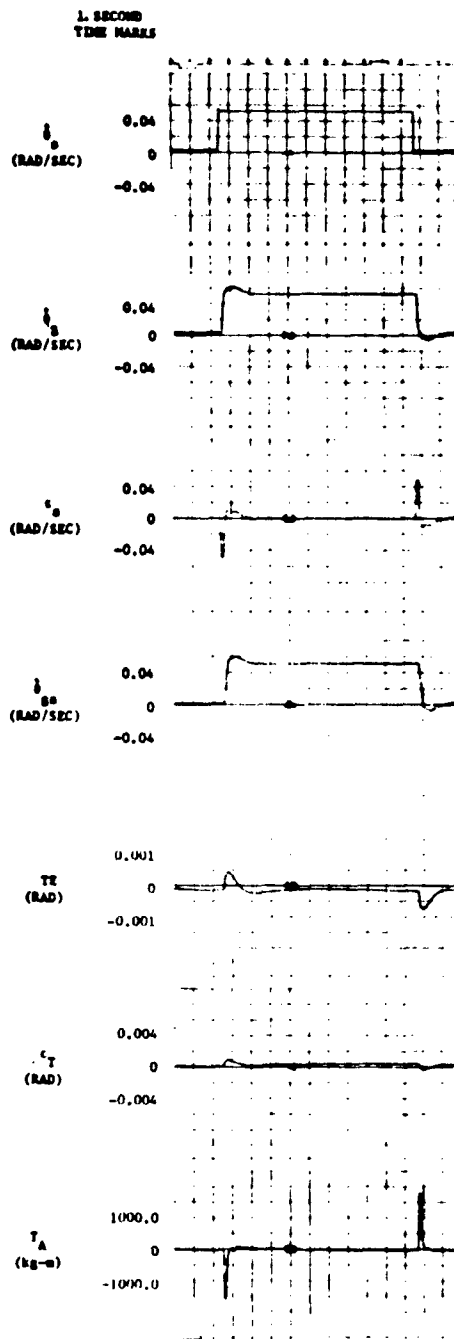


Figure 6-3. Response to a Command Step Input - Elevation Rate Control with Electric Gyros

The error rate signal ϵ_s given by $\epsilon_s = \dot{\theta}_s - \dot{\theta}_{gs}$ is the input for the open loop response. The open loop response is given by:

$$\frac{\dot{\theta}_{gs}}{\dot{\theta}_s - \dot{\theta}_{gs}}$$

The variable $\dot{\theta}_{gs}$ (sensed gun rate) is the output signal for the open loop response. The variables θ_s and θ_{gs} are used mainly for determining frequency response, gain margin, and phase margin. These variables are also used as an aid in tuning the system.

The tracking error TE and the sensed tracking error ϵ_T are defined as:

$$TE = \theta_s - \theta_g$$

$$\epsilon_T = \int \epsilon_s dt = \theta_s - \theta_{gs}$$

The variable TE originates at an open loop integration and therefore tends to drift. The variable ϵ_T is obtained from within the closed loop and generally does not drift. These two signals are nearly identical except when sensor deadband or a high frequency input are used. The actuator torque T_A is also shown.

The response to a sinusoidal hull pitch rate is shown in Figure 6-4. The pitch rate input is:

$$\dot{\theta}_h = 0.18 \sin (2\pi \times 0.6 t) \text{ rad/s}$$

This input is approximately equal to the most severe pitch rate experienced on the simulated bump course. As shown in Figure 6-4, the resulting tracking error has a peak-to-peak amplitude of 0.18 mil and thus meets the pointing performance specification of the system.

The closed loop frequency response curves $\dot{\theta}_g/\dot{\theta}_s$ are shown in Figure 6-5. The open loop frequency response curves were used for determining the gain and phase margins. An input signal amplitude of

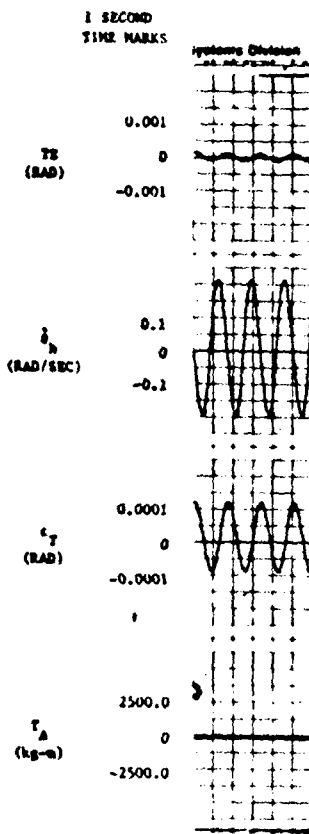


Figure 6-4. Response to Sinusoidal Pitch Rate - Elevation Rate Control with Electric Gyros

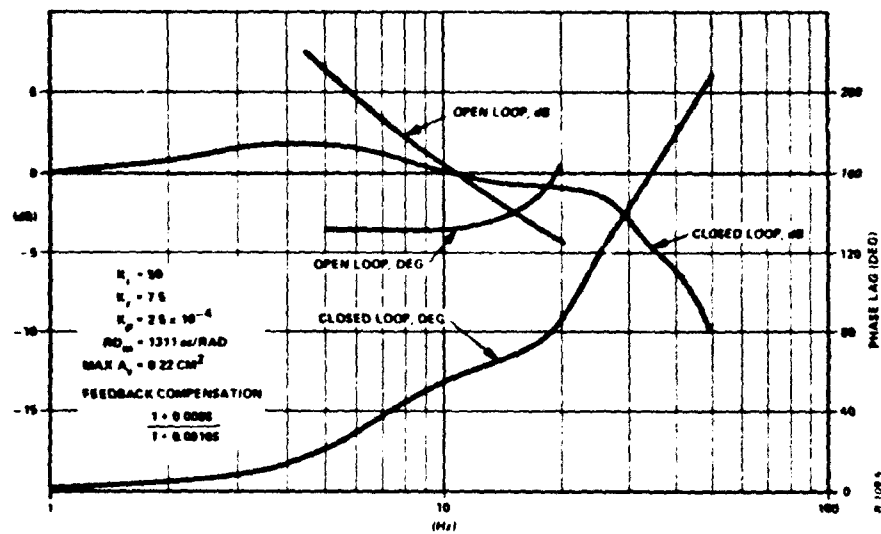


Figure 6-5. Closed Loop Frequency Response Curves - Elevation Rate Control with Electric Gyros

0.03 rad/s peak to peak was used for all frequency response tests. The frequency response results are as follows.

System bandpass: 28 Hz
Open loop phase lag
at gain crossover: 108 deg
Phase margin: 180 deg - 108 deg = 72 deg
Gain margin: 0.5

The system gain margin was determined by increasing the gain until instability resulted. It was found that the system was stable with the gain doubled, and unstable with higher gain. This is equivalent to a gain margin of 0.5.

The frequency response results meet or exceed the performance criteria specified in Section 3.3.

Time response plots using inputs consisting of vehicle rates from the simulated bump course of the HITPRO program are given in Figures 6-6 through 6-8. Graphs summarizing these results are presented in Figures 6-9 and 6-10. The maximum tracking error for nominal conditions ($K_h = 0.15$) was 0.18 mil peak to peak.

Figure 6-9 shows that a hull sensor gain error of 50 percent increased the tracking error to 0.4 mil.

Figure 6-10 shows that combined coulomb and stiction friction of 50 kg-m each, increased the tracking error to 0.4 mil.

The 0.18 mil tracking error observed with nominal conditions is well within the 0.5 mil criteria listed in Section 3.2. Note however that the combined effects of sensor gain error, sensor deadband, friction, noise, and cross-coupling of axes will increase the tracking error. The tracking error can then be reduced by increasing the system low frequency gain. This can be accomplished by adding lag-lead compensation in the forward path, of the form:

$$\frac{\tau_2}{\tau_1} \frac{1 + \tau_1 s}{1 + \tau_2 s}$$

A graph demonstrating dynamic stiffness is presented in Figure 6-11. These results were obtained by applying a sinusoidal disturbance torque, and recording tracking error as the output signal. Stiffness is the ratio of the torque amplitude to the tracking error. The minimum stiffness was found to be 111 dB. The dynamic stiffness should be high to minimize the effects of coupling and bending mode vibration.

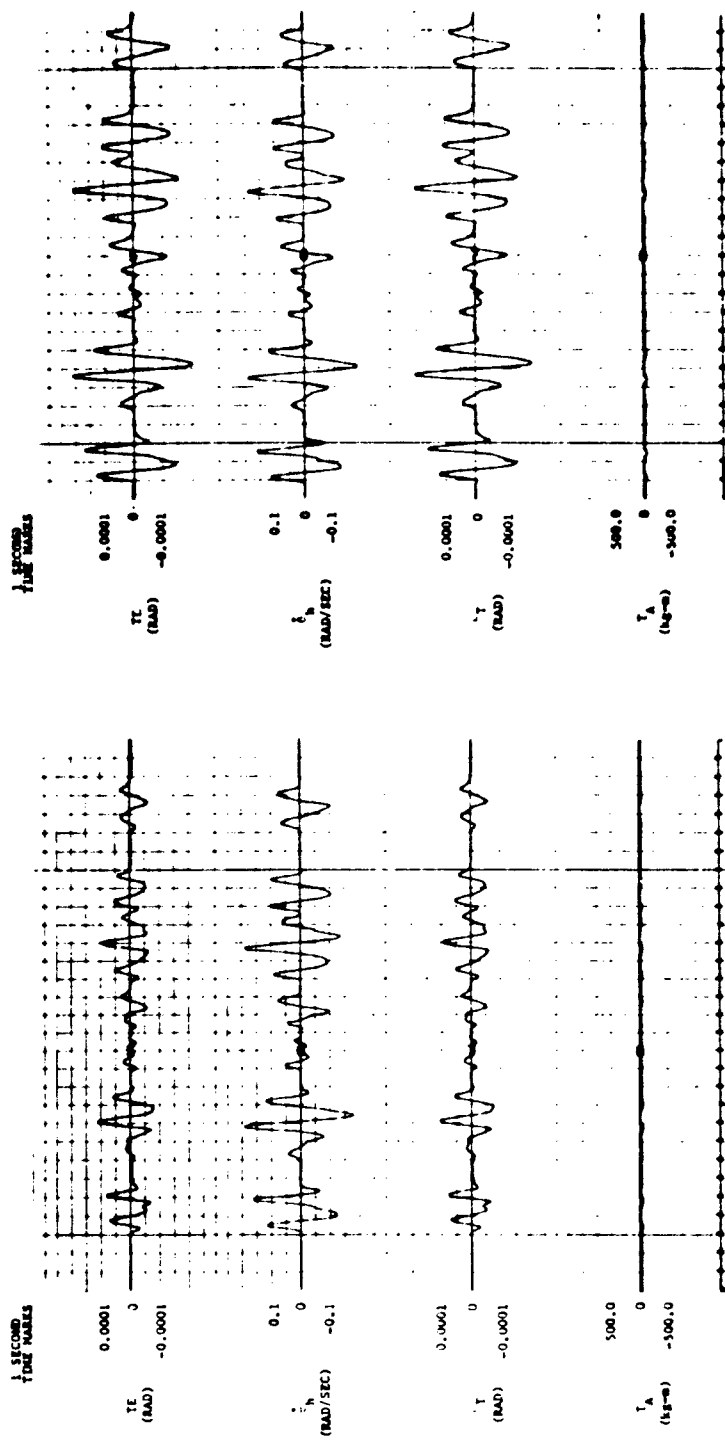


Figure 6-6. Response to HITPRO Simulated Bump Course - Elevation Rate Control with Electric Gyros

Figure 6-7. Response to HITPRO Bump Course with Hull Sensor Gain Error - Elevation Rate Control with Electric Gyros

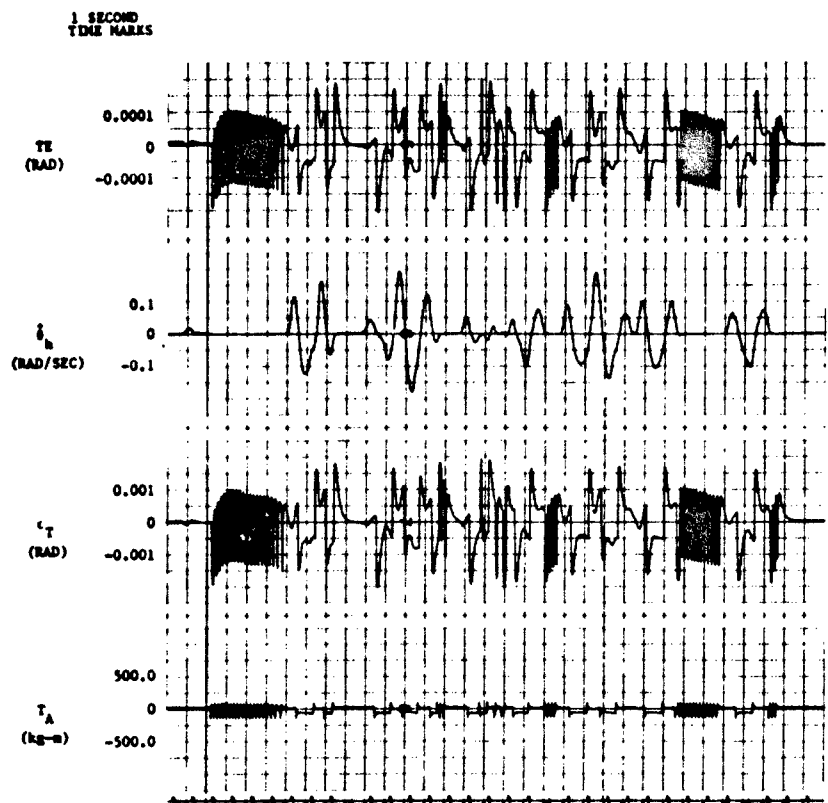


Figure 6-8. Response to HITPRO Bump Course with Coulomb and Stiction Friction - Elevation Rate Control with Electric Gyros

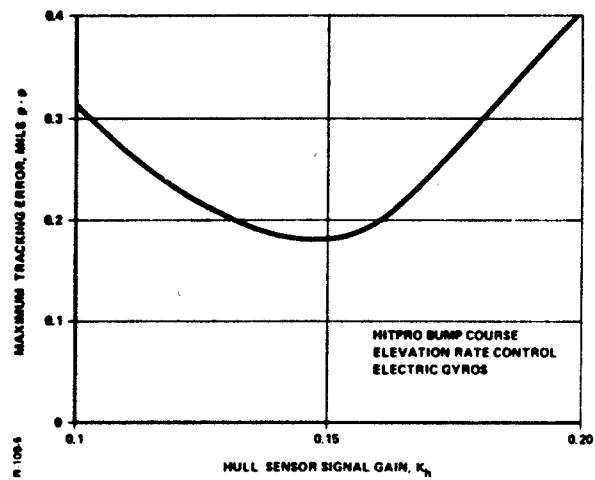


Figure 6-9. Graph of Tracking Error Versus Hull Sensor Gain Error - Elevation Rate Control with Electric Gyros

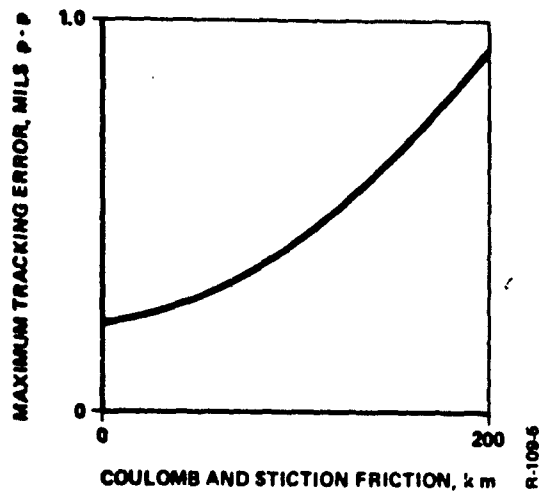


Figure 6-10. Graph of Tracking Error Versus Friction - Elevation Rate Control with Electric Gyros

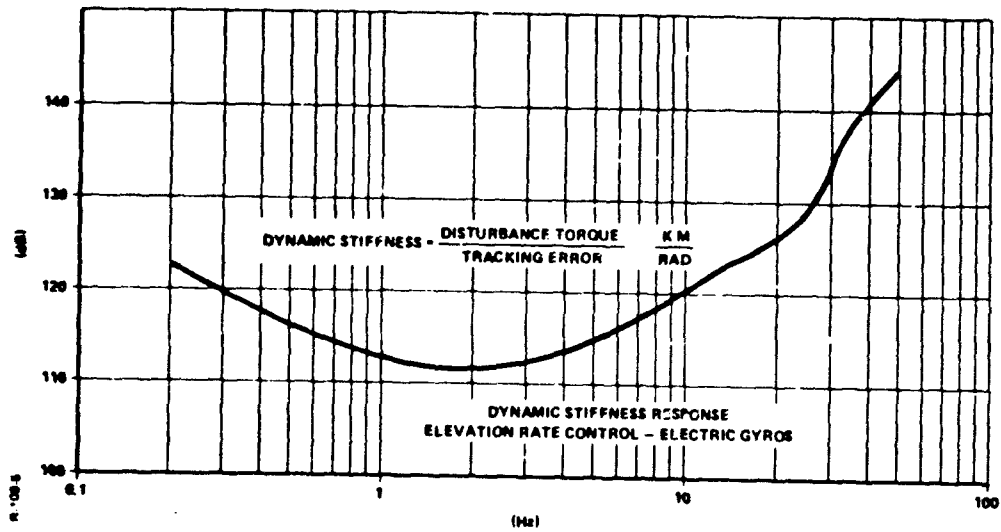


Figure 6-11. Dynamic Stiffness - Elevation Rate Control with Electric Gyros

6.5.2 Evaluation of Hydraulic Rate Sensor

Figure 5-6 is a block diagram of the stabilization system with the hydraulic rate sensor. The basic configuration is the same as with two electric gyros. Control gains and feedback compensation were identical to those used with the electric gyros.

Using the hybrid computer, the response of the system to a step rate command θ_s was obtained. As shown in Figure 6-12, this step response exhibited a 20 percent overshoot. The response time is about the same as for the system with two rate gyros.

The response to sinusoidal hull motion of an amplitude equivalent to the bump course is shown in Figure 6-13. The tracking error observed was 0.12 mil peak to peak.

The frequency response results shown in Figure 6-14 can be summarized as follows.

Bandpass: 13 to 37 Hz
Gain margin: 0.53
Phase margin: 50 deg

Note that the amplitude ratio is down 3 dB at 13 Hz and drops to -5 dB at 21 Hz. Modification of the feedback compensation network will allow improvement of the system bandpass.

The response to the HITPRO simulated bump course is shown in Figures 6-15 through 6-17. Figure 6-18 shows the maximum observed tracking error versus hull sensor gain error. A gain error of 33 percent increased the maximum tracking error to 0.38 mil. The maximum tracking error versus sensor threshold or deadband is shown in Figure 6-19. A deadband of 6 mils increases the tracking error to 2 mils. The effects of combined deadband and friction effects are shown in Figure 6-20. A small amount of friction has the effect of reducing the tracking error. Larger amounts of friction increase the tracking error. The combination of deadband and friction increases the tendency for limit cycling.

6.5.3 Evaluation of Integrating Accelerometer

The block diagram of the stabilization system with an integrating accelerometer is presented in Figure 5-7. Only a single sensor, mounted on the gun, is used. The processed sensor signal is proportional to acceleration at frequencies below 0.1 Hz and to rate above 0.1 Hz. In the simulation model, the compensation network was designed to integrate the sensor signal below 0.1 Hz and thus to provide a rate signal at all frequencies.

Since there is no hull sensor, the system gain must be increased to reduce the tracking error. To achieve this, compensation was used in the forward path. The type of compensation increases the

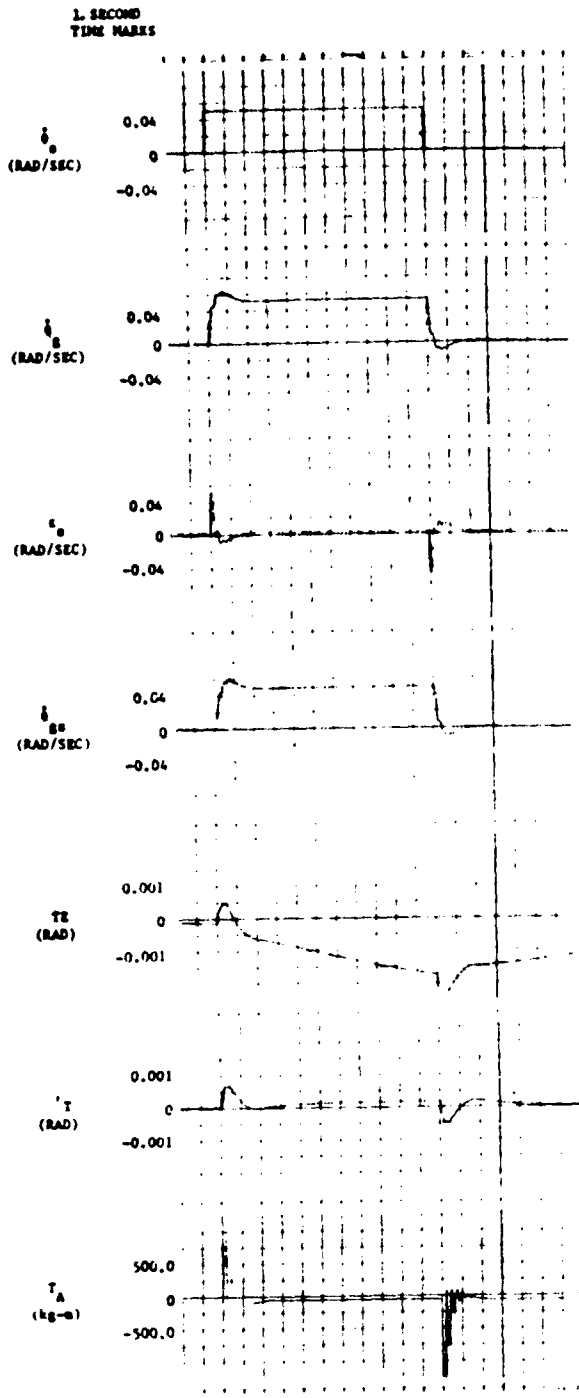


Figure 6-12. Response to a Step Rate Command - Hydraulic Rate Sensor

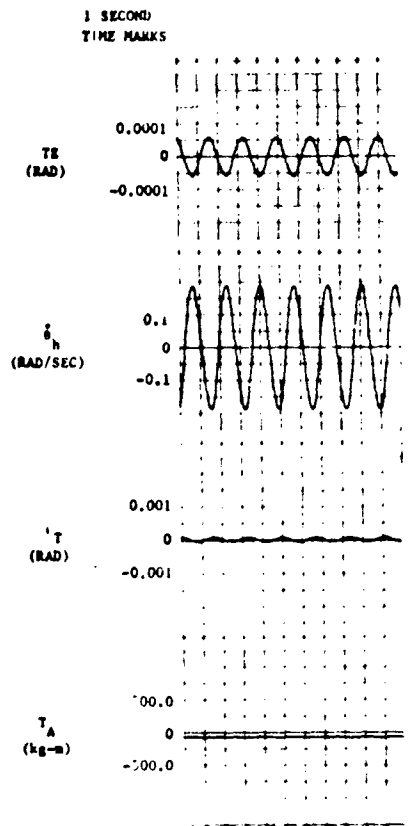


Figure 6-13. Response to Sinusoidal Hull Motion - Hydraulic Rate Sensor

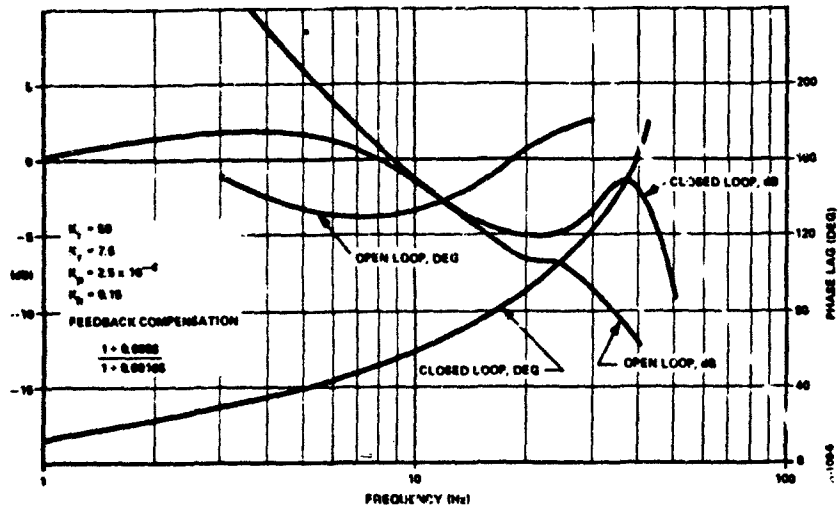


Figure 6-14. Frequency Response - Hydraulic Rate Sensor

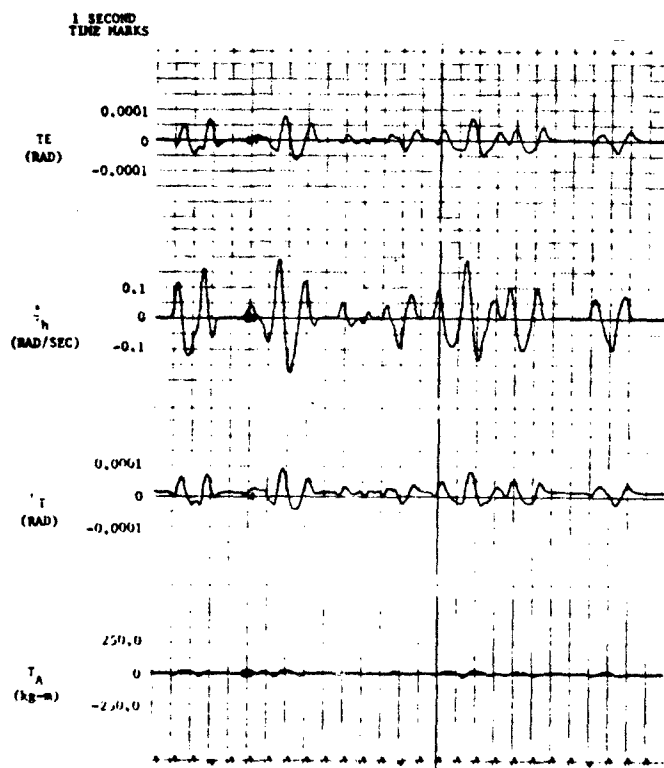


Figure 6-15. Response to HITPRO Simulated Bump Course - Hydraulic Rate Sensor

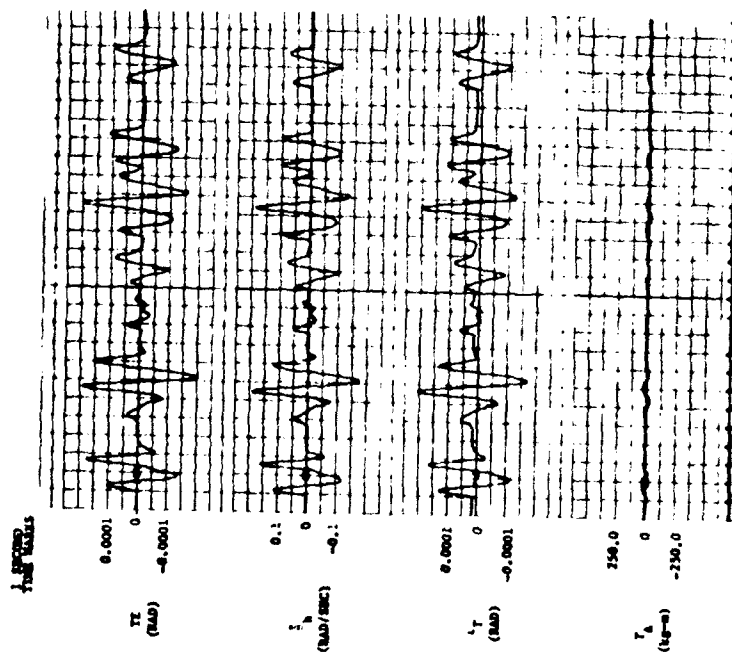


Figure 6-16. Response to HITPRO Bump Course with Hull Sensor Gain Error - Hydraulic Rate Sensor

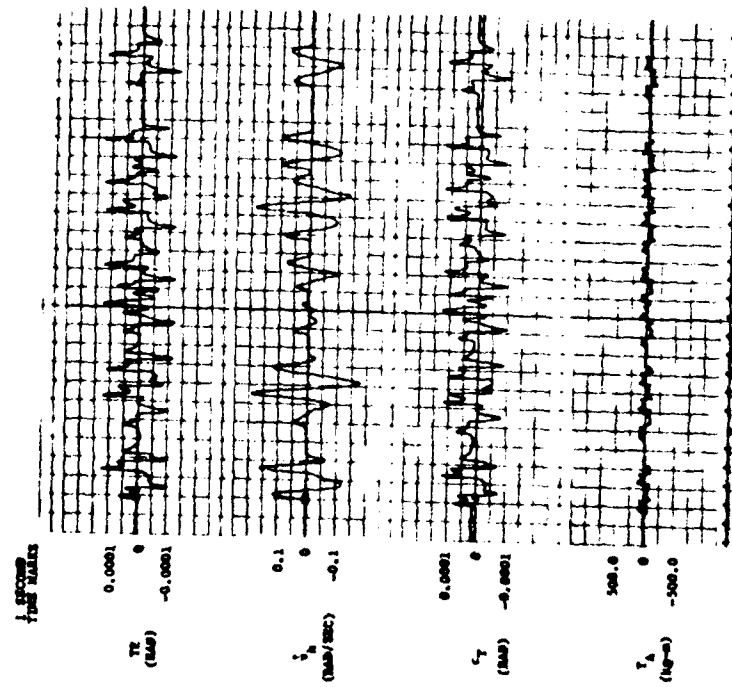


Figure 6-17. Response to HITPRO Bump Course with Coulomb and Stiction Friction - Hydraulic Rate Sensor

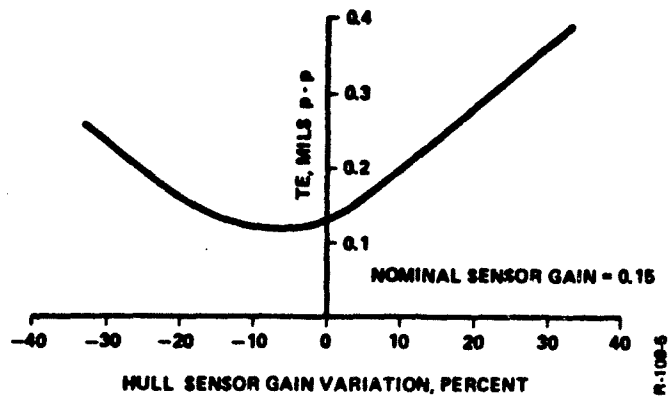


Figure 6-18. Graph of Tracking Error Versus Hull Sensor Gain Error - Hydraulic Rate Sensor

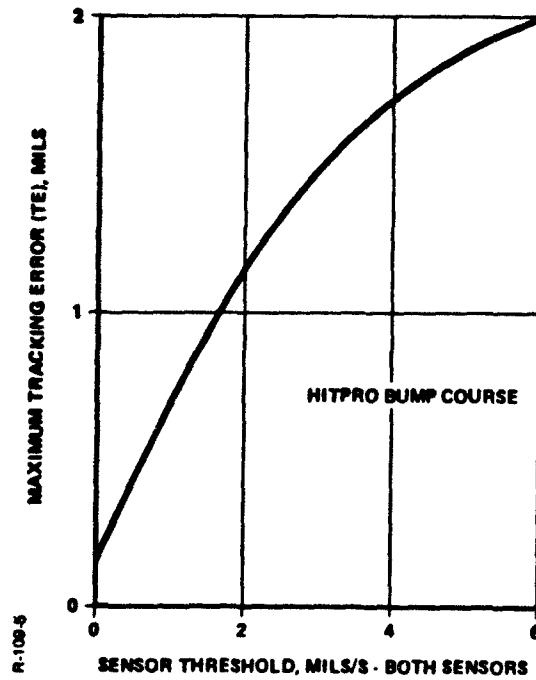


Figure 6-19. Tracking Error Versus Sensor Deadband - Hydraulic Rate Sensor

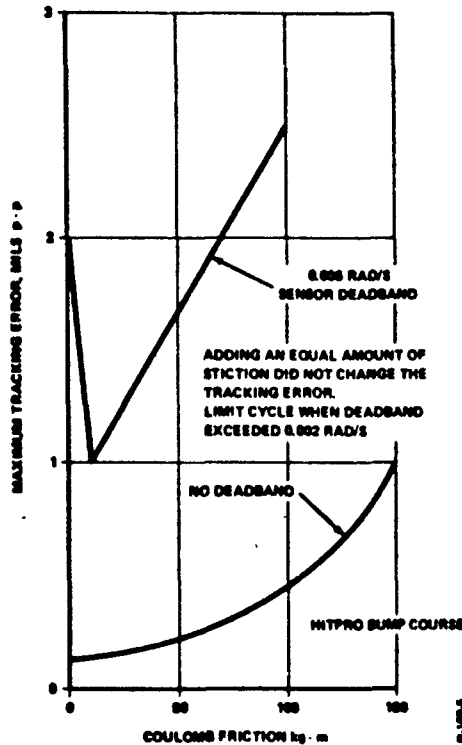


Figure 6-20. Effects of Combined Hull Sensor Deadband and Friction - Hydraulic Rate Sensor

gain at low frequencies and decreases the gain at high frequencies as is required for stability. The forward compensation and system gains established using the hybrid computer simulation are as follows:

$$\text{Forward compensation: } 10 \frac{1 + 0.055 s}{1 + 0.55 s}$$

$$\begin{aligned} \text{Control gains: } \quad K_I &= 250 \\ K_T &= 7.5 \\ K_P &= 2.5 \times 10^{-4} \end{aligned}$$

The step response of this sensor configuration to a command rate input is shown in Figure 6-21. The response has a 60 percent overshoot. This overshoot can be reduced significantly using a lead-lag feedback compensation.

The response to a sinusoidal hull input, equivalent in amplitude to the most severe motion for the bump course, is shown in Figure 6-22. The tracking error observed was 0.11 mil peak to peak. The response to the actual HITPRO bump course is shown in Figure 6-23.

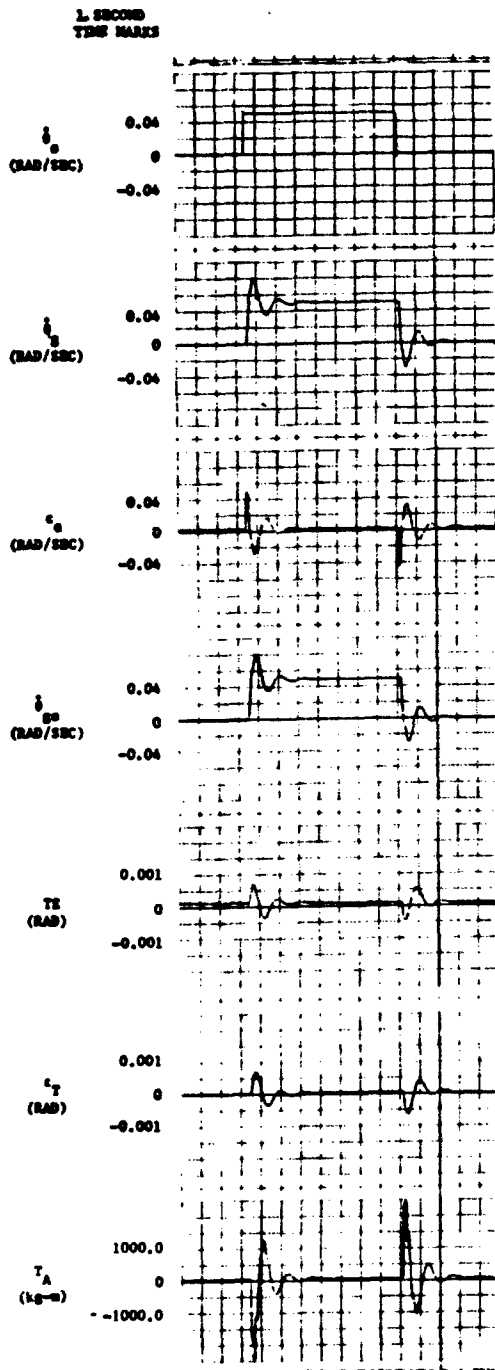


Figure 6-21. Response to a Step Rate Command - Integrating Accelerometer

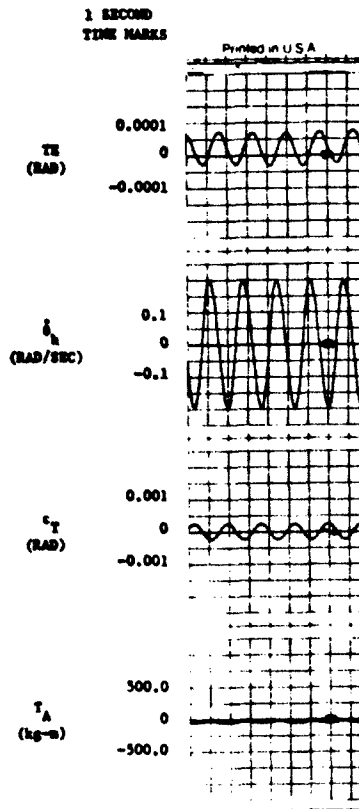


Figure 6-22. Response to Sinusoidal Hull Motion - Integrating Accelerometer

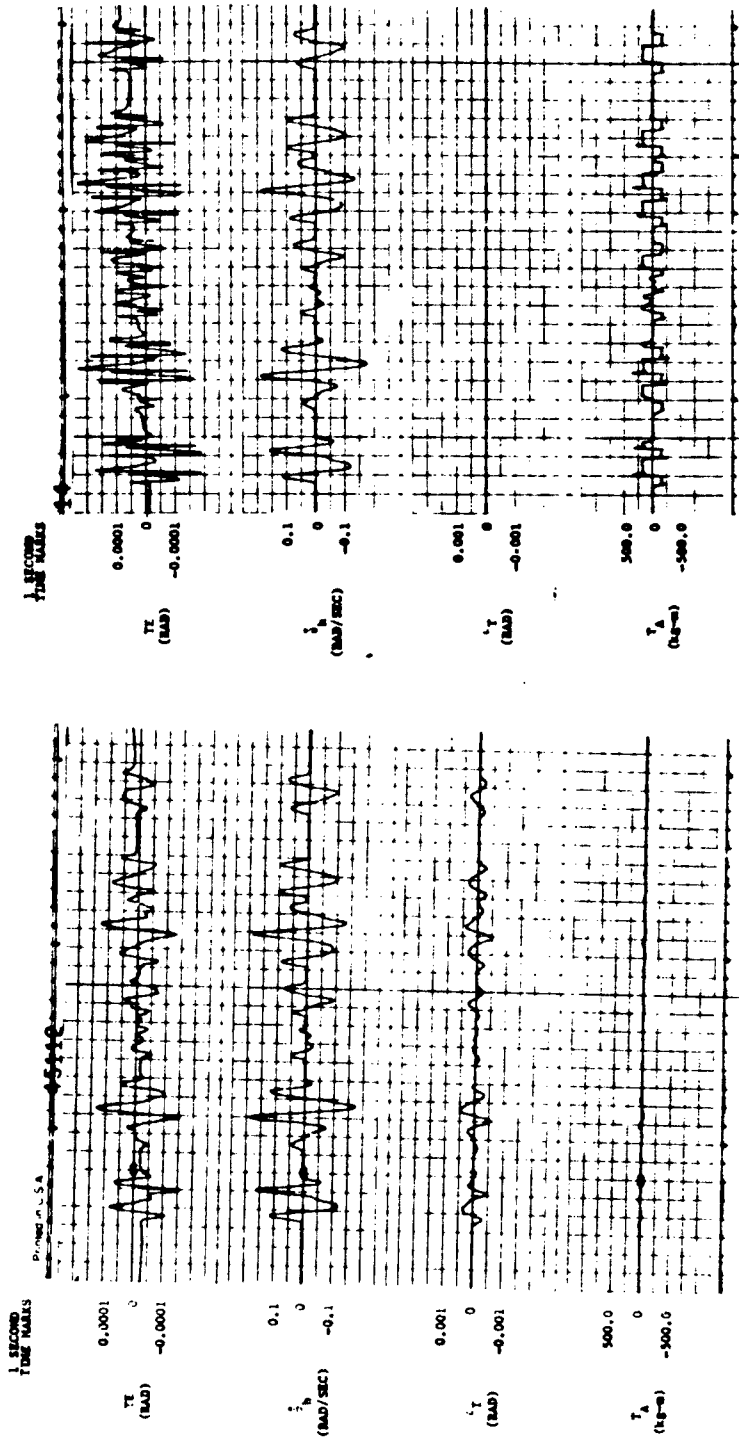


Figure 6-23. Response to HITPRO Bump Course Integrating Accelerometer

Figure 6-24. Response to HITPRO Bump Course with Coulomb and Stiction Friction - Elevation Rate Control with Integrating Accelerometer

The maximum tracking error observed is 0.28 mil peak to peak. The tracking error for the HITPRO input could be reduced by modifying the compensation.

Coulomb and stiction friction values of 100 kg-m each increased the tracking error to 0.38 mil, as shown in Figure 6-24. Figure 6-25 shows the maximum tracking error for various values of friction.

The frequency response curves are shown in Figure 6-26. The frequency response results can be summarized as follows.

Bandpass: 16 Hz
Gain margin: 0.53
Phase margin: 45 deg

6.5.4 Evaluation of Laminar Vortex Sensor

A block diagram for the rate command system with two laminar vortex sensors is shown in Figure 5-6. The sensor models consist of a single lag and a time delay. The time delay was simulated in the digital part of the hybrid computer. To achieve this for the gun rate sensor, the gun rate signal from the analog computer was fed into the digital computer, delayed in time, and then fed back to the analog computer. For the hull sensor, the hull rate from the HITPRO program was delayed in time in the sensor path, but used without time delay in the remaining portion of the simulation.

The step response to a rate command input is shown in Figure 6-27. A 30 percent overshoot is exhibited.

The response to the simulated bump course using the HITPRO program is shown in Figures 6-28 and 6-29 for hull sensor gains of 0.15 and 0.20, respectively. A plot of tracking error versus hull sensor gain K_h is shown in Figure 6-30. From this graph, a gain of 0.15 was selected as the nominal value with the minimum tracking error. Increasing K_h to 0.20 increased the tracking error to 0.6 mil. Decreasing K_h to 0.10 increased the tracking error to 0.28 mil.

The sinusoidal hull input response was not obtained for this sensor.

The frequency response curves are shown in Figure 6-31. The frequency response results are summarized as follows.

Bandpass: 25 Hz
Gain margin: 0.50
Phase margin: 50 deg

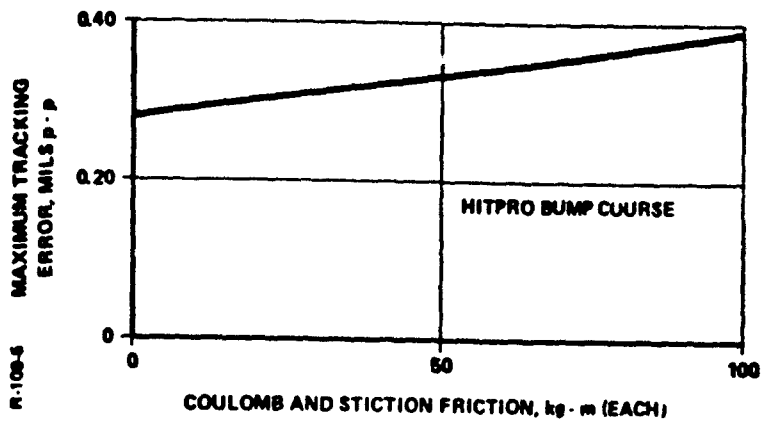


Figure 6-25. Maximum Tracking Error Versus Friction - Integrating Accelerometer

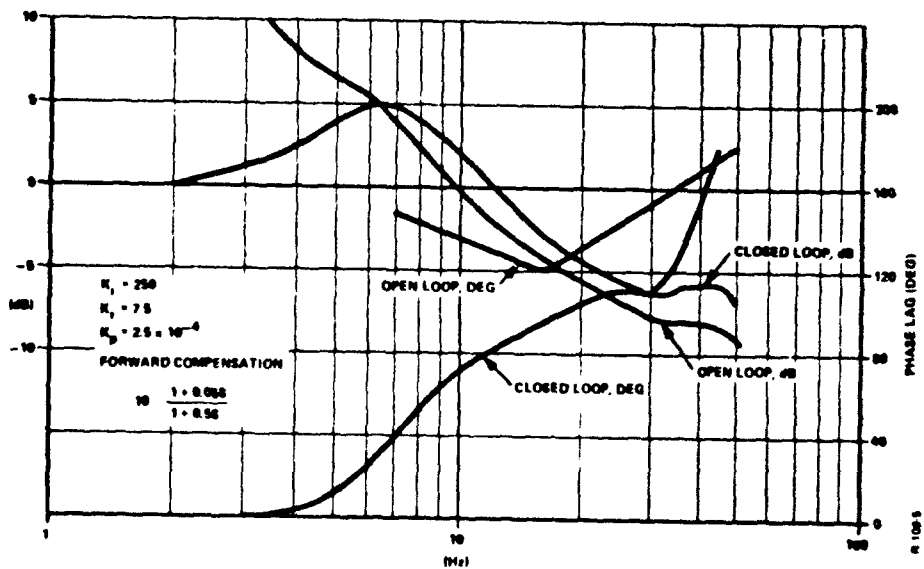


Figure 6-26. Frequency Response - Integrating Accelerometer

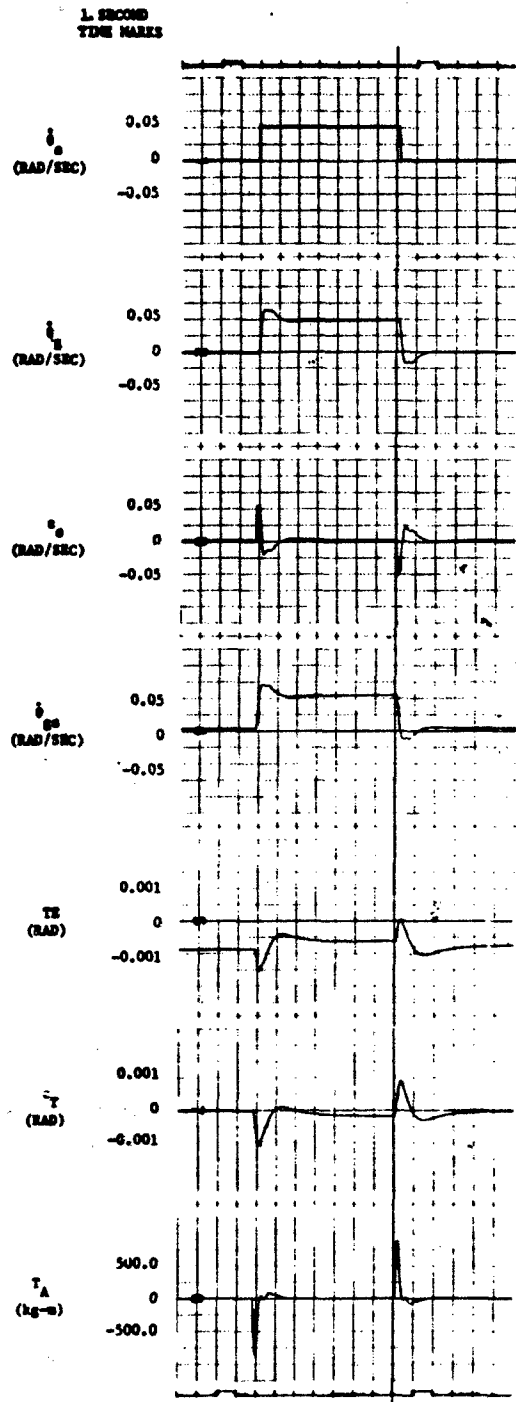


Figure 6-27. Response to a Step Rate Command - Laminar Vortex Sensor

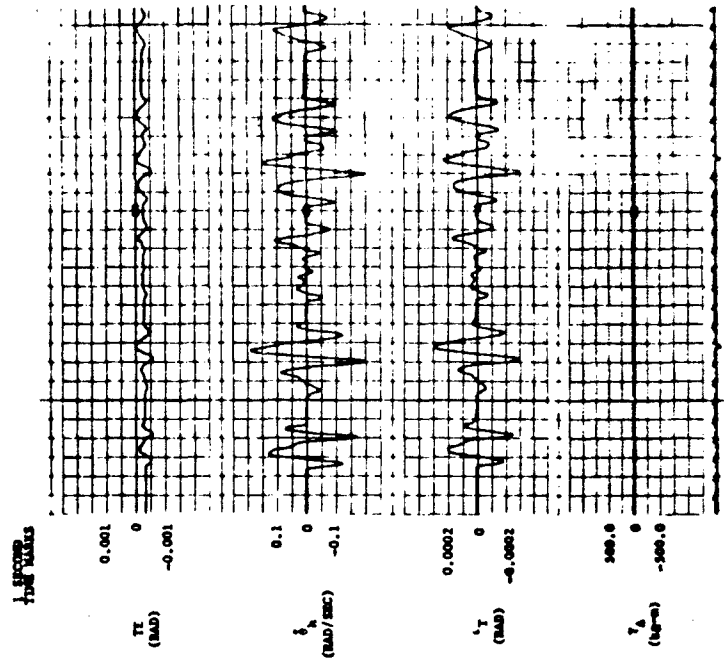


Figure 6-29. Response to HIFRO Bump Course with Hull Sensor Gain Error - Laminar Vortex Sensor

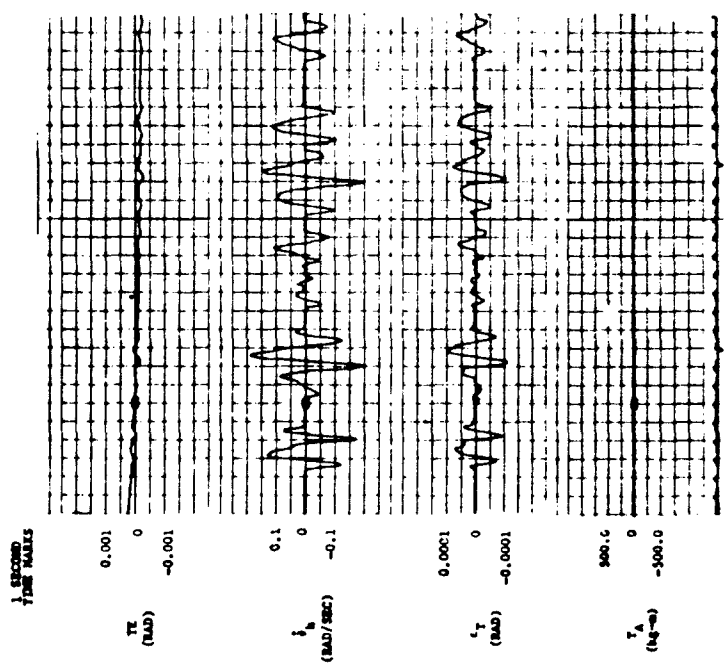


Figure 6-28. Response to HIFRO Bump Course - Laminar Vortex Sensor

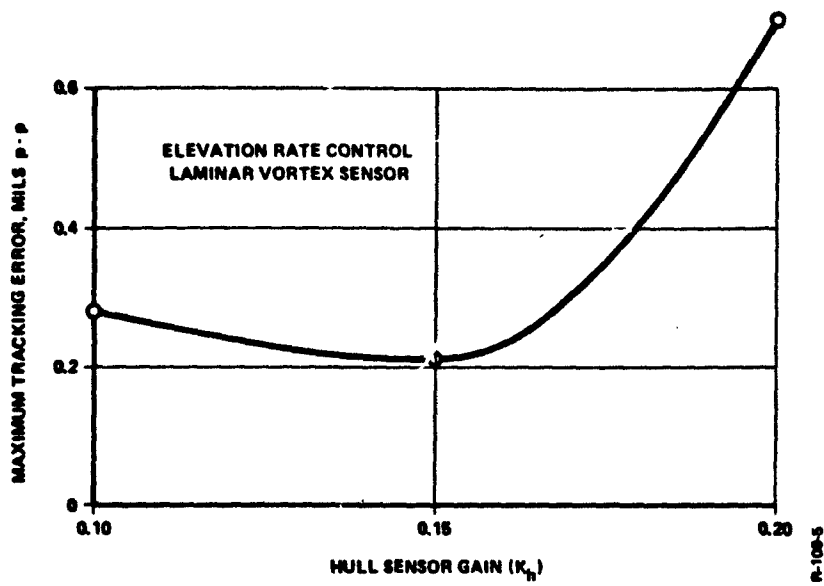


Figure 6-30. Tracking Error Versus Hull Sensor Gain - Laminar Vortex Sensor

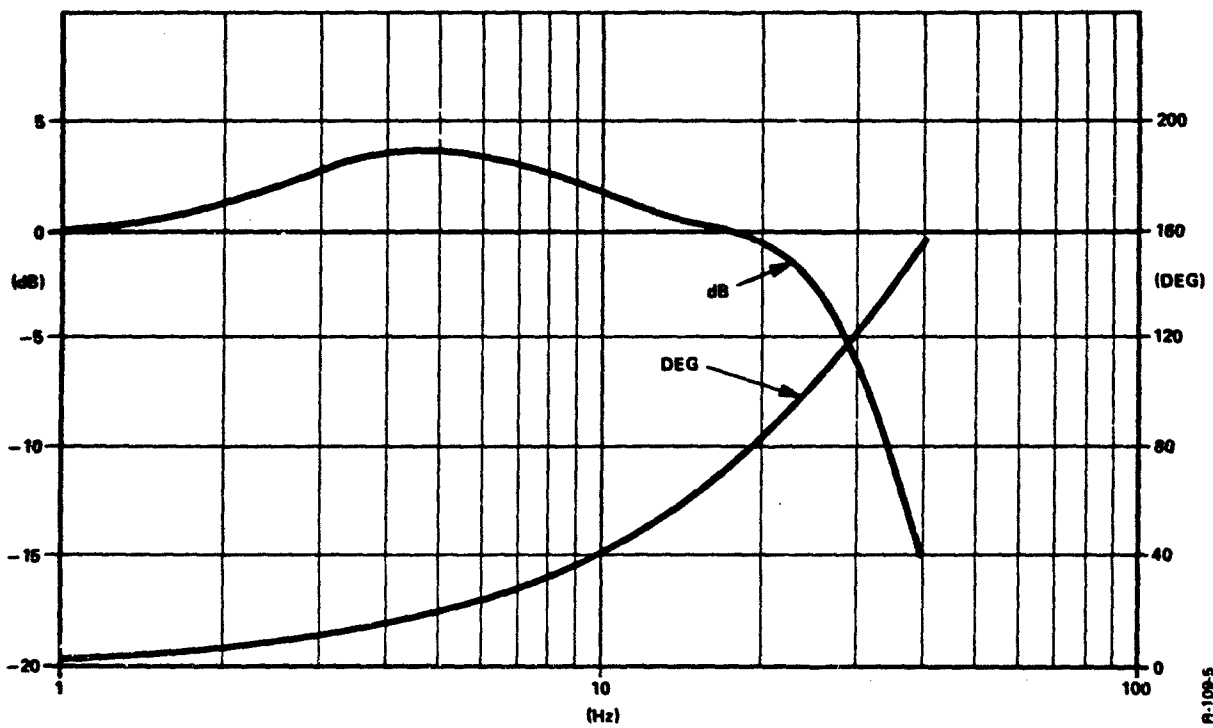


Figure 6-31. Frequency Response - Laminar Vortex Sensor

6.6 EVALUATION OF SENSORS IN AZIMUTH AXIS

6.6.1 Evaluation of Electric Rate Gyros

The block diagram of the azimuth stabilization system with two electric rate gyros, shown in Figure 5-6, is identical to the block diagram for the elevation axis. Only some of the parameters were changed to allow for hardware differences between axes. (See Tables 2-1 and 2-2.)

Using the hybrid computer simulation, the step response of the system to a rate command input was obtained and is shown in Figure 6-32. The observed overshoot is 36 percent.

The response to sinusoidal hull motion equivalent in amplitude to the bump course is shown in Figure 6-33. The observed tracking error was 0.03 mil peak-to-peak.

The response of the system using the simulated HITPRO bump course is shown in Figure 6-34. The maximum tracking error is also 0.03 mil peak to peak. The response of the system to the bump course with a 20 percent hull sensor gain error was also investigated and the results are as shown in Figure 6-35. This amount of gain error increased the tracking error to about 0.07 mil.

The effects of hull sensor gain variations for both the bump course and sinusoidal hull motions are summarized in Figure 6-36. It is evident that the observed tracking error is approximately the same for either input.

Additional simulation studies were conducted to determine the response to the bump course with 2 and 6 mil/s sensor deadband. These results are shown in Figures 6-37 and 6-38, respectively.

The effects of deadband and friction on the tracking error are summarized in Figure 6-39. Coulomb friction of 100 kg-m increased the tracking error to 0.5 mil. The addition of an equal amount of stiction friction did not change the tracking error. Sensor deadband of 2 mils/s increased the tracking error to 0.07 mil. For larger deadband, a limit cycle occurred, and the tracking error was greatly increased.

The frequency response curves are shown in Figure 6-40. The frequency response results are numerated as follows.

Bandpass: 21 Hz
Gain margin: 0.50
Phase margin: 55 deg

The response of the system to a pivot steer maneuver is shown in Figure 6-41. In a pivot steer maneuver, the tank is turning at its maximum rate, i.e., 180 deg in 8 s. In practice, it is desired that the gun remain pointing at the target during this maneuver. As shown in Figure 6-41, there is a momentary tracking error of 0.09 mil. The tracking error then decays to zero after about 0.5 s.

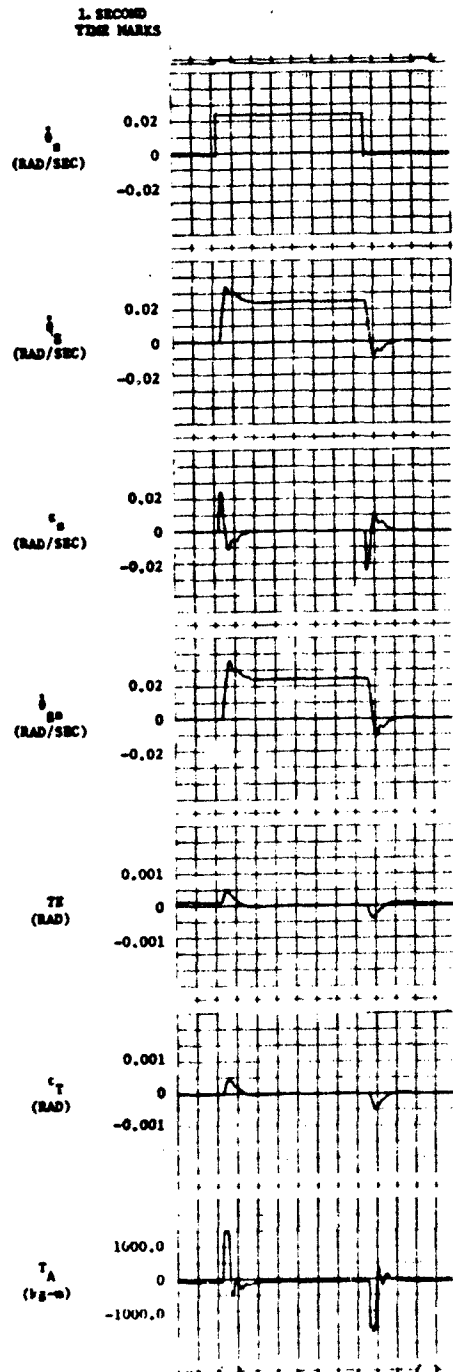


Figure 6-32. Step Response - Azimuth Rate Control with Electric Gyros

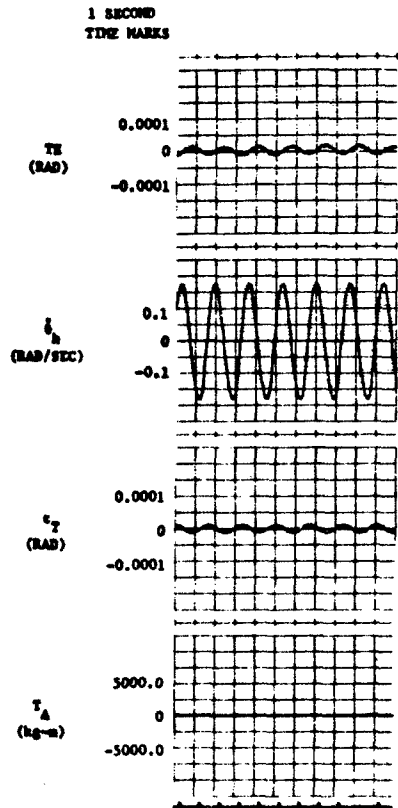


Figure 6-33. Response to Sinusoidal Hull Motion - Azimuth Rate Control with Electric Gyros

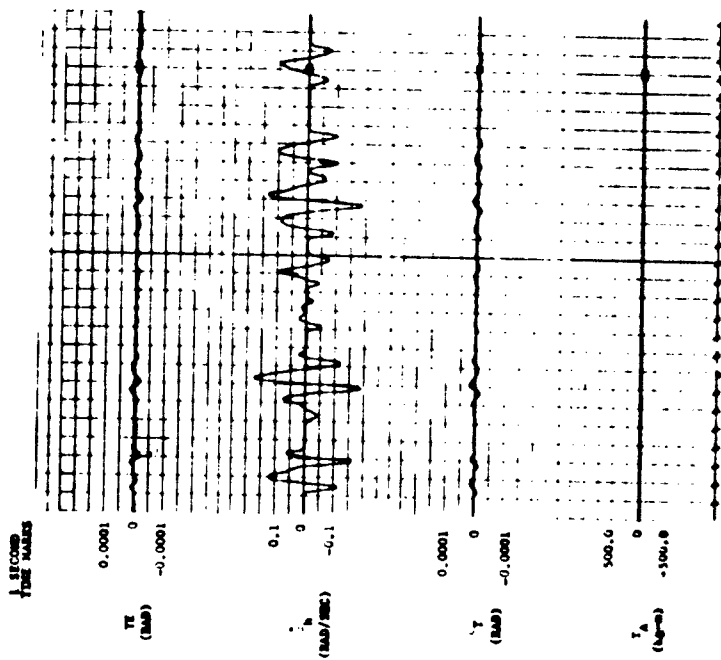


Figure 6-34. Response to HITPRO Bump Course - Azimuth Rate Control with Electric Gyros

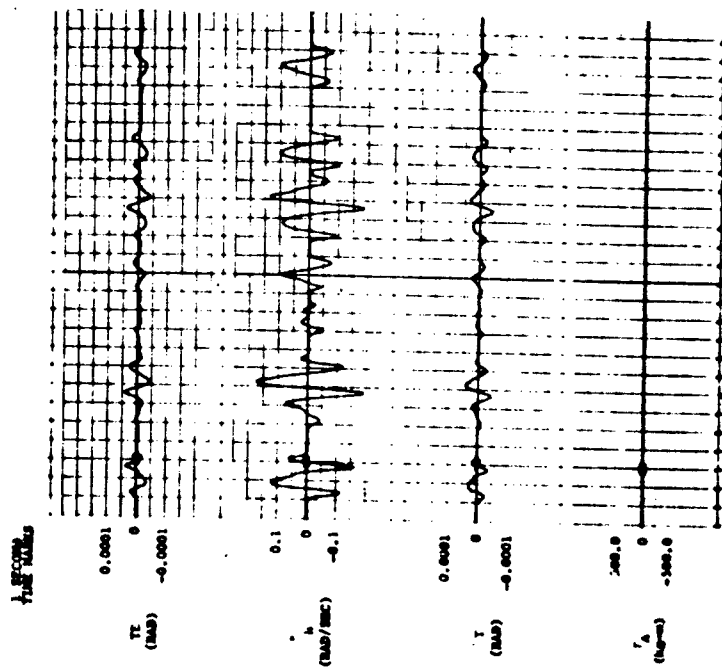


Figure 6-35. Response to HITPRO Bump Course with Hull Sensor Gain Error - Azimuth Rate Control with Electric Gyros

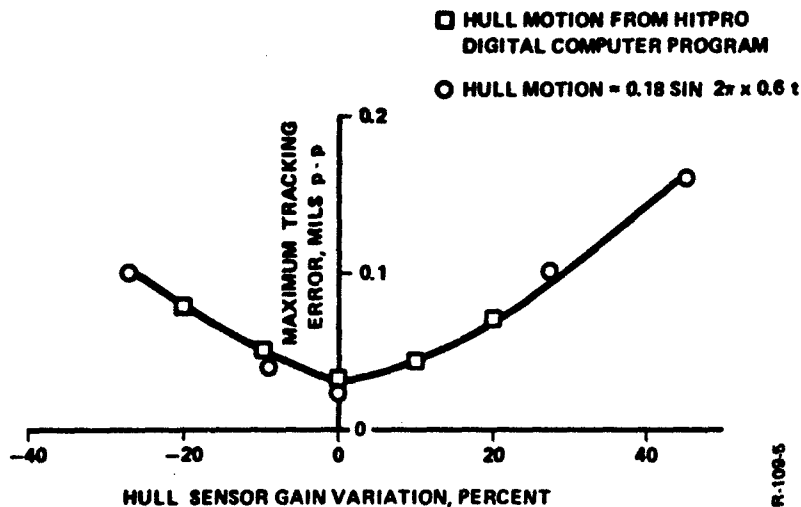


Figure 6-36. Tracking Error Versus Hull Sensor Gain Error - Azimuth Rate Control with Electric Gyros

6.6.2 Evaluation of Pneumatic Accelerometer

A block diagram of the stabilization system for the azimuth axis using a pneumatic accelerometer is presented in Figure 5-7. The accelerometer is used for sensing turret acceleration, and the sensor output signal is integrated to obtain the turret rate signal.

A high gain loop was used to reduce the tracking error. Compensation was used in the forward path for reducing the gain at high frequency to achieve stability. In addition, feedback compensation was used to reduce the effects of sensor phase lag.

The gains and compensation networks used in the simulation were as follows.

$$K_i = 35$$

$$K_r = 10$$

$$K_p = 2 \times 10^{-4}$$

$$\text{Forward compensation: } 10 \frac{1 + 0.05 s}{1 + 0.5 s}$$

$$\text{Feedback compensation: } \frac{1 + 0.010 s}{1 + 0.002 s}$$

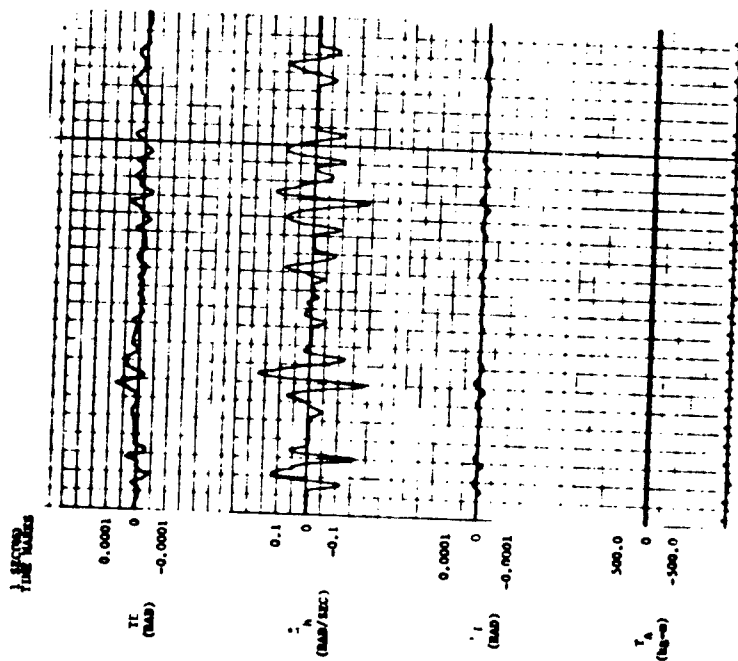


Figure 6-37. Response to HITPRO Bump Course with 2 ms Sensor Deadband - Azimuth Rate Control with Electric Gyros

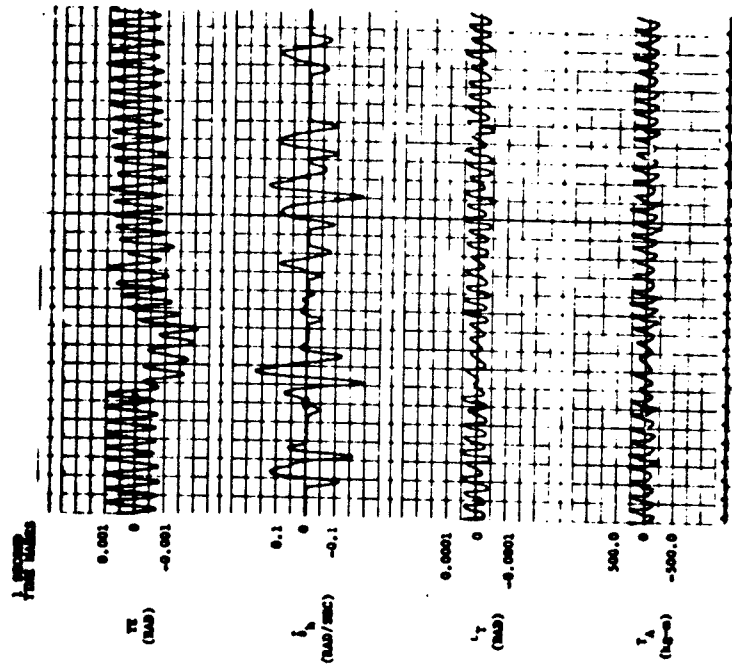


Figure 6-38. Response to HITPRO Bump Course with 6 ms Sensor Deadband

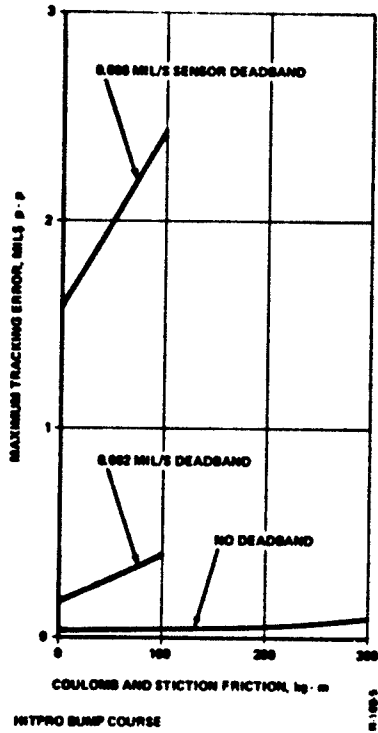


Figure 6-39. Effects of Deadband and Friction on Tracking Error - Azimuth Rate Control with Electric Gyros

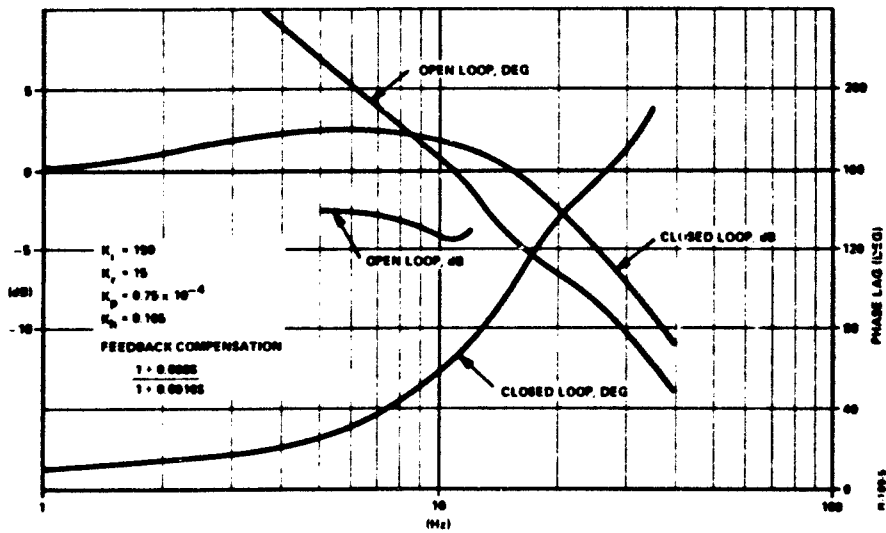


Figure 6-40. Frequency Response - Azimuth Rate Control with Electric Gyros

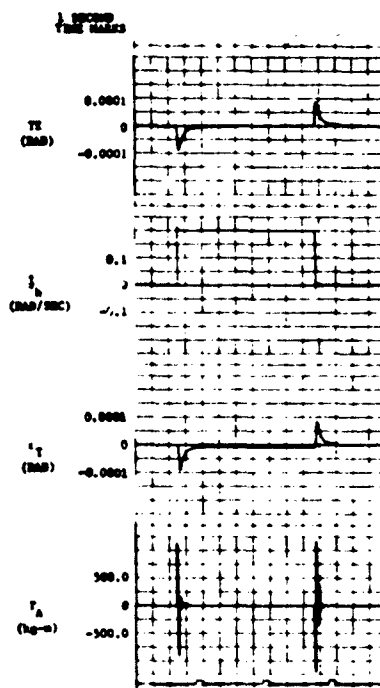


Figure 6-41. Response to Pivot Steer Maneuver - Azimuth Rate Control with Electric Gyros

The step response obtained with the hybrid computer simulation is shown in Figure 6-42. An overshoot of 44 percent was observed.

The response to sinusoidal hull motion equivalent in amplitude to the maximum hull motion for the bump course is shown in Figure 6-43. The observed tracking error was 0.2 mil peak to peak.

The response to the HITPRO bump course is shown in Figure 6-44. The effect of adding 100 kg-m coulomb friction and 100 kg-m stiction friction is shown in Figure 6-45. The resulting maximum tracking error was again 0.25 mil. The friction caused an increase in the maximum tracking error for larger values of friction, as shown in Figure 6-46.

The frequency response curves are shown in Figure 6-47. The frequency response results can be summarized as follows.

Bandpass:	15 Hz
Gain margin:	0.55
Phase margin:	36 deg

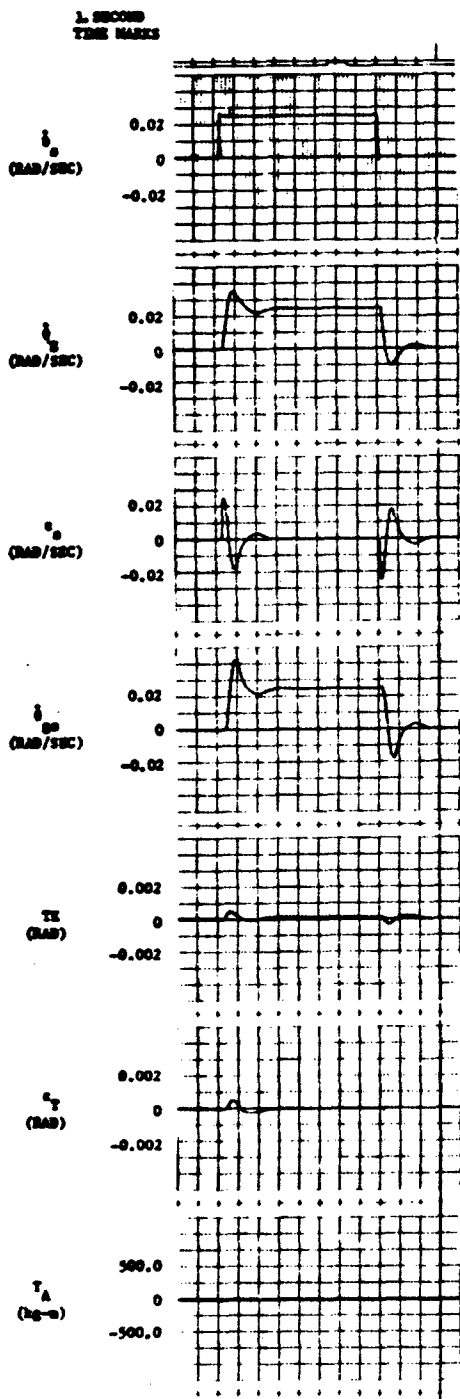


Figure 6-42. Step Response - Pneumatic Accelerometer

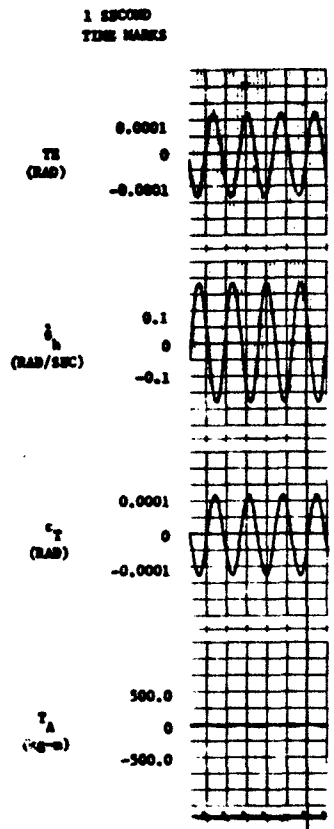


Figure 6-43. Response to Sinusoidal Hull Motion - Pneumatic Accelerometer

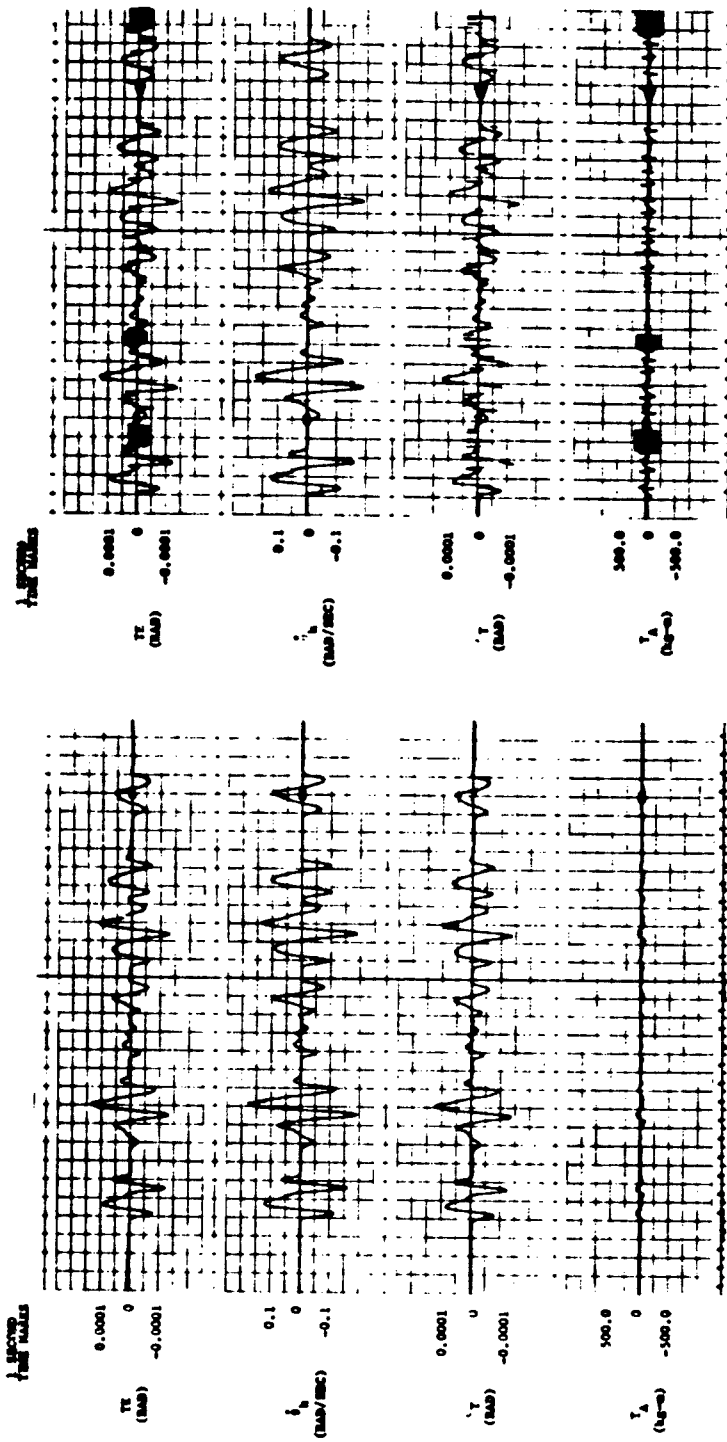


Figure 6-44. Response to HITPRO Bump Course - Pneumatic Accelerometer

Figure 6-45. Response to HITPRO Bump Course with Coulomb and Stiction Friction - Pneumatic Accelerometer

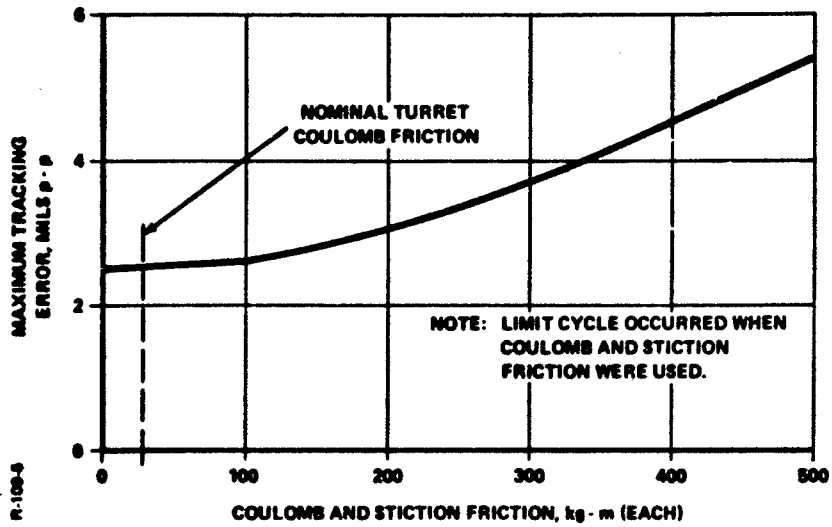


Figure 6-46. Maximum Tracking Error Versus Friction - Pneumatic Accelerometer

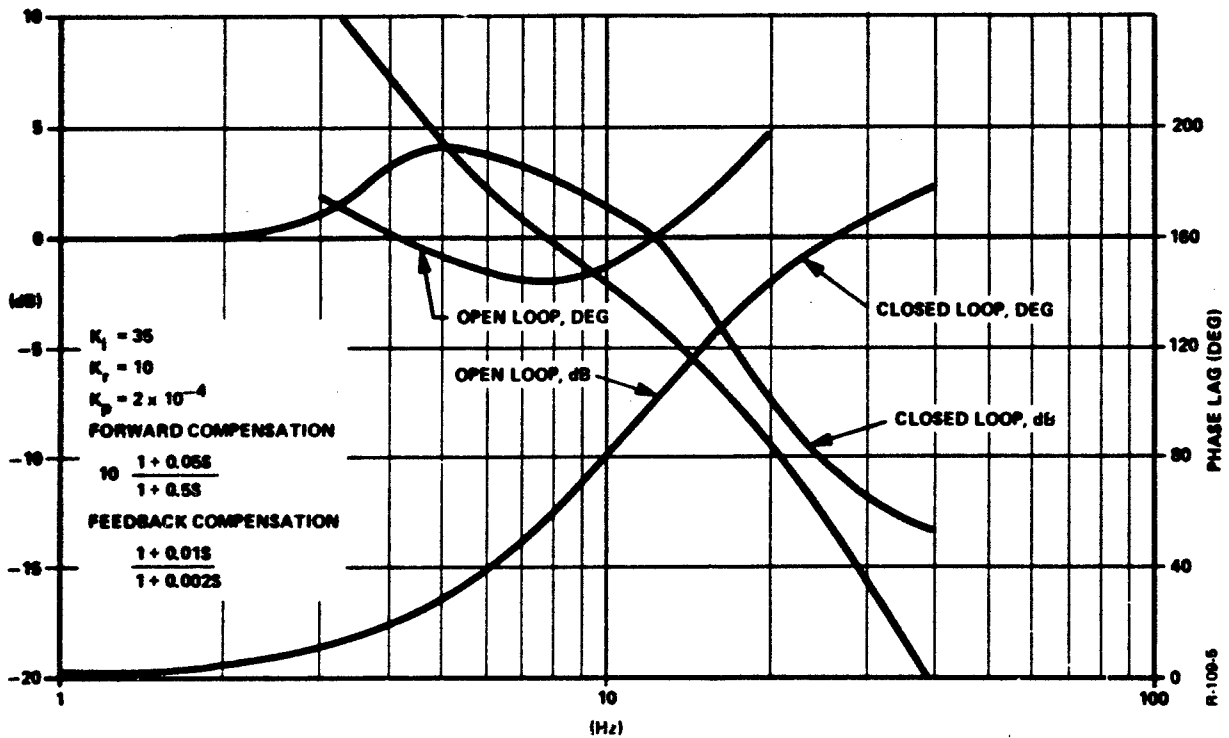


Figure 6-47. Frequency Response - Pneumatic Accelerometer

6.7 SUMMARY OF SIMULATION RESULTS

Simulation of the stabilization system has produced the following results.

- (1) The linear servovalve-actuator model provided a means of estimating required system gains but was not sufficiently accurate to be used in the sensor evaluation study. The nonlinear model was therefore used for sensor evaluations.
- (2) Hull dynamics had a negligible effect on system response and tracking error.
- (3) A summary of the results of the sensor evaluation study is presented in Table 6-1.

Table 6-1(A) summarizes the results for the rate sensors. For each of these systems, a rate sensor was mounted in the gun and the hull axis.

Table 6-1(B) summarizes the results for the accelerometers studied. For both of these systems, an accelerometer was mounted in the gun axis only.

It is to be noted that the systems represented in the table were not fully optimized in this study. An absolute comparison of the sensors is therefore not entirely justified.

As indicated by Table 6-1, the performance criteria were met for all of the sensor configurations.

- (4) A hull sensor gain error of 25 percent can be tolerated without exceeding the tracking error requirement.
- (5) Coulomb friction of 100 kg-m increases the tracking error by approximately 0.5 mil peak to peak.

Table 6-1 - Results of the Sensor Evaluation Study

A. Rate Sensor Results - Gun and Hull Sensor

Axis	System Command	Sensors	Gains				Bandpass (Hz)	Phase Margin (deg)	Gain Margin	Max. Tracking Error (Mils P-P)	Step Response Overshoot (percent)
			K _i	K _r	K _p	K _h					
Elevation	Rate	2 Elec. Gyros	50	7.5	2.5×10^{-4}	0.15	28	0.50	0.18	15	
Elevation	Rate	2 G.E. Fluidic	50	7.5	2.5×10^{-4}	0.15	13	0.53	0.11	20	
Elevation	Rate	2 Honeywell Vortex	40	4.8	2.0×10^{-4}	0.15	25	0.50	0.21	30	
Azimuth	Rate	2 Elec. Gyros	50	4.0	0.2×10^{-4}	0.165	14	0.50	0.03	36	
Elevation	Position	2 Elec. Gyros	50	7.5	2.5×10^{-4}	0.135	28	0.50	0.13	15	

B. Acceleration Sensor Results - Gun Sensor Only

Axis	System Command	Sensors	Gains				Bandpass (Hz)	Phase Margin (deg)	Gain Margin	Max. Tracking Error (Mils P-P)	Step Response Overshoot (percent)
			K _i	K _r	K _p	K _h					
Elevation	Rate	1 Bendix Int. Accel.	250	7.5	2.5×10^{-4}	-	16	0.53	0.28	60	
Azimuth	Rate	1 Aitesearch Accel.	35	10.0	2.0×10^{-4}	-	15	0.55	0.25	44	

NOTE: Tracking error values are for HITPRO bump course with nominal gains, no coulomb and stiction friction, and no deadband.

SECTION 7

CONCLUSIONS

A mathematical model of a suitable stabilization system for the M60A1 tank main gun was formulated and programmed. The model was defined so as to include most of the significant nonlinearities such as nonlinear valve flow and hull dynamics due to gun motion. A hybrid computer analysis was performed to determine the operating characteristics of the stabilization system, to evaluate prospective sensors for sensing gun and/or hull rate, and to determine whether a rate or position command control concept is preferable with respect to specified performance criteria.

An analytical study revealed that both the rate and position control concepts required a proportional plus integral control law in order to minimize the gun tracking error. It was also shown that the rate and position concepts are equivalent in terms of nulling out the effects of hull motions and thus of stabilizing the gun after the target is in the sight. A computer analysis which followed verified this equivalence. In addition, it was possible to show that the effect of hull motions on the system can be minimized by either a high control loop gain along with a lead-lag compensation network or by using a hull sensor signal in the control law.

The extensive computer simulation analysis revealed several conclusions in the areas of stabilization control philosophy and sensor applicability. In the process of arriving at a full computer model of the system for sensor evaluation, it was found that the effect of hull dynamics on the gun was negligible. Nonlinear valve flow, however, was found to have a significant influence on system performance. A linearized flow model was not sufficiently accurate for use in this study.

It was found that all five of the sensors studied in this program meet the performance criteria set forth by the Contracting Officer's Representative. In addition, this study indicates that these criteria can be met by using only a gun sensor. If verified by further studies, the need for a corresponding hull sensor may be eliminated.

The detailed sensor study immediately revealed that automatic offset and integrator drift nulling circuits are required when using an acceleration sensor. A method which can be used for this purpose is described in Section 5.5.

In addition, increasing the gain of the acceleration sensor will decrease the sensor offset effects, and hence the drift rate. More generally, it was found in the sensor study that sensor gain errors have a small effect on the tracking error. Also, a combination of sensor deadband and gun or turret friction will cause the system to limit cycle.

In order to compensate for sensor phase lag, feedback compensation is required. Forward path compensation is desirable for obtaining stability with higher loop gains for this system.

SECTION 8
RECOMMENDATIONS

It is recommended that in future system studies and sensor evaluations, additional system characteristics including realistic bending modes and hardware compliance model be added. The effects of providing an extensive model for friction which separates the effects of stiction coulomb, and running friction through switching logic should also be investigated. Sensor models should be utilized allowing for sensor errors due to noise, deadband, gain variation, and offset. It is also of importance on a complete system model to include integrator drift and an automatic nulling circuit. When these effects have been included in the model, a statistical analysis of the pointing error output data will be required in order to afford more detailed and objective performance comparisons. Inclusion of the additional nonlinearities mentioned will also make it possible to better optimize the system gains and compensation networks.

It is also recommended that a gunner model be included in the tracking loop, in order to arrive at additional data for comparing the rate and position command control concept. A display of tracking error can be developed using an oscilloscope for which a human operator can issue realistic commands to the system to simulate target tracking. Inclusion of an operator model in the simulation will allow a determination of the tracking and stabilization capabilities of the system.

In addition, it is recommended that steps be taken to verify the results of this simulation study by means of field test data with an M60A1 tank. Additional insight into the system operating characteristics and the effects of significant nonlinearities could be gained. A verification study would consist of obtaining recordings of measurements of hull and gun rates and achieved pointing accuracies on various types of terrain, and comparing these with the results of this study.

An optimal control theory approach to the stabilization of the M60A1 tank gun may also be desirable in the future if additional performance specifications are defined for the gun or if conventional techniques fail to achieve the goals when additional nonlinearities are included.

SECTION 9
BIBLIOGRAPHY

1. A Mathematical Representation of the M60A1 Azimuth and Elevation Control and Add-On Stabilization System, Report No. CDE-SA-TR-71-09, Chrysler Corporation, Defense Division, 2 November 1971.
2. Performance Requirements for Turret, Cupola, and Gun Control System, 19207-11608400, U.S. Army Tank Automotive Center, Warren, Michigan, 24 October 1968.
3. HITPRO, Volume II (User's Manual), Technical Report No. RE-TR-71-63, GEOS. No. FDU 71-6, U.S. Army Weapons Command, Rock Island, Illinois, 15 November 1971.
4. An Analysis and Simulation of the M60A1E2 Tank Main Gun's Elevation Control System, Report No. RG-TR-69-14, U.S. Army Missile Command, August 1969.
5. Final Report - Hull Angular Motions for the M601A Vehicle With Add-On Stabilization System, Report No. RS 1663, Chrysler Corporation, Defense Operations Division, 15 July 1970.
6. Functional Checkout and Troubleshooting Instructions for M60A1 Tank Stabilized Gun Control System, Cadillac Gage Company, 8 March 1967.
7. Final Report - Product Improvement Test of Gun Mount, 105-MM, M140, for M601A Tank, Report No. APG-MT-4064, Aberdeen Proving Ground, May 1972.

APPENDIX A
ACTUATOR SIZING STUDY AND
DIGITAL CHECK SOLUTIONS

PART I
ACTUATOR SIZING
STUDY

PAGE 1

SYSTEMS REAL-TIME MONITOR-4.0

ACTUATOR

CO. 01 48

ACTUATOR-10.0
SUBTYPE 3
REVOLVE FOR TRM

MAIN

```

1 1
2 2
3 3
4 4
5 5
6 6
7 7
8 8
9 9
10 10
11 11
12 12
13 13
14 14
15 15
16 16
17 17
18 18
19 19
20 20
21 21
22 22
23 23
24 24
25 25
26 26
27 27
28 28
29 29
30 30
31 31
32 32
33 33
34 34
35 35
36 36
37 37
38 38
39 39
40 40
41 41
42 42
43 43
44 44
45 45
46 46
47 47
48 48
49 49
50 50
51 51
52 52
53 53

```

```

EXTERNAL DIFEC
DIMENSION I00(20)
DIMENSION RVV(20), VCC(20)
DIMENSION DTH(1000), DTND(1000), DCDV(1000), TT(1000)
DIMENSION DUMMY(3)
DIMENSION Y(4), DY(4), VM(4), VP(4), AI(4,4)
PEAR J
COMMON/VAPES/DH,C2,J,OP,DT,VM,TA
V(1)=THO
V(2)=THO
V(3)=V
V(4)=PS
IH=0
3 IH=IH+1
5 READ 5, RVV(IH)
5 FORMAT(F10.3)
IF (RVV(IH) .EQ. 99999) GO TO 7
GO TO 3
7 KRV=IH-1
IH=0
13 IH=IH+1
5 READ 5, VCC(IH)
IF (VCC(IH) .EQ. 99999) GO TO 15
GO TO 13
15 KVC=IH-1
16 READ 17, DM, (100(IH), IH=L,KRV)
17 FORMAT(F10.3, 20I1)
IF (DM .EQ. 99999) STOP
DO 709 IB=L,KVC
VC=VCC(IB)
DO 600 JN=L,KRV
IF (100(JN) .NE. 1) GO TO 600
RV=RVV(JN)
24 PRINT 23, RV, DM, VC
23 FORMAT(1H1. /, /, RV, DM, VC, /, 3F20.3)
25 PRINT 25
25 FORMAT(/, 12X, 'TIME', 11X, 'THEIR', 0X, 'THEIR DOT', 30X, 'PS', 15X,
1' V', 14X, 'VC', 14X, 'TA', /)
NP=0
PI=3.14159
V(2)=0
V(1)=0
VP(2)=0
VP(3)=0
DY=0
V(3)=VC
TO=0
DT= 01
TEND=5
OP=77
J=23681
V(4)=J000
VM=2.0VC

```

```

54 C2=2.0 * GAINC*(100. * RV )**2
55 KK=1
56 N=1
57 CALL FILLIN(KK,V,UV,TD,DT,VAL,VP,TH,AL,DIFEC)
58 N=N+100
59 TU=TN
60 PDTH=V(2)*100 /PI
61 IFANT=CON(10+10) EQ. 0)PRINT 200,
62 1 TO,PDTH,PE,THD,V(1),VC,V(3),V(4),TR
63
64
65
66
67
68
69
70
71
72
73
74
75
76
77
78
79
80
81
82
83
84
85
86
87
88
89
90
91
92
93
94
95
96
97
98
99
100
101
102
103
104
105
200 CONTINUE
    IF(TO.LT.TEND)GO TO 100
    PRINT 300,TO,TEND,MP,MT
    300 FORMAT(' TO, TEND, MP, MT = ',2F15.5,2I7)
    *****FIND MAX AND MINS
    BMAX=DTM(1)
    BMIN=DTM(1)
    XMIN=TT(NP)
    XMAX=TT(NP)
    DO 400 I=1,MP
    IF(BMAX.LT.DTM(I))BMAX=DTM(I)
    IF(BMIN.GT.DTM(I))BMIN=DTM(I)
    IF(XMIN.GT.DTM(I))XMIN=DTM(I)
    IF(XMAX.LT.DTM(I))XMAX=DTM(I)
    IF(CMIN.LT.TT(I))CMIN=TT(I)
    IF(CMAX.GT.TT(I))CMAX=TT(I)
    400 CONTINUE
    XMIN=0
    YMIN=0
    NC=1
    CALL SLOT(TT,DTM,MP,XMIN,XMAX,BMIN,BMAX,MT,NC)
    PRINT 510
    CALL SLOT(TT,DTM,MP,XMIN,XMAX,BMIN,BMAX,MP,NC)
    PRINT 520
    CALL SLOT(TT,DEDM,MP,XMIN,XMAX,BMIN,BMAX,MP,NC)
    PRINT 530
    510 FORMAT(' ',THETA DEG VERSUS TIME')
    520 FORMAT(' ',THETA DOT DEG VERSUS TIME')
    530 FORMAT(' ',V DEG VERSUS TIME')
    600 CONTINUE
    700 CONTINUE
    GO TO 15
    END
    
```

00570
 00580
 00590
 00600
 00610
 00620
 00630
 00640
 00650
 00660
 00670
 00680
 00690
 00700
 00710
 00720
 00730
 00740
 00750
 00760
 00770
 00780
 00790
 00800
 00810
 00820
 00830
 00840
 00850
 00860
 00870
 00880
 00890
 00900
 00910
 00920
 00930
 00940
 00950
 00960
 00970
 00980
 00990
 01000
 01010
 01020
 01030
 01040
 01050
 01060
 01070
 01080

LINE:

1
2
3
4
5
6
7
8
9
10
11
12
13
14
15

C

```

SUMMATIVE DIFF(V,VP,T,N)
DIMENSION Y(4),CV(4),VK(4),VP(4),AI(4,4)
REAL I
COMMON TABLESON,C2,I,OP,DT,VM,TA
T= (VM + V(4) - C2*(I+V2))/I2
VF(1)=TA/J
VP(2)=V(1)
OP=OP+V(1)
VP(3)=0
IF(OT GT OP)VP(3)=OP-OP
IF(V(3) GT VM)V(3)=VM
VK(4)=-1 + V(4) * VP(3)/V(3)
RETURN
END

```

01000
01100
01110
01120
01130
01140
01150
01160
01170
01180
01190
01200
01210
01220
01230

```

1  SUBROUTINE RI(N, V, VO, DV, XOS, DX, VL, VP, NL, AI, DIFEC)
2  DIMENSION YOUN, DY(N), YH(N), YP(N), YI(N,4)
3  DOUBLE PRECISION XO
4  I = 1
5  GO TO (1,2,3,4,5), I
6  XH = XO
7  DO 6 J = 1, N
8  YH(J) = VO(J)
9  CALL DIFEC(VL, VP, NL, N)
10 DO 7 J = 1, N
11 RI(J, I) = DX*VP(J)
12 I = I + 1
13 GO TO 6
14 XH = XO + 0.5*DX
15 DO 9 J = 1, N
16 YH(J) = VO(J) + 0.5*RI(J, 1)
17 GO TO 10
18 DO 11 J = 1, N
19 YH(J) = VO(J) + 0.5*RI(J, 2)
20 GO TO 10
21 XH = XO + DX
22 DO 12 J = 1, N
23 YH(J) = VO(J) + RI(J, 3)
24 GO TO 10
25 DO 13 J = 1, N
26 DY(J) = (0.5*RI(J, 1) + RI(J, 4)) * RI(J, 2) * RI(J, 3) / 2.0
27 YH(J) = VO(J) + DY(J)
28 IF (I.E. 1) RETURN
29 CALL DIFEC(VL, VP, NL, N)
30 RETURN
31 END

```

01240
01250
01260
01270
01280
01290
01300
01310
01320
01330
01340
01350
01360
01370
01380
01390
01400
01410
01420
01430
01440
01450
01460
01470
01480
01490
01500
01510
01520
01530
01540
01550
01560
01570

SYSTEMS 8706 FORTRAN IV COMPILER (REV. 0)

00 05 51 ACTUATOR

```

SLOT
1
2
3
4
5
6
7
8
9
10
11
12
13
14
15
16
17
18
19
20
21
22
23
24
25
26
27
28
29
30
31
32
33
34
35
36
37
38
39
40
41
42
43
44
45
46
47
48
49
50
51
52
53

C
SUBROUTINE SLOT(X,V,MP,XMIN,XMAX,VMIN,VMAX,NT,NC)
DIMENSION IPT(76),SCLX(6),ICR(3),X(NC,MP),Y(NC,MP)
DATA ICR/1,2,3,4,5,6,7,8,9,10,11,12,13,14,15,16,17,18,19,20,21,22,23,24,25,26,27,28,29,30,31,32,33,34,35,36,37,38,39,40,41,42,43,44,45,46,47,48,49,50,51,52,53
10 IF(XP.LT.2)RETURN
20 XMIN=XMIN
30 XMAX=XMAX
40 VMIN=VMIN
50 VMAX=VMAX
60 IF(NT.NE.0)GO TO 50
70 X=X(XI-1)
80 Y=Y(YI-1)
90 V=V(VI-1)
100 DO 20 J=L,MP
110 IF(X(J,K).GT.XMIN)X=X(XI-1)+V
120 IF(Y(J,K).LT.YMIN)Y=Y(YI-1)+V
130 IF(X(J,K).GT.YMIN)Y=Y(YI-1)+V
140 CONTINUE
150 X=X(XI-1)+V
160 Y=Y(YI-1)+V
170 IF(X(XI,K).GT.XMAX)X=X(XI-1)+V
180 IF(Y(XI,K).LT.YMIN)Y=Y(YI-1)+V
190 IF(X(XI,K).GT.YMIN)Y=Y(YI-1)+V
200 CONTINUE
210 XFCT=75./XMAX-XMIN
220 YFCT=45./YMAX-YMIN
230 BITX=(XMIN-XIN)/3.0
240 BITY=(YMIN-YIN)/3.0
250 SCLX(1)=XMIN
260 SCLY(1)=YMIN
270 DO 30 K=2,5
280 SCLX(K)=SCLX(K-1)+BITX
290 SCLY(K)=SCLY(K-1)+BITY
300 CONTINUE
310 SCLX(6)=XMAX
320 SCLY(6)=YMAX
330 PRINT 999,(SCLX(N),N=1,6)
340 DO 100 I=L,46
350 DO 110 J=L,76
360 IPT(I)=IBNK
370 CONTINUE
380 DO 111 J=L,76.45
390 IPT(J)=ILNE
400 CONTINUE
410 DO 120 K=L,MP
420 DO 120 J=L,NC
430 INT=(XMAX-Y(J,K))*XFCT+1.5
440 IF(XINT.NE.1)GO TO 120
450 IX=(X(J,K)-XMIN)*XFCT+1.5
460 IF(IX.GT.0.AND.IX.LE.76)IPT(IX)=ICR(J)
470 CONTINUE
480 DO 130 K=L,6

```

01590 01590 01600 01610 01620 01630 01640 01650 01660 01670 01680 01690 01700 01710 01720 01730 01740 01750 01760 01770 01780 01790 01800 01810 01820 01830 01840 01850 01860 01870 01880 01890 01900 01910 01920 01930 01940 01950 01960 01970 01980 01990 02000 02010 02020 02030 02040 02050 02060 02070 02080 02090 02100

00.0.51 RETURN: SYSTEMS REAL-TIME MONITOR-4.0
SYSTEMS 05/86 FORTRAN IV COMPILER (REV. 6)

PAGE 7

```

SLOT
54 INT=(MPC-SOLY(K))*PCT+1.5
55 IF(LINT EQ 1)GO TO 140
56 CONTINUE
57 PRINT 998,(IPT(J),J=L,76)
58 GO TO 100
59 DO 150 J=L,76
60 IF(IPT(J).EQ.1DNK)IPT(J)=1DSH
61 CONTINUE
62 PRINT 997,(SOLY(K),(IPT(J),J=L,76)
63 CONTINUE
64 PRINT 996,(SOLX(N),N=L,6)
65 RETURN
66 FORMAT(' ',9X,01.4,6,2X,76R1)
67 FORMAT(' ',21X,76R1)
68 FORMAT(' ',9X,6F13.2)
69 FORMAT(' ',9X,6F13.2)
70 END

```

```

02110
02111
02112
02113
02114
02115
02116
02117
02118
02119
02120
02121
02122
02123
02124
02125
02126
02127

```

```

EXTERNAL DIPEC
DIMENSION IOG (20)
DIMENSION AVV (20), VCC (20)
DIMENSION OTH (1000), DTH (1000), DEGV (1000), TT (1000)
DIMENSION DUMMY (3)
DIMENSION Y (4), DY (4), YN (4), YP (4), AI (4,4)

```

REAL J

COMMON/NAMES/DH, C2, J, GP, DT, VH, TA

C	Y (1) = THO	YP (1) = THO0
C	Y (2) = TH	YP (2) = THO
C	Y (3) = V	YP (3) = VO
C	Y (4) = PS	YP (4) = PS0

IN=0

A1 2

3 IN=IN+1

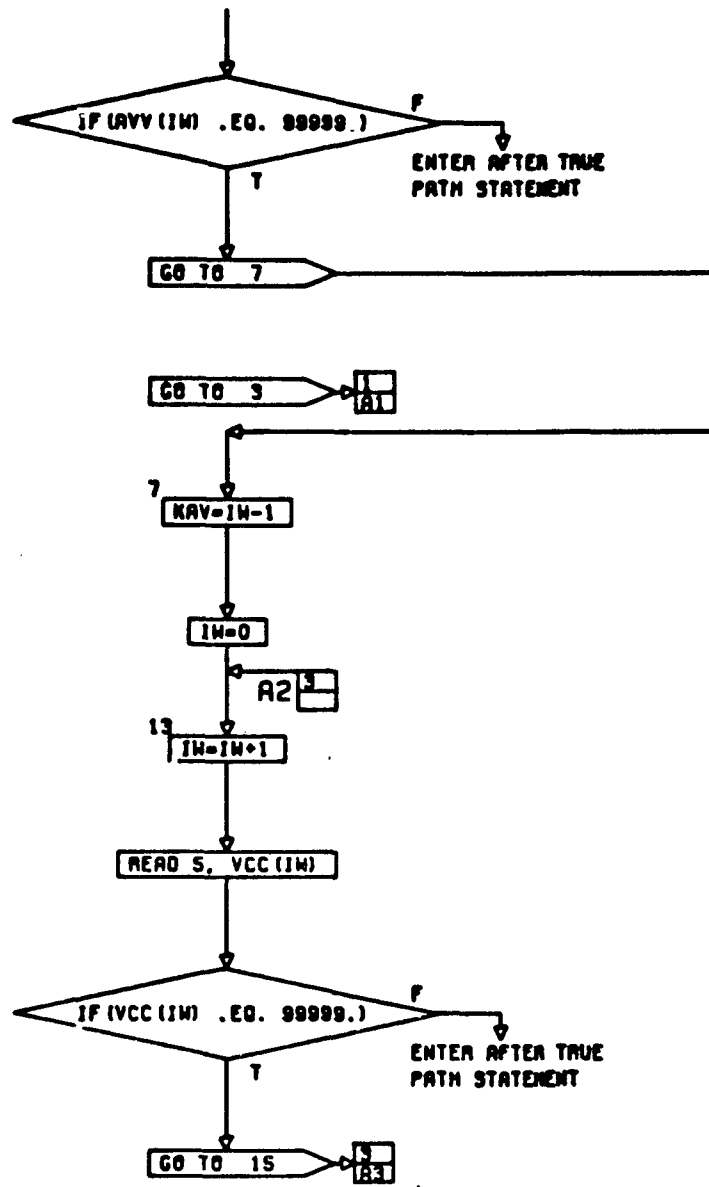
READ 5, AVV (IN)

5 FORMAT (F10.3)

CONT. ON PG 2

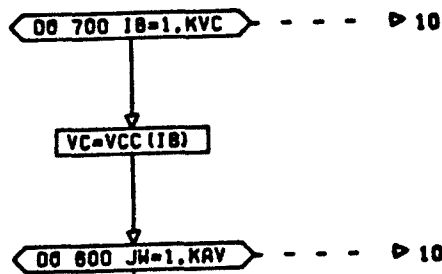
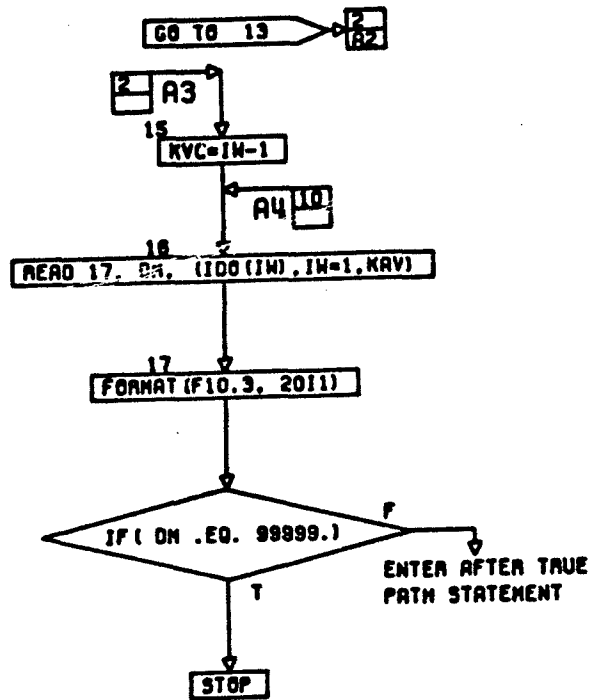
PG 1 OF 10

A-11



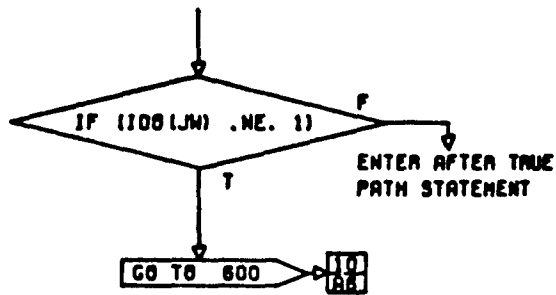
CONT. ON PG 3

PG 2 OF 10



CONT. ON PG 4

PG 3 OF 10



AV=AVV(JM)

24
PRINT 23, AV, OM, VC

23
FORMAT (1H1, /, ' AV, OM, VC=', 3F20.3)

PRINT 25

25
FORMAT (/ , 12X, 'TIME', 11X, 'THETA', 8X, 'THETA DOT', 30X, 'PS', 15X,
'V', 14X, 'VC', 14X, 'TA', /)

NP=0
PI=3.14159
Y(2)=0.
Y(1)=0.
YP(2)=0.
YP(3)=0.0
OV=0.
Y(3)=VC

CONT. ON PG 5

PG 5 OF 10

T0=0.
DT=.01
TEND=5.
QP=77.
J=23681.
Y(4)=3000.
VM=2.*VC
C2=2.0 * DN**3/(100. * AV)**2

KK=1
N=4

AS

100
CALL RK(N, KK, Y, DT, T0, DT, YH, YP, TN, AI, DIFEC)

NT=TN-100
TC=TN
PDTH=Y(2)*180./PI
PDTHO=Y(1)*180./PI

IF (NT - (NT/10) = 10) .EQ. 0

F
ENTER AFTER TRUE
PATH STATEMENT

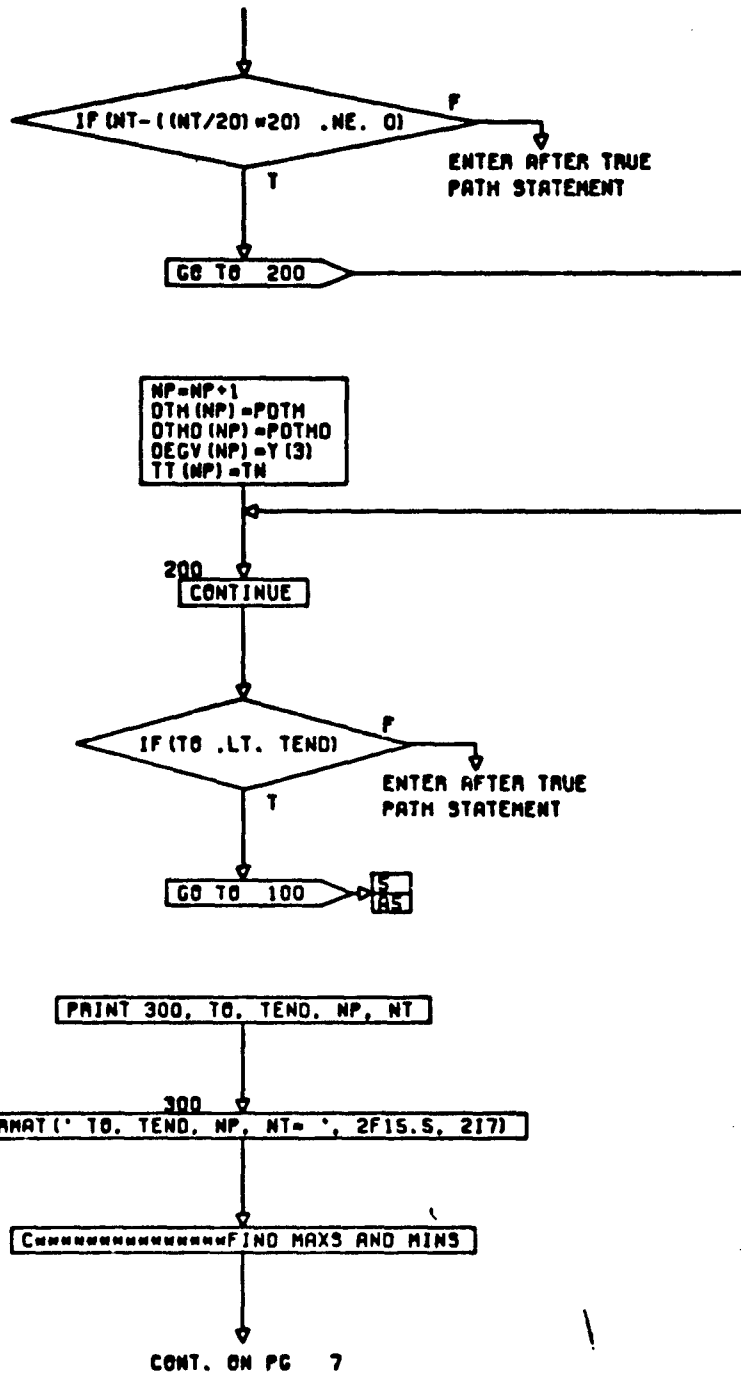
T

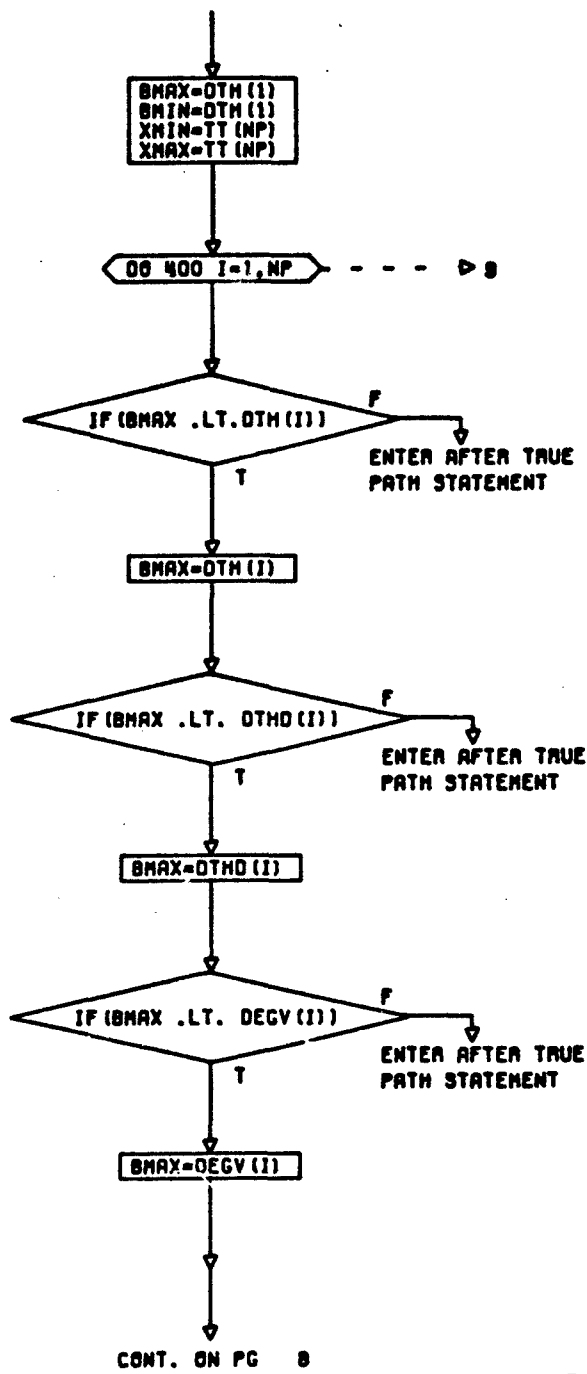
250
PRINT 250,
T0, PDTH, PDTHO, Y(1), VC, Y(3), Y(4), TA

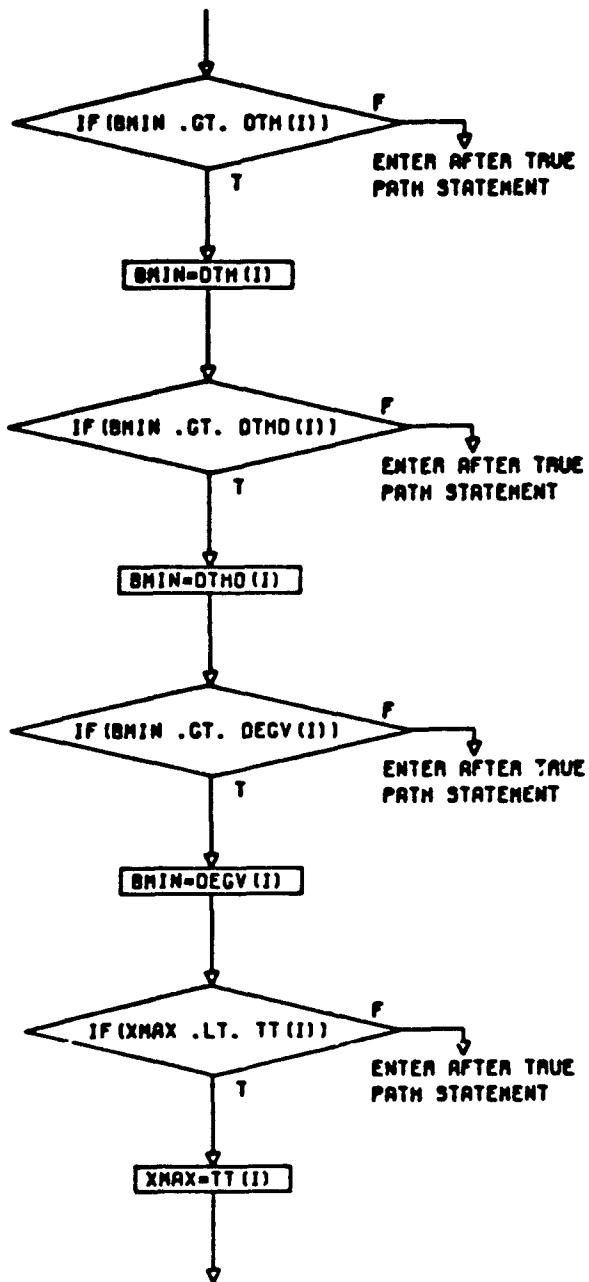
250
FORMAT (8F16.5)

CONT. ON PG 6

PG 5 OF 10

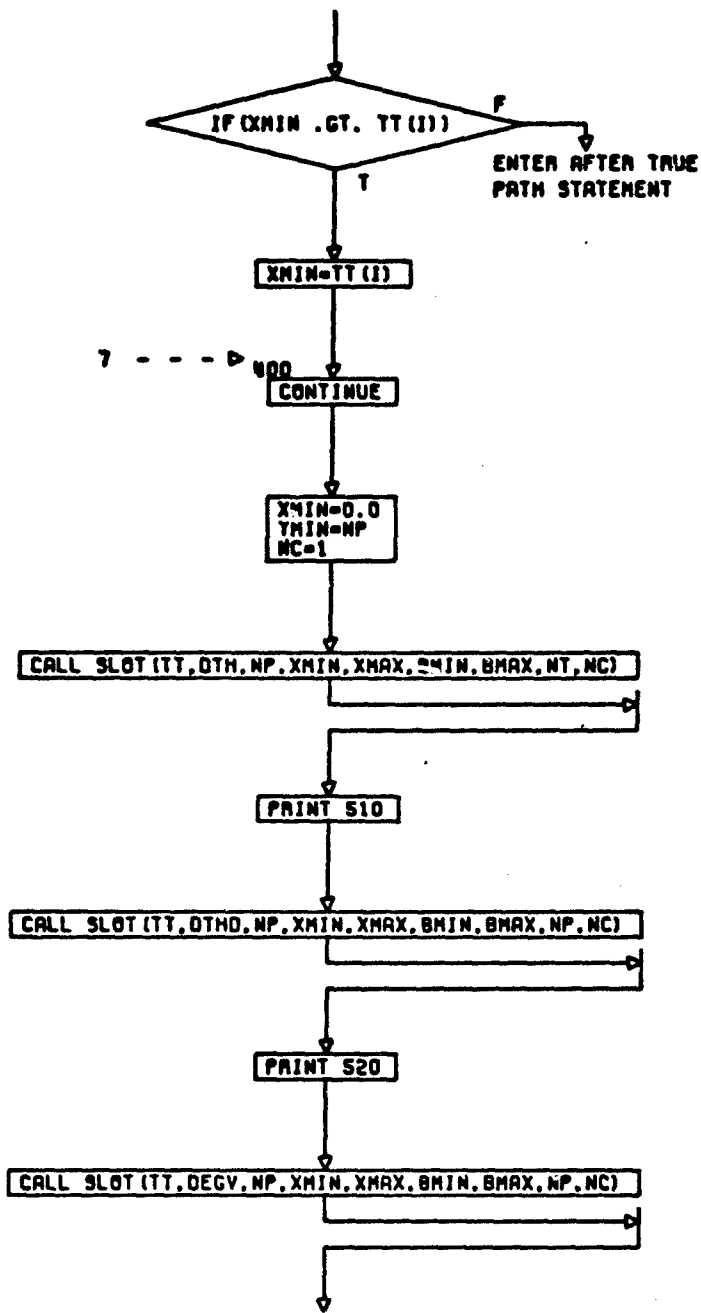






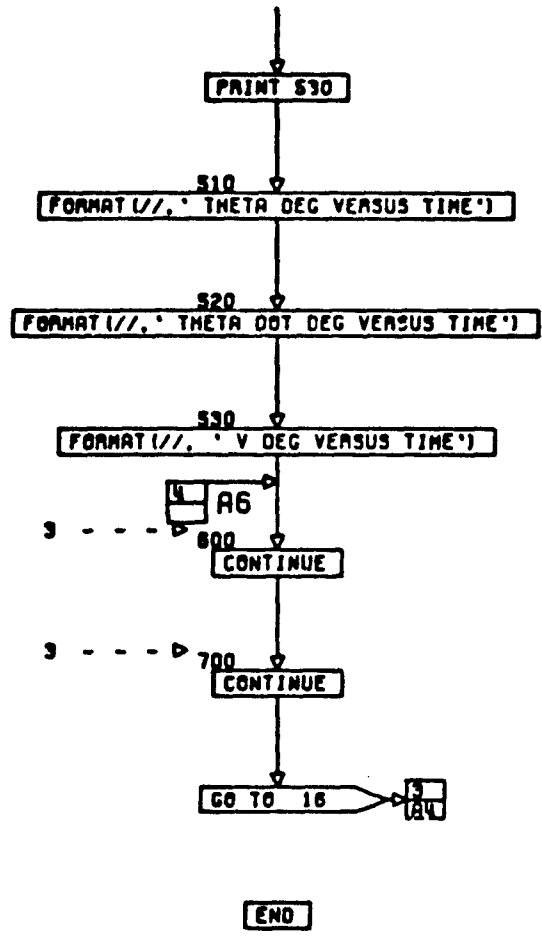
CONT. ON PG 9

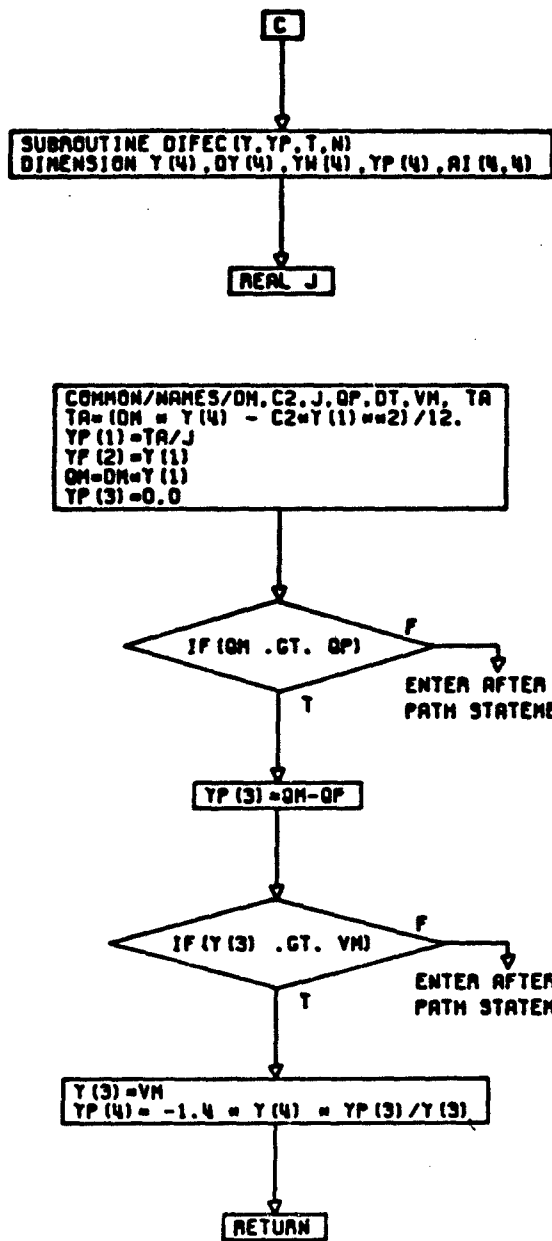
PG 8 OF 10



CONT. ON PG 10

PG 9 OF 10





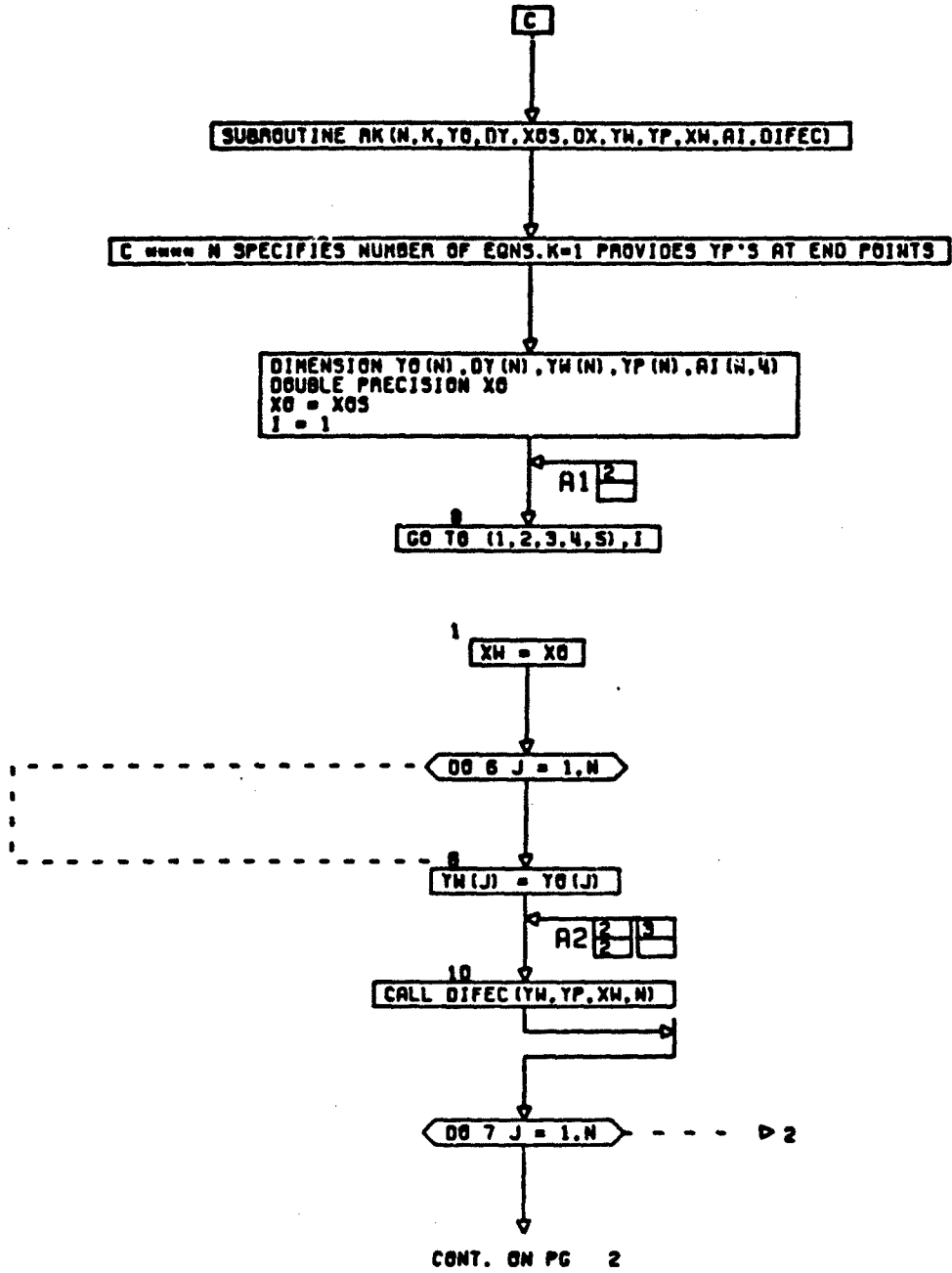
CONT. ON PG 2

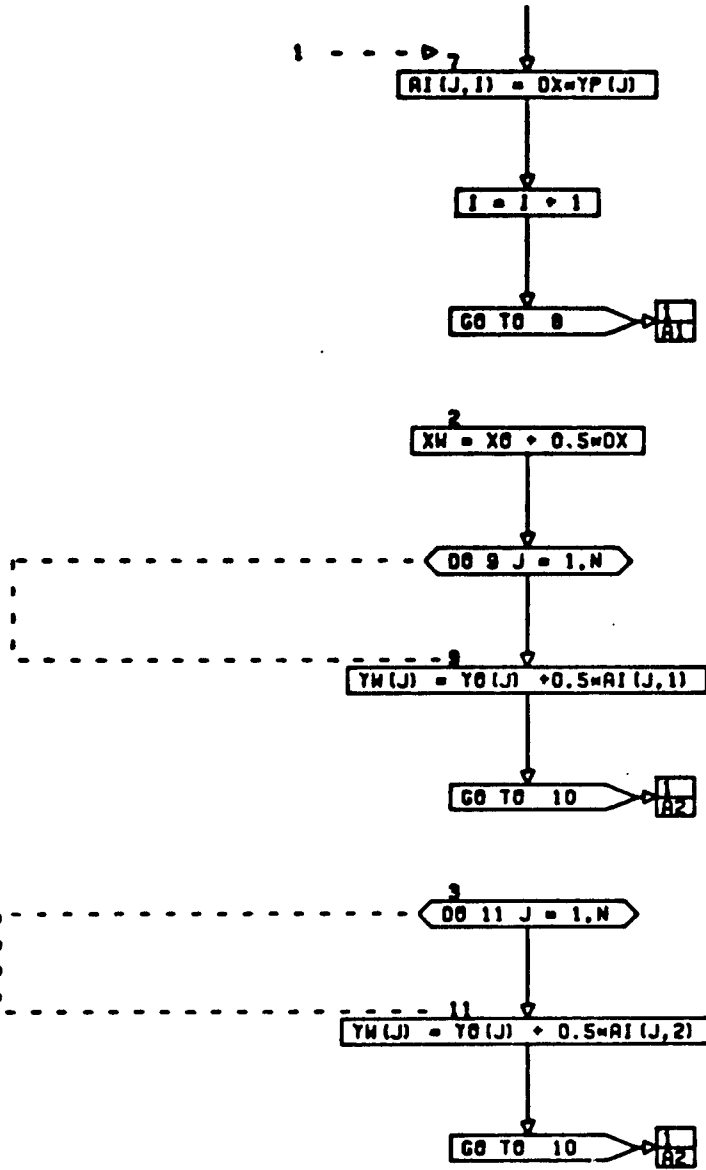
PG 1 OF 1

END

PG 2 FINAL

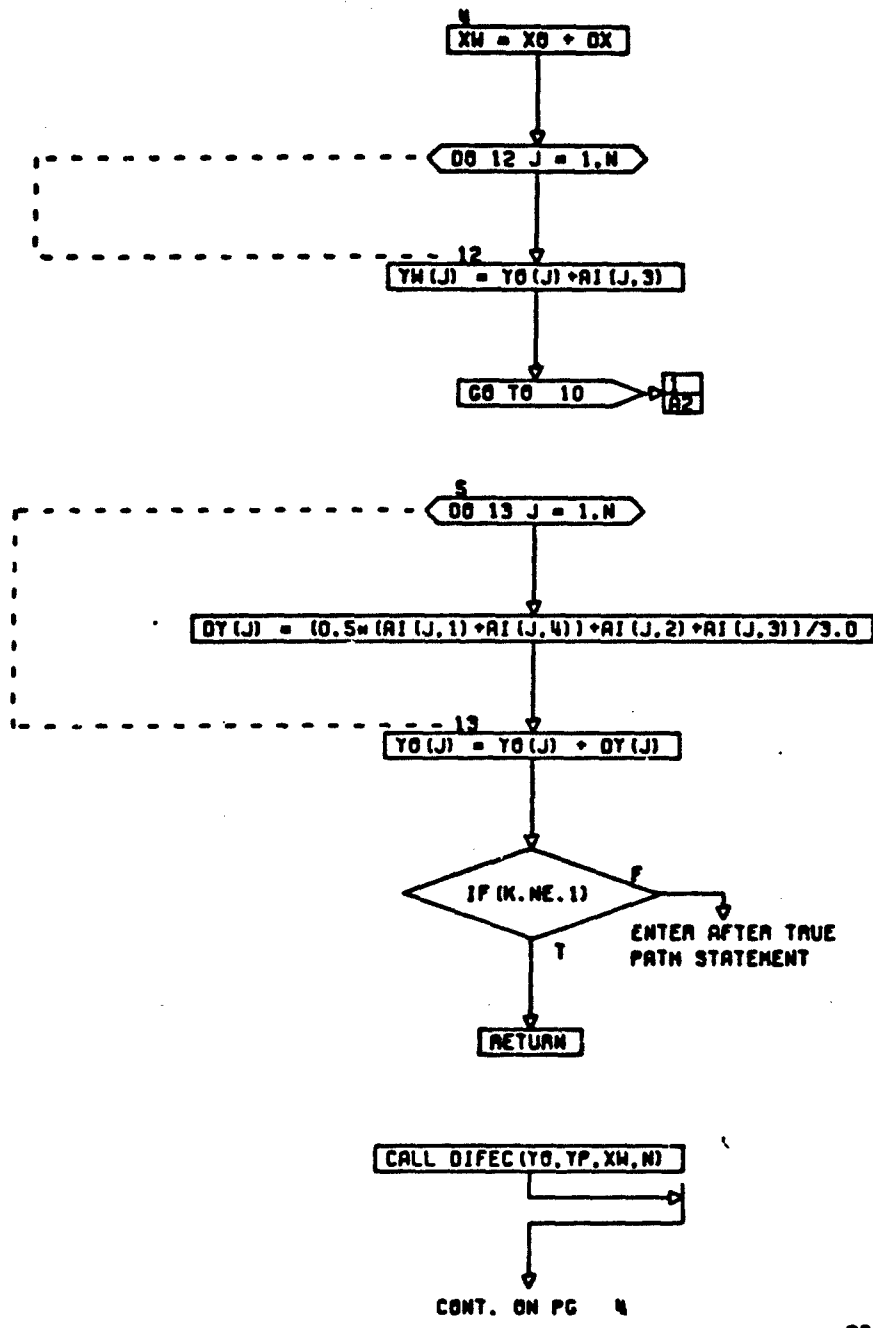
A-22





CONT. ON PG 3

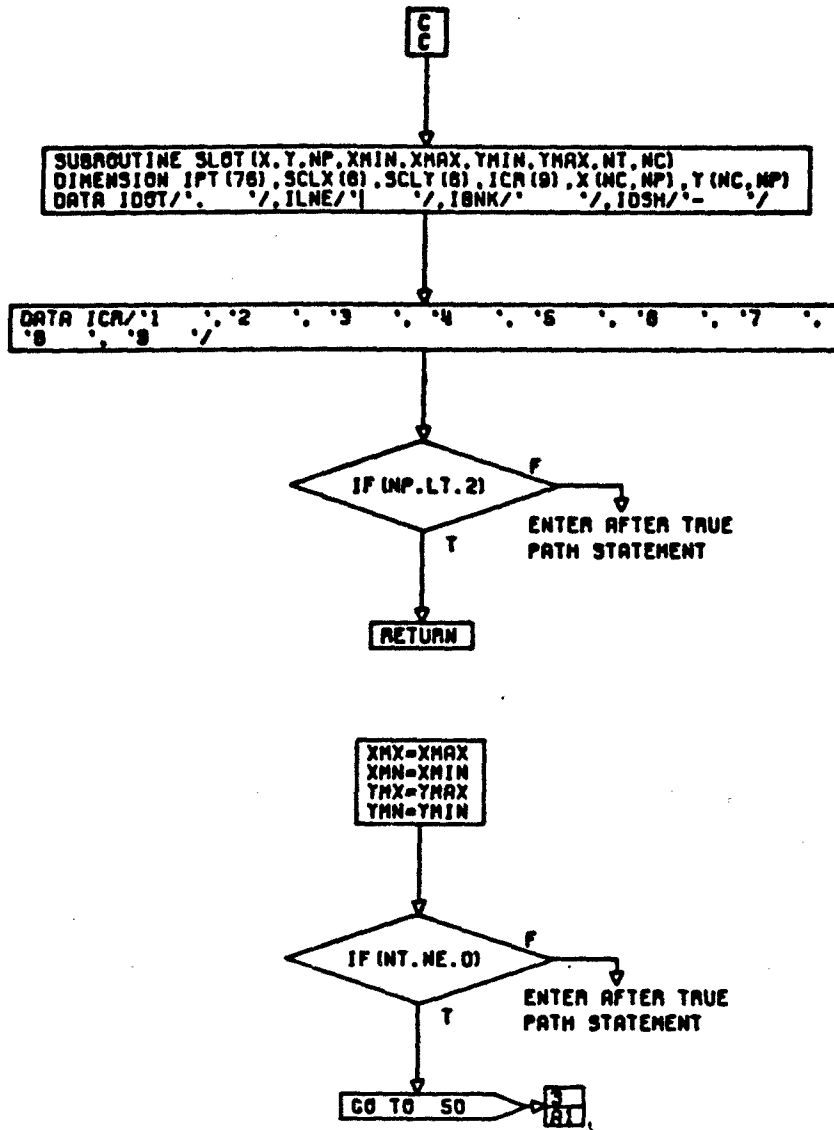
PG 2 OF 4



↓
RETURN

END

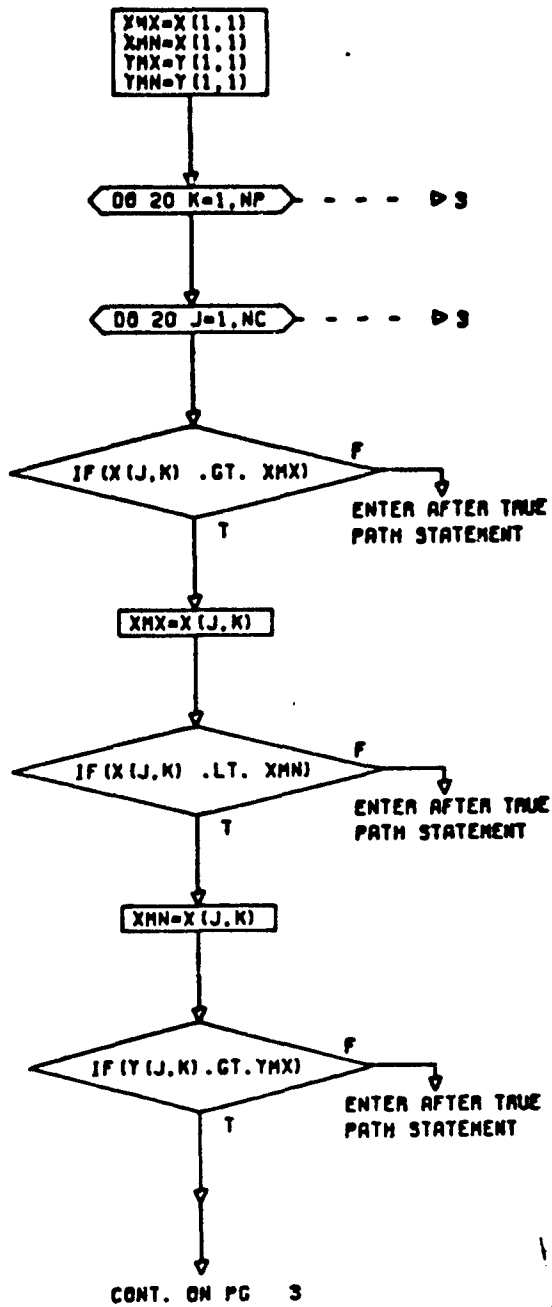
CE 3 FINAL

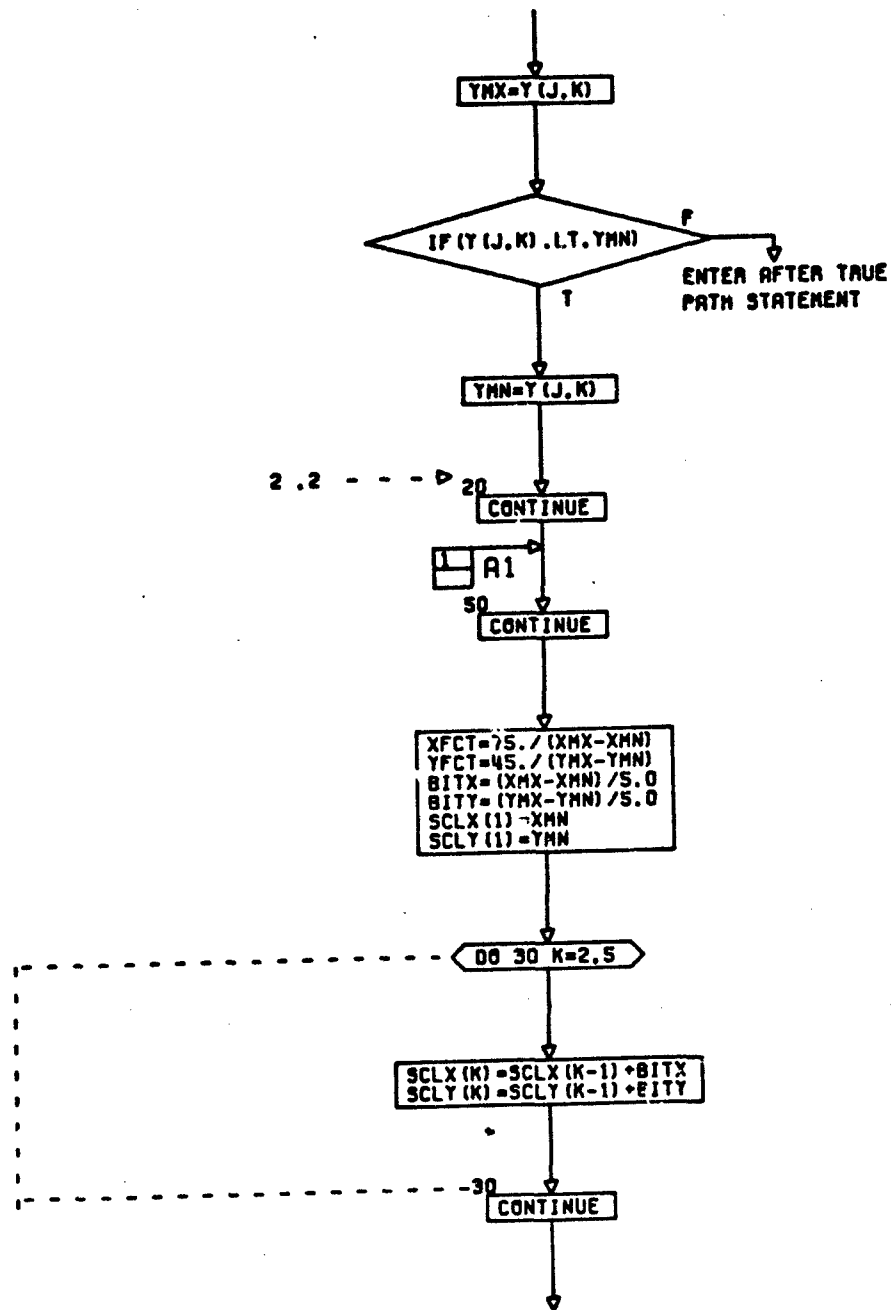


CONT. ON PG 2

PG 1 OF 7

A-27





CONT. ON PG 4

PG 3 OF 7

SCLX (8) = XM
SCLY (8) = YM
PRINT 999, (SCLX (M), M=1, 8)

DO 100 I=1, 48 ----- > 7

DO 110 J=1, 78

IPT (J) = IBNK

110
CONTINUE

DO 111 J=1, 78, 15

IPT (J) = ILNE

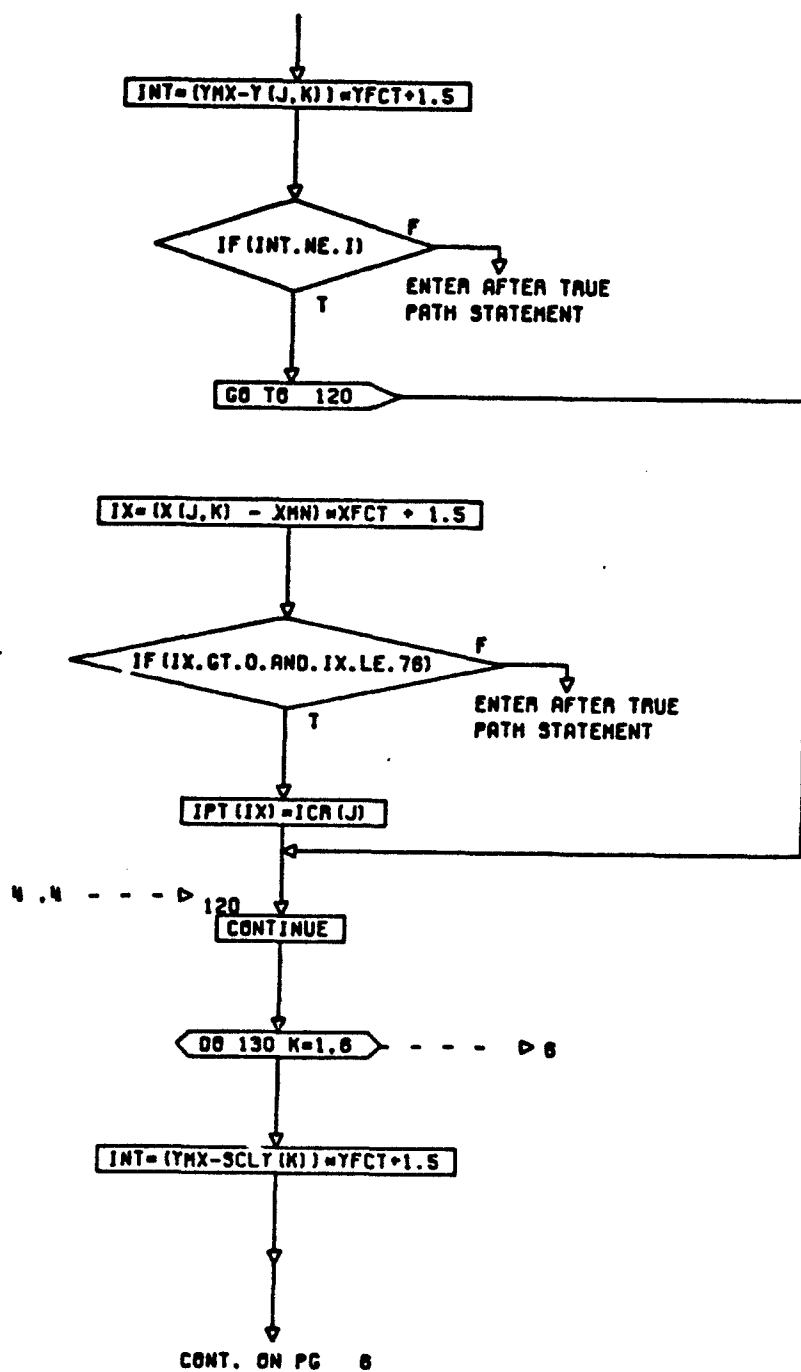
111
CONTINUE

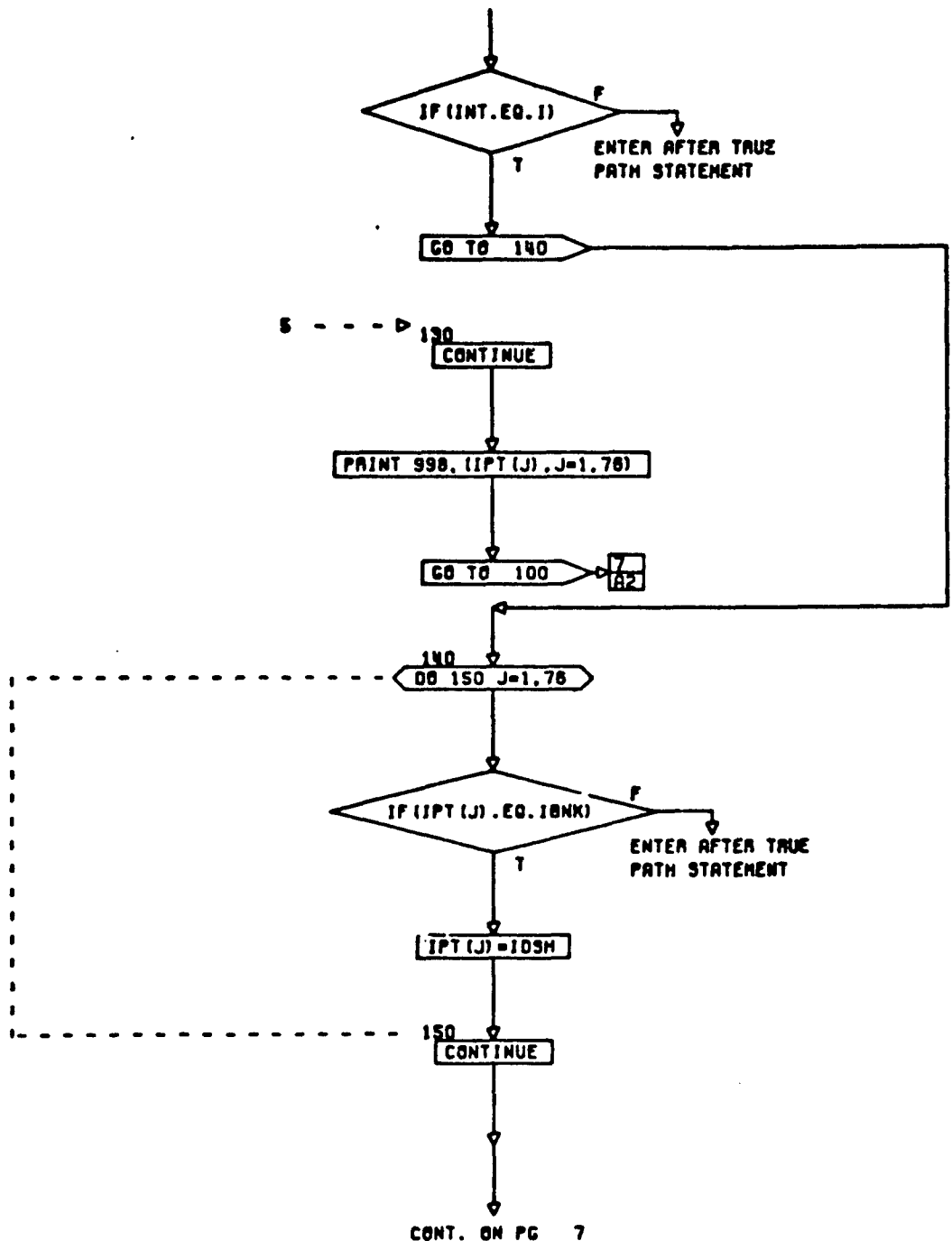
DO 120 K=1, NP ----- > 5

DO 120 J=1, NC ----- > 5

CONT. ON P; 5

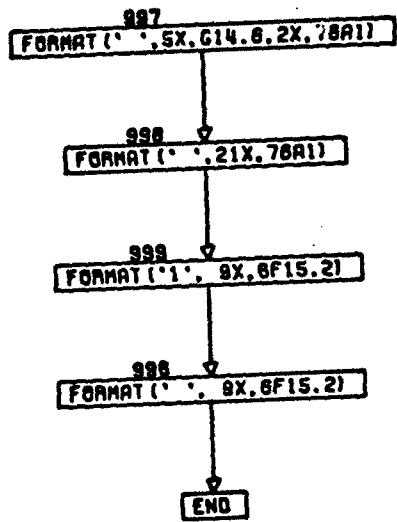
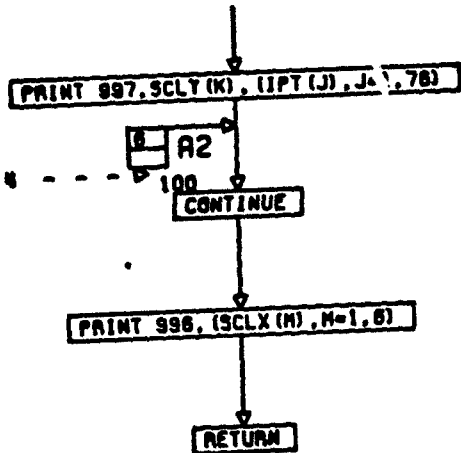
PG. 4 OF 7





CONT. ON PG 7

PG 8 OF 7



PART II
DIGITAL CHECK
SOLUTIONS

107,974 02.01.00 1030:0
11.11.2010
10.11.2010
11.11.2010

1030:0

SYSTEMS REAL-TIME MONITOR-4.0

PAGE 1

IN IN

```

54 NCS=JES46 1
55 MCD=MD46 1
56 NCU=NU46 1
57 NOP=NP46 1
58 THCD=0
59 LINCNT=1
60 ICHT=CTP/DT *8.5
61 MCD=21
62 DO 50 K=L,NEO
63 VPK=0
64 VCK=0
65 CONTINUE
66 T=0
67 PAHI=0
68 CALL DIFEG(VP,T,NEO)
69 LONTIME
70 IF(LINCNT EQ 0) GO TO 31
71 TEMP=THCD/THCNT
72 CONTINUE
73 LINCNT=LINCNT-1
74 IF(LINCNT NE 0) GO TO 40
75 LINCNT=50
76 PRINT 997,(H01(J,NCS),J=L,0),(H02(L,NCD),L=L,0)
77 PRINT 997,(H04(K),K=L,20)
78 PRINT 997,(H04(K),K=L,20)
79 PRINT 997,(H04(K),K=L,20)
80 PRINT 999
81 NPT=NPT+1
82 IF(NPT GT 350)NPT=350
83 XEL(OUT)=T
84 VPL(1,NPT)=EPT
85 IF(NCS EQ 1)GO TO 41
86 IF(NCS EQ 4)GO TO 41
87 VPL(2,NPT)=THCD
88 VPL(3,NPT)=TR
89 GO TO 42
90 VPL(2,NPT)=THCD
91 VPL(3,NPT)=TR
92 CONTINUE
93 PRINT 998,' ',9014,6,7136,8014,6)
94 FORMAT(' ',F14.3,F14.4,F14.5,F14.6,F14.7,F14.8,F14.9,F14.10,F14.11,F14.12)
95 IF(T GE THD)GO TO 200
96 DO 50 K=L,ICNT
97 LL=0
98 CALL BK(NEO,LL,V,DV,T,DT,VM,VP,TR,RI,DIFEG)
99 NUM=NUM+1
100 T=THCNT
101 CALL DIFEG(VP,T,NEO)
102 PRINT 998,T,(V(J),J=L,NEO),(VP(L),L=L,NEO)
103 CONTINUE
104 GO TO 30
105 PRINT 998,' ',F14.3,F14.4,F14.5,F14.6,F14.7,F14.8,F14.9,F14.10,F14.11,F14.12)
106

```

```

00140
00150
00160
00170
00180
00200
00210
00220
00230
00250
00240
00270
00200
00300
00330
00350
00370
00380

```


12/19/74 8:41 AM MARIIC SYSTECS REAL-TIME MONITOR-0.0
SYSTEMS 8506 FORTRAN IV COMPILER (REV. 0)

```

107 PRINT
108
109
110
111
112
113
114
115
116
117
118
119
120
121
122
123
124
125
126
127
128
129
130
131
132
133
134
135
136
137
999 FWRITE(1,9%,TIME,60,THRO DOT,100,EPST,120,TR,
1 17,LP5,60,THIN DOT,50,THRD DOT,120,DR,100,DR...')
203 GO TO 201,200,202,201,NC5
201 VNC(1)=005
VNC(2)=01
VNC(3)=500
VNC(4)=005
VNC(5)=01
VNC(6)=500
NS%1
GO TO 203
202 VNC(1)=005
VNC(2)=10
VNC(3)=500
VNC(4)=005
VNC(5)=10
VNC(6)=500
NS%2
203 NMI=0
DOP=450TP
MCS=0.71
DO 204 I=1,2
PRINT 997,(MCS(I),MCS),I=1,2,(MCS(L,NC5),L=1,2)
1 (MCS(MC),MCS),M=1,6,(MCS(N,NP),N=1,7)
PRINT 907,(MCS(K),K=1,20)
CALL FLOT(XPL,VPL,NPT,MBC,MBC,VBC,MBC)
XMI=000
XMC=0000000
204 CONTINUE
GO TO 10
END

```

SYSTEMS : SUBPROGRAMS : TRANSLATION : COMPILER (REV. 0)

SYMBOL	USAGE	MODE	STATEMENT	LOCATION IN MAIN
DIM	VARIABLE	REAL	PARS	C0007C
DHE	VARIABLE	REAL	PARS	C0007C
CJE	VARIABLE	REAL	PARS	C0007C
DT	VARIABLE	REAL	PARS	C0007C
DTP	VARIABLE	REAL	PARS	C0007C
DIN	VARIABLE	REAL	LOCAL	P00204
UV	VARIABLE	REAL	EXTERNAL	P00208
DI1ED	PROCEDURE	REAL	EXTERNAL	X02119
LL	VARIABLE	REAL	PARS	C0008C
EPOT	VARIABLE	REAL	LOCAL	P00083
EPS	VARIABLE	REAL	LOCAL	P00083
EPT	VARIABLE	REAL	LOCAL	P00083
EXIT	PROCEDURE	REAL	EXTERNAL	P00083
F	VARIABLE	REAL	PARS	C00058
Q OT	PROCEDURE	REAL	EXTERNAL	X0217C
HD	VARIABLE	REAL	PARS	C0009C
HD1	APPAY	REAL	HEAD	C00148
HD2	APPAY	REAL	HEAD	C00198
HD3	APPAY	REAL	HEAD	C00228
HD4	APPAY	REAL	HEAD	C00228
HEAD	COMMON BLOCK	REAL	S00248	
HEADL	APPAY	REAL	HEAD	C00248
I	VARIABLE	INTEGER	LOCAL	P0032C
IINT	VARIABLE	INTEGER	LOCAL	P00338
IINTT	PROCEDURE	INTEGER	EXTERNAL	X00104
J	VARIABLE	INTEGER	LOCAL	P00324
K	VARIABLE	INTEGER	LOCAL	P00328
L	VARIABLE	INTEGER	LOCAL	P0032C
LL	VARIABLE	INTEGER	LOCAL	P00348
LNCONT	VARIABLE	INTEGER	LOCAL	P00344
M	VARIABLE	INTEGER	LOCAL	P00348
MAIN	PROCEDURE	INTEGER	ENTRY	P0146C
N	VARIABLE	INTEGER	LOCAL	P0034C
NCD	VARIABLE	INTEGER	CASE	C00084
NCH	VARIABLE	INTEGER	CASE	C00088
NCS	VARIABLE	INTEGER	CASE	C00088
NOEL	VARIABLE	INTEGER	TABLES	C00088
NOI	VARIABLE	INTEGER	TABLES	C00088
NON	VARIABLE	INTEGER	TABLES	C00088
NPY	VARIABLE	INTEGER	CASE	C00088
NSH	VARIABLE	INTEGER	CASE	C00088
NUM	VARIABLE	INTEGER	LOCAL	P00354
O	VARIABLE	INTEGER	LOCAL	P00358
OUT	APPAY	REAL	LOCAL	P0035C
PARS	COMMON BLOCK	REAL	S00014	
PE	VARIABLE	REAL	S0000C	
PFDT	VARIABLE	REAL	LOCAL	P0008C
PLOT	PROCEDURE	REAL	LOCAL	P00088
PN	VARIABLE	REAL	EXTERNAL	X02158
PIOT	VARIABLE	REAL	LOCAL	P00088
PS	VARIABLE	REAL	LOCAL	P00064
PTE	VARIABLE	REAL	PARS	C00048
			PARS	C0004C

SYSTEMS : 3.06 FORTRAN IV COMPILER (REV Q)

SYMBOL	USAGE	TYPE	STRUCTURE	LOCATION IN MAIN
UNKPT0	VARIABLE	REAL	LOCAL	P00238
UNKPT1	VARIABLE	REAL	LOCAL	P00283
UNKPT2	VARIABLE	REAL	LOCAL	P00330
UNKPT3	VARIABLE	REAL	LOCAL	P00377
UNKPT4	VARIABLE	REAL	LOCAL	P00424
UNKPT5	VARIABLE	REAL	LOCAL	P00471
UNKPT6	VARIABLE	REAL	LOCAL	P00518
UNKPT7	VARIABLE	REAL	LOCAL	P00565
UNKPT8	VARIABLE	REAL	LOCAL	P00612
UNKPT9	VARIABLE	REAL	LOCAL	P00659
UNKPT10	VARIABLE	REAL	LOCAL	P00706
UNKPT11	VARIABLE	REAL	LOCAL	P00753
UNKPT12	VARIABLE	REAL	LOCAL	P00800
UNKPT13	VARIABLE	REAL	LOCAL	P00847
UNKPT14	VARIABLE	REAL	LOCAL	P00894
UNKPT15	VARIABLE	REAL	LOCAL	P00941
UNKPT16	VARIABLE	REAL	LOCAL	P00988
UNKPT17	VARIABLE	REAL	LOCAL	P01035
UNKPT18	VARIABLE	REAL	LOCAL	P01082
UNKPT19	VARIABLE	REAL	LOCAL	P01129
UNKPT20	VARIABLE	REAL	LOCAL	P01176
UNKPT21	VARIABLE	REAL	LOCAL	P01223
UNKPT22	VARIABLE	REAL	LOCAL	P01270
UNKPT23	VARIABLE	REAL	LOCAL	P01317
UNKPT24	VARIABLE	REAL	LOCAL	P01364
UNKPT25	VARIABLE	REAL	LOCAL	P01411
UNKPT26	VARIABLE	REAL	LOCAL	P01458
UNKPT27	VARIABLE	REAL	LOCAL	P01505
UNKPT28	VARIABLE	REAL	LOCAL	P01552
UNKPT29	VARIABLE	REAL	LOCAL	P01599
UNKPT30	VARIABLE	REAL	LOCAL	P01646
UNKPT31	VARIABLE	REAL	LOCAL	P01693
UNKPT32	VARIABLE	REAL	LOCAL	P01740
UNKPT33	VARIABLE	REAL	LOCAL	P01787
UNKPT34	VARIABLE	REAL	LOCAL	P01834
UNKPT35	VARIABLE	REAL	LOCAL	P01881
UNKPT36	VARIABLE	REAL	LOCAL	P01928
UNKPT37	VARIABLE	REAL	LOCAL	P01975
UNKPT38	VARIABLE	REAL	LOCAL	P02022
UNKPT39	VARIABLE	REAL	LOCAL	P02069
UNKPT40	VARIABLE	REAL	LOCAL	P02116
UNKPT41	VARIABLE	REAL	LOCAL	P02163
UNKPT42	VARIABLE	REAL	LOCAL	P02210
UNKPT43	VARIABLE	REAL	LOCAL	P02257
UNKPT44	VARIABLE	REAL	LOCAL	P02304
UNKPT45	VARIABLE	REAL	LOCAL	P02351
UNKPT46	VARIABLE	REAL	LOCAL	P02398
UNKPT47	VARIABLE	REAL	LOCAL	P02445
UNKPT48	VARIABLE	REAL	LOCAL	P02492
UNKPT49	VARIABLE	REAL	LOCAL	P02539
UNKPT50	VARIABLE	REAL	LOCAL	P02586
UNKPT51	VARIABLE	REAL	LOCAL	P02633
UNKPT52	VARIABLE	REAL	LOCAL	P02680
UNKPT53	VARIABLE	REAL	LOCAL	P02727
UNKPT54	VARIABLE	REAL	LOCAL	P02774
UNKPT55	VARIABLE	REAL	LOCAL	P02821
UNKPT56	VARIABLE	REAL	LOCAL	P02868
UNKPT57	VARIABLE	REAL	LOCAL	P02915
UNKPT58	VARIABLE	REAL	LOCAL	P02962
UNKPT59	VARIABLE	REAL	LOCAL	P03009
UNKPT60	VARIABLE	REAL	LOCAL	P03056
UNKPT61	VARIABLE	REAL	LOCAL	P03103
UNKPT62	VARIABLE	REAL	LOCAL	P03150
UNKPT63	VARIABLE	REAL	LOCAL	P03197
UNKPT64	VARIABLE	REAL	LOCAL	P03244
UNKPT65	VARIABLE	REAL	LOCAL	P03291
UNKPT66	VARIABLE	REAL	LOCAL	P03338
UNKPT67	VARIABLE	REAL	LOCAL	P03385
UNKPT68	VARIABLE	REAL	LOCAL	P03432
UNKPT69	VARIABLE	REAL	LOCAL	P03479
UNKPT70	VARIABLE	REAL	LOCAL	P03526
UNKPT71	VARIABLE	REAL	LOCAL	P03573
UNKPT72	VARIABLE	REAL	LOCAL	P03620
UNKPT73	VARIABLE	REAL	LOCAL	P03667
UNKPT74	VARIABLE	REAL	LOCAL	P03714
UNKPT75	VARIABLE	REAL	LOCAL	P03761
UNKPT76	VARIABLE	REAL	LOCAL	P03808
UNKPT77	VARIABLE	REAL	LOCAL	P03855
UNKPT78	VARIABLE	REAL	LOCAL	P03902
UNKPT79	VARIABLE	REAL	LOCAL	P03949
UNKPT80	VARIABLE	REAL	LOCAL	P04000
UNKPT81	VARIABLE	REAL	LOCAL	P04051
UNKPT82	VARIABLE	REAL	LOCAL	P04102
UNKPT83	VARIABLE	REAL	LOCAL	P04153
UNKPT84	VARIABLE	REAL	LOCAL	P04204
UNKPT85	VARIABLE	REAL	LOCAL	P04255
UNKPT86	VARIABLE	REAL	LOCAL	P04306
UNKPT87	VARIABLE	REAL	LOCAL	P04357
UNKPT88	VARIABLE	REAL	LOCAL	P04408
UNKPT89	VARIABLE	REAL	LOCAL	P04459
UNKPT90	VARIABLE	REAL	LOCAL	P04510
UNKPT91	VARIABLE	REAL	LOCAL	P04561
UNKPT92	VARIABLE	REAL	LOCAL	P04612
UNKPT93	VARIABLE	REAL	LOCAL	P04663
UNKPT94	VARIABLE	REAL	LOCAL	P04714
UNKPT95	VARIABLE	REAL	LOCAL	P04765
UNKPT96	VARIABLE	REAL	LOCAL	P04816
UNKPT97	VARIABLE	REAL	LOCAL	P04867
UNKPT98	VARIABLE	REAL	LOCAL	P04918
UNKPT99	VARIABLE	REAL	LOCAL	P04969
UNKPT100	VARIABLE	REAL	LOCAL	P05020

INPUT

```

1 SUBROUTINE INPUT
2 COMMON/ND2/ND1(20,4),ND2(10,2),ND3(2,4,6),ND4 (7,6),NDALL(20)
3 COMMON/ND3/ND5,ND6(55)
4 DIMENSION NAME(55)
5 DATA NAME / KI, KR, KP, KH, PTN, ROM, J, PTE,
6 TRUC, TRUP, TRUV, DCH, ANCH, L, C, V, B,
7 FR, PS, NCS, NCD, NCH, F, DT, TD, DTP,
8 NE, CH2, DSE, KSE, JHE, DHE, TGF, NOP, ORV,
9 ZET, GSH, DMO, TRUJ, HO, TALM, KEO, KBH, TRQ,
10 TRM, TBO, TBH, EI, TRUL, TRU2, RI, TRU3, TRU4,
11 TRU, TRU5,
12 10 REHD 999, 10, VRL
13 IF (10 GT 100) STOP 1
14 IF (10 EQ 100) GO TO 20
15 PARM(10)=VRL
16 GO TO 10
17 998 FORMAT ('0',/,' ',5(13,1X,A4,' ',014.6,' ',2X))
18 20 CONTINUE
19 N5=PARM(20)+0.1
20 NCD=PARM(21)+0.1
21 NCH=PARM(22)+0.1
22 NOP=PARM(23)+0.1
23 NCP=PARM(24)+0.1
24 PRINT 997,(HO1(J,NCS),J=1,8),(ND2(L,NCD),L=1,8),
25 (ND3(NCD,NCH,ND),ND=1,6),(ND4(N,NOP),N=1,7),
26 FORMAT('0',40X,20H4)
27 1 (ND3(NCD,NCH,ND),ND=1,6),(ND4(N,NOP),N=1,7)
28 PRINT 998,(K,NAME(K),PARM(K),K=1,55)
29 FORMAT('1',31H4)
30 RETURN
31 END

```

SYSTEMS REAL-TIME MONITOR-4.0

12.19.77 05.01.03 HS0010

S Y S T E M S F O R T R A N I V C O M P I L E R (R E V . 0)

SYMBOL	USAGE	MODE	STORAGE	LOCATION IN INPUT
>A	LABEL	TRANSFER	LOCAL	P0015C
>A1	LABEL	TRANSFER	LOCAL	P001B8
>A2	LABEL	FORMAT	LOCAL	P00073
>A3	LABEL	FORMAT	LOCAL	P00037
>A8	LABEL	FORMAT	LOCAL	P00068
>A9	VARIBLE	INTEGER FULLWORD	LOCAL	P00041
>A01	VARIBLE	INTEGER FULLWORD	LOCAL	P003CC
>A02	VARIBLE	INTEGER FULLWORD	LOCAL	P00309
C.0001	CONSTANT	REAL	LOCAL	P00304
C.0002	CONSTANT	REAL	LOCAL	P003E8
C.0003	CONSTANT	INTEGER FULLWORD	LOCAL	P003E4
C.0004	CONSTANT	INTEGER FULLWORD	LOCAL	P003E8
C.0005	CONSTANT	INTEGER DOUBLE	LOCAL	P003E8
R. IF	PROCEDURE	REAL	LOCAL	P003E8
C. RI	PROCEDURE	REAL	EXTERNAL	P003E8
EXIT	PROCEDURE	REAL	EXTERNAL	X001F0
HD1	APPHY	REAL	EXTERNAL	X007C8
HD2	APPHY	REAL	EXTERNAL	C00100
HD3	APPHY	REAL	EXTERNAL	C00140
HD4	APPHY	REAL	EXTERNAL	C00250
IC:RD	COMMON BLOCK	REAL	EXTERNAL	C00250
ID	APPHY	REAL	EXTERNAL	C002F8
INPUT	APPHY	REAL	EXTERNAL	P0094C
J	PROCEDURE	INTEGER FULLWORD	LOCAL	P00158
K	PROCEDURE	INTEGER FULLWORD	LOCAL	P00059
L	PROCEDURE	INTEGER FULLWORD	LOCAL	P00059
N	PROCEDURE	INTEGER FULLWORD	LOCAL	P00054
N	PROCEDURE	INTEGER FULLWORD	LOCAL	P00058
N	PROCEDURE	INTEGER FULLWORD	LOCAL	P0005C
N	PROCEDURE	INTEGER FULLWORD	LOCAL	P00060
N	PROCEDURE	INTEGER FULLWORD	LOCAL	P00064
N	PROCEDURE	INTEGER FULLWORD	LOCAL	P00140
N	PROCEDURE	INTEGER FULLWORD	LOCAL	P00144
N	PROCEDURE	INTEGER FULLWORD	LOCAL	P00148
N	PROCEDURE	INTEGER FULLWORD	LOCAL	P0014C
N	PROCEDURE	INTEGER FULLWORD	LOCAL	C00000
N	PROCEDURE	INTEGER FULLWORD	LOCAL	C00000
N	PROCEDURE	REAL	EXTERNAL	X0015C
N	PROCEDURE	REAL	EXTERNAL	P00154
N	PROCEDURE	REAL	EXTERNAL	X00150
N	PROCEDURE	REAL	EXTERNAL	X001C0
N	PROCEDURE	REAL	EXTERNAL	P00150
N	PROCEDURE	REAL	EXTERNAL	X00160

DIFEO

```

1 2 3 4 5 6 7 8 9 10 11 12 13 14 15 16 17 18 19 20 21 22 23 24 25 26 27 28 29 30 31 32 33 34 35 36 37 38 39 40 41 42 43 44 45 46 47 48 49 50 51 52 53
COMMON LINE: C,IF,OV,VP,T,NEO)
COMMON/TAH/CS/IN/LLC,500):TOTDLC,500),NOEL,TOLD,NOH
COMMON/TAH/EP:UT,XTAP,THIDT,THGS
COMMON/TAH/SP:KXT,SR,XP,XTM,PTG,RDM,XJ,PTC,TRAP,TRUM,DGN
1 1 RVH: XL, C, V, XA, P, S, XNC, XNC, XNC, XNC, F, DT, TND, DTP, XG
1 1 CHZ, DSE, XSE, XHE, DHE, TOF
1 1 XOP, MI, ZET, DSH, DSO, TRUL, HO, TALM
1 1 XAG, XWH, TEG, TGH, TBO, TSH
1 1 EL, TGH, TPU, RL, TAU, TRM, ZD, TRUS
COMMON/TAH/CS/IN/LLC,500):TOTDLC,500),NOEL,TOLD,NOH
DIMENSION Y(NEO), VP(NEO)
TMPT1=283165
THG= Y(1)
THG0= Y(2)
IF(Y(3) GT. TALM)Y(3)=TALM
IF(Y(3) LT. -TALM)Y(3)=-TALM
TA= Y(2)
PF= Y(4)
PN= Y(5)
EPT= Y(6)
THS= Y(7)
IF(Y(8) LT. -RVR)Y(8)=-RVR
IF(Y(8) GT. RVR)Y(8)=RVR
RV= Y(8)
THM= Y(9)
THG= Y(10)
THID= Y(11)
TGF= Y(12)
TGF0= Y(13)
THS= Y(14)
THS0= Y(15)
THS= Y(16)
THS= Y(17)
THS= Y(18)
EPS= Y(19)
PHS= Y(20)
VP(12)= Y(13)
THG= Y(21)
THRT= 0
THDT= 0
TD= 0
THIDT= 0
THSDT= 0
00 TO (10,20),NCO
10 GO TO (11,12,13,14),NCH
11 THSDT=F
IF(T,GT.(F/RL))GO TO 50
THSDT=R1
00 TO 50
12 THDT=F
00 TO 50
13 TD=1000

```

020610

020660
020670
020680
020690
021100
021110
021120
021130

02140
02150
02160

02170

FILE

```

14 THROT=0
   THROT=THROT+THROT
GO TO 50
20 GO TO (21,22,23,24),NCH
21 THROT=0.015*SIN(THROT+0.5)
GO TO 50
22 THROT=0.18*SIN(THROT+0.6)
GO TO 50
23 THROT=0.18*SIN(THROT+0.6)
GO TO 50
24 THROT=0.6*SIN(THROT+0.5)
   THROT=THROT+THROT
90 CONTINUE
   IF(TOLD.EQ.1)GO TO 123
   TOL=THROT/NCH
   TOL=ABS(TOL)
   TOL=(NCH)*TOL
   TOL=(NCH)*TOL
   TOLD=1
NON=NON+1
   IF(NON.GT.NEL)NON=1
123 CONTINUE
   IF(ZONE.EQ.0)GO TO 124
   TOL=THROT
   TOL=THROT
124 CONTINUE
   TOSPT=TOSPT+TOSPT
   THSPOT=THSPOT
GO TO (150,250,350,450,550,650),NCP
150 CONTINUE
160 CONTINUE
C*****
C *****
C *****
181 EPS=XI*(THS-TM)-NON*(THD-NCH)*THOT
   TAD=(EPS+PF)-PTM*(THD-TMOT) -TA)/TRUC
   IF(TA.GE.TAL)TAD=0.0)TAD=0.0
   IF(TA.LE.-TAL)TAD=0.0)TAD=0.0
   TAD=ABS(TAD)
   THROT=(TAD+TD-DCH*(THD-TMOT))/N
   TAD=0.0
   EPOT=0.0
   AMOT=0.0
   EPT=THS-TM
   V(G)=EPT
GO TO 400
200 CONTINUE
C *****
C *****
C *****
EPR=XB*(NKI+EPT)+NON*(THSD-TMOT)

```



```

DIFER
107 EPS=LR-NH*THD
108 TROT=(FILE+EPS+FF)-PNA*(THD-THD0) -TR)/TRUC
109 IF (TR < TRUM AND TRD GT 0.) TRD0=0
110 IF (TR LE TRLM AND TRD LT 0.) TRD0=0
111 FF0=XND*(EM*P+TRC(-FF)/TRUP
112 EPDT=(HSDT-THD0
113 PHDT=0 0
114 PHDT=0 0
115 GO TO 499
116 THD0T=(TR+TD-CGM*(THD-THD0))/NJ
117
118
119
120
121
122
123
124
125
126
127
128
129
130
131
132
133
134
135
136
137
138
139
140
141
142
143
144
145
146
147
148
149
150
151
152
153
154
155
156
157
158
159
201 EPS=LR-NH*THD
202 TROT=(FILE+EPS+FF)-PNA*(THD-THD0) -TR)/TRUC
203 IF (TR < TRUM AND TRD GT 0.) TRD0=0
204 IF (TR LE TRLM AND TRD LT 0.) TRD0=0
205 FF0=XND*(EM*P+TRC(-FF)/TRUP
206 EPDT=(HSDT-THD0
207 PHDT=0 0
208 PHDT=0 0
209 GO TO 499
210 THD0T=(TR+TD-CGM*(THD-THD0))/NJ
211
212
213
214
215
216
217
218
219
220
221
222
223
224
225
226
227
228
229
230
231
232
233
234
235
236
237
238
239
240
241
242
243
244
245
246
247
248
249
250
251
252
253
254
255
256
257
258
259
260
261
262
263
264
265
266
267
268
269
270
271
272
273
274
275
276
277
278
279
280
281
282
283
284
285
286
287
288
289
290
291
292
293
294
295
296
297
298
299
300
301
302
303
304
305
306
307
308
309
310
311
312
313
314
315
316
317
318
319
320
321
322
323
324
325
326
327
328
329
330
331
332
333
334
335
336
337
338
339
340
341
342
343
344
345
346
347
348
349
350
351
352
353
354
355
356
357
358
359
360
361
362
363
364
365
366
367
368
369
370
371
372
373
374
375
376
377
378
379
380
381
382
383
384
385
386
387
388
389
390
391
392
393
394
395
396
397
398
399
400
401
402
403
404
405
406
407
408
409
410
411
412
413
414
415
416
417
418
419
420
421
422
423
424
425
426
427
428
429
430
431
432
433
434
435
436
437
438
439
440
441
442
443
444
445
446
447
448
449
450
451
452
453
454
455
456
457
458
459
460
461
462
463
464
465
466
467
468
469
470
471
472
473
474
475
476
477
478
479
480
481
482
483
484
485
486
487
488
489
490
491
492
493
494
495
496
497
498
499
500

```

00000

```

160 NTRP=0R*(THSDT-THSD)*2.14EPT
161 V(19)=EPS
162 RETURN
163 C*****
164 C ***** FLUM MODEL - POSITION CONTROL
165 C*****
166 500 EPI=THS-THD
167 V(C)=EPI
168 EFC=0.0
169 EP3=2.14EPT-3AR*THSD-80M*THD
170 GO TO 301
171 IF(FLH GT PS)FHP=PS
172 T=RCM*FHP/CL
173 THSDT=(THSD-DHM*(THSD-THD))/XJ
174 TEMP=0.
175 IF(THSD GT DSD)TEMP=THSDT-DSD
176 IF(THSD GT -DSD)TEMP=THSDT+DSD
177 TGP3D=(V(B)*TBU+TEMP-TGSPD)/TBU
178 VP(13)=TGP3D
179 PH3SD=(TRG+TGP3D+TGSPD+E1)/TRG
180 VP(20)=PH3SD
181 THSDC=(TRU3+PH3SD+PHSD-THSD)/TRU4
182 VP(18)=THSDC
183 VP(17)=V(18)
184 EPSR=7.1*(THS-THSD)+XOR*(THSDT-THSD)
185 EPSD=XKI*(THSDT-THSD)+XKR*(THSDT-THSD)
186 EPSDT=(TRU2/TRU1)*(TRU1*EPSD+EPSR)-EPS)/TRU2
187 VP(19)=EPSDT
188 GO TO (101,202,303,501),ICS
189 TGP3D=10.4*H1+H2*(THSD-THSD)-2.4*ZET+H3*TGSPD-H4*H5*TGSPD
190 VP(13)=TGP3D
191 PH3SD=(10.4*H1+H2*TGSPD+TGSPD+PHSD)/H3
192 TH3SD=(TRU3+PH3SD+PHSD-THSD)/TRU4
193 VP(20)=PH3SD
194 VP(18)=TH3SD
195 VP(17)=V(18)
196 EPS=XKI*(THS-THSD)+XKR*(THSDT-THSD)
197 GO TO 301
198 PHTD=THCEL
199 PHD=0.0
200 IF(LIMIT GT DSH)PHD=PHTD-DSH
201 IF(PHTD LT -DSH)PHD=PHTD+DSH
202 TH2SD=(PHD-THSD)/TRUS
203 VP(21)=TH2SD
204 PTD=TDDEL
205 PHD=0.0
206 IF(PTD GT DSD)PHD=PTD-DSD
207 IF(PTD LT -DSD)PHD=PTD+DSD
208 PH3SD=(XK3D+PHD-THSD)/TRUS
209 VP(30)=PH3SD
210 TH3SD=(TRU3+PH3SD+PHSD-THSD)/TRU4
211 VP(18)=TH3SD
212

```

12/19/74 09:01:03 MGNUG SYSTEMS 8.5.86 FORTRAN IV COMPILER (REV 0)

DI:EQ

```

213 VP(17)=V(18)
214 LPS=K*(I*(THS-THGS)+X*(THSDT-THGSD)-XCN*THMSD
215 GO TO 203
216 STOP CLO
217 250 TOSK=C*(MIN*THGD-2.*ZET*H*+TOSPOO-M*H*H*+TOSPO
218 THSP=C*(MIN*THGD-2.*ZET*H*+THSPOO-M*H*H*+THSPO
219 THSD=THSPD
220 THMSD=0
221 IF (THSD GT 164) THMSD=THSPD-D84
222 IF (THSD LT. (-684)) THMSD=THSPD+D84
223 THMSD=0
224 IF (THSD GT D86) THMSD=THSPD-D86
225 IF (THSD LT. (-D86)) THMSD=THSPD+D86
226 V(18)=THMSD
227 THSDT=(TRUI*THMSD+THSS )/TRUI
228 TOSK=THG-TTH*THSS
229 EPS=X*(I*(THS-TGSS)-XCN*THGSD-XCN*THMSD
230 THSDT=0
231 THGSD=(TRUI*THGSD+TOSPO-THGSD)/TRUI
232 VP(18)=THGSD
233 VP(12)=THSPDT
234 VP(13)=THSPDT
235 VP(14)=THSPDT
236 VP(15)=THSPDT
237 VP(16)=THSDT
238 VP(17)=THGSD
239 GO TO (101,202,307,501),NCS
240 EPS=X*(I*(THS-THGS)+XCN*(THSDT-THGSD)-XCN*THMSD
241 GO TO 201
242 EPS=X*(I*(THS-THGS)+XCN*(THSDT-THGSD)-XCN*THMSD
243 GO TO 303
244 EPT=THS-THG
245 Y(6)=EPT
246 GO TO 381
247 END
248

```

SYSTEMS 8306 FORTRAN IV COMPILER (REV. G)

SYMBOL	USAGE	NAME	STORAGE	LOCATION IN DIFED
>10	LABEL	TRANSFER	LOCAL	P00480
>100	LABEL	TRANSFER	LOCAL	P00500
>101	LABEL	TRANSFER	LOCAL	P00500
>11	LABEL	TRANSFER	LOCAL	P00484
>12	LABEL	TRANSFER	LOCAL	P00418
>123	LABEL	TRANSFER	LOCAL	P00614
>124	LABEL	TRANSFER	LOCAL	P00628
>13	LABEL	TRANSFER	LOCAL	P004E4
>14	LABEL	TRANSFER	LOCAL	P004F0
>150	LABEL	TRANSFER	LOCAL	P00664
>20	LABEL	TRANSFER	LOCAL	P00508
>208	LABEL	TRANSFER	LOCAL	P0078C
>201	LABEL	TRANSFER	LOCAL	P007E0
>202	LABEL	TRANSFER	LOCAL	P012F4
>21	LABEL	TRANSFER	LOCAL	P00524
>22	LABEL	TRANSFER	LOCAL	P00548
>23	LABEL	TRANSFER	LOCAL	P0056C
>24	LABEL	TRANSFER	LOCAL	P00590
>250	LABEL	TRANSFER	LOCAL	P0116C
>300	LABEL	TRANSFER	LOCAL	P0082C
>301	LABEL	TRANSFER	LOCAL	P0083C
>303	LABEL	TRANSFER	LOCAL	P008F0
>307	LABEL	TRANSFER	LOCAL	P0132C
>322	LABEL	TRANSFER	LOCAL	P005A4
>350	LABEL	TRANSFER	LOCAL	P00508
>351	LABEL	TRANSFER	LOCAL	P006F4
>400	LABEL	TRANSFER	LOCAL	P00000
>450	LABEL	TRANSFER	LOCAL	P0049C
>50	LABEL	TRANSFER	LOCAL	P00EE4
>500	LABEL	TRANSFER	LOCAL	P0058C
>501	LABEL	TRANSFER	LOCAL	P00C98
>550	LABEL	TRANSFER	LOCAL	P01164
>650	LABEL	TRANSFER	LOCAL	P01000
>650	LABEL	TRANSFER	LOCAL	P01164
>701	VARIABLE	INTEGER FULLWORD	LOCAL	P01398
>712	VARIABLE	INTEGER FULLWORD	LOCAL	P0139C
>813	VARIABLE	INTEGER FULLWORD	LOCAL	P01380
>814	VARIABLE	INTEGER FULLWORD	LOCAL	P01384
>805	VARIABLE	INTEGER FULLWORD	LOCAL	P01388
>806	VARIABLE	INTEGER FULLWORD	LOCAL	P0138C
>807	VARIABLE	INTEGER FULLWORD	LOCAL	P01390
>808	VARIABLE	INTEGER FULLWORD	LOCAL	P01394
>809	VARIABLE	INTEGER FULLWORD	LOCAL	P01398
>80A	VARIABLE	INTEGER FULLWORD	LOCAL	P0139C
>80B	VARIABLE	INTEGER FULLWORD	LOCAL	P013A0
>80C	VARIABLE	INTEGER FULLWORD	LOCAL	P013A4
>80D	VARIABLE	INTEGER FULLWORD	LOCAL	P013A8
>80E	VARIABLE	INTEGER FULLWORD	LOCAL	P013AC
>80F	VARIABLE	INTEGER FULLWORD	LOCAL	P013B0
>807	VARIABLE	INTEGER FULLWORD	LOCAL	P013B4
>80H	VARIABLE	INTEGER FULLWORD	LOCAL	P013B8
>80I	VARIABLE	INTEGER FULLWORD	LOCAL	P013BC
>80J	VARIABLE	INTEGER FULLWORD	LOCAL	P013C0
>80K	VARIABLE	INTEGER FULLWORD	LOCAL	P013C4
>80L	VARIABLE	INTEGER FULLWORD	LOCAL	P013C8
>80M	VARIABLE	INTEGER FULLWORD	LOCAL	P013CC
>80N	VARIABLE	INTEGER FULLWORD	LOCAL	P013D0
>80O	VARIABLE	INTEGER FULLWORD	LOCAL	P013D4
>80P	VARIABLE	INTEGER FULLWORD	LOCAL	P013D8
>80Q	VARIABLE	INTEGER FULLWORD	LOCAL	P013DC
>80R	VARIABLE	INTEGER FULLWORD	LOCAL	P013E0
>80S	VARIABLE	INTEGER FULLWORD	LOCAL	P013E4
>80T	VARIABLE	INTEGER FULLWORD	LOCAL	P013E8
>80U	VARIABLE	INTEGER FULLWORD	LOCAL	P013EC
>80V	VARIABLE	INTEGER FULLWORD	LOCAL	P013F0
>80W	VARIABLE	INTEGER FULLWORD	LOCAL	P013F4
>80X	VARIABLE	INTEGER FULLWORD	LOCAL	P013F8
>80Y	VARIABLE	INTEGER FULLWORD	LOCAL	P013FC
>80Z	VARIABLE	INTEGER FULLWORD	LOCAL	P01300

12/19/77 09:01:03 H-01:10 SYSTEMS MIL-TIME COMPILER (REV. 0)

SYMBOL	USAGE	KIND	STORAGE	LOCATION IN DIFEO
DATA	VARIABLE	INTEGER FULLWORD	LOCAL	P013E4
DATA	VARIABLE	INTEGER FULLWORD	LOCAL	P013E8
DATA	VARIABLE	INTEGER FULLWORD	LOCAL	P013EC
DATA	VARIABLE	INTEGER FULLWORD	LOCAL	P013F0
DATA	VARIABLE	INTEGER FULLWORD	LOCAL	P013F4
DATA	VARIABLE	INTEGER FULLWORD	LOCAL	P013F8
DATA	VARIABLE	INTEGER FULLWORD	LOCAL	P013FC
DATA	VARIABLE	INTEGER FULLWORD	LOCAL	P01400
DATA	VARIABLE	INTEGER FULLWORD	LOCAL	P01404
DATA	VARIABLE	INTEGER FULLWORD	LOCAL	P01408
C.0001	CONSTANT	REAL	LOCAL	P01410
C.0002	CONSTANT	REAL	LOCAL	F0141C
C.0003	CONSTANT	REAL	LOCAL	P01420
C.0004	CONSTANT	REAL	LOCAL	P01424
C.0005	CONSTANT	REAL	LOCAL	P01428
C.0006	CONSTANT	REAL	LOCAL	P0143C
C.0007	CONSTANT	REAL	LOCAL	P01438
C.0008	CONSTANT	REAL	LOCAL	P01434
C.0009	CONSTANT	REAL	LOCAL	P01438
C.0010	CONSTANT	REAL	LOCAL	P0143C
C.0011	CONSTANT	REAL	LOCAL	P01440
C.0012	CONSTANT	REAL	LOCAL	P01444
C.0013	CONSTANT	REAL	LOCAL	P01410
AL	VARIABLE	INTEGER DOUBLE	LOCAL	P000C8
AV	VARIABLE	REAL	PARS	P00008
A:DT	VARIABLE	REAL	LOCAL	P00004
B:AN	VARIABLE	REAL	LOCAL	P00004
B	VARIABLE	REAL	PARS	C00030
C	VARIABLE	REAL	PARS	C00030
CH2	COMMON BLOCK	REAL	PARS	C00038
DB0	VARIABLE	REAL	PARS	C0006C
DBH	VARIABLE	REAL	PARS	C00094
DGH	VARIABLE	REAL	PARS	C00090
DHE	VARIABLE	REAL	PARS	C0002C
DSE	VARIABLE	REAL	PARS	C0007C
DT	VARIABLE	REAL	PARS	C00078
DTP	VARIABLE	REAL	PARS	C0005C
DIFEB	PROCEDURE	REAL	PARS	C00064
E1	VARIABLE	REAL	ENTRY	P0000C
EPOT	VARIABLE	REAL	PARS	C0000C
EPR	VARIABLE	REAL	LOCAL	F00008
EPS	VARIABLE	REAL	LOCAL	P0000C
EPT	VARIABLE	REAL	OUTPUT	C00000
EXIT	PROCEDURE	REAL	LOCAL	P00010
EXDOT	VARIABLE	REAL	EXTERNAL	X01394
EPSFD	VARIABLE	REAL	LOCAL	P00014
EPSPR	VARIABLE	REAL	LOCAL	P00018
F	VARIABLE	REAL	LOCAL	P0001C
F:PR	PROCEDURE	REAL	PARS	C00058
G:OT	PROCEDURE	REAL	EXTERNAL	X000E0
HD	VARIABLE	REAL	EXTERNAL	X012D8
NCD	VARIABLE	INTEGER FULLWORD	PARS	C0003C
			CRSE	C00004

SYSTEMS TIME - JUNE 40

SYSTEMS FORTRAN IV COMPILER (REV 0)

SYMBOL USAGE INDEX

SYMBOL	USAGE	INDEX	SUBNAME	LOCATION IN DIR
VP	ARRAY	REAL	DUMMY	PODNEC
ZD	VARIABLE	REAL	PARS	COBEN
ZET	VARIABLE	REAL	PIPS	COBUC


```

1 SUBROUTINE FLOT(X,V,IP,N,N1,N2,N3,N4,N5,N6,N7,N8,N9,N10)
2 DIMENSION X(10),V(2,10),VFN(3),VFK(3),IPT(10),ICR(3,2),
3 I=1
4 SOLV(1,1)=IH(3,2),VFCT(3)
5 DATA IPR, E, G, ILNE, ISTR, O, E, O, T, T, T, T, T, T
6 DATA IH, EPST, THOD, TR, EPST, THOD, TR
7 DO 10 I=1,3
8 BV=(VFN(K)-VFK(K))/O 1
9 SOLV(I,1)=VFN(I)
10 DO 11 J=2,10
11 SOLV(I,J)=SOLV(I,J-1)+BTV
12 CONTINUE
13 SOLV(I,11)=VFN(K)
14 PRINT 998,(SOLV(K,I),J=1,11),IH(K,NS),ICR(K,NS)
15 CONTINUE
16 XECT=45/(OMX+YMN)
17 DO 12 K=1,3
18 VECT(K)=108/(VFN(K)-VFK(K))
19 CONTINUE
20 PRINT 999
21 DO 100 J=1,46
22 DO 101 J=1,101
23 IPT(J)=IBK
24 CONTINUE
25 DO 102 J=1,NP
26 I=(C*(J)-NM)/XECT+1 5
27 IF(IX NE K)GO TO 102
28 DO 103 I=1,3
29 I=(C*(I J)-FK(I))/VFCT(I)+1 5
30 IF(IY LT 1 OR IY GT 10)GO TO 103
31 IF(IPT(IY) NE IBK AND IPT(IY) NE ICR(I,NS))IPT(IY)=ISTR
32 IF(IPT(IY) EQ IBK)IPT(IY)=ICR(I,NS)
33 CONTINUE
34 XOUT=NM*(K-1)/XECT
35 DO 104 J=1,101,10
36 IF(IPT(J) EQ IBK)IPT(J)=ILNE
37 CONTINUE
38 PRINT 997,XOUT,(IPT(J),J=1,101)
39 CONTINUE
40 PRINT 998
41 RETURN
42 FORMAT('F10 2,26,101A1)
43 FORMAT('13G',,10(' '),',')
44 FORMAT(7F,11F10,3,2X,A4,1X,(' ,ML. '))
45 END

```


SYSTEM, REAL-TIME -A10K-4.0

SYNCHRONIZATION OF DATA

SYNCHRONIZATION OF DATA IN COMPILER (PEV G)

SYNCHRONIZATION OF DATA IN COMPILER (PEV G)

SYNCHRONIZATION OF DATA IN COMPILER (PEV G)

STORAGE

DUPPLY

FILE

FILE

FILE

FILE

101974 030103 180010 SYSTEMS FORTRAN IV COMPILER (REV. 0)

```

1 SUBROUTINE ZONE(Y, NP, YMR, YMR, NC)
2 DIMENSION YMR(NP), YMR(NC), YMR(NC)
3 GO TO 1, 1, NC
4 YMR=0
5 DO 20 I=1, NP
6 YMR=ABS(YMR(I))
7 IF (YMR .GT. YMR) YMR=YMR
8 CONTINUE
9 NP=NP
10 INT=YMR
11 IF (INT NE 0) GO TO 40
12 YMR=YMR*10
13 NP=NP*10-1
14 GO TO 20
15 IF ((YMR-INT) .GT. 1 E-5) INT=INT+1
16 YMR=INT*10 **NPN
17 YMR=YMR*10
18 CONTINUE
19 RETURN
20 END

```

SYSTEMS PERL-TIME MONITOR-4.0

12/19/74 09:01:03 M00016

SYSTEMS PERL-TIME MONITOR-4.0 COMPILER (REV. G)

SYMBOL	USAGE	MODE	STORED	LOCATION IN SCALE
0	LABEL	TRANSFER	IMPERATIVE	100000
00	LABEL	TRANSFER	IMPERATIVE	100000
01	LABEL	TRANSFER	LOCAL	100008
02	LABEL	TRANSFER	LOCAL	100013
03	VAR LABEL	INTEGER FULLWORD	LOCAL	100170
04	VAR LABEL	INTEGER FULLWORD	LOCAL	100174
05	VAR LABEL	INTEGER FULLWORD	LOCAL	100178
06	VAR LABEL	INTEGER FULLWORD	LOCAL	10017C
07	CONSTANT	REAL	LOCAL	100180
08	CONSTANT	REAL	LOCAL	100184
09	PROCEDURE	REAL	EXTERNAL	100120
10	PROCEDURE	INTEGER FULLWORD	EXTERNAL	10012C
11	PROCEDURE	REAL	EXTERNAL	100130
12	PROCEDURE	REAL	EXTERNAL	10013C
13	PROCEDURE	REAL	EXTERNAL	100140
14	PROCEDURE	REAL	EXTERNAL	10014C
15	PROCEDURE	REAL	EXTERNAL	100150
16	PROCEDURE	REAL	EXTERNAL	10015C
17	PROCEDURE	REAL	EXTERNAL	100160
18	PROCEDURE	REAL	EXTERNAL	10016C
19	PROCEDURE	REAL	EXTERNAL	100170
20	PROCEDURE	REAL	EXTERNAL	10017C
21	PROCEDURE	REAL	EXTERNAL	100180
22	PROCEDURE	REAL	EXTERNAL	100184
23	PROCEDURE	REAL	EXTERNAL	100188
24	PROCEDURE	REAL	EXTERNAL	100192
25	PROCEDURE	REAL	EXTERNAL	100196
26	PROCEDURE	REAL	EXTERNAL	100200
27	PROCEDURE	REAL	EXTERNAL	100204
28	PROCEDURE	REAL	EXTERNAL	100208
29	PROCEDURE	REAL	EXTERNAL	100212
30	PROCEDURE	REAL	EXTERNAL	100216
31	PROCEDURE	REAL	EXTERNAL	100220
32	PROCEDURE	REAL	EXTERNAL	100224
33	PROCEDURE	REAL	EXTERNAL	100228
34	PROCEDURE	REAL	EXTERNAL	100232
35	PROCEDURE	REAL	EXTERNAL	100236
36	PROCEDURE	REAL	EXTERNAL	100240
37	PROCEDURE	REAL	EXTERNAL	100244
38	PROCEDURE	REAL	EXTERNAL	100248
39	PROCEDURE	REAL	EXTERNAL	100252
40	PROCEDURE	REAL	EXTERNAL	100256
41	PROCEDURE	REAL	EXTERNAL	100260
42	PROCEDURE	REAL	EXTERNAL	100264
43	PROCEDURE	REAL	EXTERNAL	100268
44	PROCEDURE	REAL	EXTERNAL	100272
45	PROCEDURE	REAL	EXTERNAL	100276
46	PROCEDURE	REAL	EXTERNAL	100280
47	PROCEDURE	REAL	EXTERNAL	100284
48	PROCEDURE	REAL	EXTERNAL	100288
49	PROCEDURE	REAL	EXTERNAL	100292
50	PROCEDURE	REAL	EXTERNAL	100296
51	PROCEDURE	REAL	EXTERNAL	100300
52	PROCEDURE	REAL	EXTERNAL	100304
53	PROCEDURE	REAL	EXTERNAL	100308
54	PROCEDURE	REAL	EXTERNAL	100312
55	PROCEDURE	REAL	EXTERNAL	100316
56	PROCEDURE	REAL	EXTERNAL	100320
57	PROCEDURE	REAL	EXTERNAL	100324
58	PROCEDURE	REAL	EXTERNAL	100328
59	PROCEDURE	REAL	EXTERNAL	100332
60	PROCEDURE	REAL	EXTERNAL	100336
61	PROCEDURE	REAL	EXTERNAL	100340
62	PROCEDURE	REAL	EXTERNAL	100344
63	PROCEDURE	REAL	EXTERNAL	100348
64	PROCEDURE	REAL	EXTERNAL	100352
65	PROCEDURE	REAL	EXTERNAL	100356
66	PROCEDURE	REAL	EXTERNAL	100360
67	PROCEDURE	REAL	EXTERNAL	100364
68	PROCEDURE	REAL	EXTERNAL	100368
69	PROCEDURE	REAL	EXTERNAL	100372
70	PROCEDURE	REAL	EXTERNAL	100376
71	PROCEDURE	REAL	EXTERNAL	100380
72	PROCEDURE	REAL	EXTERNAL	100384
73	PROCEDURE	REAL	EXTERNAL	100388
74	PROCEDURE	REAL	EXTERNAL	100392
75	PROCEDURE	REAL	EXTERNAL	100396
76	PROCEDURE	REAL	EXTERNAL	100400
77	PROCEDURE	REAL	EXTERNAL	100404
78	PROCEDURE	REAL	EXTERNAL	100408
79	PROCEDURE	REAL	EXTERNAL	100412
80	PROCEDURE	REAL	EXTERNAL	100416
81	PROCEDURE	REAL	EXTERNAL	100420
82	PROCEDURE	REAL	EXTERNAL	100424
83	PROCEDURE	REAL	EXTERNAL	100428
84	PROCEDURE	REAL	EXTERNAL	100432
85	PROCEDURE	REAL	EXTERNAL	100436
86	PROCEDURE	REAL	EXTERNAL	100440
87	PROCEDURE	REAL	EXTERNAL	100444
88	PROCEDURE	REAL	EXTERNAL	100448
89	PROCEDURE	REAL	EXTERNAL	100452
90	PROCEDURE	REAL	EXTERNAL	100456
91	PROCEDURE	REAL	EXTERNAL	100460
92	PROCEDURE	REAL	EXTERNAL	100464
93	PROCEDURE	REAL	EXTERNAL	100468
94	PROCEDURE	REAL	EXTERNAL	100472
95	PROCEDURE	REAL	EXTERNAL	100476
96	PROCEDURE	REAL	EXTERNAL	100480
97	PROCEDURE	REAL	EXTERNAL	100484
98	PROCEDURE	REAL	EXTERNAL	100488
99	PROCEDURE	REAL	EXTERNAL	100492

```

PK 1 1 SUBROUTINE RA(N,K,VO,DV,XOS,DX,VA,VP,XU,AL,DIFEC)
2 2 C **** N SPECIFIES NUMBER OF EQNS. P=1 PROVIDES VP'S AT END POINTS
3 3 DIMENSION Y0(N),DY(N),YK(N),YK(D),VP(N),AL(N,4)
4 4 X0 = XOS
5 5 I = 1
6 6 DO 10 (1,2,3,4,5),I
7 7 1 XH = X0
8 8 DO 6 J = 1,N
9 9 YK(J) = Y0(J)
10 10 CALL DIFEC(VH,VP,XU,N)
11 11 DO 7 J = 1,N
12 12 Y AT(J,1) = DX*VP(J)
13 13 I = I + 1
14 14 GO TO 8
15 15 2 XH = X0 + 0.5*DX
16 16 DO 9 J = 1,N
17 17 YH(J) = Y0(J) + 0.5*AL(J,1)
18 18 GO TO 10
19 19 3 DO 11 J = 1,N
20 20 YH(J) = Y0(J) + 0.5*AL(J,2)
21 21 YH(J) = Y0(J) + 0.5*AL(J,2)
22 22 GO TO 10
23 23 4 XH = X0 + DX
24 24 DO 12 J = 1,N
25 25 YH(J) = Y0(J) + AL(J,3)
26 26 GO TO 10
27 27 5 DO 13 J = 1,N
28 28 DY(J) = (0.5*AL(J,1)+AL(J,4)+AL(J,2)+AL(J,3))/2.0
29 29 Y0(J) = Y0(J) + DY(J)
30 30 IF (K.NE.1) RETURN
31 31 DO 16 J = 1,N
32 32 YH(J) = Y0(J)
33 33 CALL DIFEC(VH,VP,XU,N)
34 34 RETURN
35 35 END
03710
03720
03730
03740
03750
03760
03770
03780
03790
03800
03810
03820
03830
03840
03850
03860
03870
03880
03890
03900
03910
03920
03930
03940
03950
03960
03970
03980
03990
04000
04010
04020
04030
04040
04050

```

USAGE MODE STORAGE LOCATION IN PK

SYMBOL	USAGE	MODE	STORAGE	LOCATION IN PK
>1	LABEL	TRANSFER	LOCAL	P00090
>10	LABEL	TRANSFER	LOCAL	P00098
>11	LABEL	TRANSFER	INACTIVE	I00000
>12	LABEL	TRANSFER	INACTIVE	I00000
>13	LABEL	TRANSFER	INACTIVE	I00000
>16	LABEL	TRANSFER	INACTIVE	I00000
>2	LABEL	TRANSFER	LOCAL	P00140
>3	LABEL	TRANSFER	LOCAL	P001C8
>4	LABEL	TRANSFER	LOCAL	P00278
>5	LABEL	TRANSFER	LOCAL	P003E8
>6	LABEL	TRANSFER	LOCAL	I00000
>7	LABEL	TRANSFER	INACTIVE	I00000
>8	LABEL	TRANSFER	INACTIVE	I00000
>9	LABEL	TRANSFER	INACTIVE	I00000
>A0	VARIABLE	INTEGER FULLWORD	LOCAL	P00060
>A1	VARIABLE	INTEGER FULLWORD	LOCAL	P0040C
>A2	VARIABLE	INTEGER FULLWORD	LOCAL	P0040C
>A3	VARIABLE	INTEGER FULLWORD	LOCAL	P00410
>A4	VARIABLE	INTEGER FULLWORD	LOCAL	P00414
>A5	VARIABLE	INTEGER FULLWORD	LOCAL	P00418
>A6	VARIABLE	INTEGER FULLWORD	LOCAL	P0041C
>A7	VARIABLE	INTEGER FULLWORD	LOCAL	P00424
>A8	VARIABLE	INTEGER FULLWORD	LOCAL	P00428
>A9	VARIABLE	INTEGER FULLWORD	LOCAL	P0042C
>B0	VARIABLE	INTEGER FULLWORD	LOCAL	P00430
>B1	VARIABLE	INTEGER FULLWORD	LOCAL	P00434
C.0001	CONSTANT	REAL	LOCAL	P00438
C.0002	CONSTANT	REAL	LOCAL	P0043C
RI	ARRAY	REAL	DUMMY	P00044
DX	VARIABLE	REAL	DUMMY	P00034
DY	VARIABLE	REAL	DUMMY	P00034
DIFEC	PROCEDURE	REAL	DUMMY	P0002C
EXIT	PROCEDURE	REAL	DUMMY	P00048
F.PR	PROCEDURE	REAL	EXTERNAL	X00404
G.OT	PROCEDURE	REAL	EXTERNAL	X00404
I	VARIABLE	REAL	EXTERNAL	X00018
J	VARIABLE	REAL	EXTERNAL	X00018
K	VARIABLE	REAL	EXTERNAL	X00018
N	VARIABLE	REAL	EXTERNAL	X00018
RET.	PROCEDURE	REAL	EXTERNAL	X00018
KK	PROCEDURE	REAL	EXTERNAL	X00018
X0	VARIABLE	DOUBLE	LOCAL	P00014
X05	VARIABLE	DOUBLE	LOCAL	P00014
X1	VARIABLE	REAL	DUMMY	P00030
Y0	ARRAY	REAL	DUMMY	P00040
Y1	ARRAY	REAL	DUMMY	P00040
Y1	ARRAY	REAL	DUMMY	P00028
Y1	ARRAY	REAL	DUMMY	P0003C
Y1	ARRAY	REAL	DUMMY	P00038

EXTERNAL DIFED
COMMON/TABLES/TMTOL (500) , TCTOL (500) , NOEL, TOLD, NOM
COMMON/OPUT/EP5, QH, XTHP, THIDT, THGS

COMMON/PARS/XKI, XKA, XKP, XKH, PTN, ROM, XJ, PTE, TAUC, TAUP, TAVU, OGH,
AVMX, XL, C, V, B, XKA, PS, XNCS, XNCO, XNCN, F, DT, TNO, OTP, XKB
.CH2, OSE, XKSE, XJHE, OHE, TGF
.XNOP, WN, ZET, O8H, O8G, TAU1, MO, TALM
.XK8G, XK8H, TAG, TAH, T8G, T8H
.E1, TAU1, TAU2, A1, TAU3, TAU4, TD, TAUS

COMMON/CASE/NCS, NCO, NCM, NOP
DIMENSION XPL (350), YPL (3, 350), YMX (3), YMN (3)
DIMENSION Y (21), YL (21), YP (21), Z (21), O (21), DY (21), YH (21), AI (4, 21)
COMMON/HEAD/MO1 (20, 4), MO2 (10, 2), MO3 (2, 4, 6), MO4 (7, 6), MOALL (20)

EQUIVALENCE (Y (1), THG) , (YP (1) , THGOT) , (Y (8), AV) ,
(Y (2), THGO) , (YP (2) , THGOT) , (YP (8), AVDT) ,
(Y (3), TA) , (YP (3) , TAOT) ,
(Y (4), PF) , (YP (4) , PFOT) ,
(Y (5), PH) , (YP (5) , PHOT) ,
(Y (6), EPT) , (YP (6) , EPOT) ,
(Y (7), THS) , (YP (7) , THSOT) ,
, (Y (9), THH) , (YP (9), THHDT) , (Y (10), THHG) , (YP (10), THHGDT) ,

(Y (11), THMGO) , (YP (11), THMGO)
, (YP (12), TCSPOT) , (Y (12), TCSPD)
, (YP (13), TCSP30) , (Y (13), TCSPDD)
, (YP (14), THSPOT) , (Y (14), THSPD)
, (YP (15), THSP30) , (Y (15), THSPDD)
, (YP (16), THSSDT) , (Y (16), THSS)

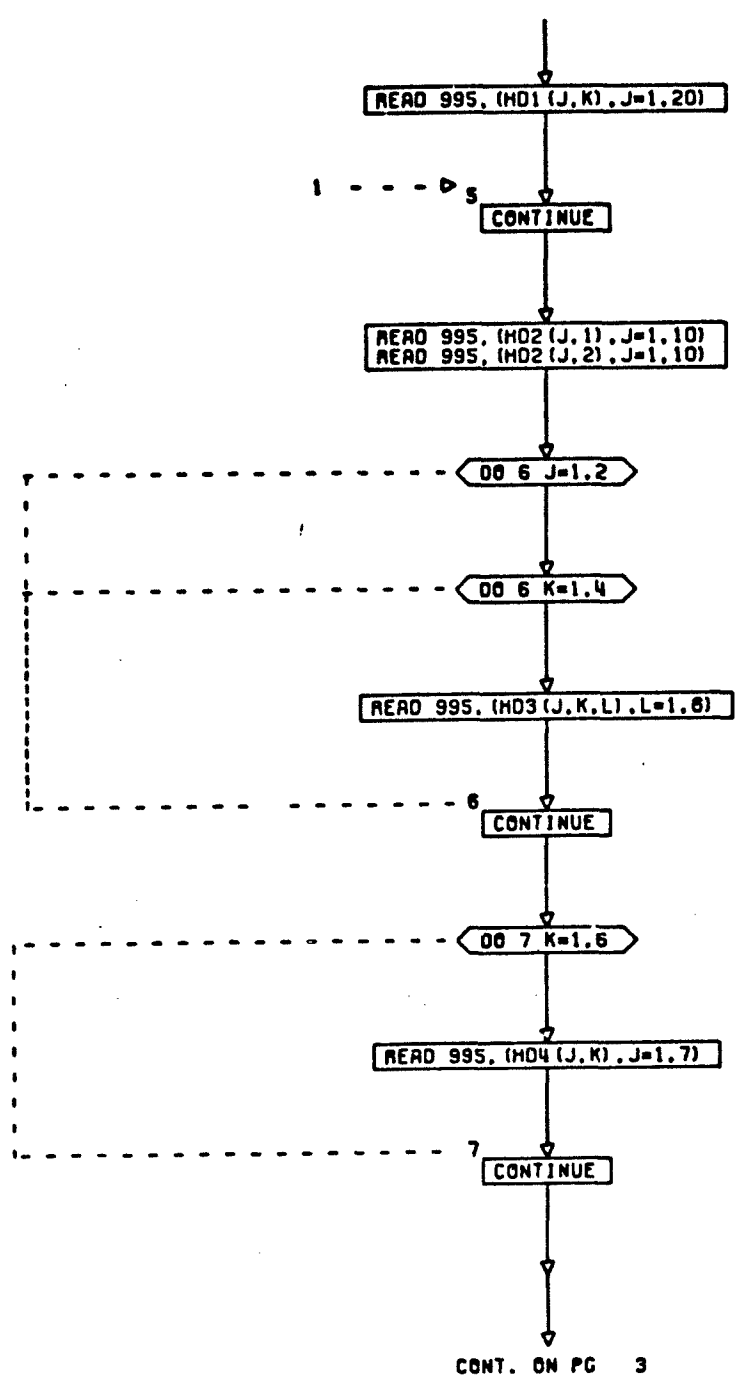
READ 995, (MDALL (K), K=1, 20)

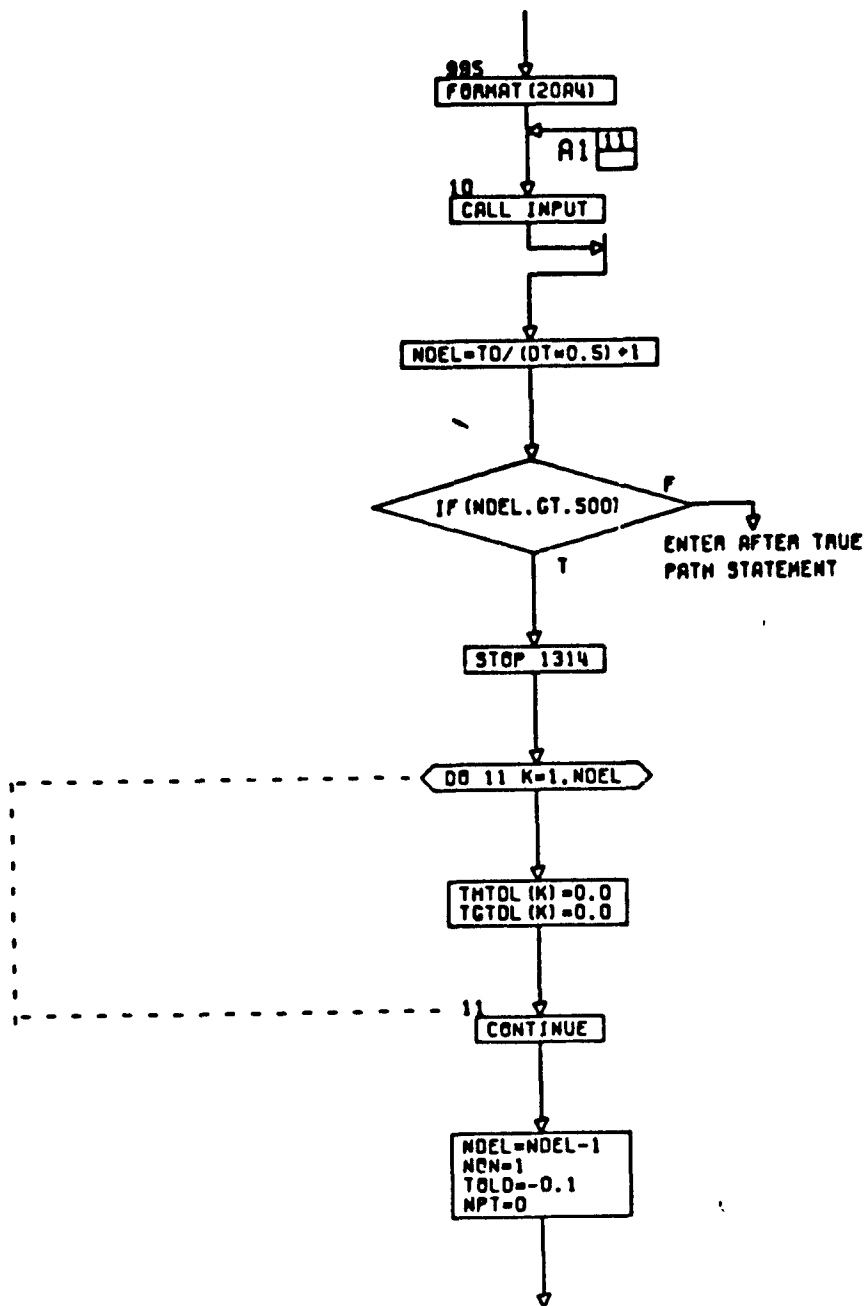
DO 5 K=1, 4 ----- > 2

CONT. ON PG 2

PG 1 OF 11

A-63

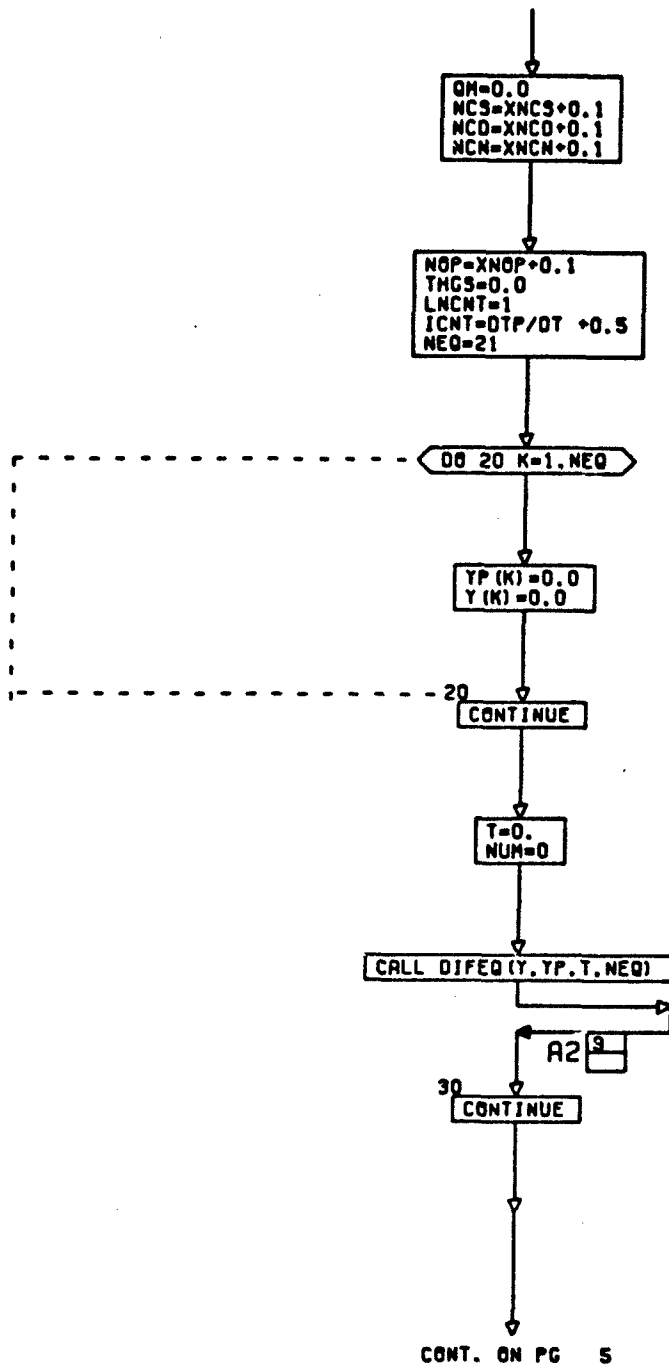


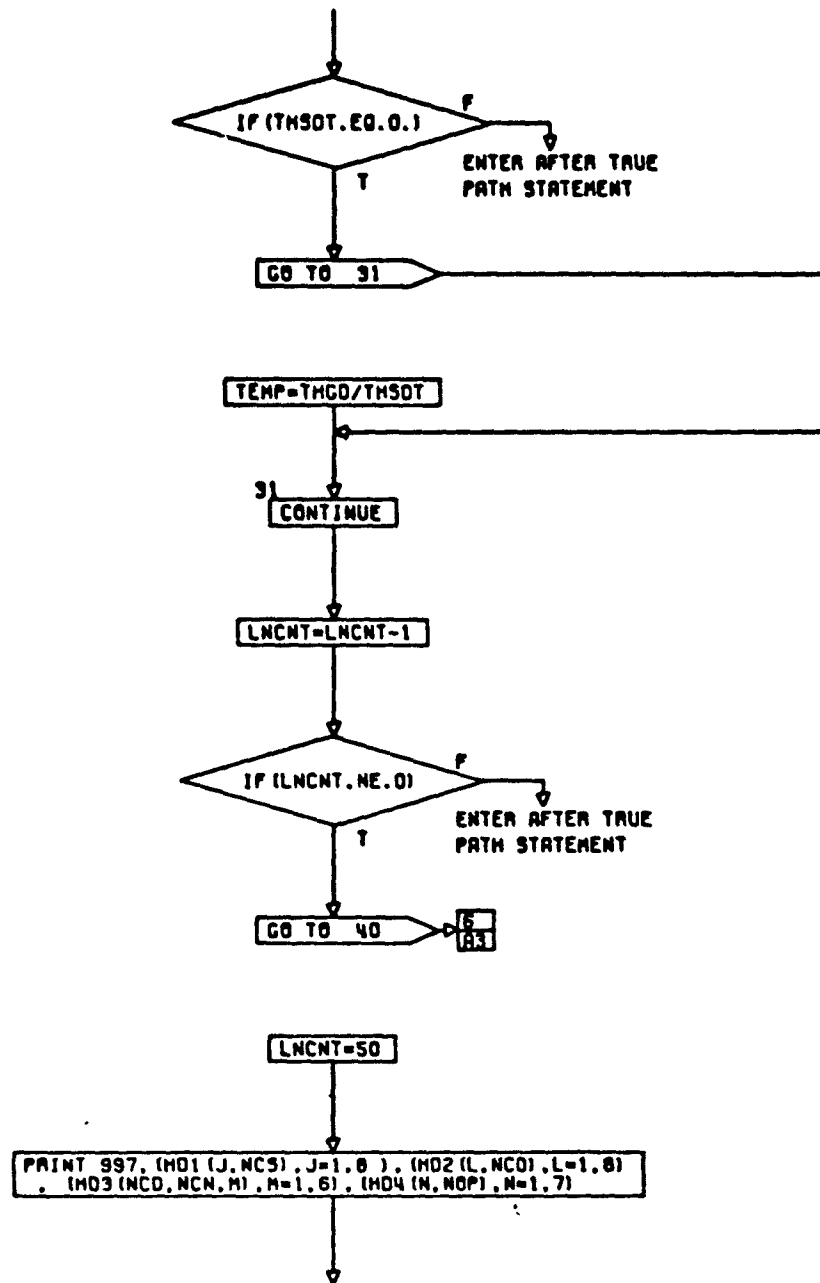


CONT. ON PG 4

PG 3 OF 11

A-65

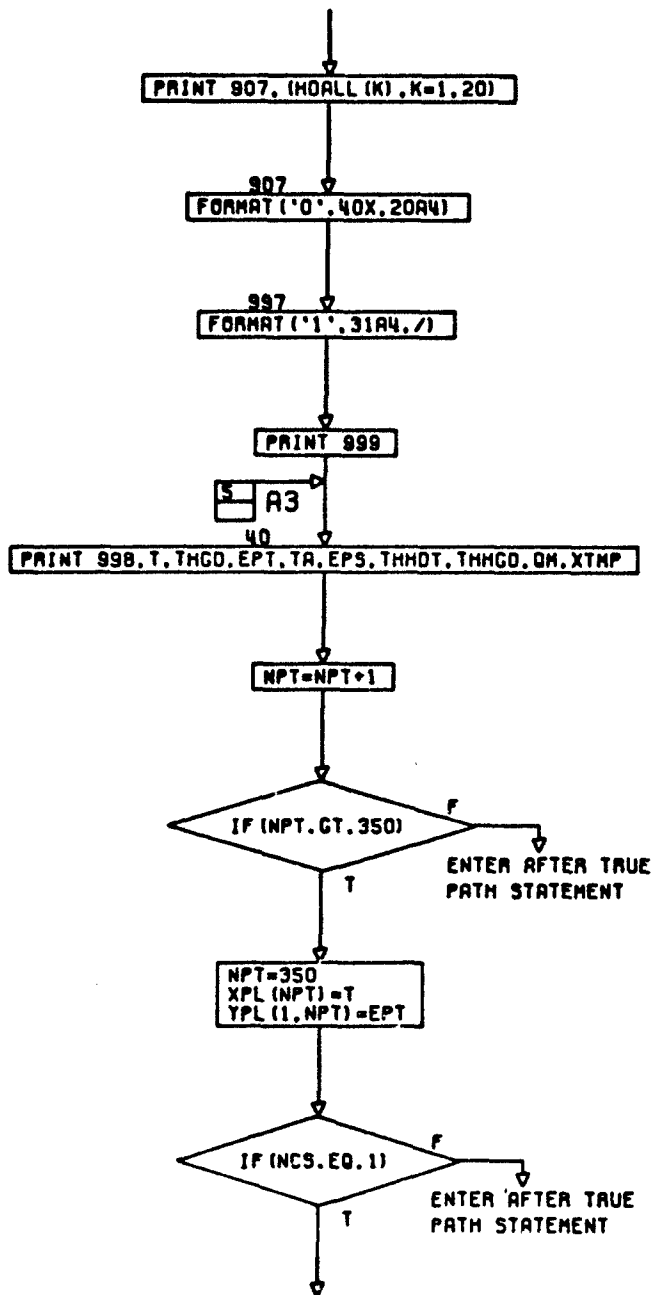




CONT. ON PG 8

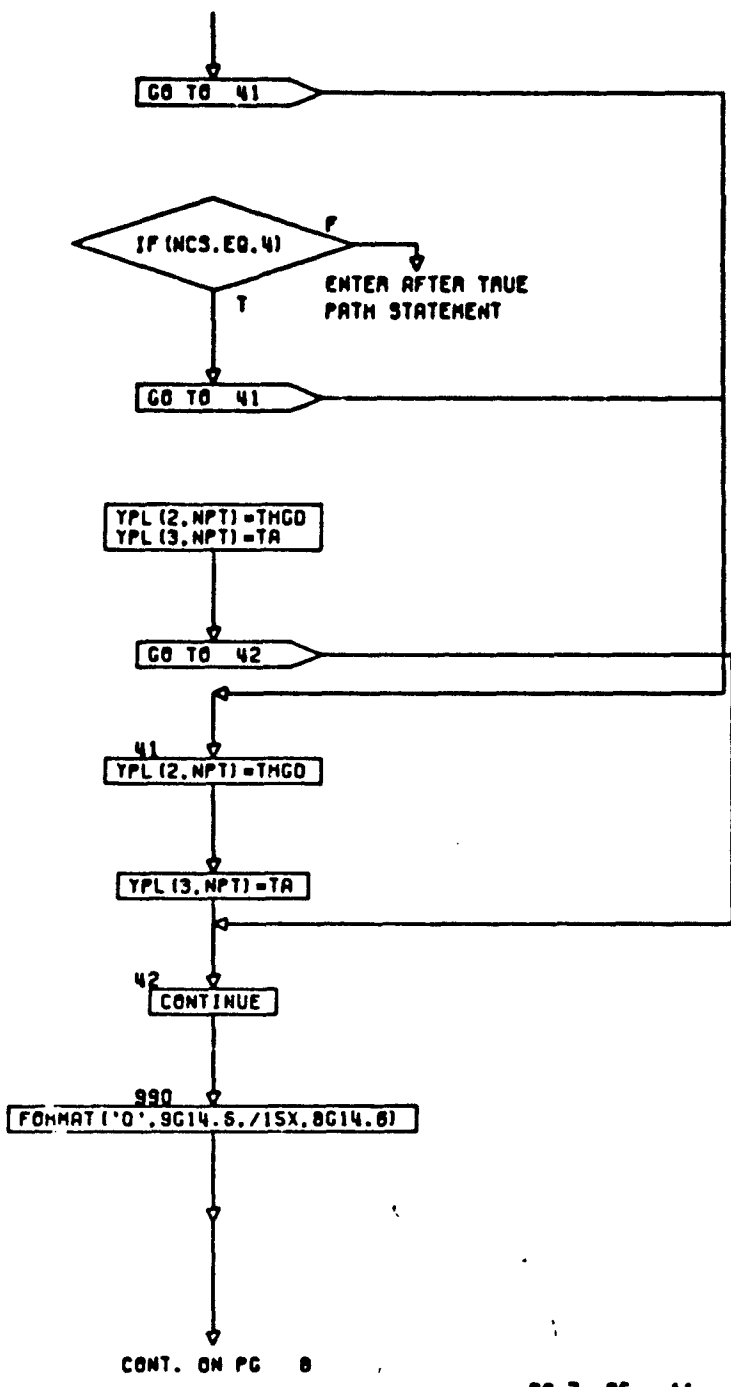
PG 5 OF 11

A-67

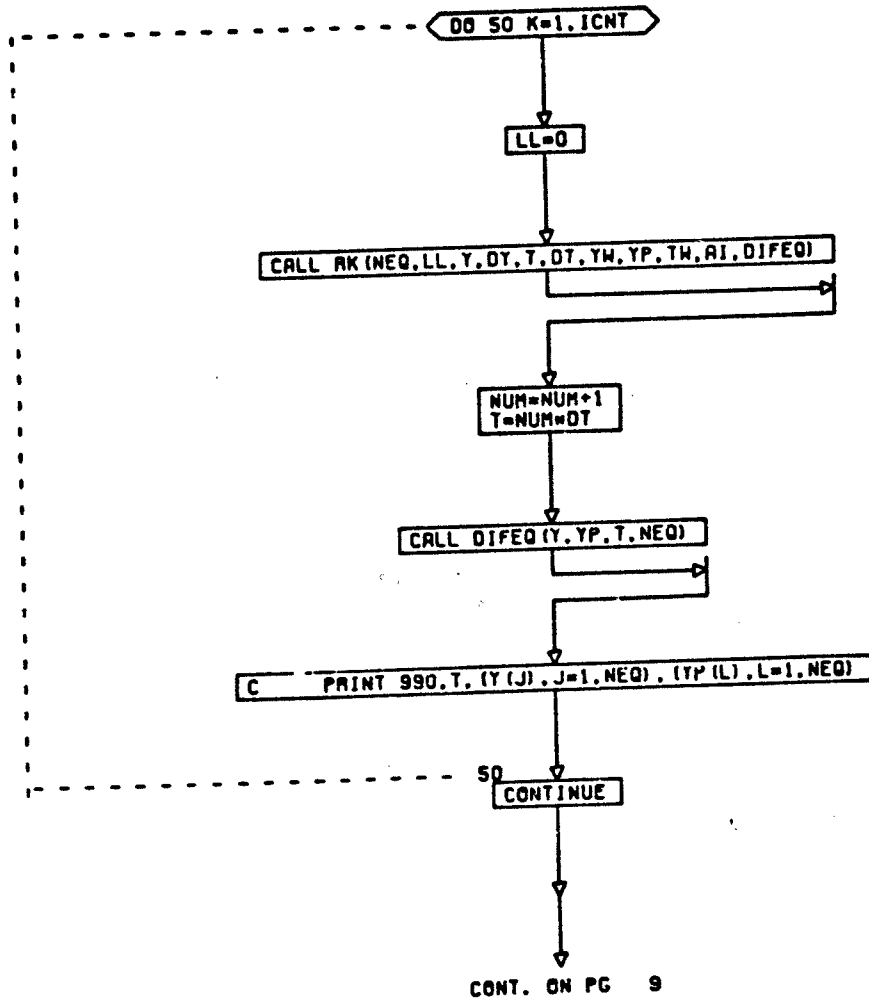
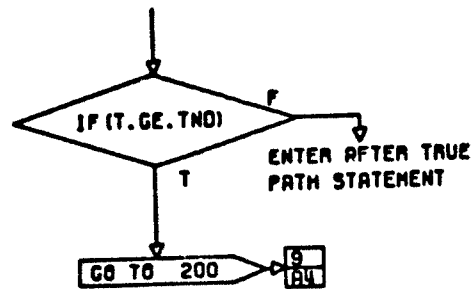


CONT. ON PG 7

PG 6 OF 11



CONT. ON PG 8



GO TO 30

999
FORMAT (' .F14.3.F14.4.F14.5.F14.0.2F14.4.F14.4.F14.1.F14.5')

999
FORMAT (' .9X.'TIME'.6X.'THTC DOT'.10X.'EPS'.12X.'TR'.
11X.'EPS'.8X.'THTM DOT'.5X.'THTHC DOT'.12X.'QM'.10X.'KR...')

R4

200
GO TO (201,202,202,201),NCS

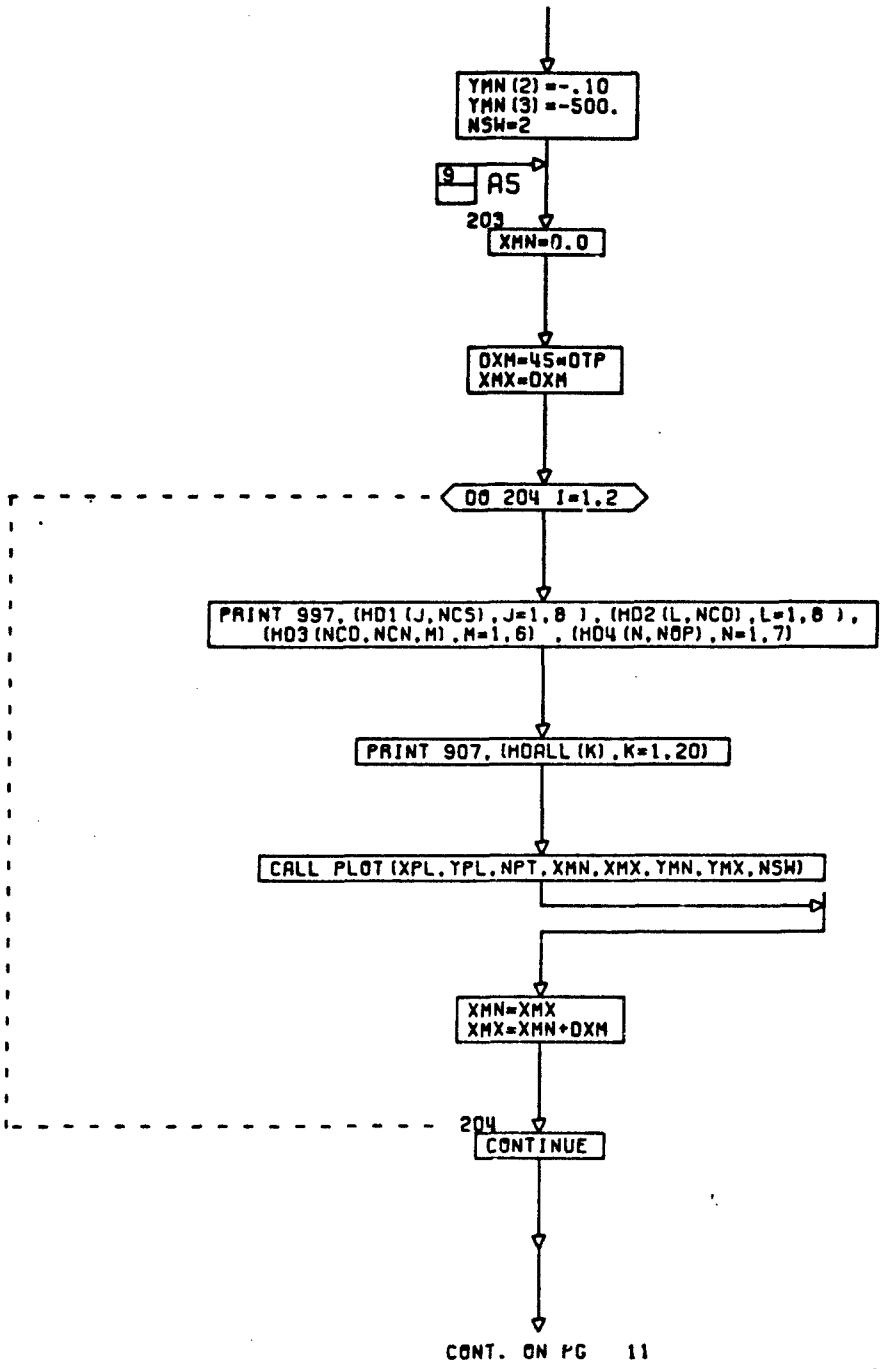
201
YMX (1) = .005

YMX (2) = 0.1
YMX (3) = 500.
YMN (1) = -.005
YMN (2) = -0.1
YMN (3) = -500.
NSM = 1

GO TO 203

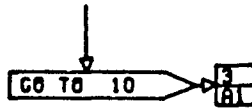
202
YMX (1) = .005

YMX (2) = .10
YMX (3) = 500.
YMN (1) = -.005



CONT. ON PG 11

PG 10 OF 11



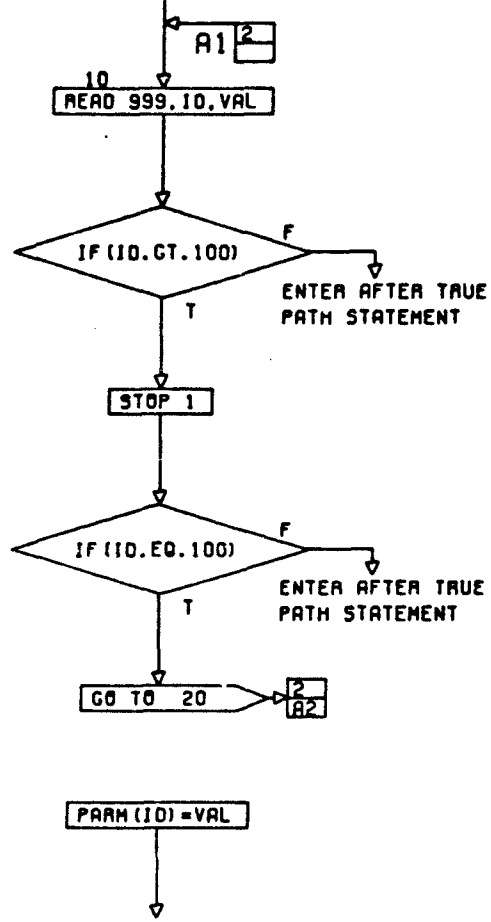
END

PG 11 FINAL

A-73

SUBROUTINE INPUT
 COMMON/HEAD/HD1 (20,4) ,HD2 (10,2) ,HD3 (2,4,6) ,HD4 (7,6) ,HDALL (20)
 COMMON/PARS/PARM (55)
 DIMENSION NAME (55)

DATA NAME/	KI	KR	KP	KH	PTN	ADM	J	PTE
TAUC	TAUP	TAUV	DGH	AVMX	L	C	V	B
KA	PS	NCS	NCO	NCN	F	DT	TND	DTP
KB	CH2	DSE	KSE	JME	OME	TGF	NOP	OMN
ZET	DBH	DBG	TAUI	HD	TALM	KBG	KBH	TAC
TAM	T8C	T8H	E1	TAU1	TAU2	A1	TAU3	TAU4
TD	TAUS	/						



CONT. ON PG 2

PG 1 OF 3

↓
GO TO 10

998
FORMAT ('0',/(' ',5(13,1X,A4,'=',G14.6,' ',.2X)))

A2
20
CONTINUE

NCS=PARAM(20)+0.1
NCD=PARAM(21)+0.1
NCN=PARAM(22)+0.1
NOP=PARAM(34)+0.1

PRINT 997, (MD1(J,NCS),J=1,8), (MD2(L,NCD),L=1,8),
(MD3(NCD,NCN,M),M=1,6), (MD4(N,NOP),N=1,7)

PRINT 907, (MDALL(K),K=1,20)

907
FORMAT ('0',40X,20A4)

997
FORMAT ('1',31A4)

PRINT 998, (K,NAME(K),PARAM(K),K=1,55)

999
FORMAT (13,G17.0)

CONT. ON PG 3

↓
RETURN

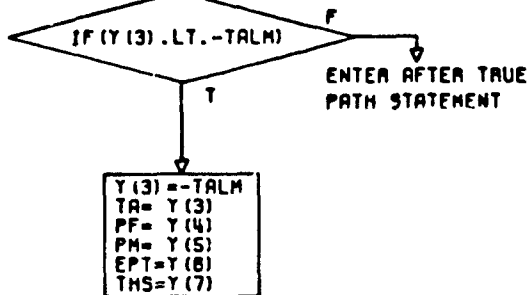
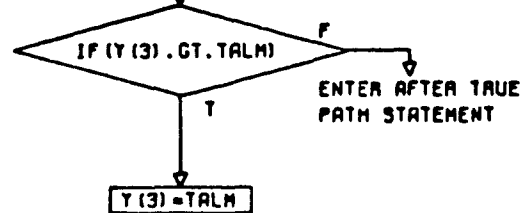
END

PG 3 FINAL

SUBROUTINE DIFEQ (Y, YP, T, NEQ)
COMMON/TABLES/TMTOL (500), TCTDL (500), NOEL, TOLD, NON
COMMON/OPUT: EPS, OM, XTMP, THIDT, THGS

COMMON/PARS/XKI, XKA, XKP, XKH, PTN, ADM, XJ, PTE, TAUC, TAUP, TAUV, OGM,
AVMX, XL, C, V, B, XKA, PS, XNCS, XNCD, XNCN, F, DT, TND, OTP, XKB
.CH2, OSE, XKSE, XJHE, OHE, TGF
.XNOP, WN, ZET, OBM, OBG, TAU1, HD, TALM
.XKBC, XKBH, TAG, TAH, TCG, TBM
.E1, TAU1, TAU2, A1, TAU3, TAU4, ZD, TAUS

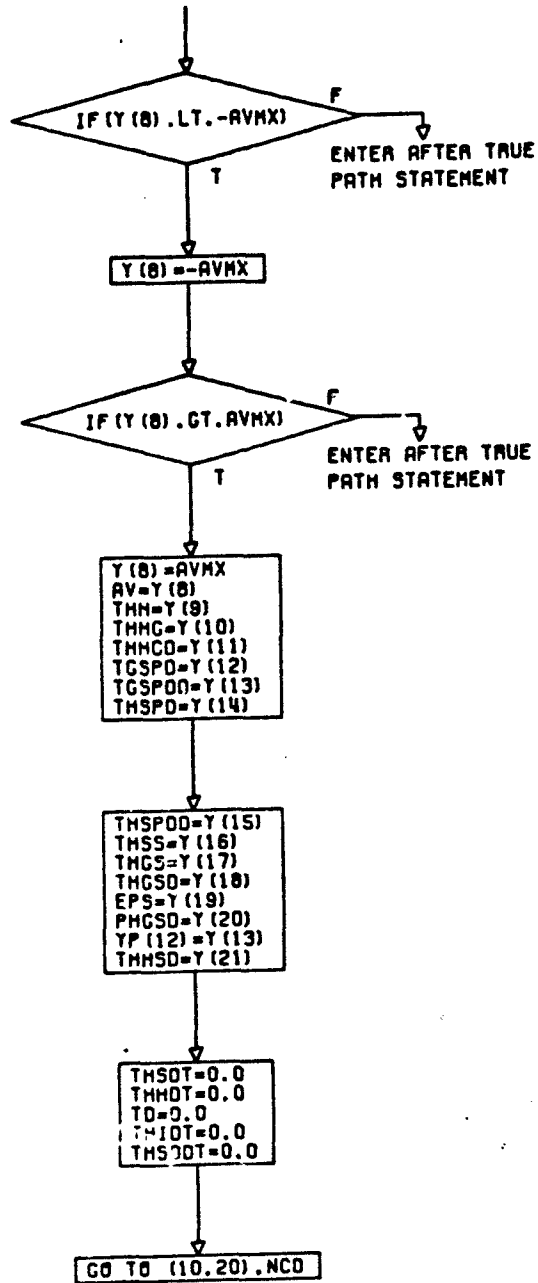
COMMON/CASE/NCS, NCO, NCN, NOP
DIMENSION Y (NEQ), YP (NEQ)
TWOPI=6.283185
THG= Y (1)
THGD=Y (2)



CONT. ON PG 2

PG 1 OF 17

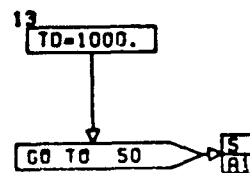
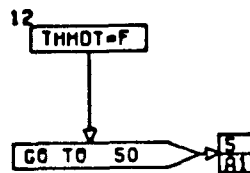
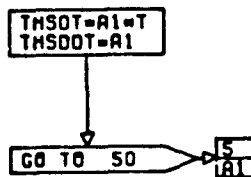
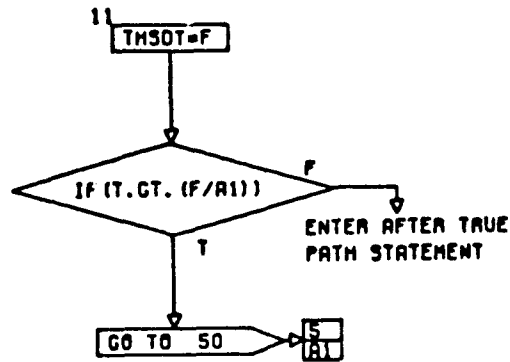
A-77



CONT. ON PG 3

PG 2 OF 17

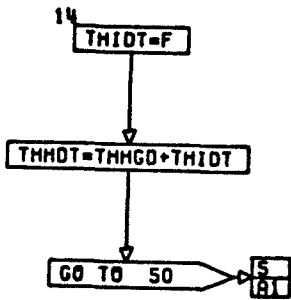
10
GO TO (11,12,13,14),NCN



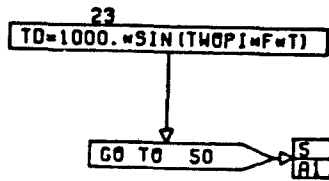
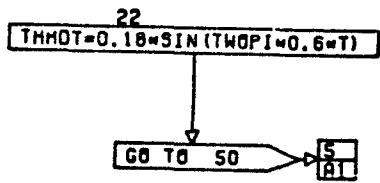
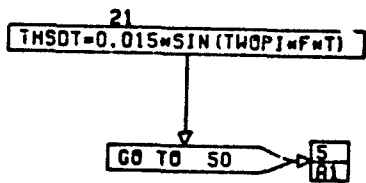
CONT. ON PG 4

PG 3 OF 17

A-79

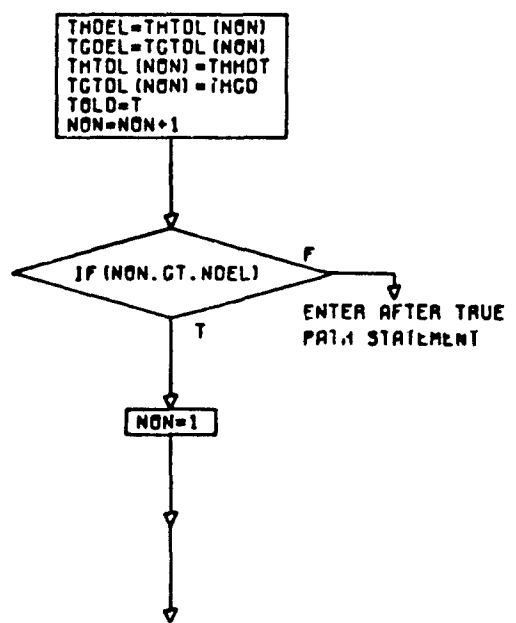
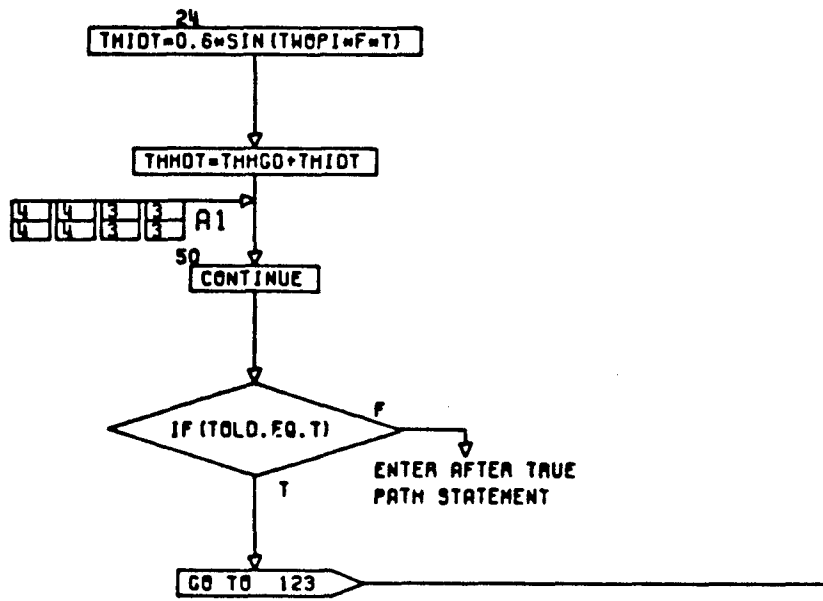


20
GO TO (21,22,23,24),NCN

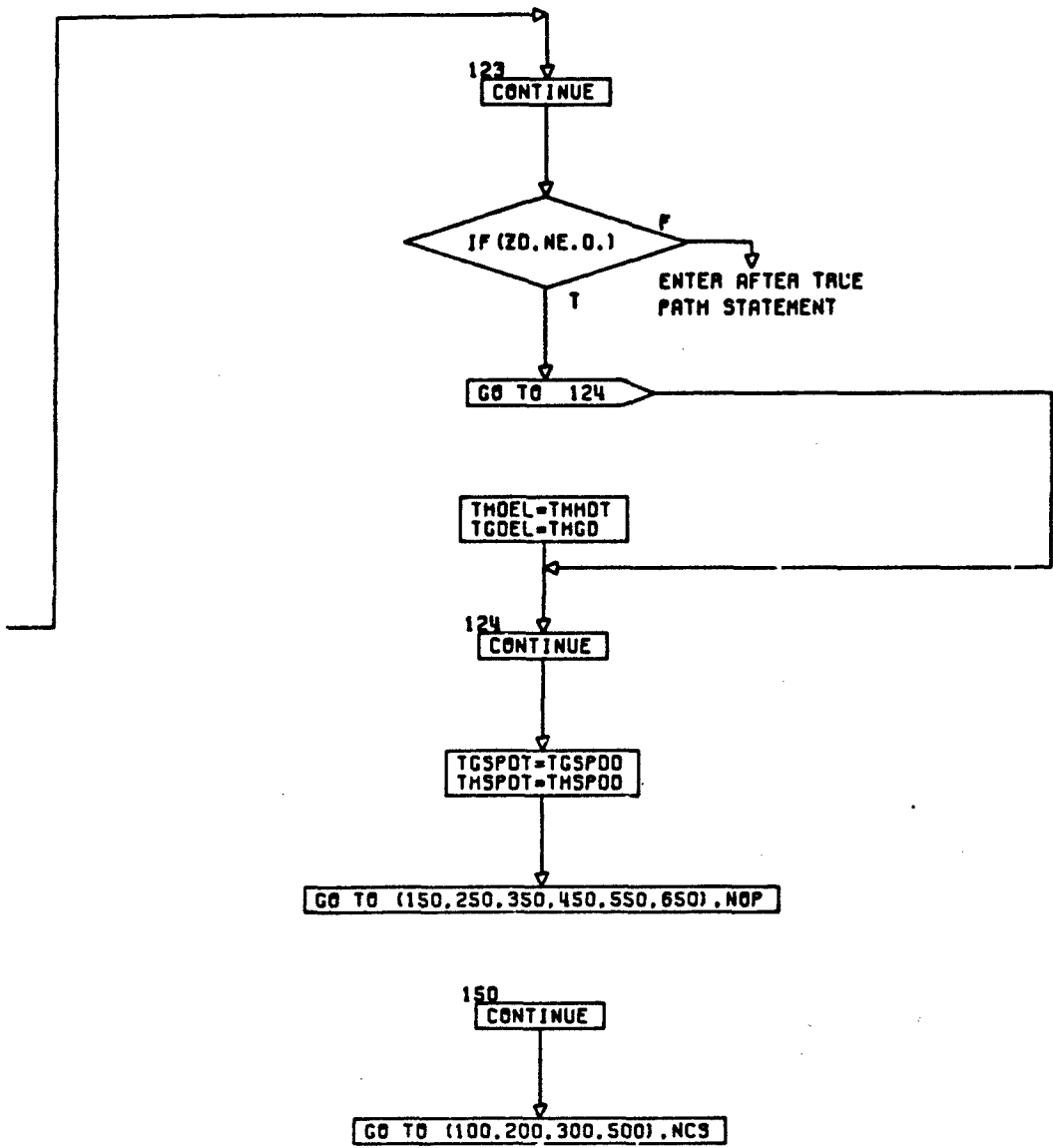


CONT. ON PG 5

PG 4 OF 17

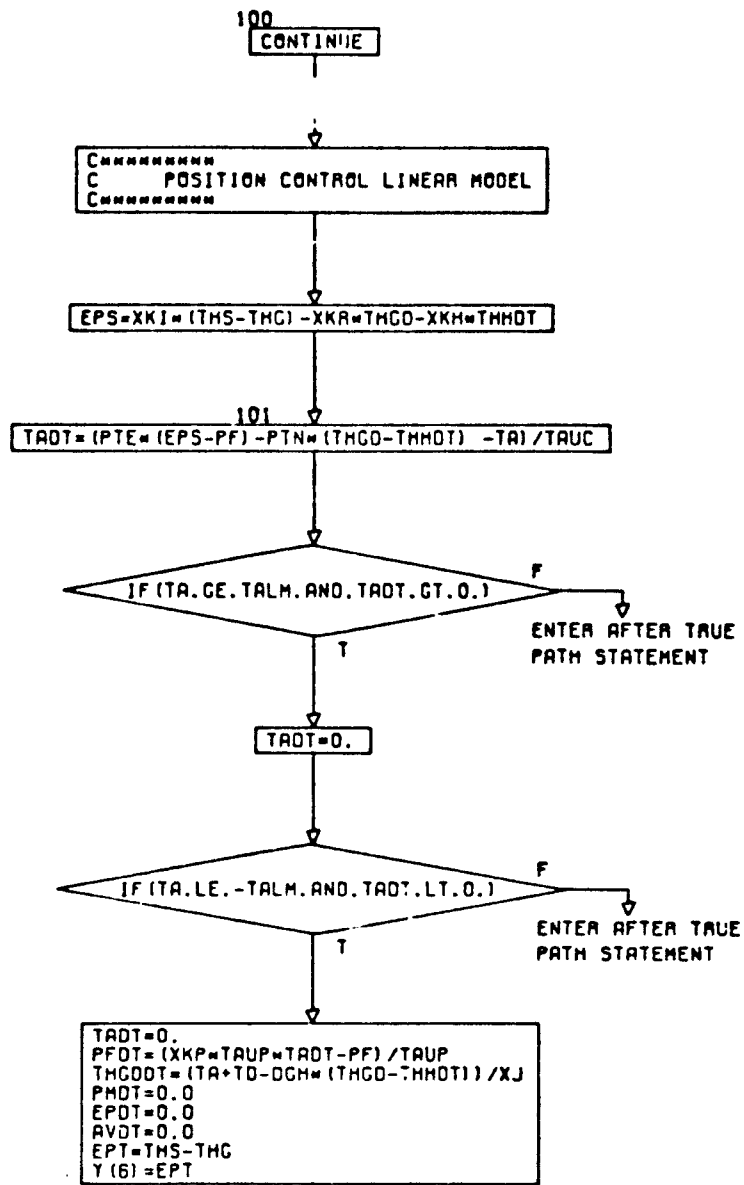


CONT. ON PG 6



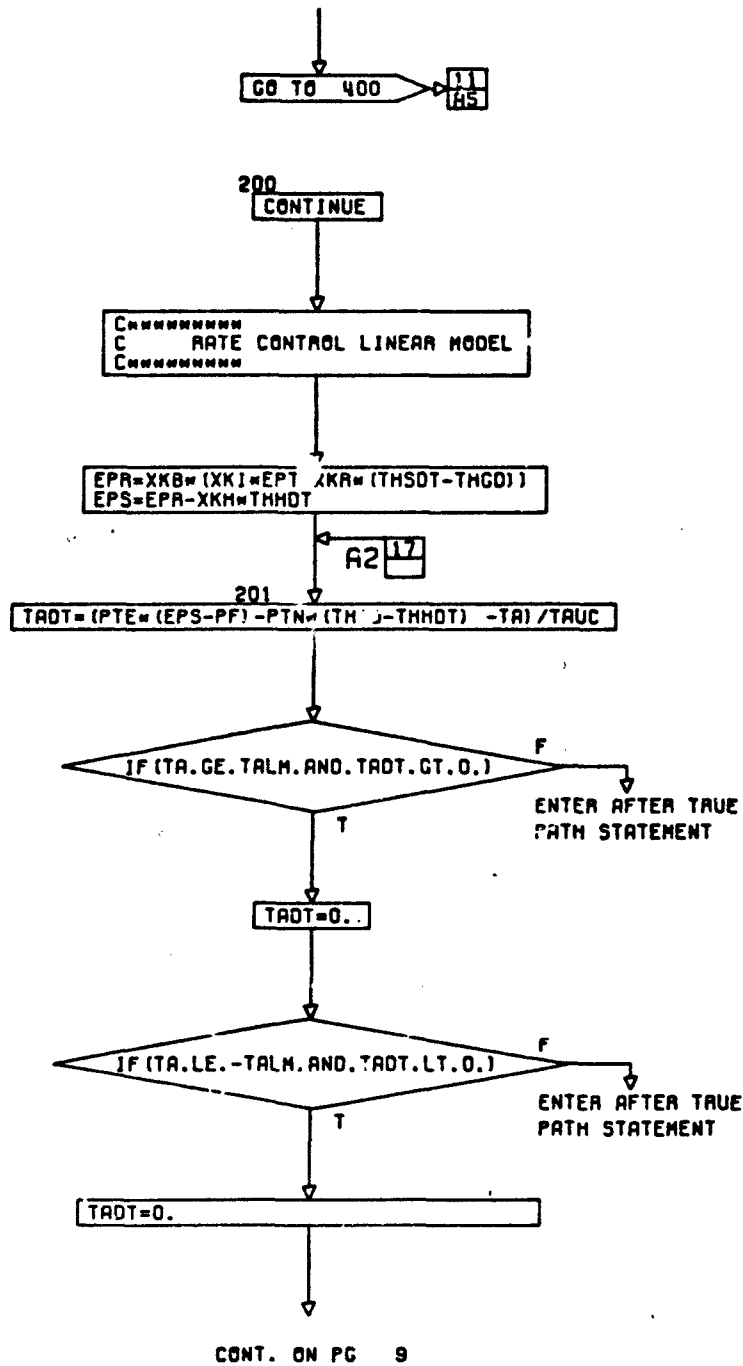
CONT. ON PG 7

PG 6 OF 17



CONT. ON PG 8

PG 7 OF 17



$PFDT = (XKP * TAUP - TADT - PF) / TAUP$
 $EPDT = THSDT - TMGD$
 $PHDT = 0.0$
 $AVDT = 0.0$
 $THGDDT = (TA + TD - DGM - (THGD - THHDT)) / XJ$

GO TO 400 →

11
A5

300
CONTINUE

C*****
 C NONLINEAR FLOW MODEL - RATE CONTROL
 C*****

$EPA = XKB * (XKI * EPT + XKA * (TK * SOT - TMGO))$
 $EPS = EPA - XKM * THHDT$

A3

14	17
16	

303
CONTINUE

EPDT = THSDT - TMGD

A4

12
17

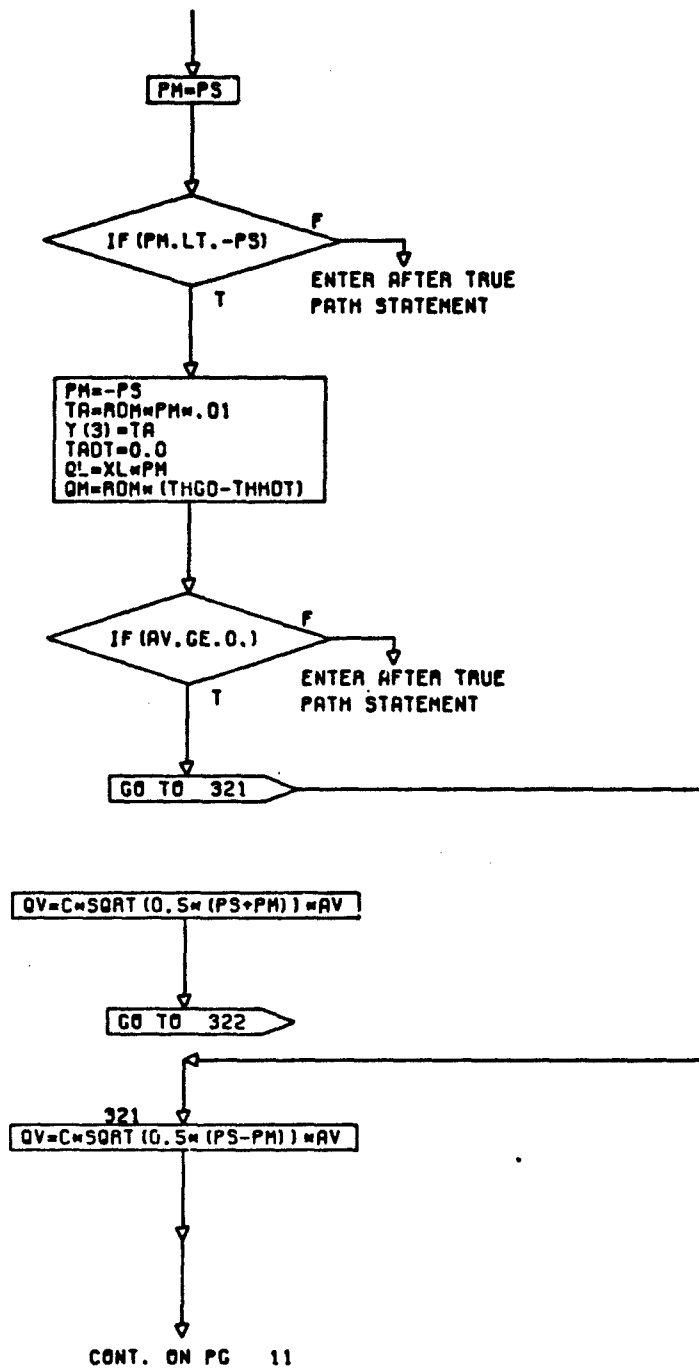
301
CONTINUE

IF (PM.GT.PS) F
ENTER AFTER TRUE
PATH STATEMENT
T

CONT. ON PG 10

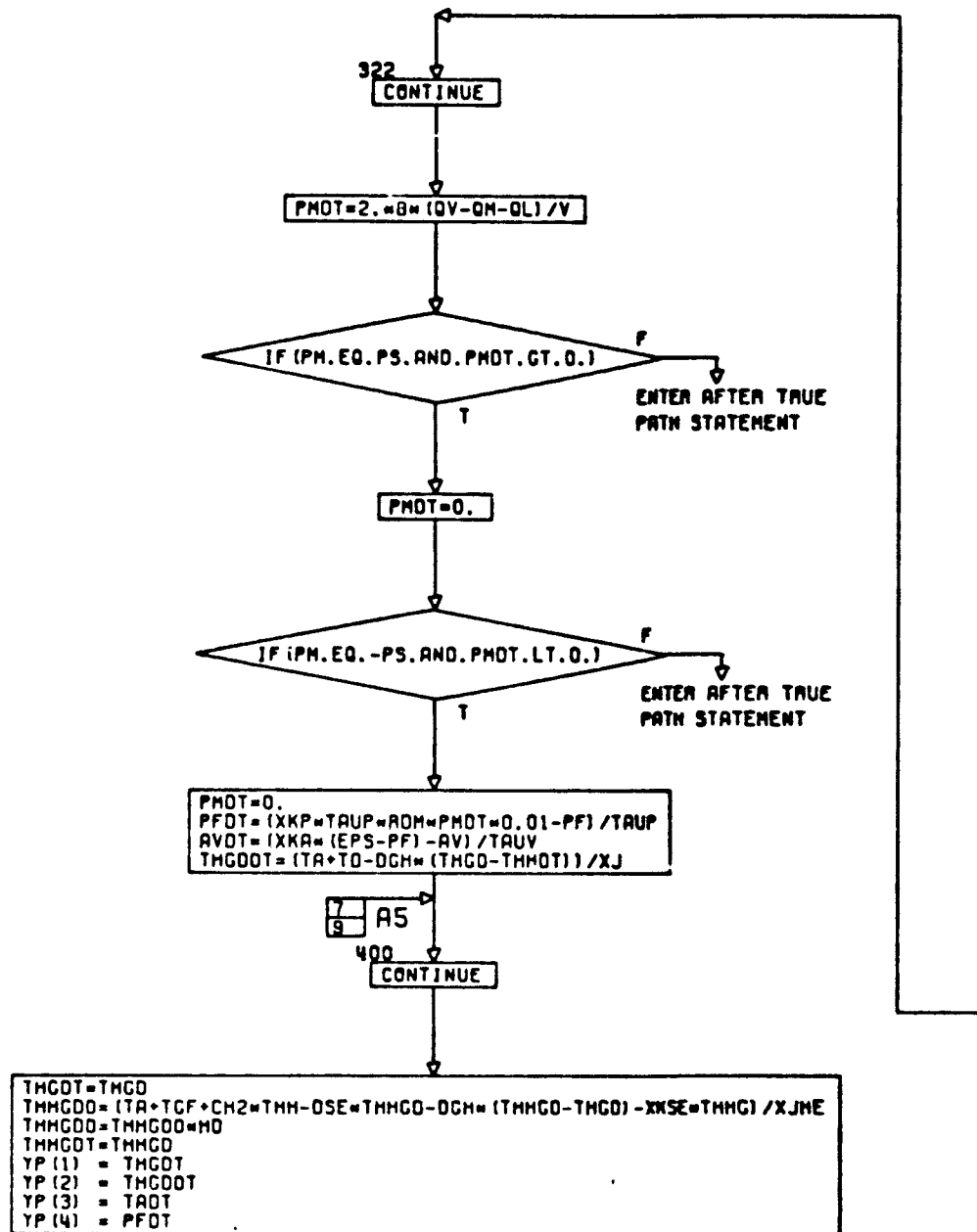
PG 9 OF 17

A-85



CONT. ON PG 11

PG 10 OF 17



CONT. ON PG 12

PG 11 OF 17

A-87


```

YP (5) = PMOT
YP (6) = EPOT
YP (7) = THSOT
YP (8) = AVOT
YP (9) = THHOT
YP (10) = THHGO
YP (11) = THHGOO
XTMP = XKA * (THSOT - THGO) + XKI * EPT

```

Y (19) = EPS

RETURN

```

C *****
C   NONLINEAR FLOW MODEL - POSITION CONTROL
C *****

```

500
EPT = TMS - THG

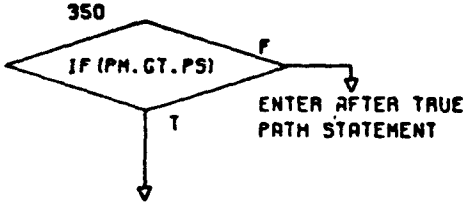
```

Y (6) = EPT
EPOT = 0.0
EPS = XKI * EPT - XKA * THGO - XKH * THHOT

```

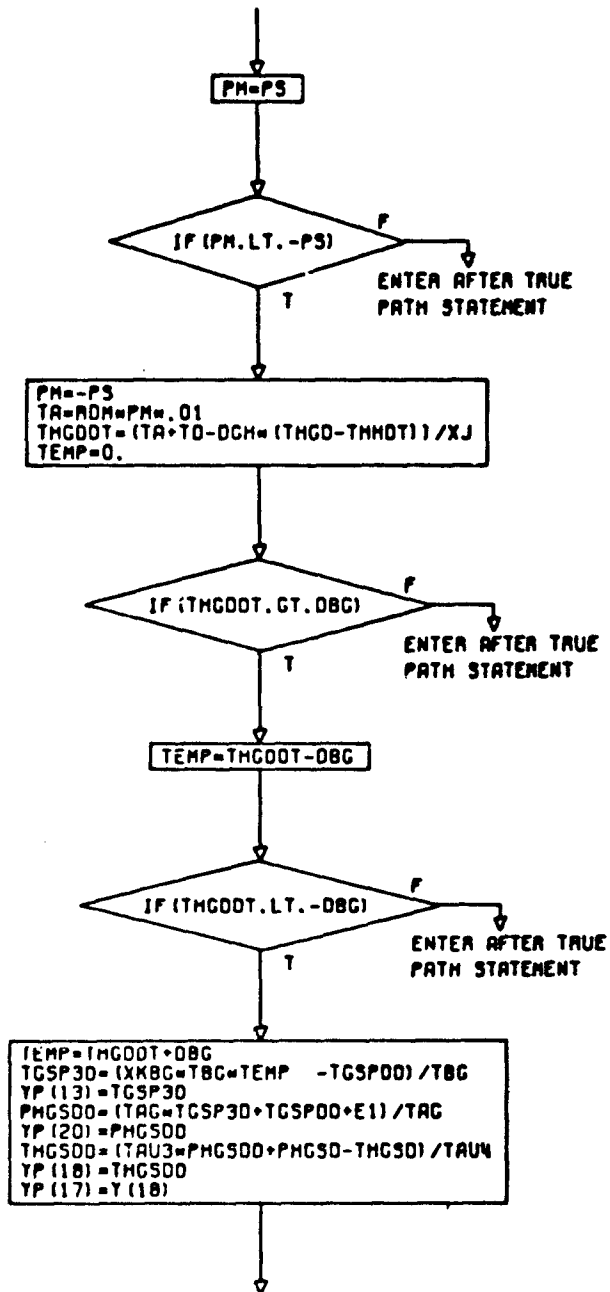
GO TO 301

9
R4



CONT. ON PG 13

PG 12 OF 17



CONT. ON PG 14

PG 13 OF 17

A-89

$EPSPA = XKI = (TMS - THCS) * XKA = (THSOT - THGSD)$
 $EPSPO = XKI = (THSOT - THGSD) * XKA = (THSOT - THGSD)$
 $EPSOT = ((TAU2 / TAU1) * (TAU1 * EPSPO + EPSPA) - EPS) / TAU2$
 $YP(19) = EPSOT$

GO TO (101, 202, 303, 501), NC9

450
 $TGSP30 = 10. * WN * WN * (THGO - PHGSD) - 2. * ZET * WN * TGSPD - WN * WN * TGSPD$

$YP(13) = TGSP30$
 $PHGS00 = 1.035 * TGSPD + TGSPD - PHGSD) / 0.007$
 $THGS00 = (TAU3 * PHGS00 + PHGSD - THGSD) / TAU4$
 $YP(20) = PHGS00$
 $YP(18) = THGS00$
 $YP(17) = Y(18)$
 $EPS = XKI = (TMS - THCS) * XKA = (THSOT - THGSD)$

GO TO 303

550
 $PHTD = THDEL$

$PMD = 0.0$

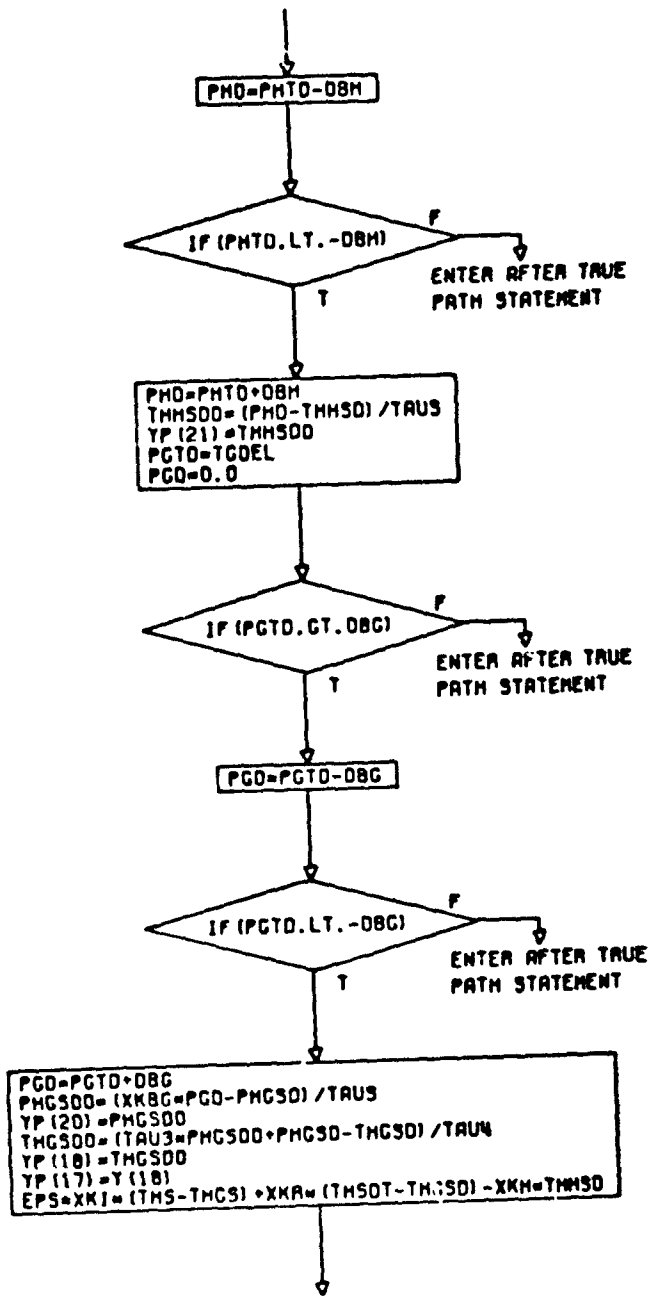
IF (PHTD. GT. DBM)

F
ENTER AFTER TRUE PATH STATEMENT

T

CONT. ON PG 15

PG 14 OF 17



CONT. ON PG 16

PG 15 OF 17

A-91

GO TO 303

650
STOP 650

250
TGSP30=WN*WN*THGD-2.*ZET=WN*TGSPDD-WN*WN*TGSPD

THSP30=WN*WN*THMDT-2.*ZET=WN*THSPDD-WN*WN*THSPD
THMSD=THSPD

```
C THMSD=0.0
C IF (THSPD.GT.DBH) THMSD=THSPD-DBH
C IF (THSPD.LT.(-DBH)) THMSD=THSPD+DBH
C THGSD=0.0
C IF (TGSPD.GT.DBG) THGSD=TGSPD-DBG
C IF (TGSPD.LT.(-DBG)) THGSD=TGSPD+DBG
C Y(18)=THGSD
C THSSDT=(TAUI*THMSD+THSS)/TAUI
```

```
C TGSS=THG-THH*THSS
C EPS=XKI*(THS-TGSS)-XKA*THGSD-XKH*THMSD
```

```
THSSDT=0.
THGSD=(TAU3*TGSPDD+TGSPD-THGSD)/TAU4
YP(18)=THGSD
YP(12)=TGSPDT
YP(13)=TGSP3D
YP(14)=THSPDT
YP(15)=THSP3D
YP(16)=THSSDT
```

351
YP(17)=THGSD

CONT. ON PG 17

PG 16 OF 17

GO TO (101, 202, 307, 501), NCS

202
 $EP^2 = XKI = (TMS - TMS) \cdot XKR = (TMSOT - TMSO) - XKH = TMSO$

GO TO 201 → 8
A2

307
 $EP^2 = XKI = (TMS - TMS) \cdot XKR = (TMSOT - TMSO) - XKH = TMSO$

GO TO 303 → 9
A3

501
 $EPT = TMS - TMS$

$Y(6) = EPT$
 $EPDT = 0.0$

GO TO 301 → 9
A4

END

SUBROUTINE PLOT (X, Y, NP, XMN, XMX, YMN, YMX, NS)

DIMENSION X (NP), Y (3, NP), YMN (3), YMX (3), IPT (101), ICR (3, 2),
SCLY (3, 11), IHD (3, 2), YFCT (3)

DATA IBNK/ ' //, ILNE/ ' //, ISTR/ 'w //
DATA ICR/ 'E ' 'C ' 'T ' 'E ' 'C ' 'T '
DATA IHD/ 'EPST ' 'THGD ' 'TA ' 'EPST ' 'THGD ' 'TA '

00 10 K=1,3 - - - > 2

BTY = (YMX (K) - YMN (K)) * 0.1
SCLY (K, 1) = YMN (K)

00 11 J=2,10

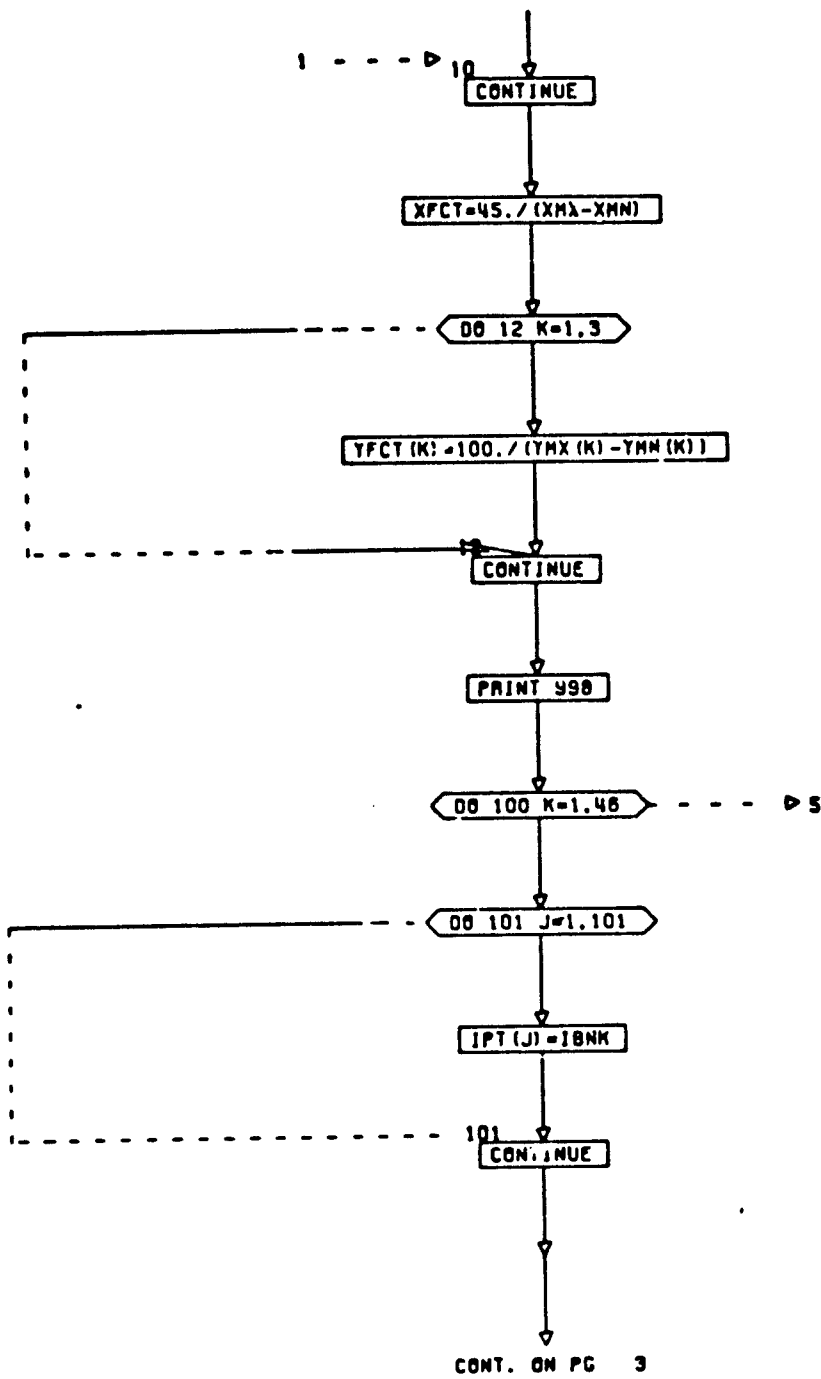
SCLY (K, J) = SCLY (K, J-1) * BTY

CONTINUE

SCLY (K, 11) = YMX (K)
PRINT 999, (SCLY (K, J), J=1, 11), IHD (K, NS), ICR (K, NS)

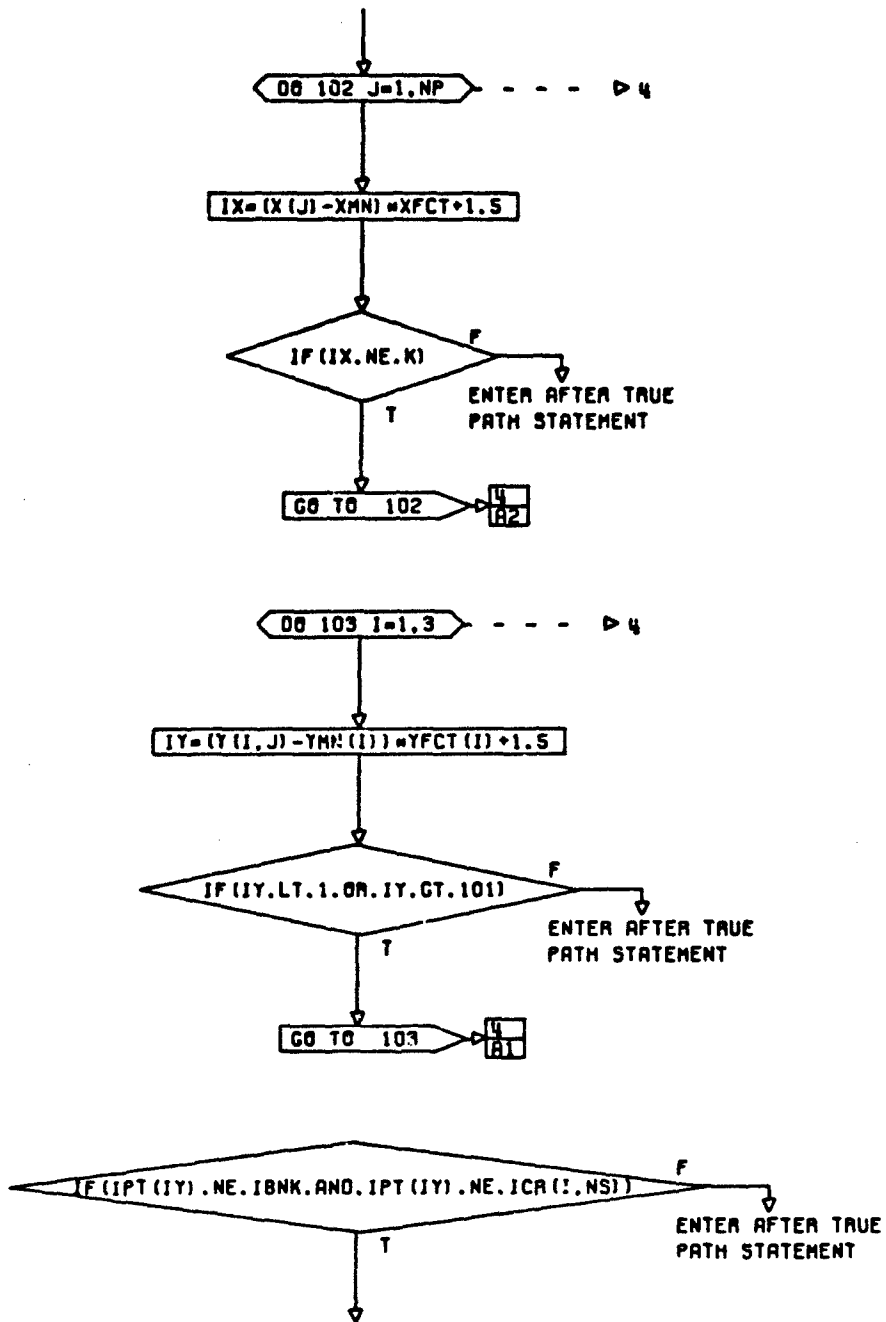
CONT. ON PG 2

PG 1 OF 5



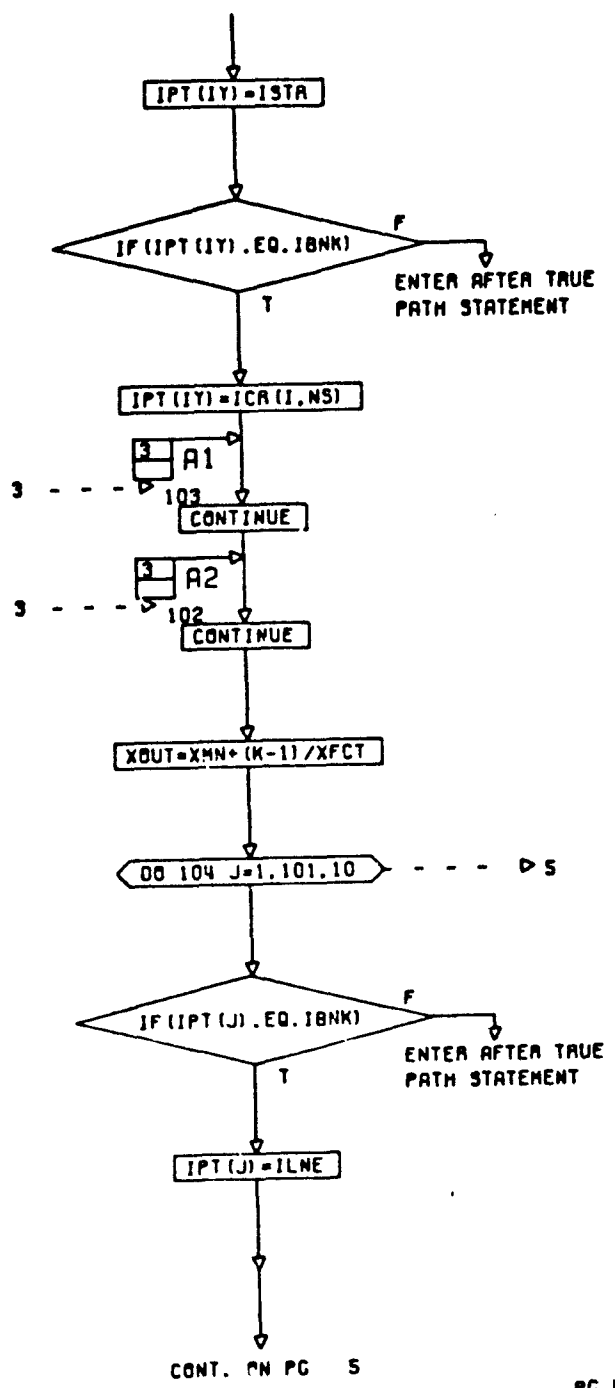
CONT. ON PG 3

PG 2 OF 5

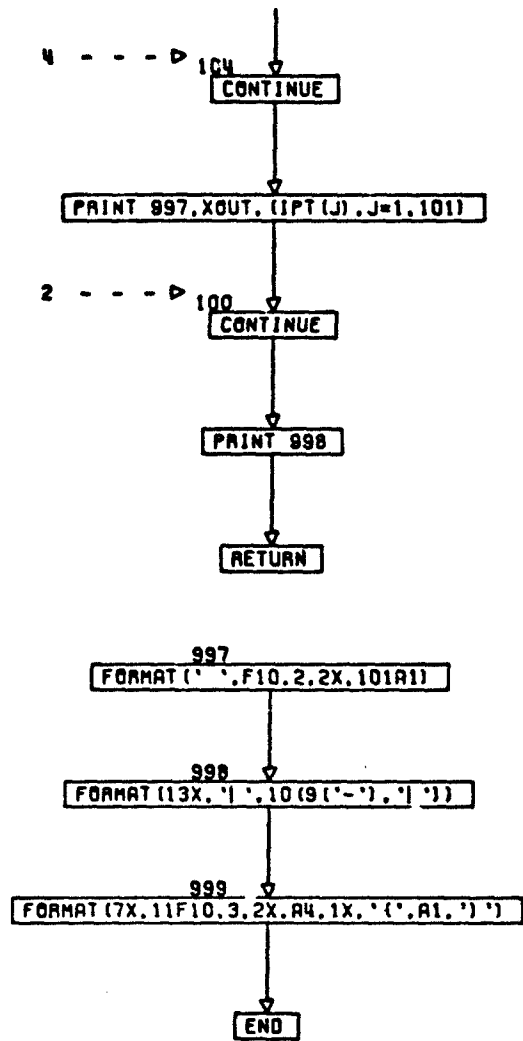


CONT. ON PG 4

PG 3 OF 5



PG 4 OF 5



SUBROUTINE SCALE (Y, NP, YMN, YMX, NC)
DIMENSION Y (NC, NP), YMN (NC), YMX (NC)

00 10 K=1, NC ----- > 3

YMAX=0.0

00 20 J=1, NP

TMP=ABS (Y (K, J))

IF (TMP.GT. YMAX)

F
ENTER AFTER TRUE
PATH STATEMENT

T
YMAX=TMP

20
CONTINUE

NPOW=0

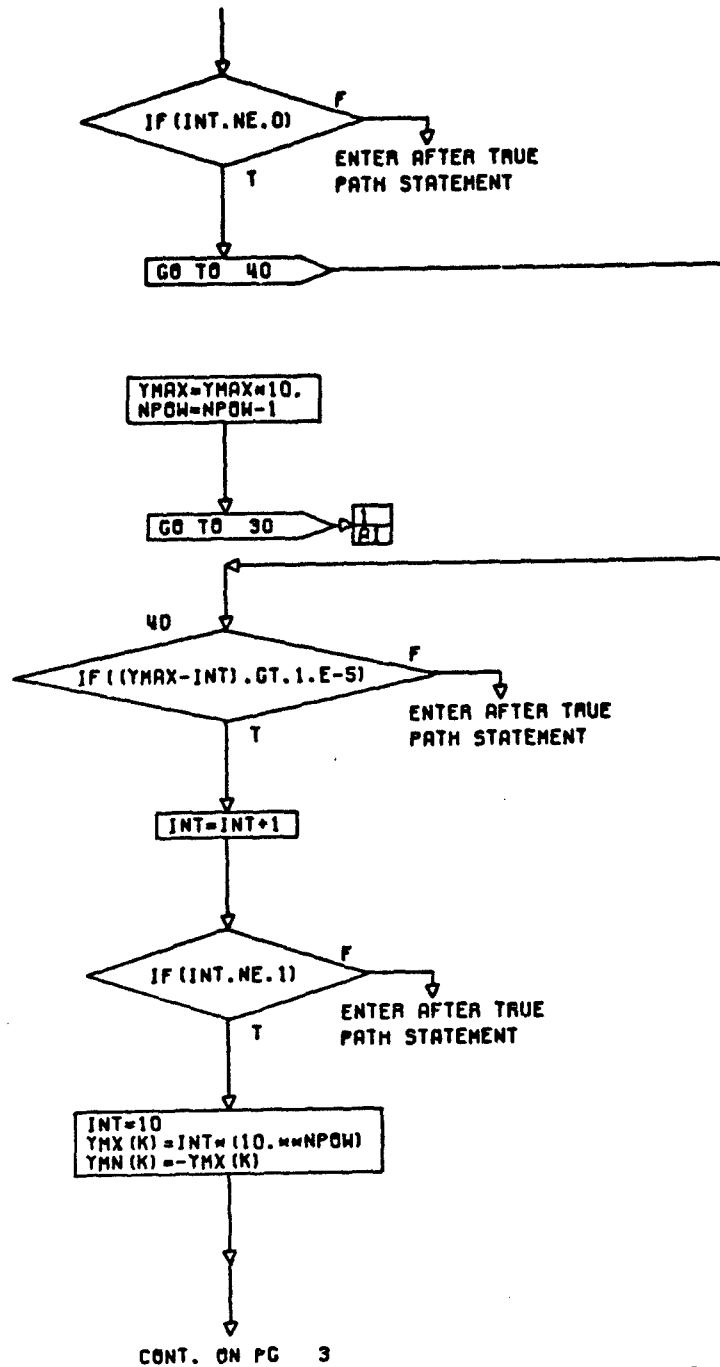
A1 2

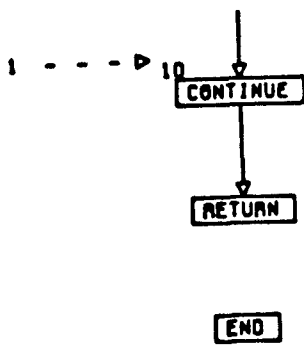
30
INT=YMAX

CONT. ON PG 2

PG 1 OF 3

A-99





PG 3 FINBL

A-101

SUBROUTINE RK (N, K, Y0, DY, X0S, DX, YW, YP, XW, AI, DIFEC)

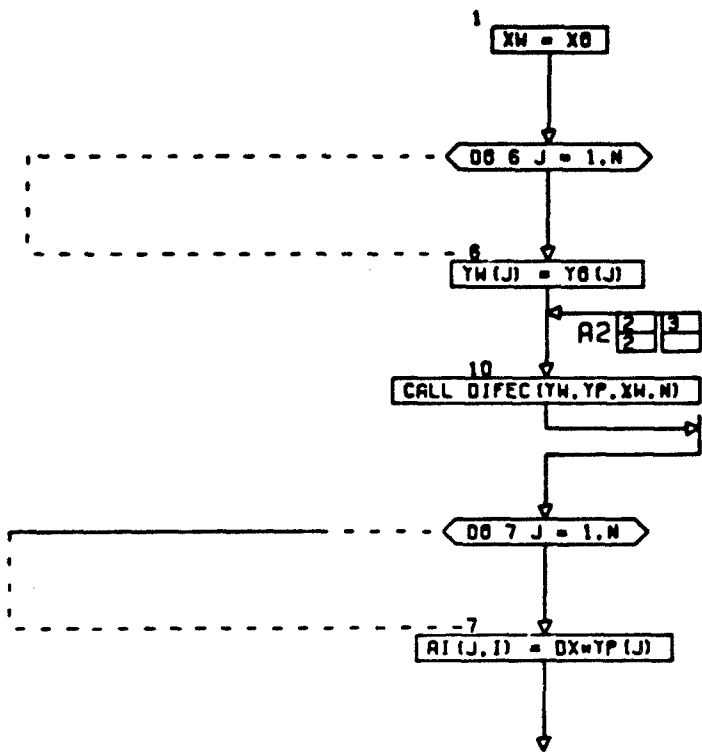
C **** N SPECIFIES NUMBER OF EQNS. K=1 PROVIDES YP'S AT END POINTS

DIMENSION Y0(N), DY(N), YW(N), YP(N), AI(N,4)
DOUBLE PRECISION X0
X0 = X0S
I = 1

A1

2	3
2	3

GO TO (1,2,3,4,5), I

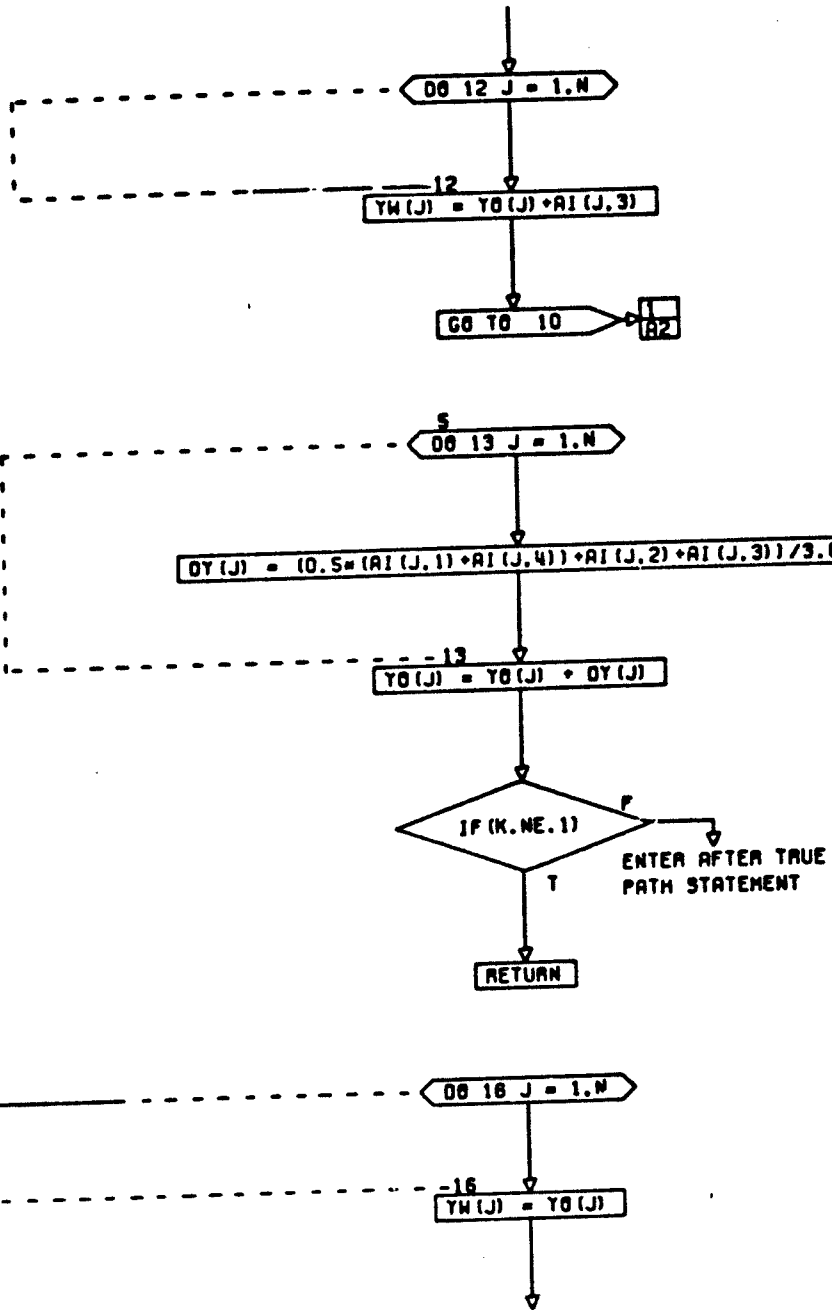


CONT. ON PG 2

PG 1 OF 4

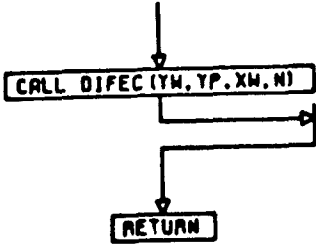


Page 2 of 4



CONT. ON PG 4

PG 3 OF 4



END

APPENDIX B
ANALOG AND HYBRID WIRING DIAGRAMS

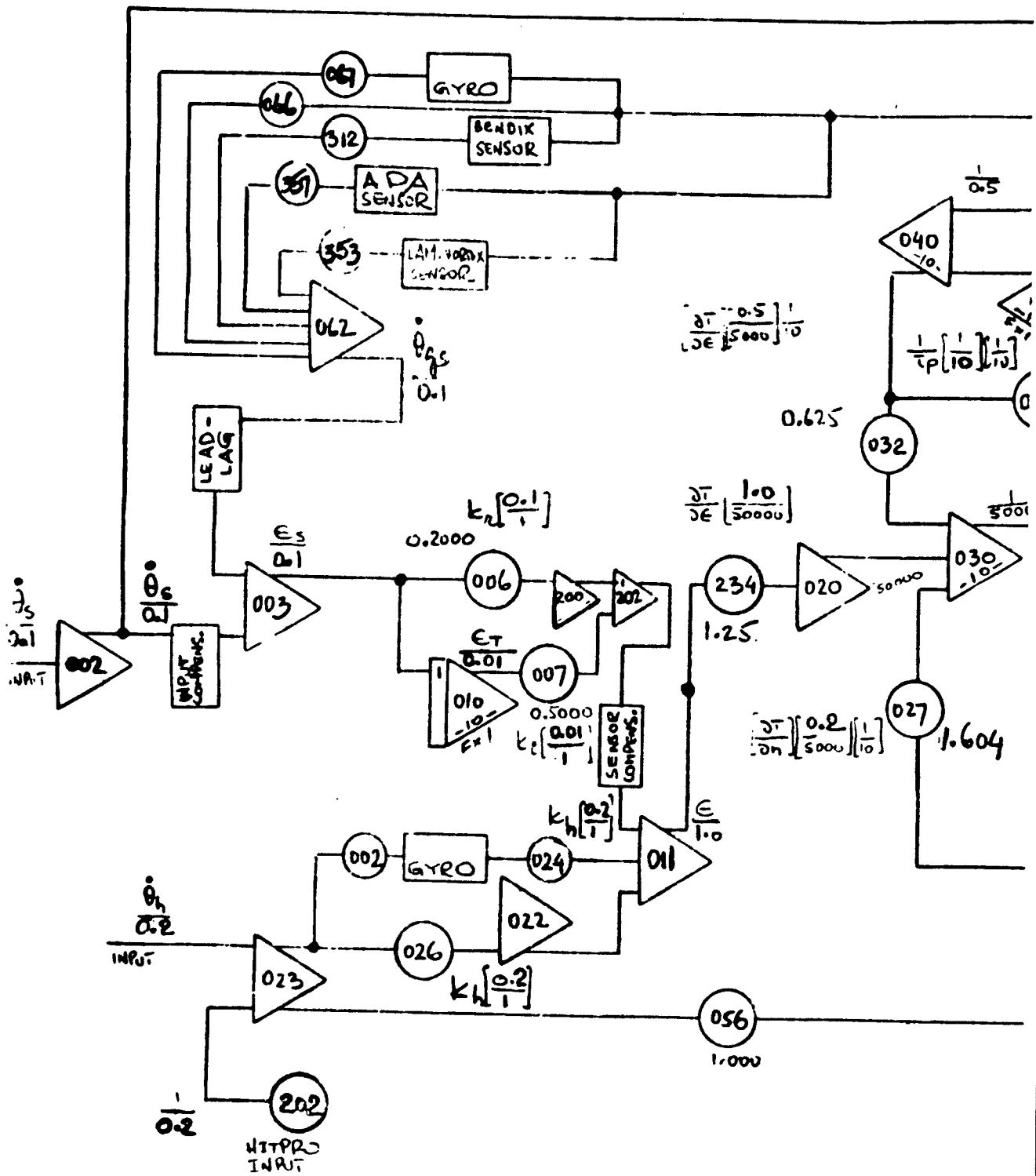


Figure B-1. Rate Control Sy

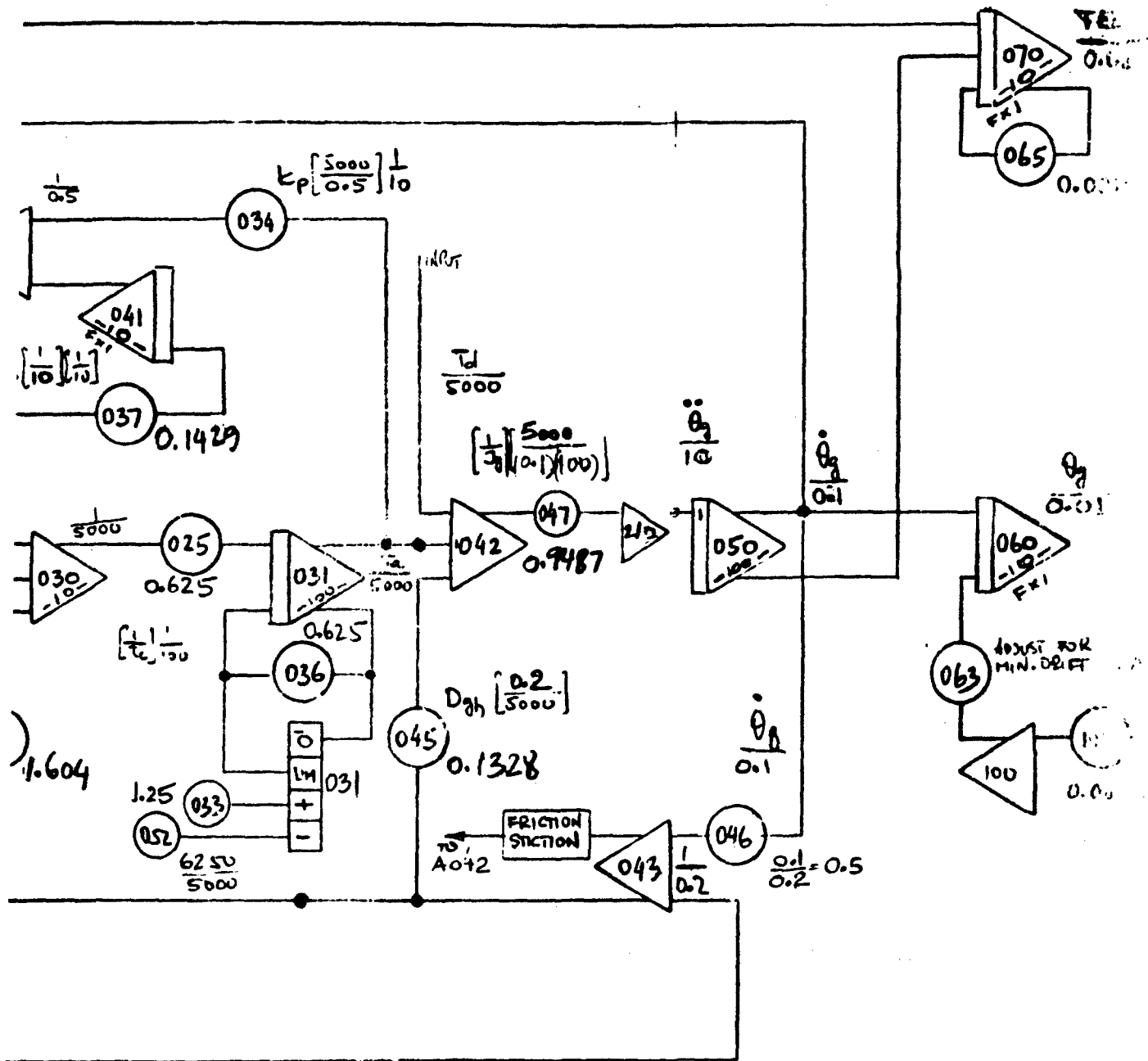


FIGURE B1
 M60 TANK 10.10.74
 RATE CONTROL - LINEAR

Control System with Linear Flow Model

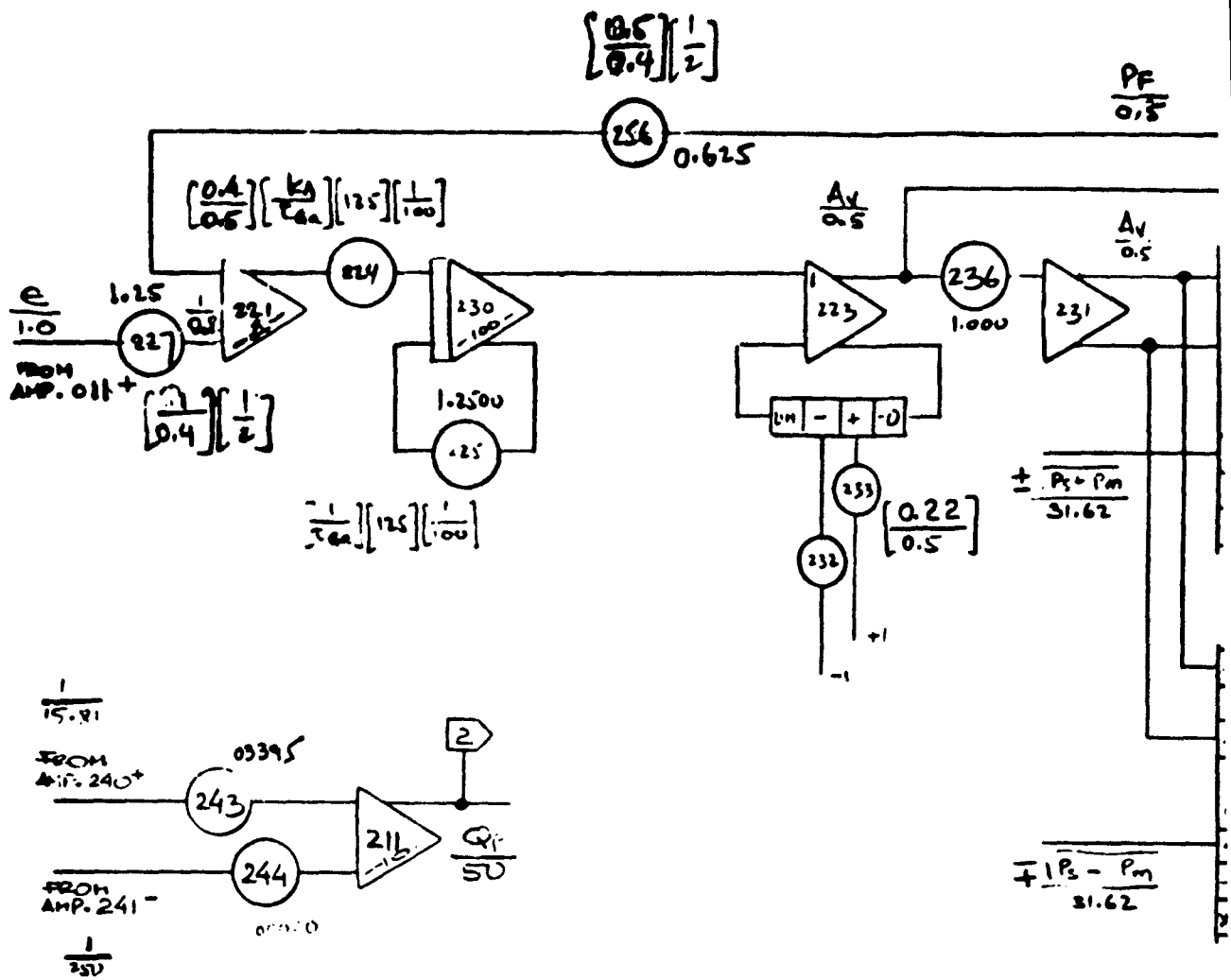


FIGURE B2
 M60 TANK $S=0.12, \sigma=7.1$
 NONLINEAR FLOW MODEL
 RATE CONTROL

DUAL SQUARE ROOT CIRCUIT

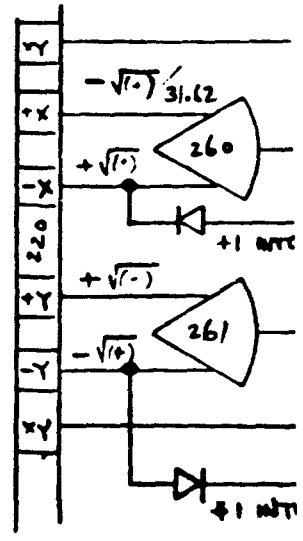
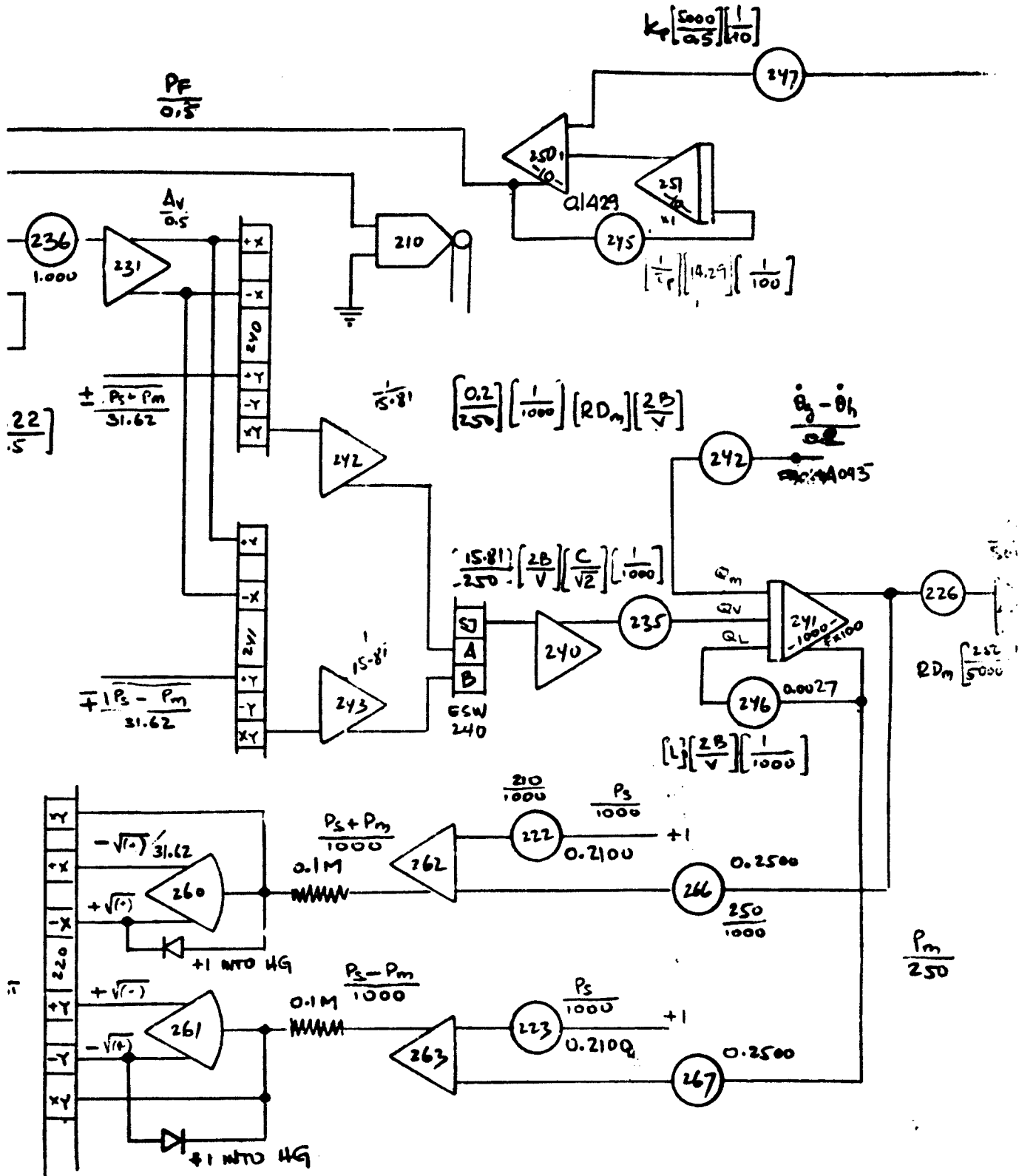
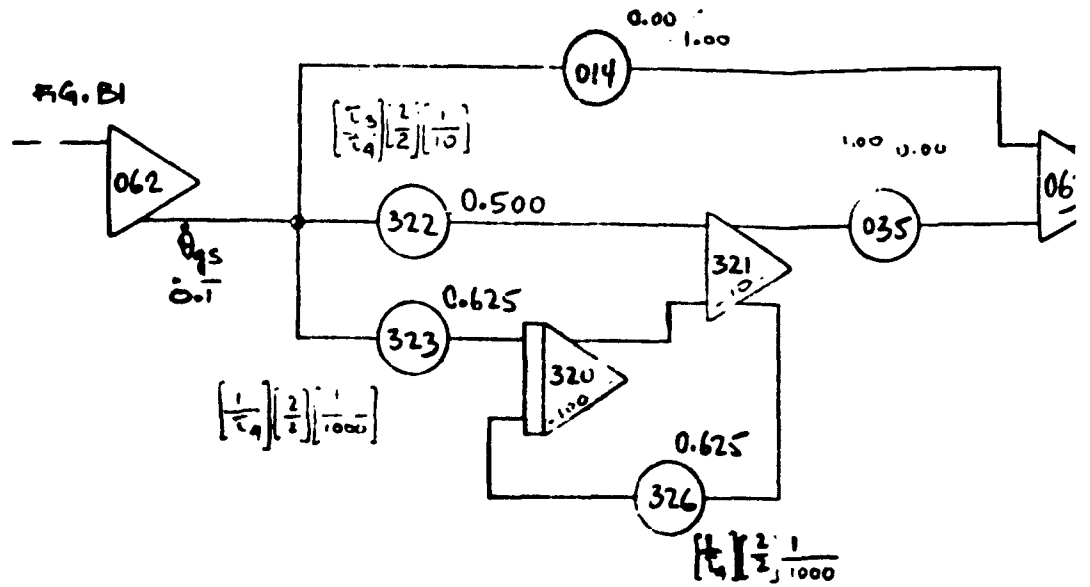


Figure B-2. Nonlinear Flow Model in Rate



Linear Flow Model in Rate Control System

LEAD-LAG



Coulomb Friction
Stiction

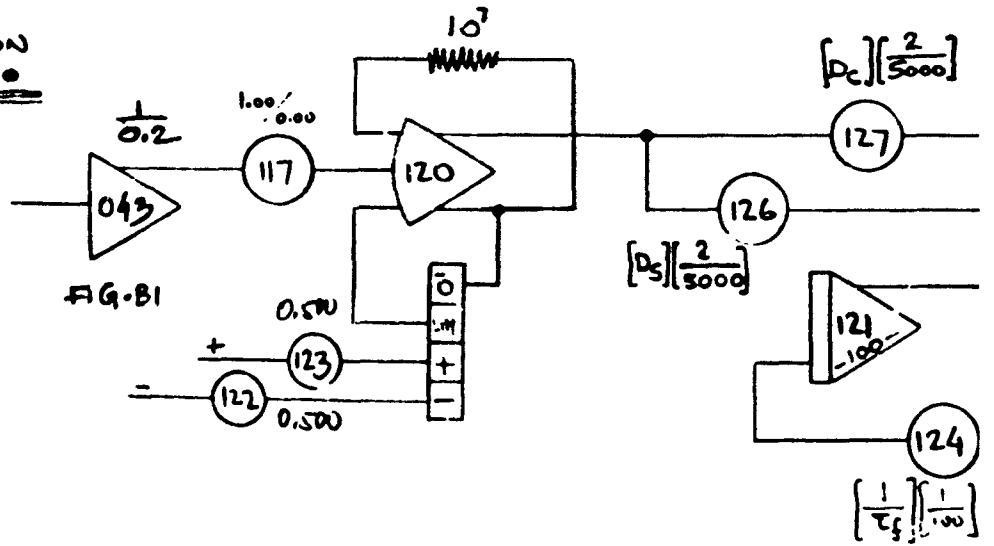
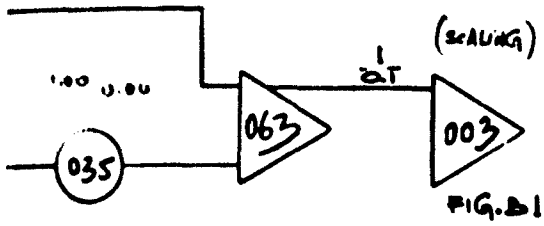
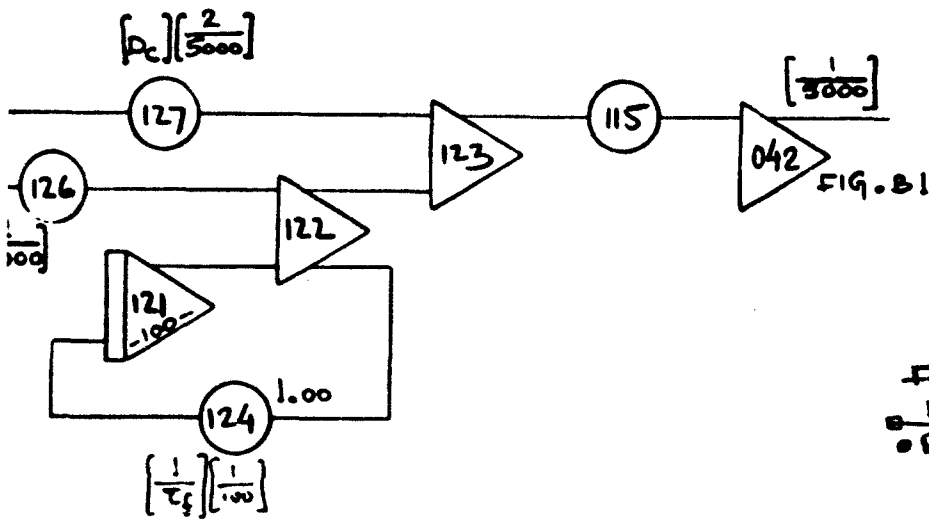


Figure B-3. Compensation Circuit



100



Compensation Circuits in Rate Control System

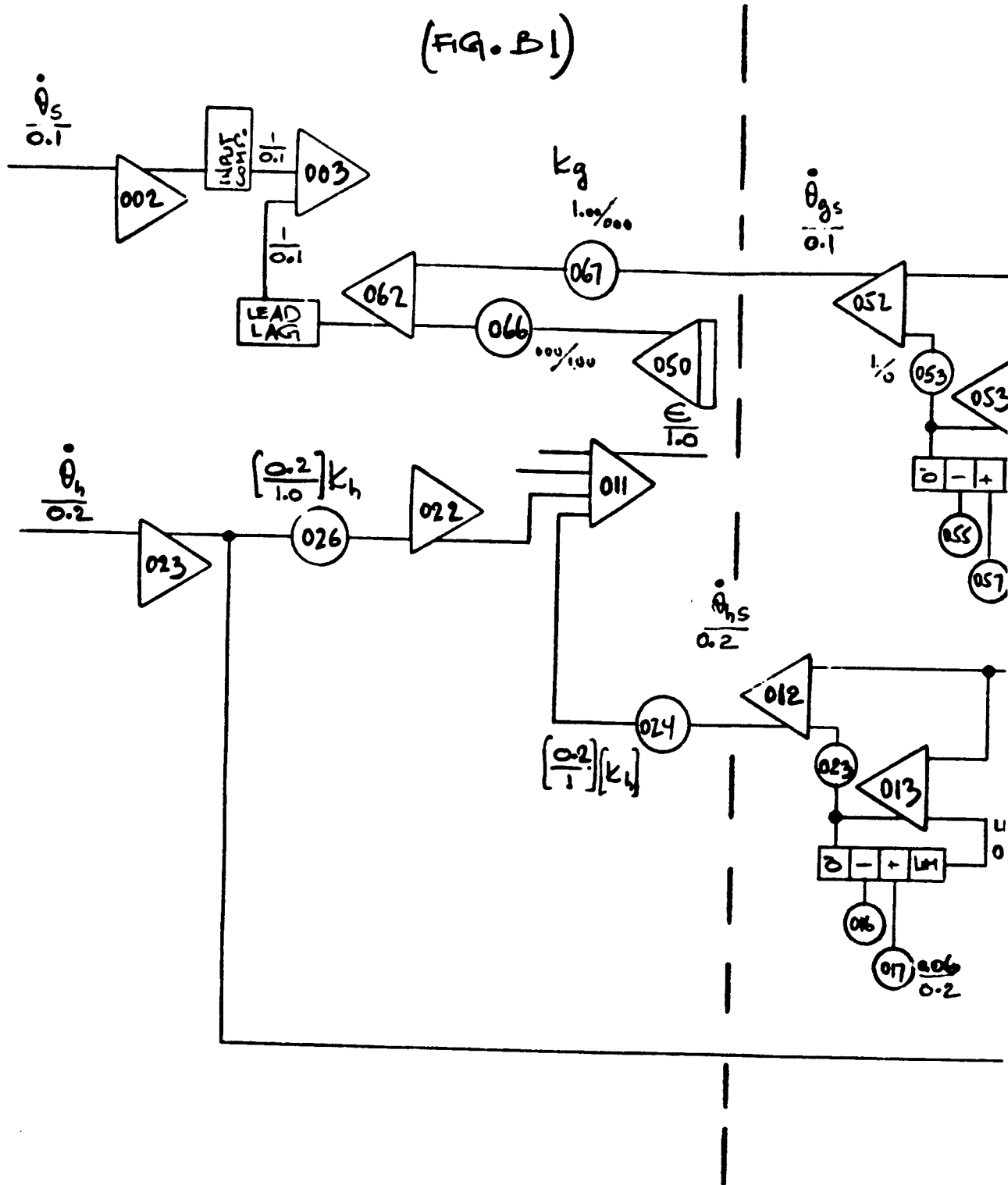


Figure B-4. Gyros in Rate Cont

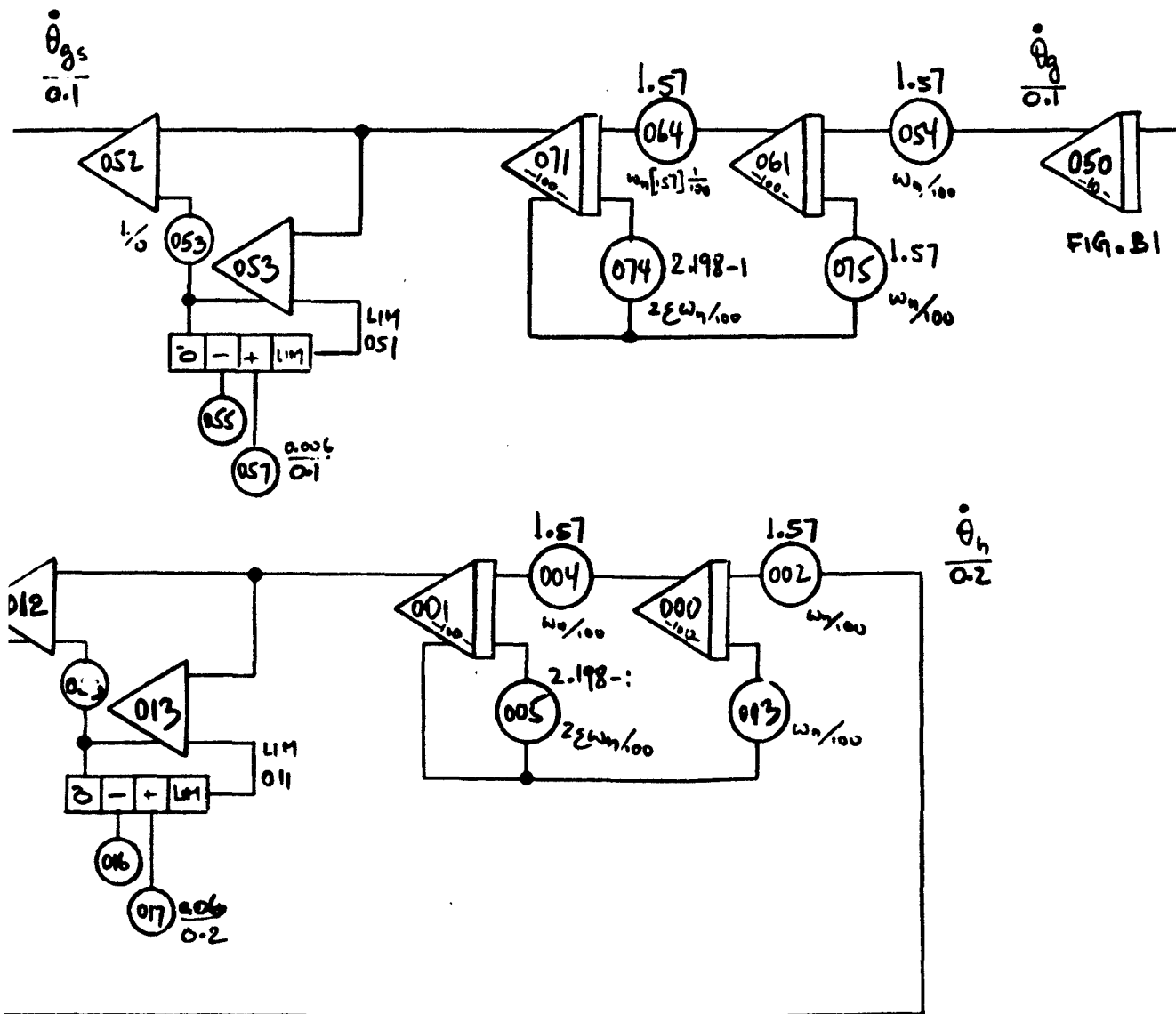


FIGURE B4
M60 • RATE CONTROL
GYROS • 10 • 4 • 74

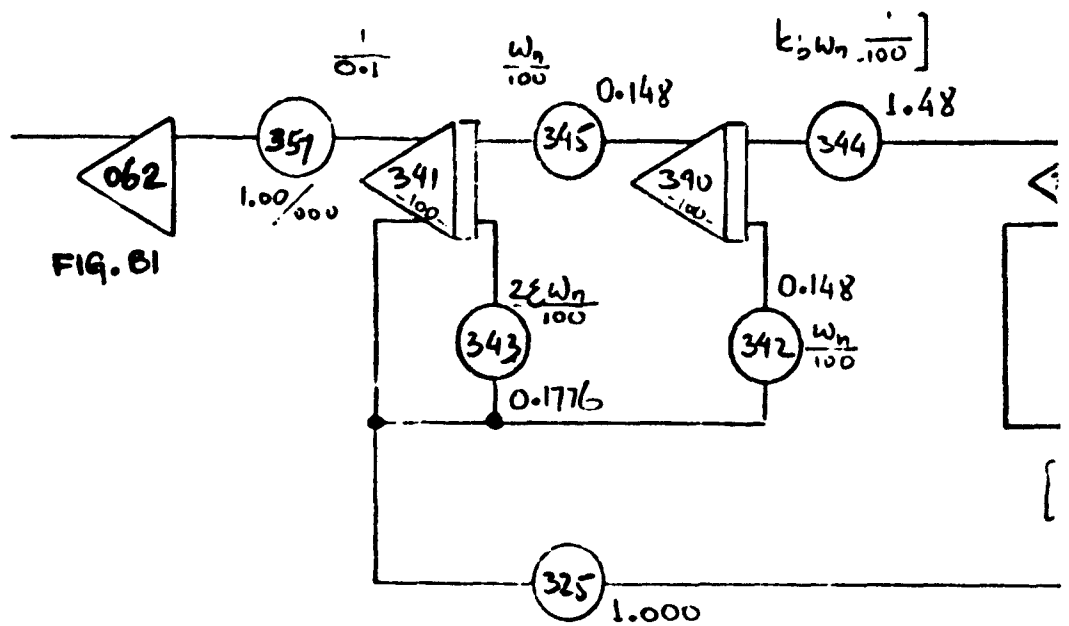
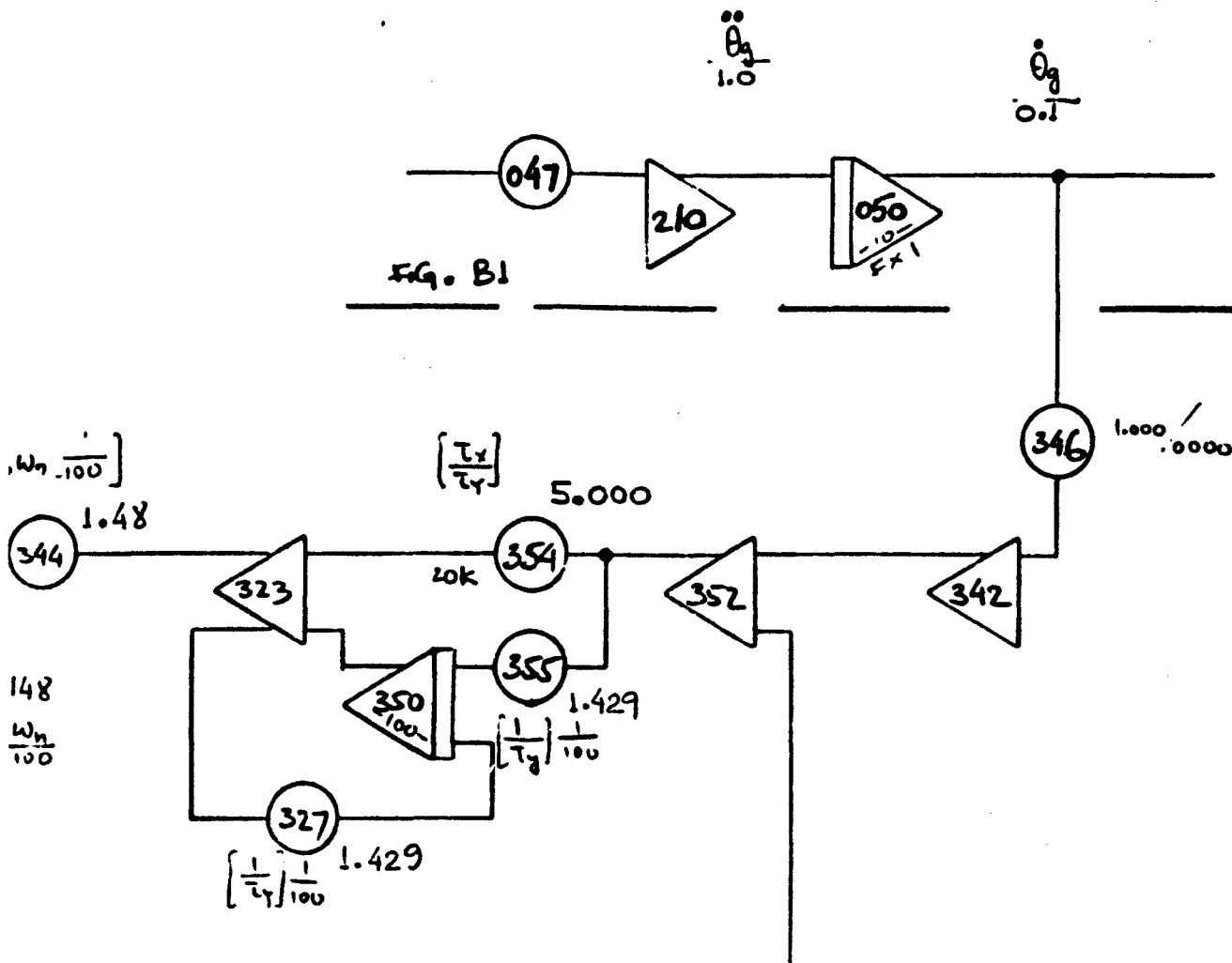


FIG. B5
 M60 TANK • RATE CONTROL
 AIRESEARCH PNEUMATIC ACCELEROMETER
 11-12-74

Figure B-5. Airesearch Pneumatic Acce



rch Pneumatic Accelerometer in Rate Control System

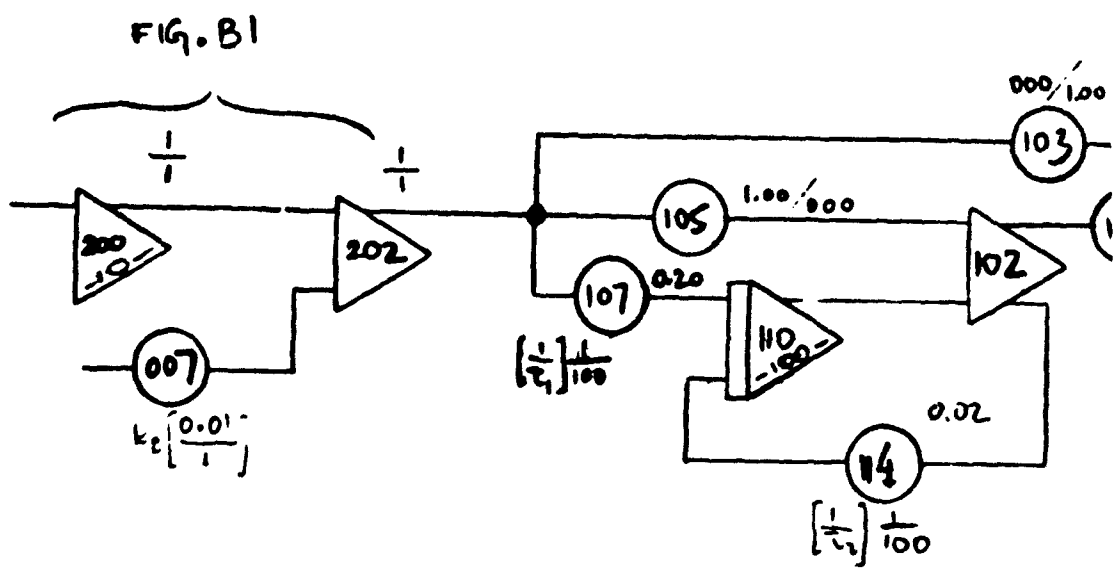
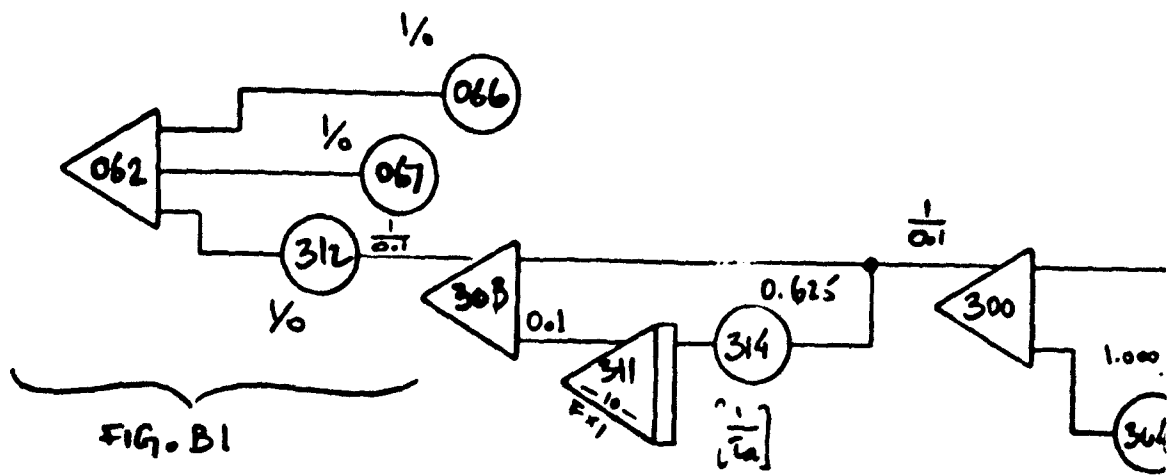


Figure B-6. Bendix Sensor in R

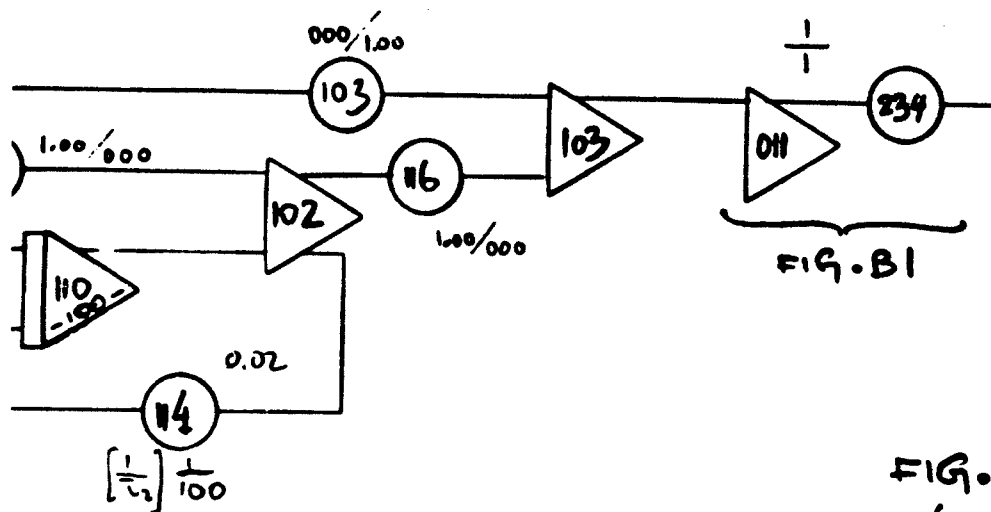
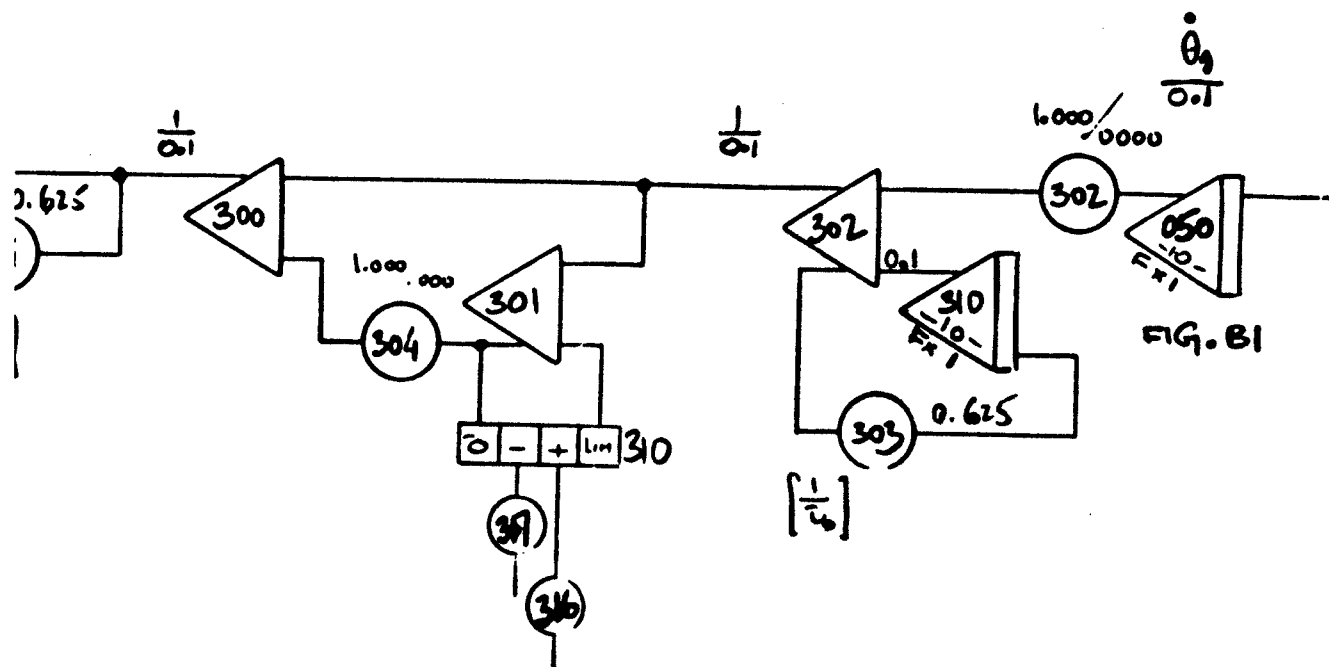


FIG. B6
M60 TANK RATE CONTROL
BENDIX SENSOR
 11-7-74

Figure B-6. Bendix Sensor in Rate Control System

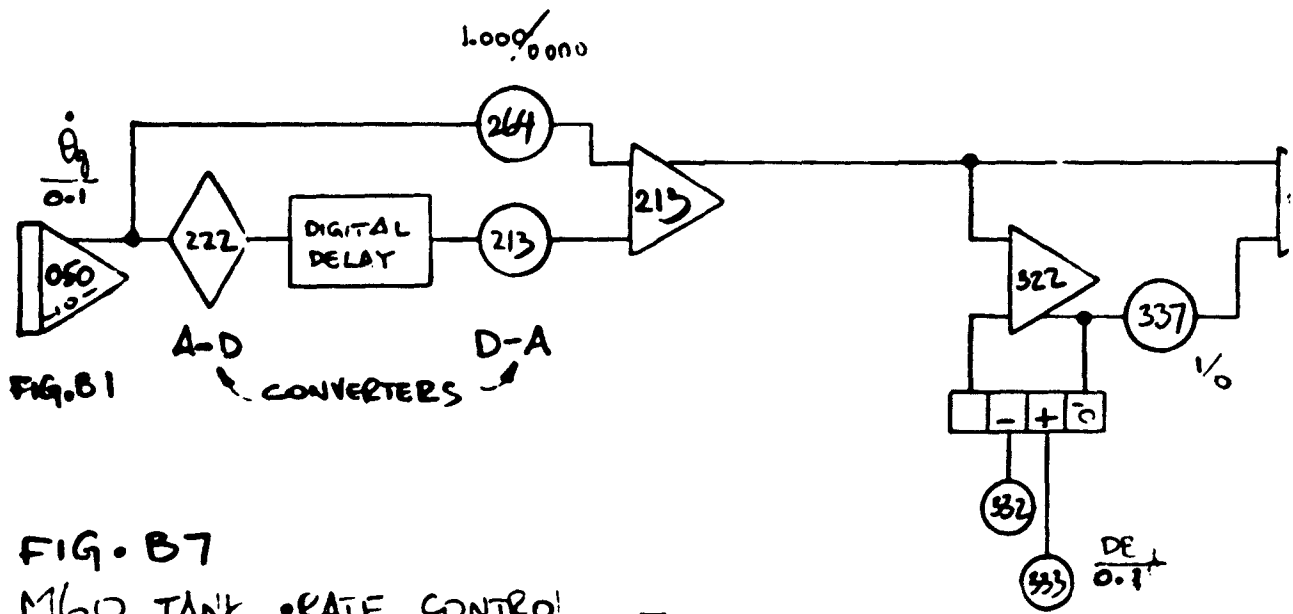
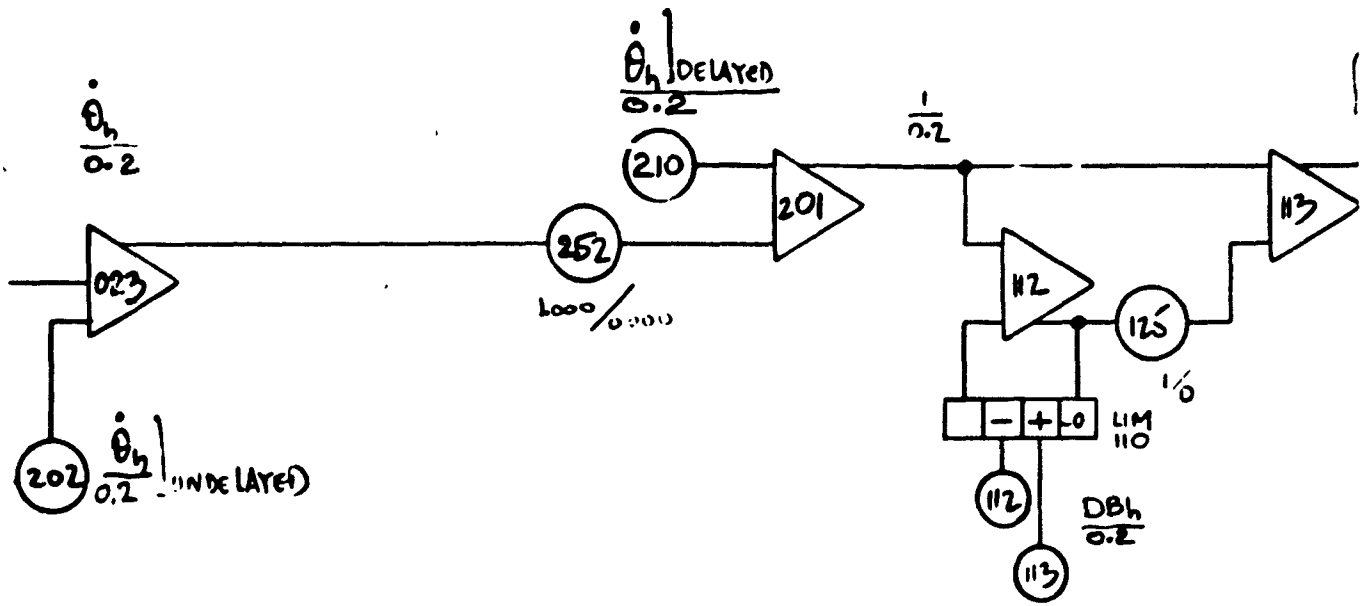
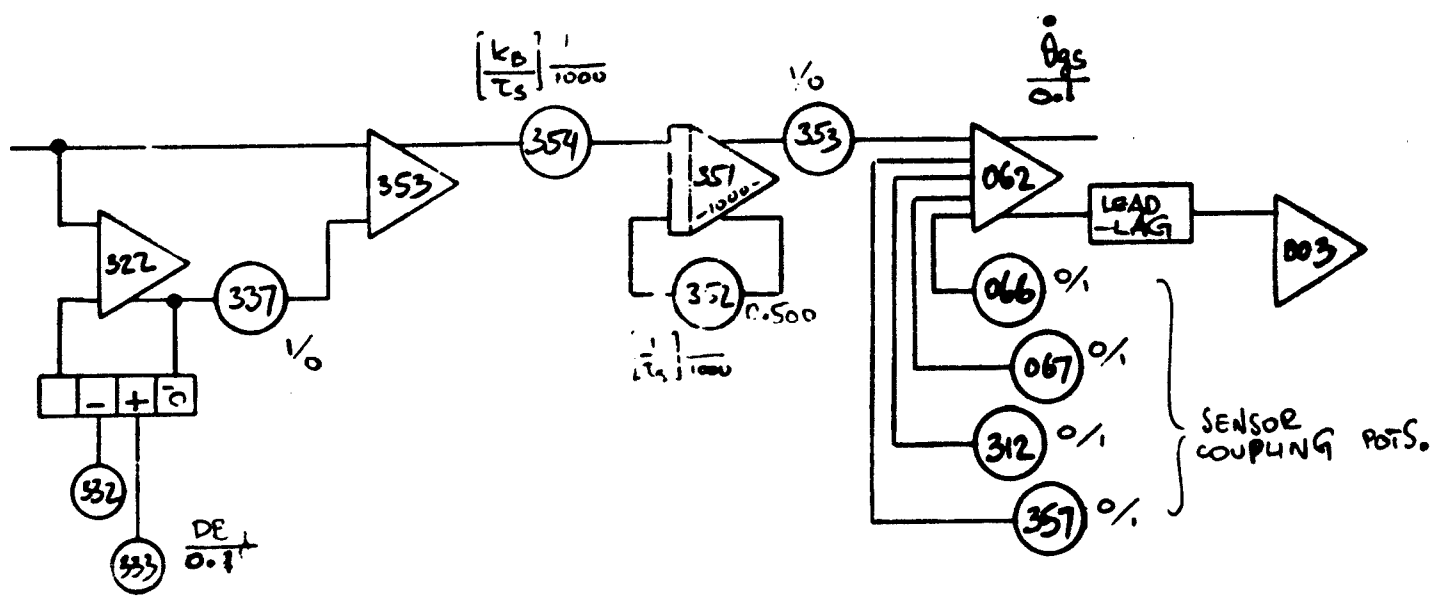
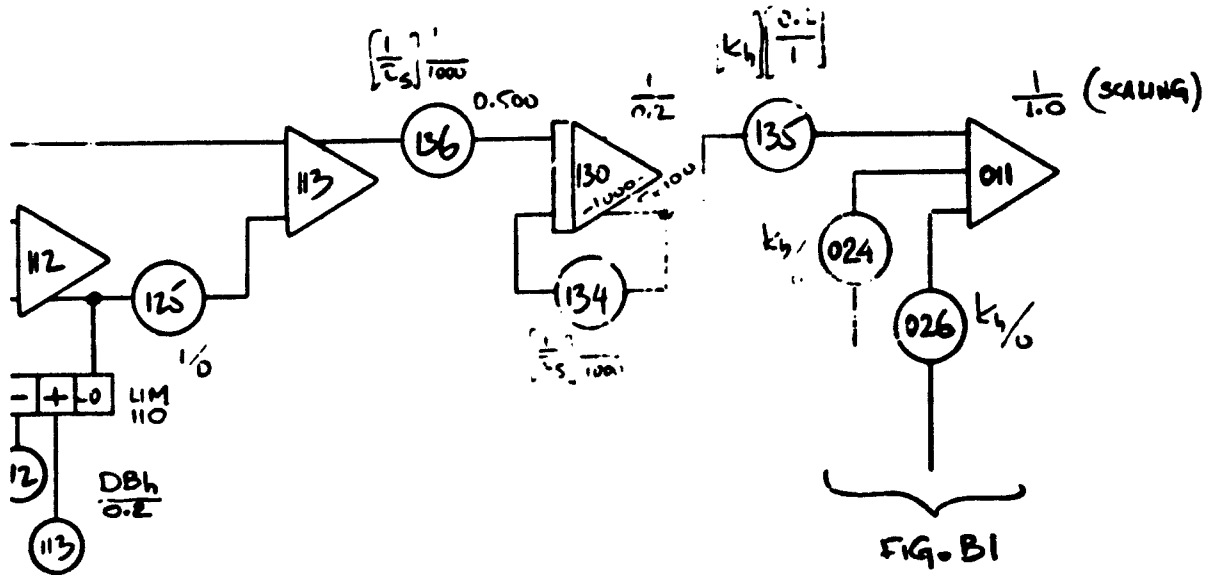


FIG. B7
M60 TANK RATE CONTROL
LAMINAR VORTEX SENSOR 11-19-74

Figure B-7. Laminar Vortex Sensor in R



Laminar Vortex Sensor in Rate Control System

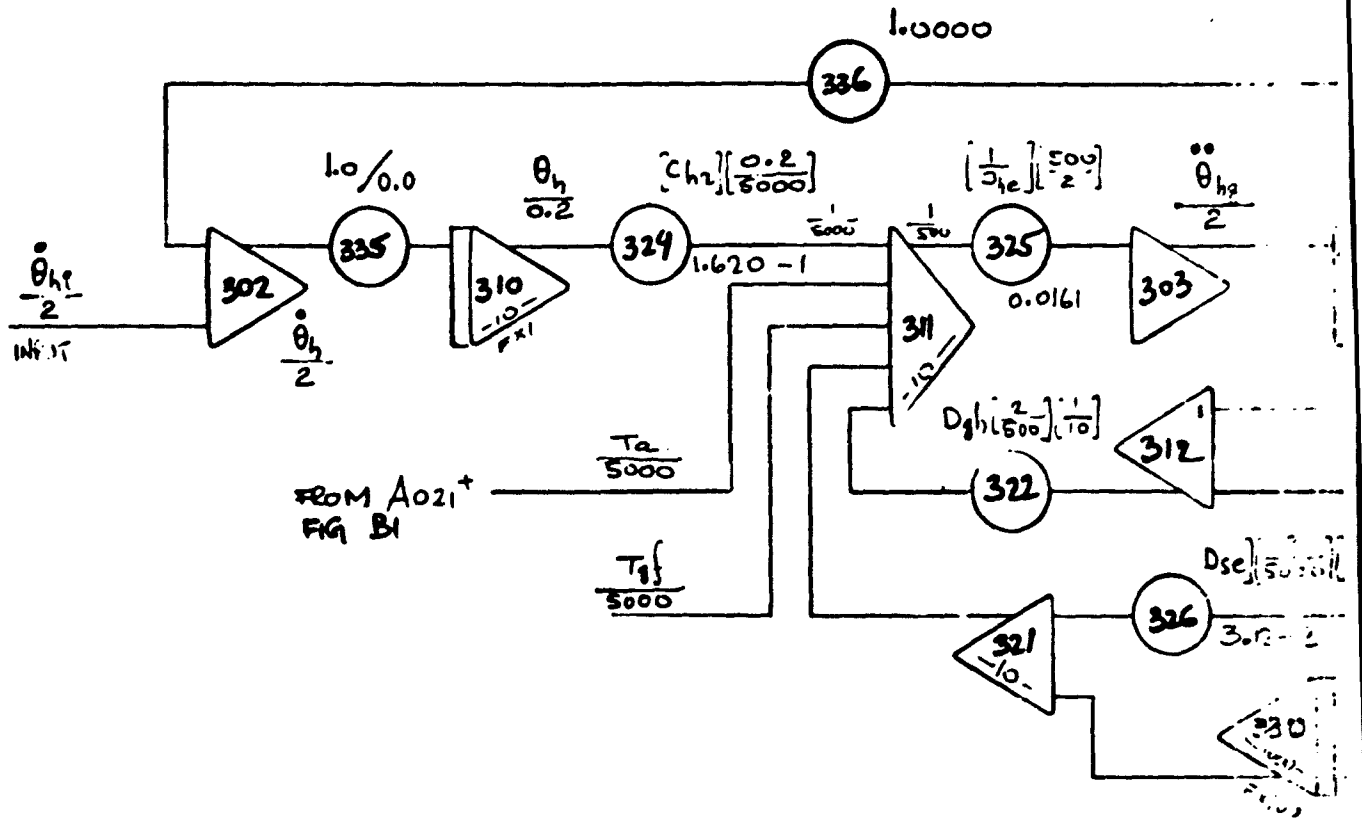


FIG. B8

MGO TANK • 10.8.74.
 RATE CONTROL • LINEAR FLOW
 HULL DYNAMICS

Figure B-8. Hull Dynamics in Rate Control System

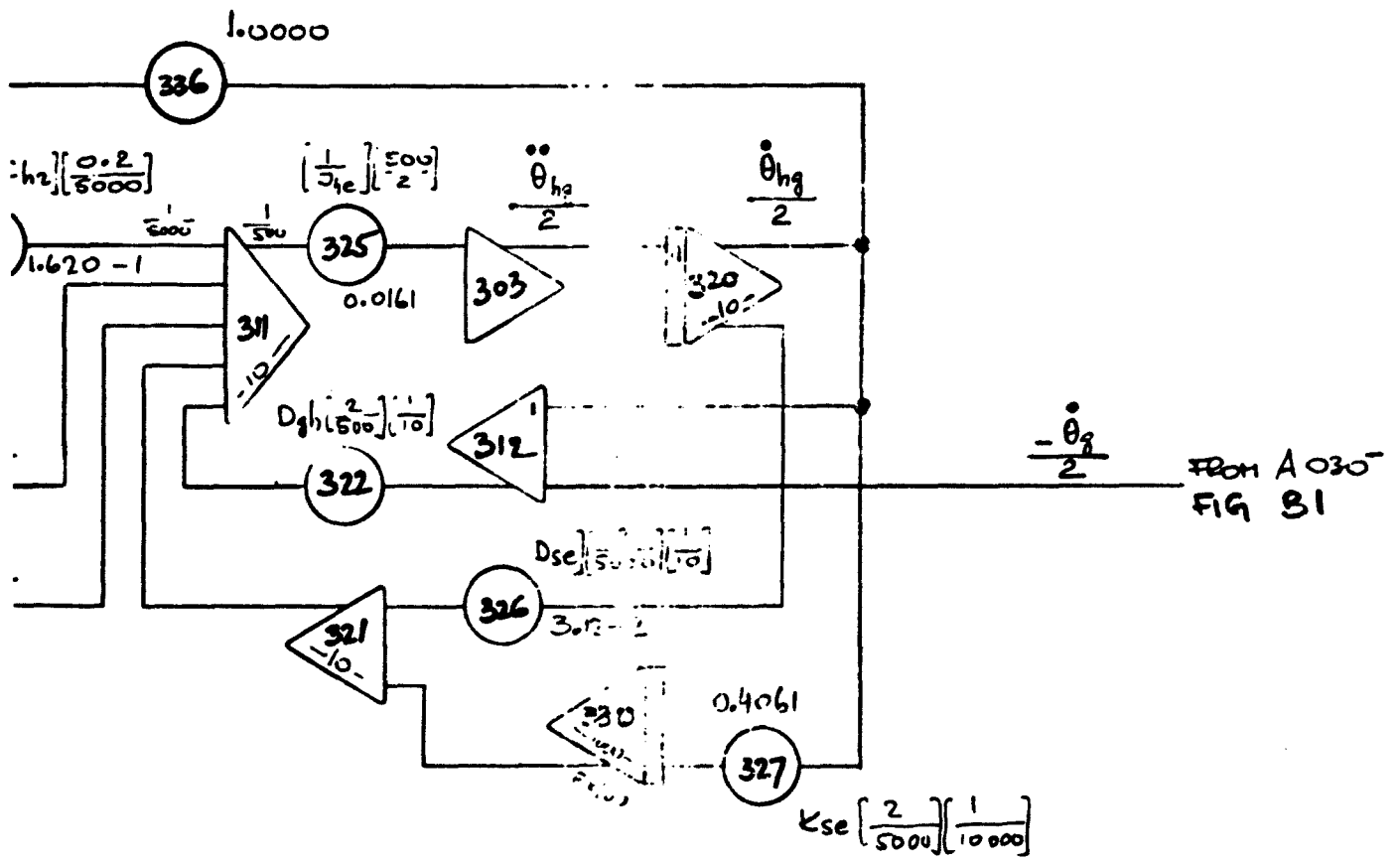


Figure B-8. Hull Dynamics in Rate Control System

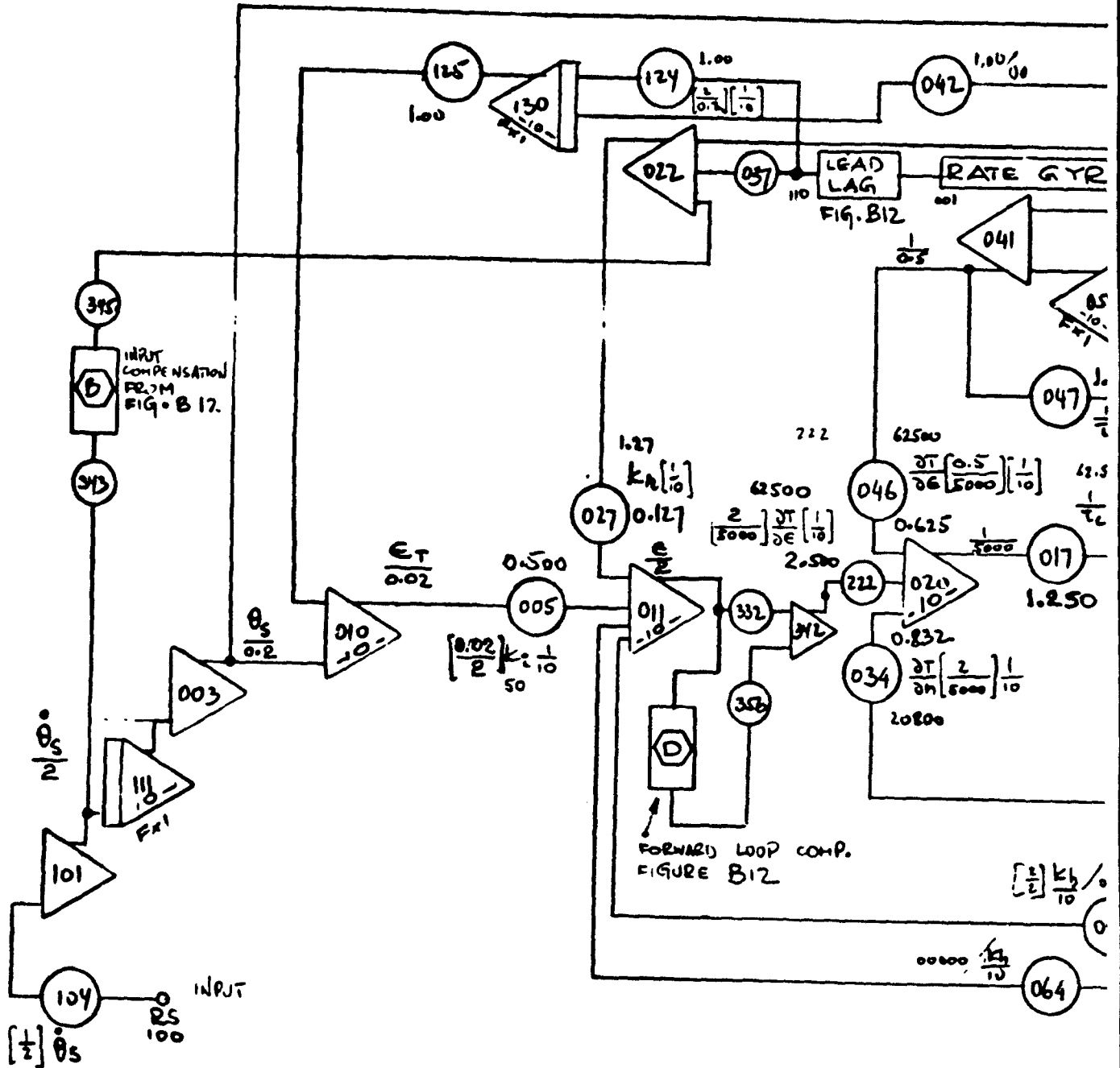
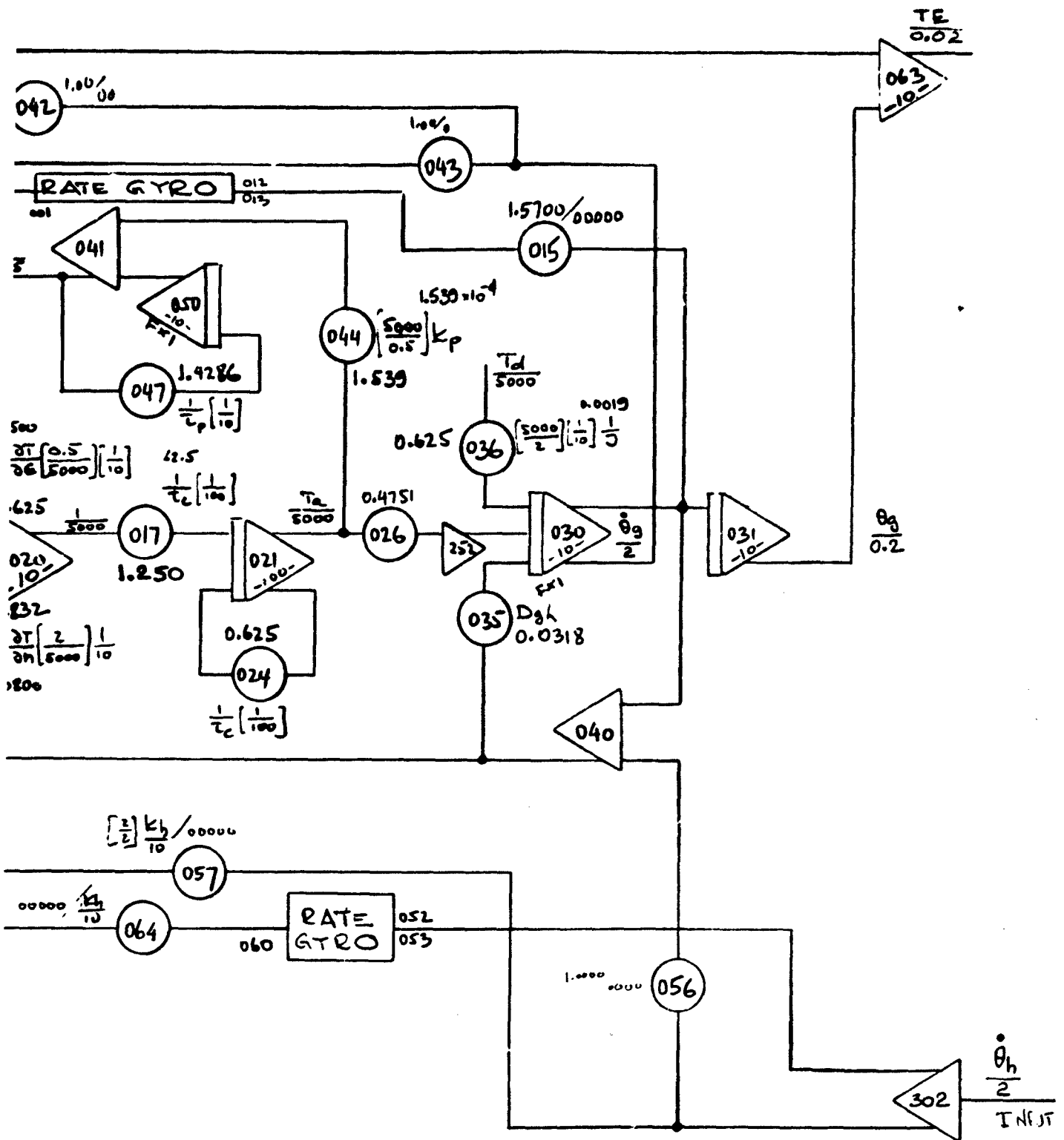


FIG. B9
 M60.10.4.74
 POSITION CONTROL - LINEAR FLOW

Figure B-9. Position Control System



tion Control System with Linear Flow Model

$$\frac{0.5}{2} = 0.25C$$

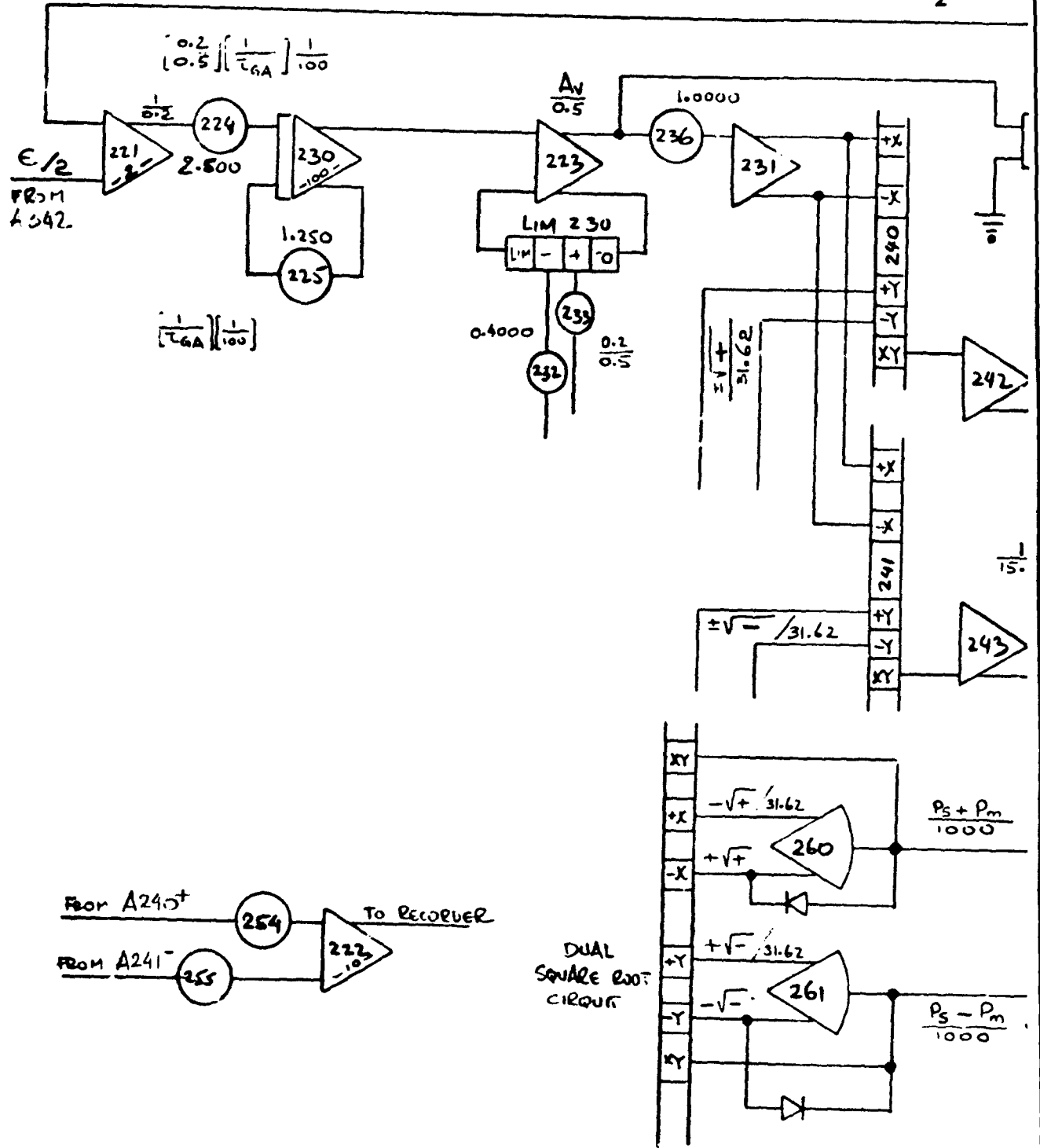


Figure B-10. Nonlinear Flow Model in 1

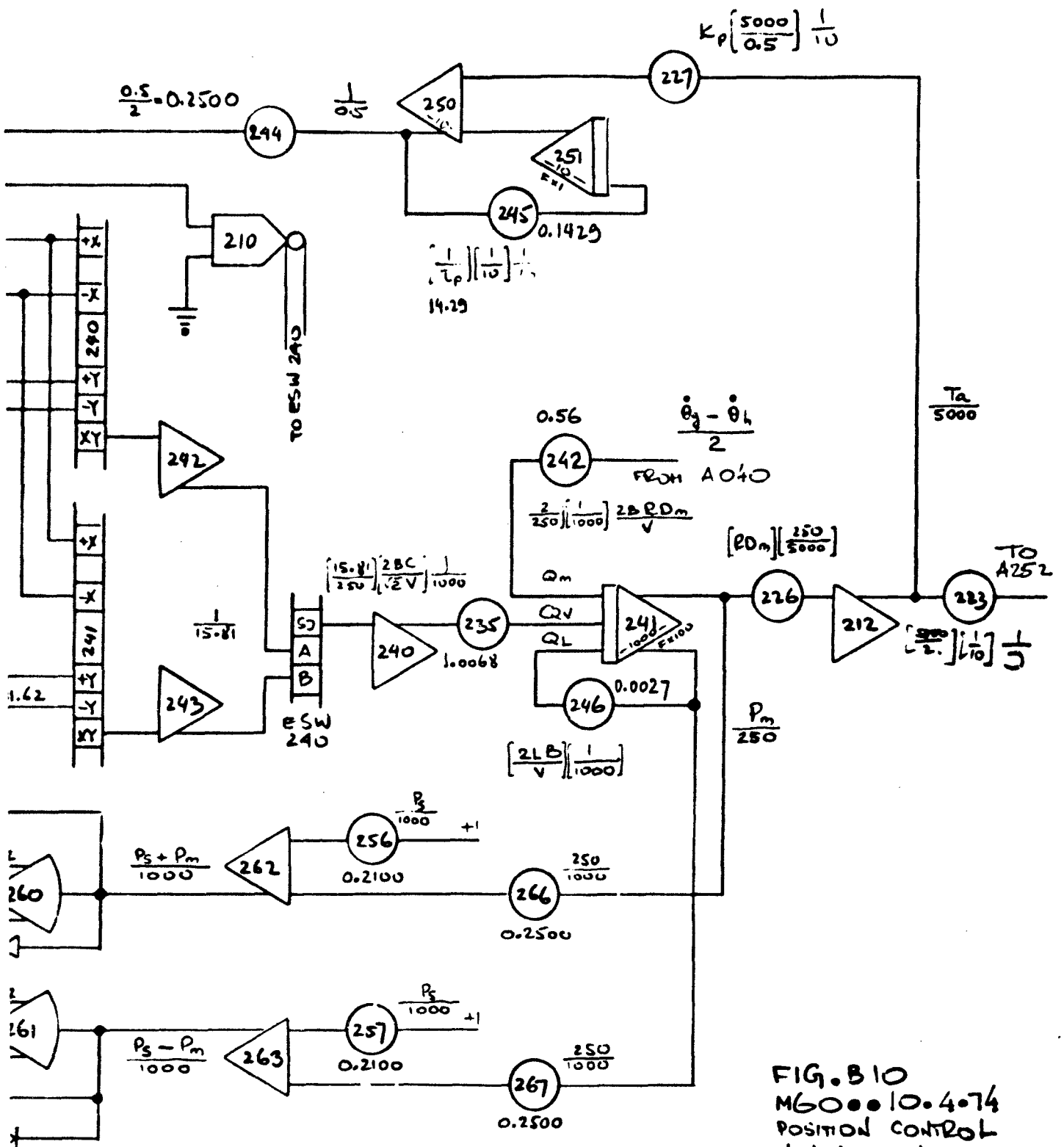


FIG. B10
 M600 • 10.4 • 74
 POSITION CONTROL
 NONLINEAR FLOW

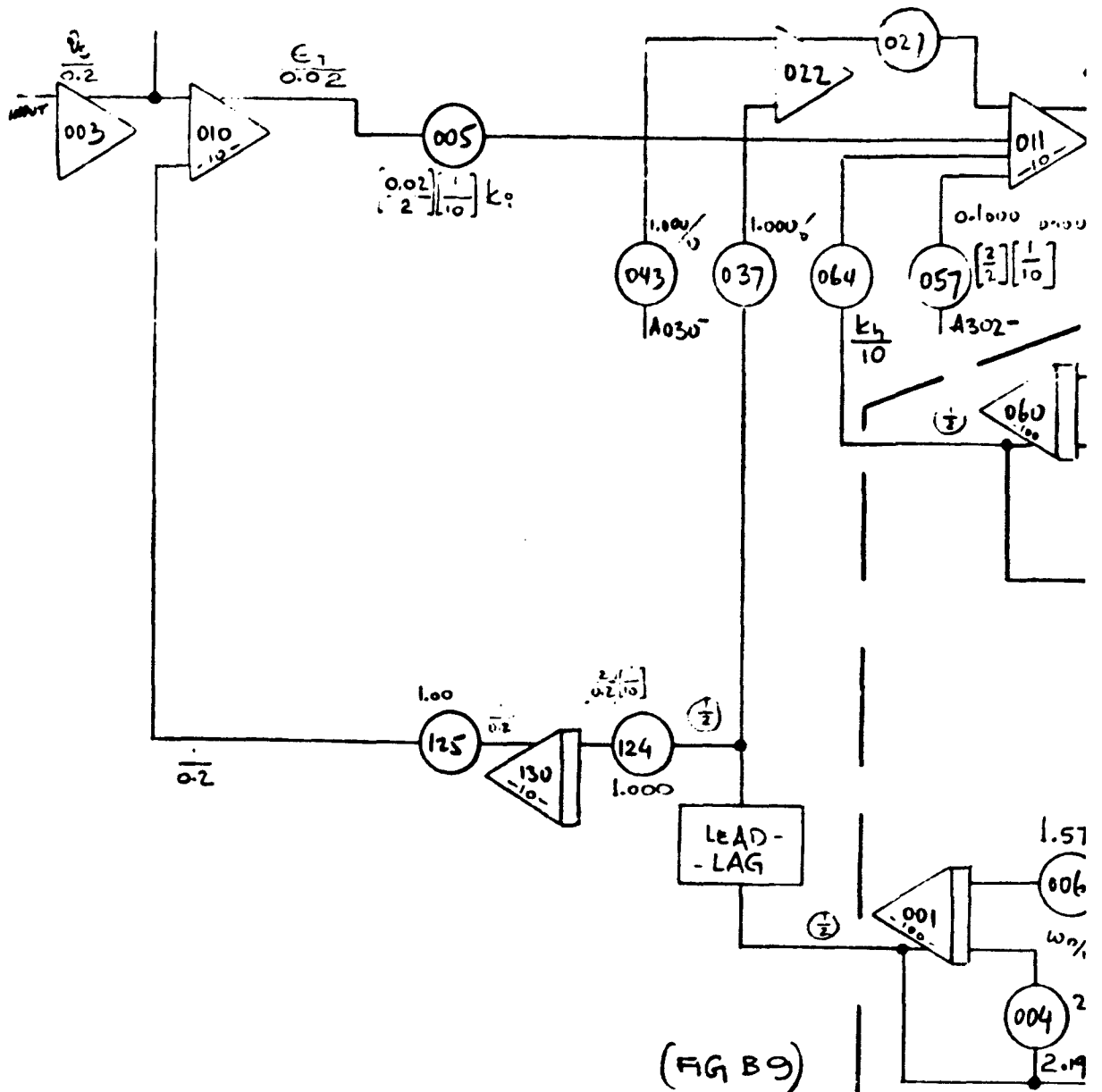
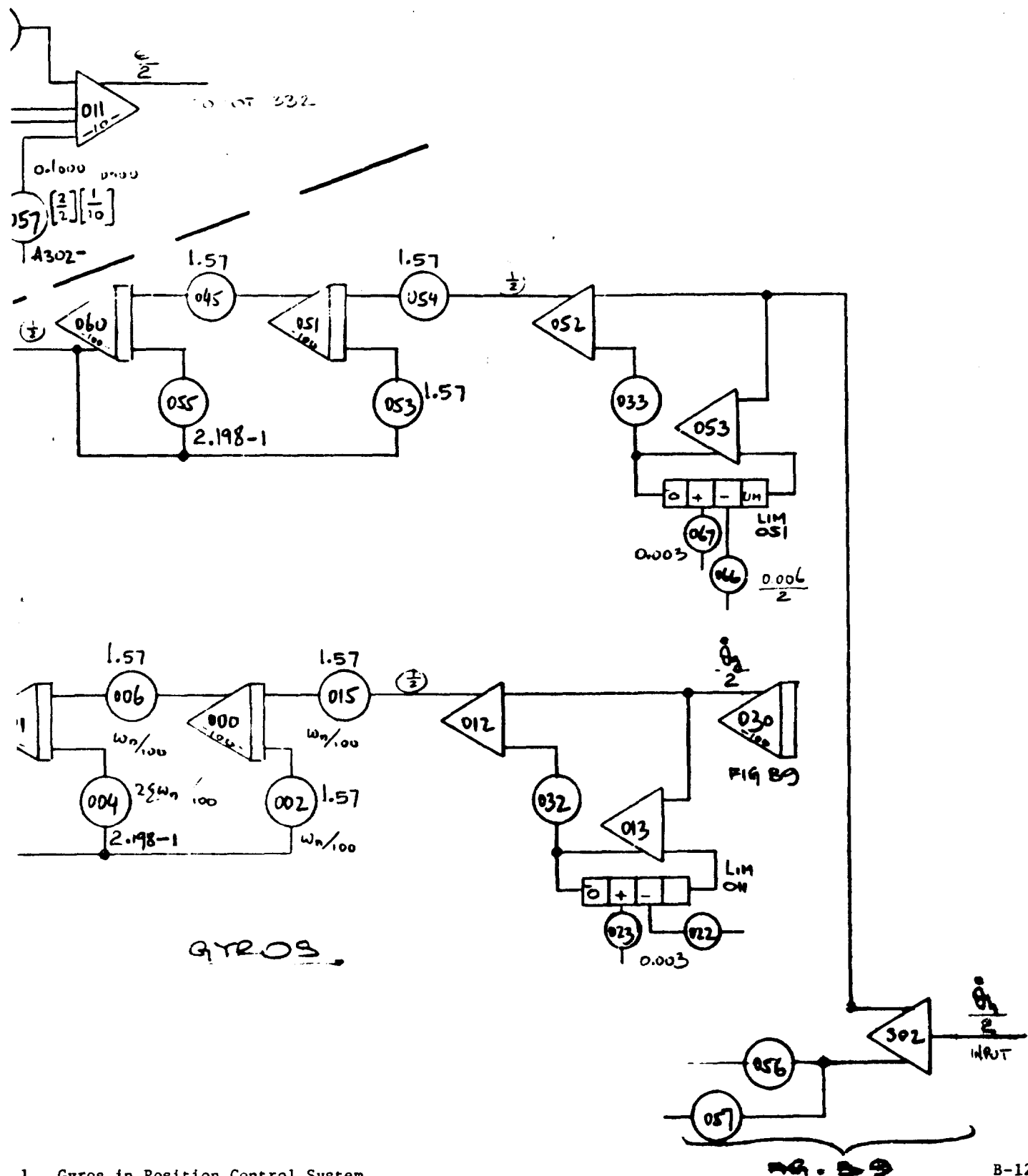


FIG. B11
 M60 TANK
 POSITION CONTROL
 GYROS
 11-26-74

Figure B-11. Gyros in I



1. Gyros in Position Control System

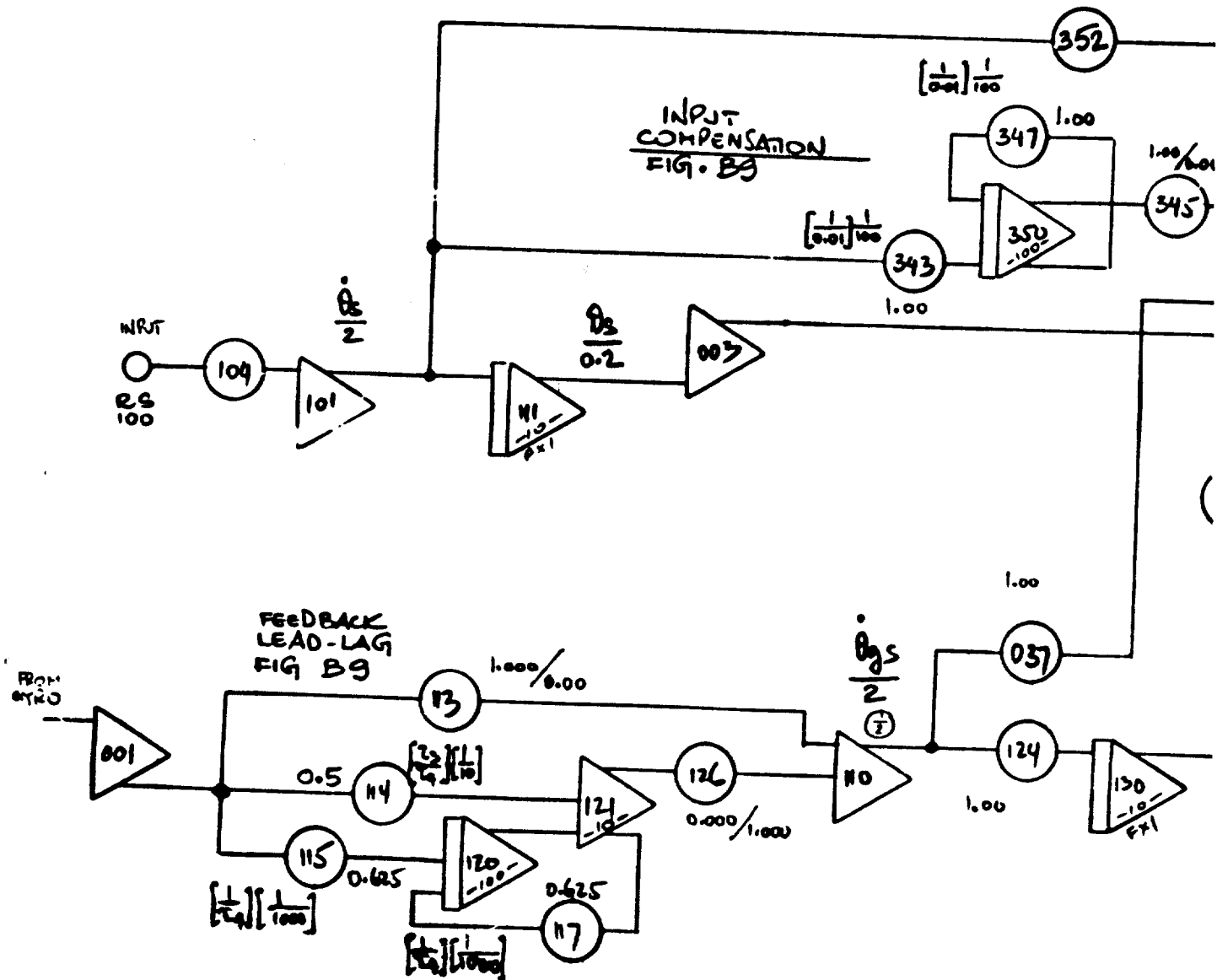
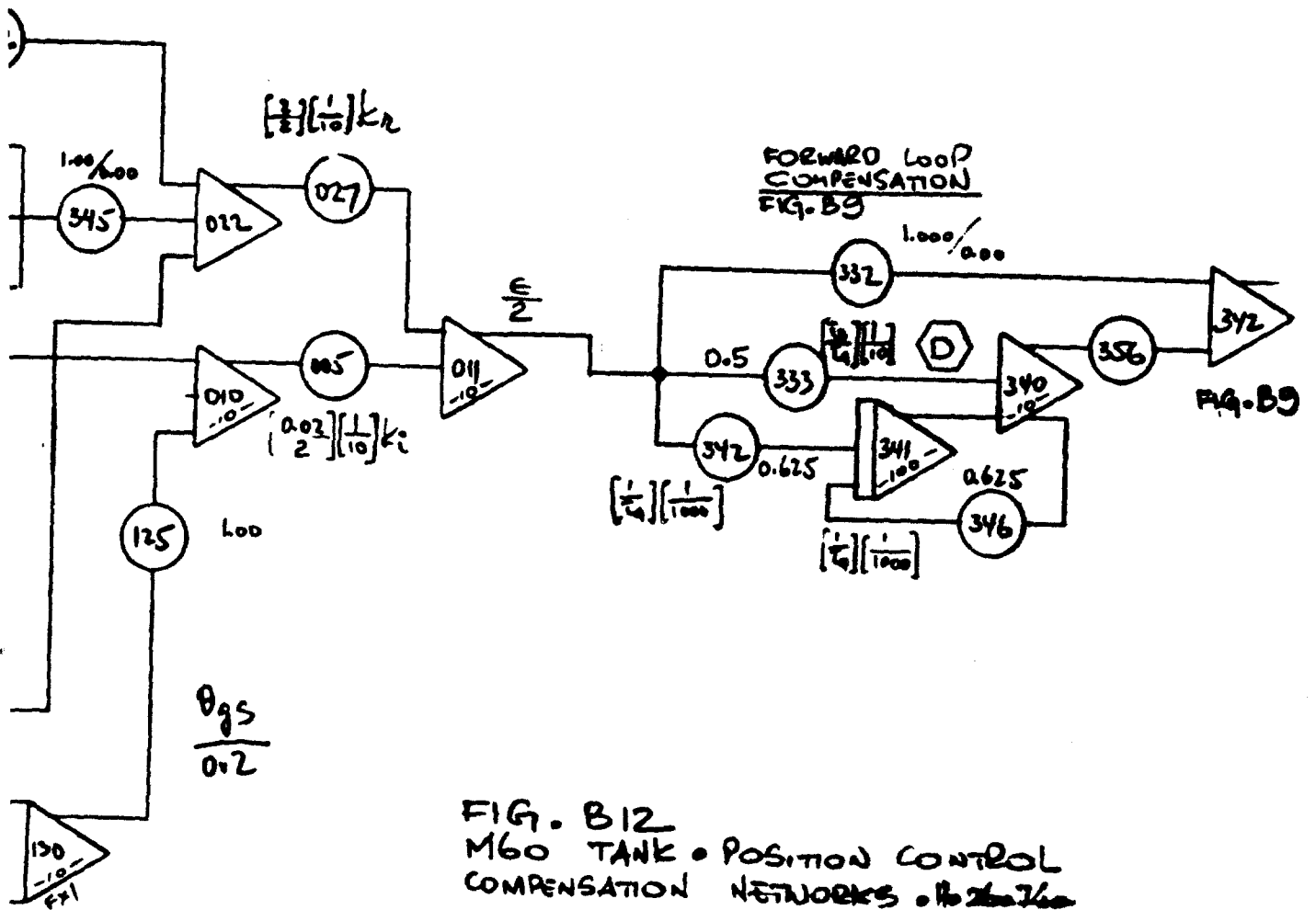


Figure B-12. Compensation Networks in

Best Available Copy

Best Available Copy



Networks in Position Control System